Comparison of the intestinal permeation enhancers, SNAC and C , for oral peptides : biophysical, in vitro and ex vivo studies

Caroline Twarog

Thèse de doctorat

NNT : 2020UPASS045

Comparison of the intestinal permeation enhancers, SNAC and C_{10}, for oral peptides: biophysical, *in vitro* and *ex vivo* studies

Thèse de doctorat de l'université Paris-Saclay

École doctorale n°569, Innovation Thérapeutique : Du fondamental à l'appliqué (ITFA)

Spécialité de doctorat : Pharmacotechnie et Biopharmacie

Unité de recherche : Université Paris-Saclay, CNRS, Institut Galien Paris-Saclay, 92296, Châtenay-Malabry, France

Référent : Faculté de Pharmacie

Thèse présentée et soutenue en visioconférence totale, le 03 Juillet 2020, par

Caroline TWAROG

Composition du Jury

M. Gilles PONCHEL Professeur, Université Paris-Saclay	Président
Mme Anne-Marie Healy Professeur, Trinity College Dublin	Rapporteur
Mme Véronique Préat Professeur, Université catholique de Louvain	Rapporteur
Mme Brigitte Illel Docteur en Sciences Pharmaceutiques, Sanofi R&D Montpellier	Examinateur
M. Alan Baird Professeur, University College Dublin	Examinateur
M. Hervé Hillaireau Maître de conférences, Université Paris-Saclay	Examinateur
M. Elias Fattal Professeur, Université Paris-Saclay	Directeur de thèse
M. David Brayden Professeur, University College Dublin	Co-Directeur de thèse

To my parents,

Acknowledgments

This thesis originates from half of my work at the Galien Institut Paris Sud and the other half at University College Dublin, with additional input from Sanofi, Montpellier. As an international collaboration, this work could not have been accomplished without the continued moral, technical and financial support of many individuals, institutions and organisations. I therefore, wish to express my sincere appreciation and gratitude to all of those who were directly or indirectly involved with my PhD project.

Firstly, I would like to thank my two co-supervisors, Prof Elias Fattal and Prof David Brayden, as well as my thesis committee comprising Dr Brigitte Illel, Dr. Hervé Hillaireau, and Dr. Rachel Vogel. Thank you for providing me this opportunity and your guidance, support and patience throughout the duration of my PhD program. Thank you very much for every piece of information you gave me that helped me to grow as a researcher.

I am immensely thankful to my Advisory Committee members, Prof Anne-Marie Healy from Trinity College Dublin, and my advisory Chairs, Prof Véronique Préat, Prof Gilles Ponchel and Prof Alan Baird for agreeing to evaluate this work.

Next, I would like to thank all people who helped me in various techniques, Prof Myriam Taverna (capillary electrophoresis), Magali Noiray (ITC, SPR), Dr. Christophe Desvignes and Loic Villemet (CMC measurement), Dr. Bridget Hogg (Cell Culture), Dr. Fiona McCartney (Ussing Chambers), Prof. Peter O'Brien and Dr. Kai Liu (High Content Analysis), Dr. Sabine Harrison (Rheology), Prof. Jeremy Simpson (Confocal Microscope), Marc Farrelly (Organ Baths), Kevin Thornton, Margot Coady and Catherine Lawson (Histology).

To Dr. Fiona McCartney, I wish to express my sincere gratitude and appreciation for the intensive technical discussions that started even when I had not yet arrived in Dublin. You always helped me no matter what the question throughout the course of my Ph.D. Thank you for your suggestions that were quite helpful for this research.

To Dr. Bridget Hogg for her continued kindness, tremendous support, advice and assistance during the research. I learn a lot from your scientific rigor and continuous curiosity about science. Thank you for your time and energy every day.

I believe that a complex project such as a PhD project cannot be done without the love and support of friends and family, and for me, a long list of people has been essential for my well-being in both good and bad times over the course of my PhD.

At the Galien Institut, I am so grateful to have had amazing desk buddies for half of my PhD. You were always ready to build the pyramid of the week: Balthazar, Federica, Céline, Sophie, Ludmila, Serra. A special thank you to Raul, Barbara and Nelly for their unlimited bliss and delightful personalities that made them valuable companions throughout this tough year. Thank you for the conversations, the laughs, the thoughts, the concerns, the enthusiasm, the support and for being you

At UCD, to all my course colleagues and friends for accepting this “foreigner from inside doors” with such great hospitality and joy. Thank you for making my time abroad so special. I have also had the distinct pleasure of crossing paths with some fantastic people during my time in UCD and I probably wouldn’t survived without all the chats and sharing of epic stories: Hugh, Jose, Nick, Sulliman, Joanne, and Amy. Also, many thanks to my cheerful and indispensable “minions” friends, Vivienne and Sarinj, I feel happy and grateful for the comfort of having such a harbor even when far from home. Also a special thanks to Jose Maria Urtesun Elizari for his constant good mood and bringing some lightness too.

To my Irish host family, Simon and Eileen: thank you for the talk, the advice, the laughs and your precious company. I will remember all the great memories at 22 Nutley Road. I will come back sooner or later so we can sit in your lovely garden and share some more scones and Queen cake. Of course, I want also to thank my past house-mates from all around the world that became friends during my stay in Dublin: Johanna, Martina, Sophia, Claire, Barbora, Duio, Cristina. Thank you for the fresh and young atmosphere in the house and for all the good “craic” together.

I would like to extend my deepest gratitude to my parents and my sister, for their encouragement and never-ending moral support particularly during this two-year period away from home to fulfill this PhD project. I dedicate this work to you. I love you so much, thank you.

To my partner in life, Simon, you stood by my side and supported me throughout this entire PhD journey, all while facing the troubles of your own research. Thank you so much for teaching me the importance of getting things done and moving forward to what is to come. I love you.

Contents

Abbreviations

4-CNAB	*N*-(4-chlorosalicyloyl)-4-aminobutyrate
5-CNAC	Sodium N-[8-(2-hydroxybenzoyl) Amino] caprylate
6-CF	6-carboxy-fluorescein
ABC	ATP-binding cassette
ACE	Affinity capillary electrophoresis
AJ	*Adherens* junctions
AME	Absorption-modifying excipients
ANOVA	Analysis of variance
API	Active pharmaceutical ingredient
AREC	Animal Research Ethics Committee
BA	Bioavailability
BCS	Biopharmaceutics Classification System
BCRP	Breast cancer resistant proteins
BW	Body weight
C-CPE	C-terminal fragment of *Clostridium perfringens enterotoxin*
C_{10}	Sodium caprate
$CaCl_2$	Calcium chloride
Caco-2	Human epithelial colorectal adenocarcinoma cells
CCh	Carbachol
Ci	Curie
CMC	Critical micelle concentration
CN	Cell number
CV	Cardiovascular
Da	Dalton
DMEM	Dulbecco's Modified Eagle Medium
DNA	Deoxyribonucleic acid
DPP-4	Dipeptidyl peptidase 4
EDTA	Ethylenediaminetetraacetic acid
eGFR	Estimated glomerular filtration rate
EU	European Union
FA	Fraction absorbed
FCCP	Carbonylcyanide-p-trifluoromethoxyphenylhydrazone
FcRn	Neonatel Fc Receptor
FD-4	FITC-labelled dextran of 4 kDa

FDA	Food and Drug Administration
FITC	Fluorescein isothiocyanate
FSH	Follicle-stimulating hormone
FTIR	Fourier-transform infrared
GalNAc	N-acetylgalactosamine
GI	Gastrointestinal
GIPET®	Gastro-Intestinal Permeation Enhancement Technology
GlcNAc	N-acetylglucosamine
GLP-1	Glucagon-like Peptide 1
GnRH	Gonadotropin-releasing hormone
GRAS	Generally Recognized As Safe
H&E	Haematoxylin/eosin stain
HbA1c	Glycated haemoglobin
HBSS	Hank's Balanced Salt Solution
HCA	High content analysis
HEPES	4-(2-hydroxyethyl)-1-piperazine ethanesulphonic acid
HepG2	Human hepatocellular carcinoma cells
hGH	Human growth hormone
HIM2	Hexyl-insulin monoconjugate-2
HIP	Hydrophobic ion-pairing
HPRA	Health Products Regulatory Authority
IBAT	Bile acid transporters
IC	Intracellular calcium
IgA	Immunoglobulin A
IP_3	Inositol 1,4,5-triphosphate
Isc	Short circuit current
ITC	Isothermal titration calorimetry
JAM	Junctional adhesion molecules
K_2HPO_4	Potassium phosphate di-basic
KCl	Potassium chloride
kDa	Kilodaltons
KH	Krebs-Henseleit
KH_2PO_4	Potassium phosphate monobasic
LDH	Lactate dehydrogenase
LMER	Lactulose:mannitol urinary excretion ratio
LMW	Low-molecular weight
M-cells	Microfold cells

MCFA	Medium Chain Fatty Acid
MEM	Modified Eagle medium
Mg^{2+}	Magnesium ion
$MgSO_4$	Magnesium sulfate
$MgSO_4.7H_2O$	Magnesium sulfate heptahydrate
MLCK	Myosin light-chain kinase
MMP	Mitochondrial membrane potential
MRP	Multidrug Resistance associated Protein
MTS	3-(4,5-dimethylthiazol-2-yl)-5-(3-carboxymethoxyphenyl)-2-(4-sulfophenyl)-2H-tetrazolium
MTT	3-(4,5-dimethylthiazol-2-yl)-2,5 diphenyltetrazolium bromide
MW	Molecular weight
NA	Nuclear area
Na_2CO_3	Sodium carbonate
$Na_2HPO_4.7H_2O$	Sodium phosphate dibasic heptahydrate
NAC	N-acetylcysteine
NaH_2PO_4	Sodium phosphate monobasic anhydrous
$NaHCO_3$	Sodium bicarbonate
NI	Nuclear intensity
NOAEL	No observed adverse effect
NP	Nanoparticle
P-gP	P-glycoprotein
PAMR	Peri-junctional actomyosin ring
P_{app}	Apparent permeability coefficient
PBO	Placebo
PBS	Phosphate-buffered saline
PD	Pharmacodynamic
PE	Permeation Enhancers
PEG	Polyethylene glycol
PIONEER	Peptide Innovation for Early Diabetes Treatment trial
PK	Pharmacokinetic
PMP	Plasma membrane permeability
ROS	Reactive Oxygen Species
s.c.	Sub-cutaneous
SBTI	Soybean Trypsin Inhibitor
sCT	Salmon calcitonin
SDS	Sodium dodecyl sulfate

SEM	Standard Error of the Mean
SGLT1	Sodium-glucose transport proteins
siRNA	Small-interfering RNA
SNAC	Sodium N-[8-92-hydroxybenzoyl)aminocaprylate]
SNEDDS	Self-Emulsifying Drug Delivery Systems
SOMA	Self-Orientation Millimeter-Scale Applicator
SPR	Surface plasmon resonance
SVCT	sodium-vitamin C co-transporter
T2D	Type 2 diabetes
TEER	Transepithelial electrical resistance
TI	Therapeutic index
TJ	Tight junction
TMRM	Tetreamethyl rhodamine ethyl ester
TNF	Tumor necrosis factor
Triton™ X-100	p-t-octyl phenol polyoxyethylene-9.5
TRIM	Thrifty Rapid Intestinal Monolayers
UCD	University College Dublin
WPI	World Precision Instruments Inc.
ZO	*Zonula occludens*

Publications Associated with this thesis

Papers

1) **C. Twarog**, S. Fattah, J. Heade, S. Maher, E. Fattal, D.J. Brayden. Intestinal Permeation Enhancers for Oral Delivery of Macromolecules: A Comparison between Salcaprozate Sodium (SNAC) and Sodium Caprate (C10), *Pharmaceutics* **2019**, *11, 78*.

2) **C. Twarog**, K. Liu, P. J. O'Brien, K. A. Dawson, E. Fattal, B. Illel, D. J. Brayden "Comparison of the mechanisms of action of the intestinal permeation enhancers SNAC and sodium caprate in Caco-2 assays", *European Journal of Pharmaceutics and Biopharmaceutics (submitted).*

Peer-reviewed conference abstracts:

1) **C. Twarog**, K. Liu, P. J. O'Brien, K. A. Dawson, E. Fattal, B. Illel, D. J. Brayden. "A Head-to-head comparison of the Intestinal Permeation Enhancers, Salcaprozate Sodium (SNAC) And Sodium Caprate (C_{10}), Using High Content Analysis In Caco-2 And HepG2 cells", Abstract number 19-A-159-CRS, *Controlled Release Society 35th Annual Meeting*, Valencia, Spain (July **2019**).

2) **C. Twarog**, K. Liu, P. J. O'Brien, K. A. Dawson, E. Fattal, B. Illel, D. J. Brayden. "A multi-parametric high content analysis of the intestinal permeation enhancers, SNAC and C10 in Caco-2 and HepG2 cells", Number 2030, *Keystone Symposia Conference, Delivering Therapeutics Across Biological Barriers,* Dublin, Ireland (May **2019**).

3) **C. Twarog,** H. Hillaireau, M. Taverna, M. Noiray, C. Desvignes, R. Vogel, B. Illel, D. Brayden, E. Fattal. "Understanding physicochemical interactions between selected intestinal permeation enhancers and peptide therapeutics to improve oral peptide formulation", *4th Annual Meeting SFNano*, Bordeaux, France (Dec **2017**).

Selected oral presentations:

1) **C. Twarog,** H. Hillaireau, M. Taverna, M. Noiray, C. Desvignes, R. Vogel, B. Illel, D. Brayden, E. Fattal. "Understanding physicochemical interactions between intestinal permeation enhancers and exenatide to improve oral peptide formulation", *11th World Meeting on Pharmaceutics, Biopharmaceutics and Pharmaceutical Technology*, Grenada, Spain (March **2018**)

General introduction

General Introduction

Due to their poor stability, large molecular weight and poor cellular transport properties, therapeutic biomolecules are predominantly limited to parenteral administration. Oral delivery of macromolecular drugs especially therapeutic peptides is highly desirable due to the ease of use and improved patient compliance when compared with injection. However, there are major concerns over the development a therapeutic peptide for oral delivery including (i) the peptide instability in the GI tract (ii) its low permeability and (iii) narrow absorption window in the intestine [1]. Engineering solutions have been developed to overcome low pH and enzymatic degradation in the stomach. However, in order for an oral delivery system to be effective, the biomolecule should be absorbed in quantities to achieve good bioavailability, enough to elicit a pharmacological effect. Poor absorption across the intestinal epithelial barrier and into the bloodstream continues to hinder clinical viability of oral protein formulation.

Incorporation of permeations enhancers (PEs) in conventional oral dosage forms is considered a relatively basic technology to address macromolecule permeability. PEs can improve macromolecule absorption by several mechanisms: (i) increasing drug solubility, (ii) opening the tight junctions (TJs); (iii) temporarily disturbing the lipid bilayer packing or fluidizing membranes; (iv) complexation or ion-pairing with the payload; (v) preventing degradation/metabolism [2]. There are currently over 50 clinical trials in which PEs were shown to increase oral absorption of poorly permeable molecules, mostly achieved using surfactants.

In this thesis, the medium-chain fatty acid (MCFA), sodium caprate (C_{10}), and the C_8 derivative, salcaprozate sodium (SNAC), are of particular interest. They have had over 20 years of development in proprietary delivery platforms and have been tested in human trials more than any other PEs [3,4]. In addition, SNAC is a key component in the first oral semaglutide formulation for treatment of Type II diabetes mellitus (T2D) from Novo Nordisk

(Copenhagen, Denmark) that received FDA approval in October 2019 (Rybelsus®). Although the first oral glucagon-like peptide 1 (GLP-1) treatment for T2D is now on the market, uncertainty remains concerning the mechanism of action of SNAC in particular its interaction with the epithelial cell layer and its designation as a "chaperone" with regards to payload and/or cytotoxicity [5].

During this PhD project, a head to head comparison between SNAC and the gold standard PE, C_{10} was carried out in order to assess the mechanistic action of each and to highlight differences and common features (Figure 1).

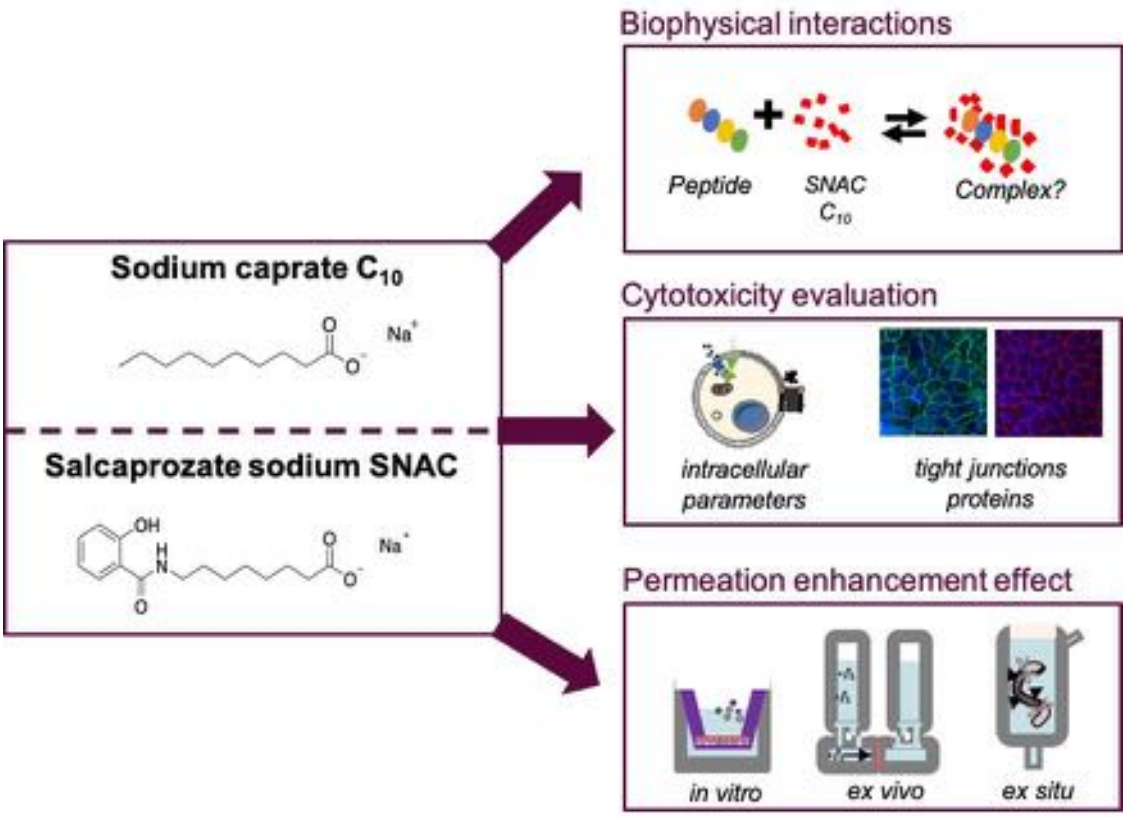

Figure 1: General overview of the thesis.

The overall aims of this thesis were:

1. To investigate physico-chemical interactions between the GLP-1 peptide analogue, exenatide, and SNAC or C_{10} using complementary analytical techniques.
2. To evaluate the relative cytotoxicity of SNAC and C_{10} in cell-based models using a range of conventional endpoint assays and High Content Analysis (HCA) and to determine effects on TJs and protein localization.

3. To compare the mechanism of enhancement of SNAC and C_{10} across the intestinal epithelium using *in vitro* (Caco-2 monolayers) and *ex vivo* models (isolated rat mucosae) and *ex situ* models (non-everted gut sacs) and measure their impact on mucus properties.

The thesis is divided into two sections. The first section is based on a published review article, further expanded to become **Chapter 1**. It describes the challenges for oral delivery of macromolecules including formulation and approaches to increase the bioavailability of therapeutic biomolecules. It goes on to attempt the first head-to-head comparison between SNAC and C_{10} under a set of criteria. Based on current understanding and *in vitro* data, distinct mechanisms of action were proposed for each, their extensive history of clinical trials was summarized, and their safety evaluation and regulatory perspectives was discussed.

The second section represents the experimental work that was carried out during this PhD project and is organized into three chapters.

In Chapter 2, the colloidal organization of SNAC or C_{10} alone or mixed with a model GLP-1 peptide analogue, exenatide, was analyzed. The interaction between SNAC or C_{10} with exenatide was then further investigated. For the first time, advanced biophysical methods (isothermal titration calorimetry, surface plasmon resonance, affinity capillary electrophoresis) are used to measure binding strengths of the PEs/exenatide complexes in simple and complex buffers.

In Chapter 3, the assessment of the *in vitro* cytotoxicity of C_{10} and SNAC was made by determining the epithelial cellular response after exposure to the PEs using conventional cytotoxicity assays and HCA. The intestinal transport route of paracellular markers was also established using Caco-2 monolayers exposed to SNAC and C_{10} as well as their effects on selected TJ protein distribution.

In Chapter 4, the permeation enhancement effect on paracellular markers by SNAC and C_{10} across isolated rat gastric, jejunal and colonic mucosae mounted in Ussing chambers and non-everted gut sacs was investigated. The morphological changes in tissue via

histological sampling were studied for each technique after *in situ* rat intestinal instillation. Finally, the impact of both PEs was also evaluated on native pig intestinal mucus by measuring viscoelastic properties of the mucus.

The thesis manuscript concludes with a general discussion on the work carried out during the PhD project, the unsolved issues, and the future possible perspectives for this work.

This research was funded by a French Government CIFRE grant No. 2016/0439, supplemented with funding from Sanofi-Aventis. Experimental work from Chapter 2 was carried out during the first 18 months of the Ph.D. at the Galien Institute Paris-Sud under the supervision of Prof Elias Fattal and Dr. Hervé Hillaireau. The data in Chapters 3 and 4 was produced during the subsequent 18 months at University College Dublin under the supervision of Prof David Brayden.

References

[1] D.J. Drucker, Advances in oral peptide therapeutics, Nature Reviews Drug Discovery, (**2019**).

[2] S. Maher, Intestinal permeation enhancers for oral peptide delivery, Adv Drug Deliv Rev, 106 (**2016**) 277-319.

[3] S.T. Buckley, Transcellular stomach absorption of a derivatized glucagon-like peptide-1 receptor agonist, Science translational medicine, 10 (**2018**).

[4] T.W. Leonard, Promoting absorption of drugs in humans using medium-chain fatty acid-based solid dosage forms: GIPET, Expert Opin Drug Deliv, 3 (**2006**) 685-692.

[5] E. Arbit, Oral heparin: status review, Thrombosis journal, 4 (**2006**) 6-6.

Introduction générale

En raison de leur faible stabilité, de leur poids moléculaire élevé et de leur faible perméabilité cellulaire, les biomolécules thérapeutiques sont principalement administrées par voie parentérale. Pourtant, les patients privilégient de loin la voie orale qui apporte une facilité d'administration des médicaments augmentant leur observance par rapport à l'injection. Toutefois, administrer par voie orale des biomolécules reste un challenge en raison de leur instabilité dans le tractus gastro-intestinal et de leur faible perméabilité au travers des membranes intestinales [1]. Des solutions galéniques existent pour diminuer leur dégradation enzymatique gastrique leur permettant d'atteindre l'intestin. Cependant, pour obtenir une biodisponibilité suffisante et donc un effet pharmacologique, la biomolécule doit être absorbée en quantités suffisante au travers de la barrière intestinale : un défi majeur qui continue d'entraver le développement clinique des formes peptidiques pour la voie orale.

L'incorporation de promoteurs d'absorption dans les formes pharmaceutiques orales classiques est considérée comme une technologie relativement simple pour améliorer la perméabilité des macromolécules. Ces promoteurs peuvent : (i) augmenter la solubilité des macromolécules, (ii) ouvrir les jonctions serrées de l'épithélium intestinale ; (iii) perturber temporairement les membranes cellulaires ; (iv) protéger les macromolécules de dégradations intestinales par formation de complexes d'interactions [2]. Plus de 50 essais cliniques ont démontré que les promoteurs d'absorption augmentent l'absorption orale de molécules peu perméables.

Dans cette thèse, deux promoteurs d'absorption nous ont semblé présenter un intérêt particulier : le caprate de sodium (C_{10}), et le dérivé en C_8, le salcaprozate de sodium (SNAC). Ils ont été développés pendant plus de 20 ans comme promoteurs d'absorption et ont été testés dans de nombreux essais cliniques chez l'homme [3,4]. Le SNAC est un composant majeur de la formulation orale du sémaglutide, un peptide thérapeutique utilisé dans le traitement du diabète de type II, développée par Novo Nordisk. Cette formulation orale à la

composition inédite a reçu l'approbation de mise sur le marché par l'agence américaine des produits alimentaires et médicamenteux en octobre 2019 et porte le nom de Rybelsus®. Il s'agit de la toute première spécialité thérapeutique disponible pour le traitement du diabète de type II par voie orale. Cependant, des incertitudes demeurent quant au mécanisme d'action du SNAC, en particulier son interaction avec les cellules épithéliales et son interaction en tant que molécule "chaperonne" avec la biomolécule [4].

Au cours de cette thèse, une comparaison entre les promoteurs SNAC et C_{10} est réalisée afin d'évaluer leur mécanisme d'action et de mettre en évidence leurs différences ou leurs points communs (Figure 1) dans leur interaction avec l'exénatide, choisi comme peptide modèle.

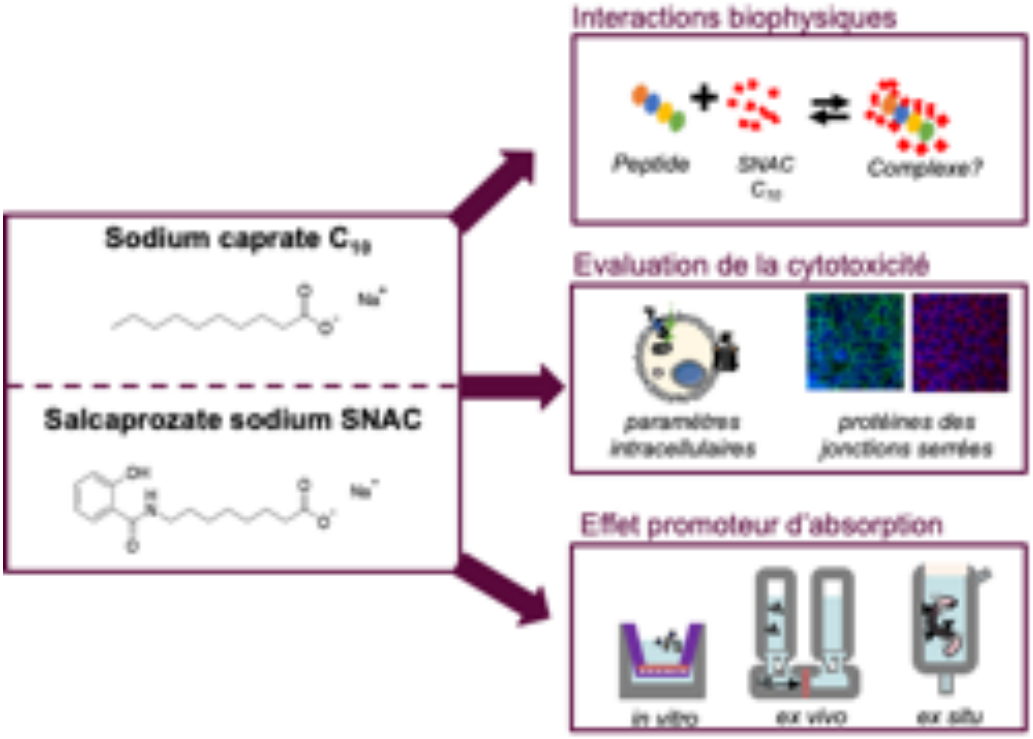

Figure 1 : Résumé général du projet de thèse.

Les objectifs principaux de cette thèse étaient les suivants :

1. Étudier les interactions physico-chimiques entre l'exénatide et le SNAC ou le C_{10} en utilisant des techniques analytiques complémentaires.

2. Évaluer la cytotoxicité du SNAC et du C_{10} sur modèles cellulaires en utilisant des tests de cytotoxicités conventionnels et par *High Content Analysis* ainsi que leur impact sur les protéines des jonctions serrées.
3. Comparer les mécanismes d'action en tant que promoteur d'absorption du SNAC et du C_{10} sur l'épithélium intestinal à l'aide de modèles *in vitro* (monocouches de cellules Caco-2), *ex vivo* (muqueuses de rat isolées) et *ex situ* (sacs intestinaux non inversés) et mesurer leur impact sur les propriétés de mucus intestinal de porc.

Le manuscrit est divisé en deux sections. La première section est basée sur un article de revue publié et enrichi pour devenir le **chapitre 1**. Elle fournit :

- Les défis rencontrés pour l'administration orale de macromolécules et les solutions développées pour augmenter leur biodisponibilité.
- La première analyse d'une comparaison directe entre le SNAC et le C_{10}. À partir des connaissances actuelles et des données *in vitro*, des mécanismes d'action distincts sont proposés pour chacun, l'historique exhaustif des essais cliniques est résumé, et l'évaluation de l'innocuité et les perspectives réglementaires sont abordées.

La deuxième section représente le travail expérimental qui a été effectué au cours de cette thèse et est organisée en trois chapitres.

Au **chapitre 2**, l'organisation colloïdale du SNAC ou du C_{10}, seul ou en mélange avec un peptide modèle, l'exénatide, est analysée. L'interaction entre les promoteurs et l'exénatide est ensuite étudiée plus en détail. Pour la première fois, des méthodes biophysiques avancées (titration calorimétrique isotherme, résonance plasmonique de surface, électrophorèse capillaire d'affinité) sont utilisées pour mesurer les forces de liaison des complexes PE/exénatide dans des tampons simples et complexes.

Au **chapitre 3**, l'évaluation de la cytotoxicité *in vitro* du C_{10} et du SNAC est réalisée à l'aide d'essais de cytotoxicité classiques et par *High Content Analysis*. Leur mécanisme d'action en tant que promoteurs d'absorption et leur l'effet sur la distribution de certaines protéines des jonctions serrées est évalué sur monocouches de cellules Caco-2.

Au **chapitre 4**, le mécanisme d'action du C_{10} et du SNAC est évalué par mesure de la perméabilité de marqueurs paracellulaires au travers de muqueuses isolées de rat montées sur chambres de Ussing (gastriques, jéjunales et coliques) et de sacs intestinaux de rats non inversés. Une évaluation histologique des tissues est ensuite réalisée ainsi que suite à une instillation *in situ* des promoteurs. Enfin, l'impact des PE est également évalué sur le mucus intestinal natif du porc en mesurant les propriétés viscoélastiques du mucus.

Au **chapitre 5**, une discussion générale sur les travaux réalisés au cours du projet de thèse, les questions non résolues et les perspectives d'avenir possibles pour ces travaux sont exposées.

Cette recherche a été financée par une bourse du gouvernement français CIFRE n° 2016/0439, complétée par un financement de Sanofi-Aventis. Les travaux expérimentaux du chapitre 2 ont été réalisés pendant les 18 premiers mois de la thèse à l'Institut Galien Paris-Sud sous la direction du Pr. Elias Fattal et du Dr. Hervé Hillaireau. Les données des chapitres 3 et 4 ont été produites pendant les 18 mois à l'University College Dublin sous la direction du Pr. David Brayden.

Références

[1] D.J. Drucker, Advances in oral peptide therapeutics, Nature Reviews Drug Discovery, (**2019**).

[2] S. Maher, Intestinal permeation enhancers for oral peptide delivery, Adv Drug Deliv Rev, 106 (**2016**) 277-319.

[3] S.T. Buckley, Transcellular stomach absorption of a derivatized glucagon-like peptide-1 receptor agonist, Science translational medicine, 10 (**2018**).

[4] T.W. Leonard, Promoting absorption of drugs in humans using medium-chain fatty acid-based solid dosage forms: GIPET, Expert Opin Drug Deliv, 3 (**2006**) 685-692.

[5] E. Arbit, Oral heparin: status review, Thrombosis journal, 4 (**2006**) 6-6.

Chapter 1

Oral peptide delivery: focus on the intestinal permeation enhancers, SNAC and C_{10}

1. Overview of oral peptide delivery

Despite an increasing trend in discovery and development in favor of injectable biopharmaceuticals, poor oral bioavailability remains a major impediment to their even more widespread application. One group of macromolecules, peptides and proteins, are especially useful due to excellent specificity, selectivity, safety, and efficacy in parenteral formats. Indeed, the therapeutic peptide market has expanded exponentially and a combined ~240 peptides and proteins have been marketed since the 1980s [1]. Of that list, 12% have <60 amino acids, representing approximately 30 peptides of that total [2]. Over 90% of peptides are injectable formulations, with just 4% delivered orally, and even lower percentages delivered via the skin and airway routes (Figure 1) [2].

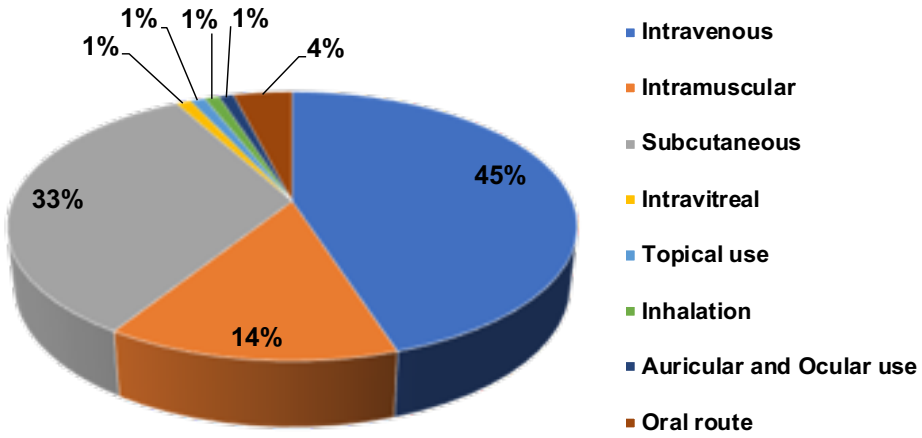

Figure 1: A schematic representation of distribution of therapeutic peptides and proteins based on route of administration. Modified from ([2]).

Those numbers reflect the typically low and variable bioavailability that is typically achieved for peptides from non-injectable routes. Injections required for long-term treatment necessitated by chronic disease are inconvenient and painful. The parenteral route also requires expertise of healthcare workers, can be associated with needle-infections, and is associated with high non-compliance [3]. Long acting formulations have been developed to reduce dosing frequency, especially for type 2 diabetes (T2D) [4]. Thus, for glucagon-like-peptide 1 (GLP-1) analogues, sub-cutaneous (s.c.) injection of exenatide has shifted from twice-a-day

administration (Byetta®; Lilly) to once weekly administration (e.g. Bydureon®, Lilly). This was achieved by the development of a microsphere-based controlled release system [5]. Other long-acting GLP-1 analogues administered once weekly include albiglutide (Tanzeum®, GlaxoSmithKline), dulaglutide (Trulicity®, Lilly) or semaglutide (Ozempic®, Novo Nordisk) which were developed using different chemistry approaches (albumin binding, fatty acid conjugation) [6,7].

The oral route offers greater patient compliance and can generate large market sales for molecules working indirectly on the same overall biological target, even if overall efficacy is lower than parenteral options [8,9]. Abramson *et al.* concluded that even considering the additional costs incurred to produce extra semaglutide for the oral formulation (dosage is on the order of 100 times as high as injection), it would lead to a greater quality of life experienced by the patient compared to a weekly injection [9]. In the treatment of T2D with two different drug classes, physicians prescribe more oral dipeptidyl peptidase 4 (DPP-4) inhibitors than injectable GLP-1 analogues [10]. Even if GLP-1 receptor agonists result in superior glycemic control and weight loss benefits, DPP-4 inhibitors are still preferred by the patients for a long-term medication. From a market perspective, sitagliptin (DPP-4 inhibitor) consequently outsells the injectable GLP-1 analogue, exenatide.

Oral administration of peptides is limited by local conditions within the gastro-intestinal (GI) tract and to date few peptides designed for systemic delivery have been approved by the FDA except for three relatively low-molecular-weight (LMW) and unconventional ones: a microemulsion (SNEDDS: Self-emulsifying Drug Delivery Systems) of cyclosporin (Neoral®, Novartis, Switzerland), a conventional solid-dose formulation of desmopressin (Minirin®, Ferring, USA) and a non-enteric coated tablet of semaglutide co-formulated with the permeation enhancer SNAC (salcaprozate sodium) (Rybelsus®, Novo Nordisk, Denmark) [11]. However, these examples are exceptions based first on the atypical macrocycle structures of the peptides (cyclosporin and desmopressin), yielding oral bioavailabilities (BA) of 30-40% for

lipophilic cyclosporin (Neoral®) and just 0.17% for the highly potent hydrophilic desmopressin, Minirin® [12]. Despite these low numbers, the Minirin® tablet is still a viable product as it is convenient to take orally and has a large therapeutic index (TI). The new mechanism of action for SNAC promoting semaglutide absorption through the stomach is also highly specific for semaglutide only.

The suitability of commercially available peptides for oral reformulation depends on their physicochemical properties (molecular weight (MW), solubility), chemical complexity, therapeutic considerations (route/frequency of administration, therapeutic index) and cost-effectiveness [13]. If the plasma half-life ($t_{½}$) is too short, it will not be economically viable to administer a peptide candidate in multiple daily oral doses, where safety, efficacy, and variability issues would also arise [13]. Similarly, a large TI is important in the context of selecting potent macromolecules as oral candidates, since efficacy and safety need to be present at the low and variable BA values that may be achieved even with successful oral formulations. Indeed, for peptides with a low TI such as insulin, a low bioavailability and high pharmacokinetic (PK) variability may result in either a lack of therapeutic effect or dangerous hypoglycemia, hence its use only as a model peptide by many researchers in the oral peptide field.

Recent progress has been made toward the development of oral formulations for peptides where there are scientific, patient acceptability, and commercial advantages over non-injectable alternatives. Indeed, the most clinically advanced oral peptide formulations are being developed for diabetes (insulin, GLP-1 analogues [4]), osteoporosis (salmon calcitonin (sCT) and teriparatide (PTH 1-34), endometriosis (leuprolide), acromegaly (octreotide), and chronic pain (difelikefalin) [12].

2. Challenges for oral delivery of peptides

Oral administration of hydrophilic macromolecules with a MW above 1000 Da remains a challenge. For peptides there is additional susceptibility to pH and gastric/small intestinal enzymes, as well as degradation due to the liver first pass metabolism. All macromolecules

are associated with low intestinal epithelial membrane permeability resulting from minimal passive- or carrier-mediated transcellular permeation across phospholipid bilayers, as well as restricted paracellular transport via tight junctions. Nucleic acid-based therapeutics face similar challenges [14]. Bioactive molecules can be classified under the Biopharmaceutics Classification System (BCS) which predicts *in vivo* performance of small molecules delivered orally based on *in vitro* measurements of solubility and permeability [15]. If they were small molecules, peptides would likely be assigned as Class III molecules typically exhibiting high aqueous solubility (but not always) and low intestinal permeability [16].

As the GI tract is dynamic, the transport of a peptide is limited but also variable. Many parameters including age, gender, fed state, time of the day, diet, and GI health status can also contribute to intra- and inter- subject PK variability, especially relevant for low TI molecules. Numerous barriers prevent an effective oral delivery of macromolecules and are discussed in reviews [17,18,19]. The following sections will describe the three main barriers to oral peptide delivery along the gastrointestinal tract and will discuss potential methods to address those limitations and enhance the oral delivery of therapeutic molecules.

2.1 Gastric and intestinal digestive barriers

2.1.1 Effect of enzymatic degradation

After oral intake, a significant challenge for oral peptide delivery is the presence of multiple digestive enzymes the purpose of which is to degrade macromolecules into absorbable nutrients. The most common form of peptide degradation is proteolysis of peptide bonds by pepsin in the stomach and by pancreatic peptidases in the small intestine (Figure 2). Trypsin, carboxypeptidase and chymotrypsin are secreted from the pancreas into the small intestine, mostly in the duodenum, where they are present in gram quantities [20]. These enzymes are responsible for 20% of the enzymatic degradation of ingested proteins and peptides. Enzymes are in the greatest abundance in the duodenum and jejunum with levels decreasing towards

the colon. However, in the colon, enzymatic fermentation processes further degrade biomacromolecules [21].

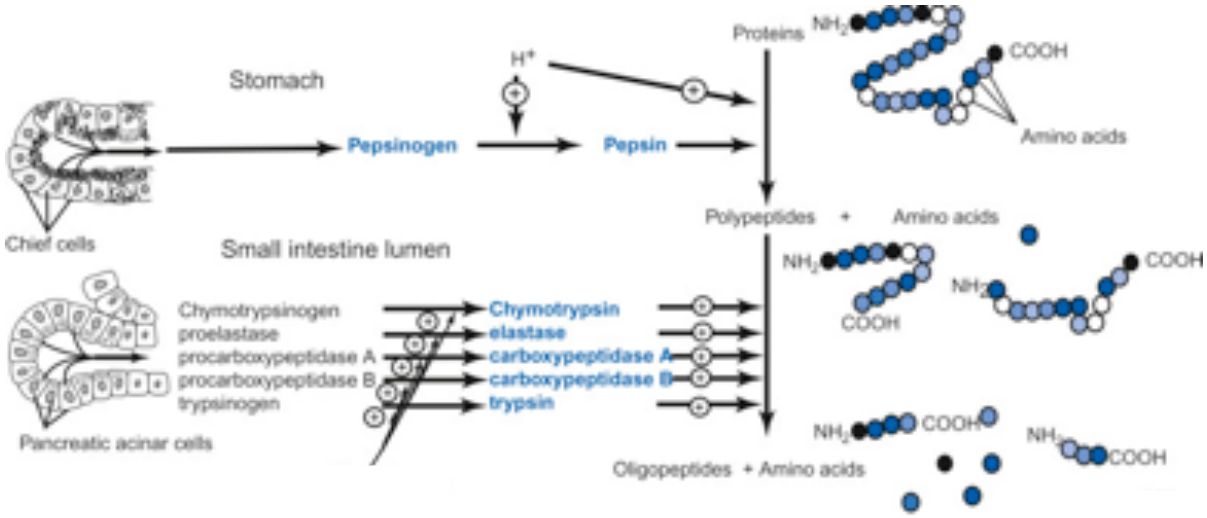

Figure 2: The events in protein digestion in the gastric and intestinal phase. Amino acids are represented by colored circles.

Wang *et al.* investigated the stability of 17 peptides drugs such as insulin in human gastric and intestinal fluids. It was found that cyclic peptides such as cyclosporin were more resistant to enzymatic cleavage due to restricted structure flexibility. Larger linear peptides (insulin, sCT, glucagon and secretin) were unstable in gastric and intestinal fluid compared to short peptides (octreotide, cyclosporin, desmopressin) due to the higher number of enzyme susceptible peptide bonds and high structural flexibility. Also, a good correlation in peptide stability was seen between fluids obtained from humans, pigs, and simulated versions [22].

2.1.2 Effect of gastric and intestinal pH

The harsh acidic conditions inside the stomach can denature many molecules [23]. A wide range of pH values varying from 1 to 7 in different regions of the GI tract affect the overall stability of the peptides [24]. Dressman *et al.* measured a median gastric pH of 1.7 and mid duodenum pH of 6.1 among 24 young healthy human subjects in the fasted state [25]. During meals, the pH in the stomach can increase to 6, but quickly returns to normal within minutes in most subjects. However, this high fasting gastric pH of 6 can be maintained for up to 6 hours in some cases and is more variable for elderly people [26]. As many tablets are enteric coated for delivery in the intestine, a high variation in pH in the stomach can lead to a premature

disintegration of the tablet with an impaired protection for the peptide against degradation. A pH in the duodenum below 5.5 was observed for cystic fibrosis patients and can affect the solubility of the peptide [27]. In addition to the acidic and enzymatic degradation, the lumen can cause other damages to therapeutic peptides. Osmotic stresses along the GI tract, peristalsis of the GI muscles, as well as the shear stresses by the flow rate of the gastric juice inside the lumen are other factors that decrease peptide efficiency due to mechanical degradation inside the lumen [28].

2.2 Intestinal mucus barrier

Orally administered therapeutics are confronted with the mucus gel layer that covers the GI tract surface [29]. With continuous secretion and rapid turnover, mucus allows removal of pathogens and lubrication of the epithelium. It has a complex gel-like substance that is composed of 95% water, mucin, immunoglobulin A (IgA) and cellular debris containing DNA, lipids and actin [30]. Mucus glycoproteins (mucins) have a high molecular weight and are encoded by more than 20 MUC genes. MUC2 and MUC5A are the main mucins secreted in the small intestine and the stomach respectively [31,32]. Mucin monomers consist of a protein backbone which is made up of repeating amino acids (serine, threonine and proline) which are heavily glycosylated with fucose, galactose, sialic acids, N-acetylglucosamine (GlcNAc) and N-acetylgalactosamine (GalNAc) [33] (Figure 3). Secreted mucins are joined together by di-sulphide bonds and these macromolecules are crosslinked to build up the mucosal layer. Mucins are responsible for the rheological properties of mucus as the glycans group bind a lot of water and thereby generate the typical gel-like properties of mucus. Indeed, mucus is a visco-elastic gel displaying shear-thinning behavior [34].

In rat the mucosal layer is heterogenous with one outer loosely adherent layer and one inner firmly adherent layer. In humans, a double layer mucus architecture is also present in the stomach and colon protecting the underlying lining from acid, enzymes and microbial aggressors [35]. The thickness and composition of mucus differs regionally which suggests a slowed-down diffusion and a lower permeability through the mucus in the GI tract for peptide-

based therapeutics [36]. For example, in colon the mucus thickness has been reported to increase from proximal to the distal regions. The mucus barrier shows large species variations with the rat intestinal mucus being thicker compared to humans. In humans, the stomach mucus thickness is around 144 μm [37], in duodenum 15.5 μm [38] and in the descending colon 69.6 μm. The mucus turnover along the GI tract of humans has been reported to be between 24 - 48 h [39].

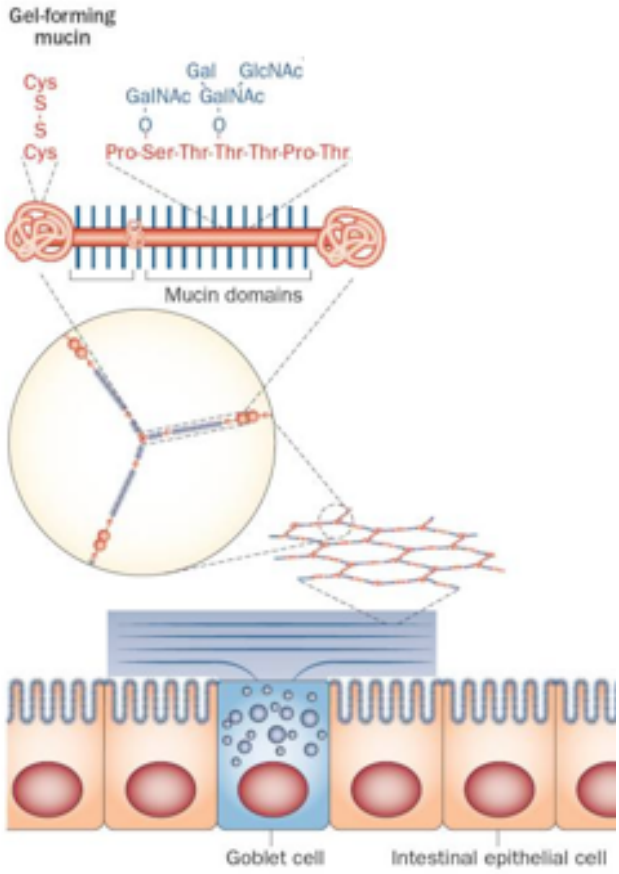

Figure 3: Simplified representation of a secreted mucin forming the mucus gel that covers the intestinal epithelium. Reproduced with permission from [33].

Mucus is composed by a three-dimensional network with size filtering properties. The mesh size is around 10-200 nm and blocks most pathogens and xenobiotics to permeate it. The larger the diameter of drugs or carrier systems, the more is their diffusion across the mucus gel layer hindered [40]. The anionic glycoproteins can interact with the peptide via electrostatic/ionic interactions, van der Waals interactions, hydrophobic forces, and hydrogen bonding, leading to poor absorption as well as alteration in the peptide structure [28,41]. The rate and extent of diffusivity of peptide through mucus to reach the intestinal epithelium is

affected by its viscous properties, its adhesive nature and its turnover. Although there is a constant water flow towards the intestinal epithelium accelerating the diffusion process of drugs through the mucus gel layer [42], it is obvious that without the aid of mucolytics and/or appropriate drug carriers, peptide-based therapeutics will have difficulty negotiating the mucus gel barrier [43].

2.3 Intestinal epithelial barrier

The epithelium lining of the GI-tract is another challenging barrier to orally administered peptides and is the most significant component of the intestinal barrier function. This barrier consists of a single layer of columnar epithelial cells supported by *lamina propria* and *muscularis mucosa* (Figure 4). The epithelium below the brush border consists of enterocytes, mucus-secreting goblet cells, Peyer's patch microfold cells (M-cells), enteroendocrine cells, and Paneth cells.

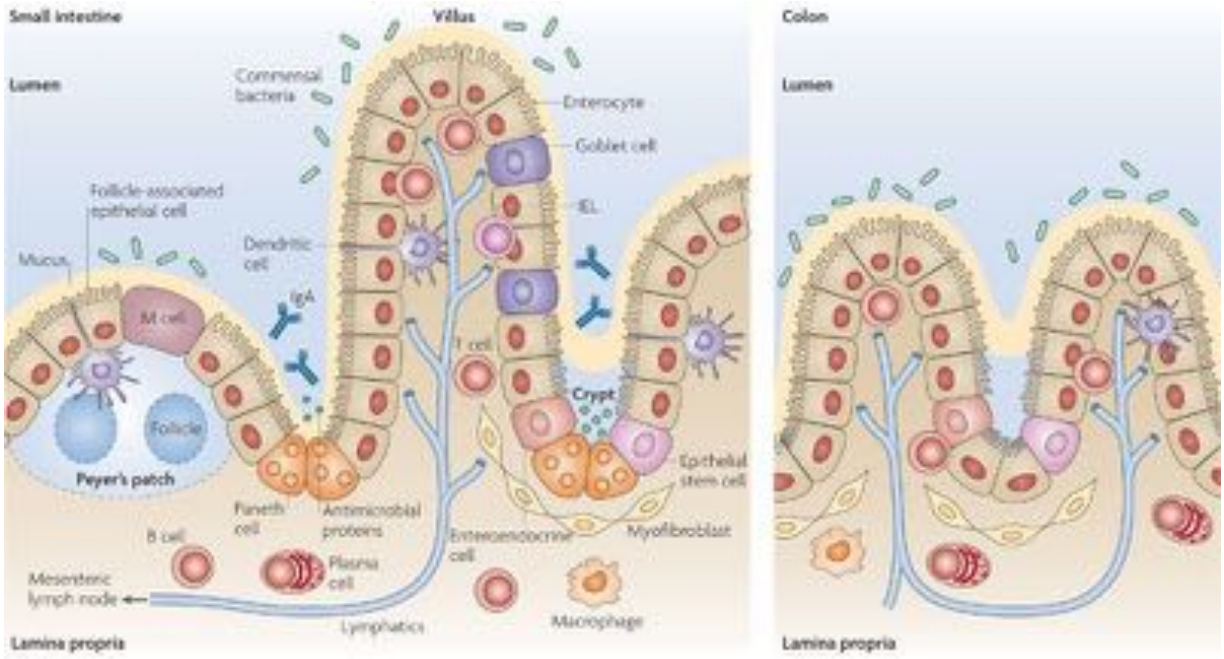

Figure 4: Anatomy of the intestinal epithelium. Reproduced with permission from [44].

2.3.1 Potential routes of cellular uptake

A high-density negative charge on the microvilli is present at the enterocyte apical membrane, which can prevent peptides interacting with the cell membrane [45]. Also, because of their hydrophilic macromolecular nature, they are unable to permeate the lipophilic phospholipid

bilayer of enterocytes. There are distinct mechanisms for molecules to cross the cell membrane: these include paracellular, receptor- or carrier-mediated uptake, absorptive transcytosis, passive diffusion, and M cell sampling (Figure 5). For peptides exhibiting a MW < 500-1000 Da the paracellular route of uptake is an option, whereas for others above that size, the capacity of that pathway is limited.

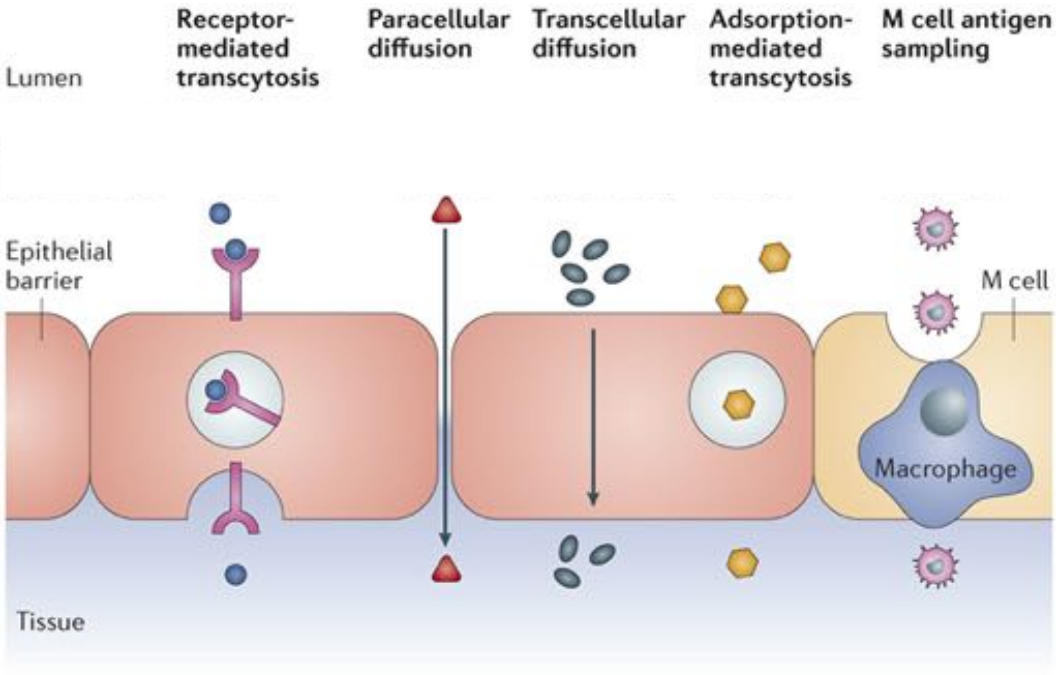

Figure 5: Representation of routes to permeate the intestinal epithelia: adsorption-mediated transcytosis and transcellular diffusion, paracellular permeation and receptor-/carrier-mediated uptake. Reproduced with permission from [46].

2.3.2 Role of P glycoprotein and cytochrome P450 enzymes

A long intestinal transit time of 4 hours allows for increased exposure of peptides to the intestinal epithelium for absorption, increasing its exposure to the brush border [47]. However, near the brush border membrane, macromolecules can undergo extensive pre-systemic intestinal metabolism and encounter active drug efflux transport [48]. In the intestine, ATP-binding cassette (ABC) transporters are among the most highly expressed transporters (colon: P-gP (5%), Breast cancer resistant protein (BCRP) (3%), Multidrug resistance-associated protein 2 (MRP2) (25%), small intestine: PgP (8%) BCRP (4%), MRP2 (10%)) [49] and together they function as a significant barrier to intestinal absorption. The abundance of P-gP increases from the proximal to the distal region of the small intestine, while the opposite is true for

CYP3A4. Due to this synergistic interplay of CYP3A4 and P-gP, intracellular metabolism remains a challenge for macromolecules [50]. As an example, cyclosporine (Sandimmune®, Novartis, Switzerland) can highly permeate the intestinal epithelium up to 86%, but the fraction absorbed (FA) is 35% due to coordinated brush border cytochrome P450 metabolism and P-gP efflux, and a further 8% is lost through hepatic metabolism to yield an oral BA of 27% [51]. Its primary problem is therefore intestinal wall metabolism, not permeability. It is known that linear lipophilic and cyclic peptides (including cyclosporine) are substrates of P-gP [52]. However, macromolecules tend not to be P-gP-substrates due to their high hydrophilic properties that will not favour interaction with P-gP [53].

2.3.3 Paracellular epithelial drug transport

The paracellular pathway consists of the intercellular space in between epithelial cells and provides an aqueous pore that permits the controlled movement of solutes into the body i.e. secretion of sodium and chloride ions. TJs localized between the intestinal epithelial cells control the paracellular diffusion of water, electrolytes, small molecules and immune cells. As multi-protein complexes, they form a highly dynamic gate-like barrier, which is impermeable to large macromolecules [54]. They also maintain epithelial polarity preventing the interaction of apical and basolateral membrane constituents (fence function) [55]. Transepithelial electrical resistance (TEER) characterizes the porosity/tightness of TJs in intestinal tissue by passing a continuous current across the tissue and measuring the changes in potential difference (PD) [56]. As the intestinal tissue has different TJ density and protein composition along the GI tract, different barrier properties and TEER values are obtained: leakier in small intestinal tissue (TEER~40 $\Omega.cm^2$) while tighter in colon (TEER~100 $\Omega.cm^2$) [57,58]. With a leakier tissue, the TEER decreases due to an increase in paracellular ionic conductance [59].

TJs are part of the intercellular junctional complexes and present at the apical side of the cells above the *adherens* junctions (AJ), gap junctions and desmosomes. A sharp molecular size cut off constitutes a major restriction to paracellular transport of peptide. Depending on the intestinal region, the TJ pore radii range from 7-9 Å for the jejunum, 3-4 Å for the ileum, and 8-

9 Å for the colon [60]. This cut off is sufficient to permit the polar sugar, mannitol (radius 3.3 Å), to permeate to a limited extent, whereas paracellular flux of the fluorescent-dextran 4 kDa (FD4) sugar, is minimal, hence their use as probes for that pathway. It is estimated that a MW <500 Da is required and the peptide must be hydrophilic for permeation via TJs [16]. The apical receptor of sodium-glucose transport proteins (SGLT1) can induce contraction of the actinomyosin ring, dilating the tight junction and increasing the pore radius to 50 Å to potentially allow further glucose absorption via solvent drag [61]. Multiple proteins control paracellular permeability via the TJs.

2.3.3.1 Composition of TJs

TJs are composed of transmembrane proteins, tight junction associated proteins and scaffolds proteins (Figure 6). TJs comprise only about 0.01% of the total absorption surface area of the intestine. Around 40 distinct proteins are involved in the TJ and the major ones are claudins, *Zonula occludens* (ZO) and occludin (Figure 6) [62].

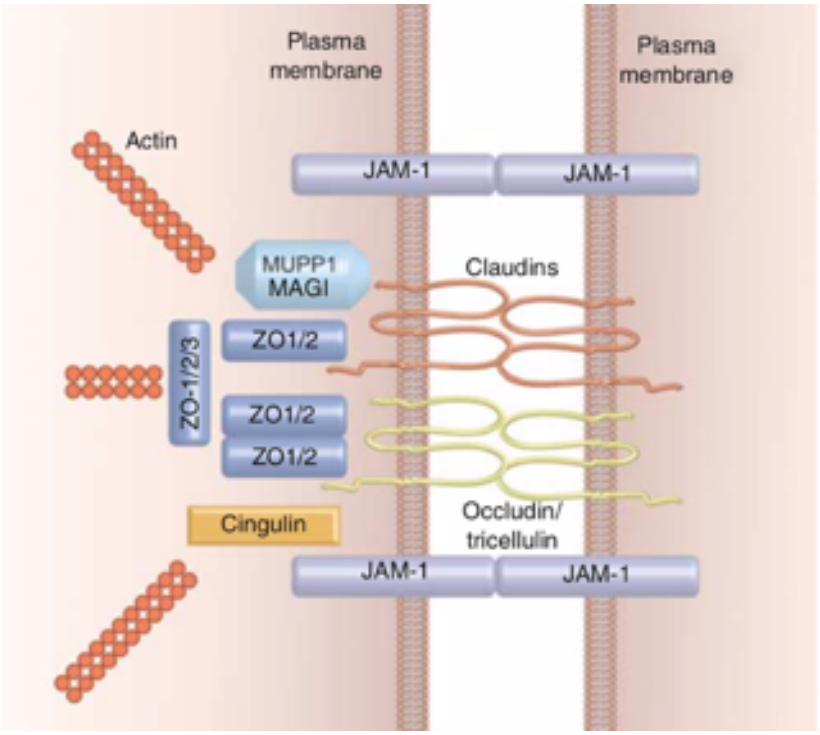

Figure 6: Representation of the basic structural membrane components of tight junction proteins. Transmembrane TJ proteins include claudins, occludins and junctional adhesion molecules (JAM-1) with cytoplasmic TJ proteins including ZO-1/2/3 and Cingulin. Reproduced with permission from [63].

Occludin is an integral transmembrane TJ protein with four transmembrane segments and two extracellular loops [64]. It interacts with the long C-terminal domain with intracellular TJ proteins including *zonula occludens*, which in turn links occludin to the cytoskeleton via F-actin (Figure 7). Occludin is thought to function in sealing the tight junction as well as in the maintenance of adhesion and polarity. However, in occludin gene knockout mice, the barrier function and structure of tight junctions remained intact even if tissue-specific effects were noted, such as chronic inflammation of the gastric epithelium [65]. Another study with occluding deficient mice found that the TEER of the tissue and the paracellular flux of mannitol were not affected by the absence of occludin [66]. However recent studies, using small-interfering RNA (siRNA) transfection against occludin in mice, suggested that occludin is responsible for the regulation of the passage of large molecules [67]. Lack of correlation between junctional strand formation and the presence of occludin led to the discovery of claudins.

Claudins are a group of around 26 transmembrane TJ-associated proteins in humans [62]. Similar to occludin, many claudins have four transmembrane domains with two extracellular loops but do not share structural homology with occludin and are smaller (Figure 7).

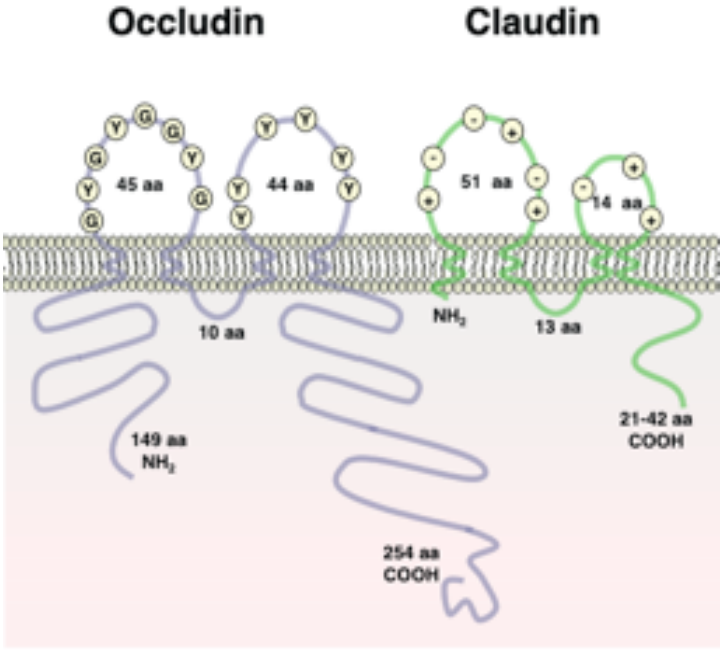

Figure 7: Structures of the transmembranes TJ proteins, occludin and claudin, adapted with permission from [68]

Claudins are central to the construction of the tight junction and maintenance of paracellular permeability forming junctional strands, even in the absence of other tight junction proteins. They maintain tight junctional barrier integrity and are responsible for size- and charge-selective pores. Each isoform is responsible for different aspects of intestinal barrier regulation and they are expressed differentially throughout the GI tract (Figure 8). For example, claudin-1, -3, -7 and -8 are expressed in the colon, while claudin-2, -7, -8 and -9 are expressed in the small intestine.

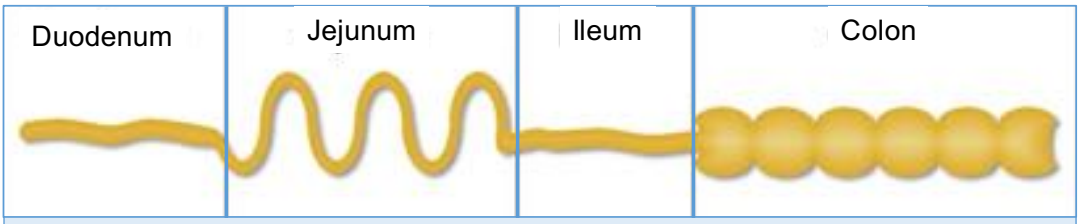

Claudin-1		
Claudin-2		
Claudin-3		
Claudin-4		
Claudin-5		Claudin-5
Claudin-7		Claudin-7
Claudin-8		Claudin-8
Claudin-12		Claudin-12
Claudin-15		Claudin-15
Claudin-18		

Figure 8: Regional expression of claudin proteins throughout the human intestinal tract. Adapted with permission from [69].

Some claudins mediate paracellular permeability (claudin 2, -7 and -12), while others control the physical- and electrical tightness of the junctions (claudin-1, -3, -4, -5 and -8) [69]. Importance of claudins involved in the formation of the paracellular barrier seal has been demonstrated with claudin-1 knockout mice dying within 24 hours of birth due to altered epidermal skin barrier function [70]. These claudins can also be categorized based on selectivity: anion selective (claudin-12), cation selective (claudin-15) and water selective (claudin-2), while others exhibit barrier properties regardless of charge (claudin-1, -3 and -5).

Claudin-2 increases trans-junctional permeability of cations such as sodium and potassium as well as water through the creation of a charge selective pore with an upper limit of molecules no greater than 3.5 Å [71]. In Crohn's disease, ulcerative colitis, coeliac disease and irritable bowel syndrome, claudin-2 was upregulated in GI epithelia [72,73]. The size selective space for paracellular flux increases along the crypt-villus axis from 6 Å at the villi tip and 60 Å in the crypt and is directly related to claudin-2 expression [74]. However, it does not facilitate the transport of larger MW molecules such as lactulose (342 kDa) [75]. A tight epithelium is characterized by overexpression of claudin-4 and -5. Claudin proteins ultimately interact with occludin and ZO-1.

ZO proteins are multidomain proteins which provide an intracellular structure and scaffold to regulate and maintain TJs [76]. They are composed by three PSD95-DIgA-ZO-1 (PDZ) domains, a central Src homology 3 domain and a region with homology to guanylate kinase ZO-1 that forms complete contiguous rings around polarized epithelial cells and mediates early assembly of TJ proteins in bilateral cells [77]. ZO-2 might play a role in recruiting claudin proteins. The first PDZ domain of ZO-1 interacts with claudin proteins, the second domain interacts with other ZO proteins (ZO-1, -2 and -3) and the third domain interacts with JAM-A. Due to this complex interaction ZO-1 plays a central role in TJ regulation and binds directly to F-actin (a cytoskeleton protein).

2.3.4 Transcellular epithelial drug transport

The epithelium of the small intestine has a multitude of transporters localized on the apical membrane which transport macromolecules and hydrophilic nutrients via the transcellular pathway by mechanisms including endocytosis and epithelial transporters. Due to their lipophilic properties, peptides are unlikely to cross the lipid bilayer of enterocytes and if a random endocytosis occurs, the majority is catabolized in lysosomes. M cells are mainly located within the epithelium of Peyer's patches and possess a higher transcytosis capacity in comparison to regular enterocytes. They represent a potential portal for oral delivery of macromolecules due to their high endocytosis ability.

Receptor-mediated endocytosis is a tightly regulated transport pathway allowing certain macromolecules to cross the phospholipid bilayer i.e. epidermal growth factor, immunoglobulins, transferrin, and cyanocobalamin (vitamin B_{12})- intrinsic protein complex. Bioactive di- and tri-peptides are carried by PepT1, calcium uptake is mediated by the vitamin D receptor, while vitamin C is carried on the sodium-vitamin C co-transporter (SVCT) [78]. Therapeutic peptides can potentially be taken up using receptor mediated delivery by targeting specific receptors as presented by Table 1.

Table 1: Representative ligand-mediated transport in oral delivery of therapeutic macromolecules. From [79].

Name	Distribution
Bile acid transporters (IBAT)	In the epithelium of ileum
UEA-1	In murine M-cells
Lectin-like protein receptors	In the intestine
Biotin receptor	In the intestine
Proton-coupled oligopeptide transporters PepT1 and PepT2	In the brush border membrane of small intestine
C-terminal Src kinase (CSK) peptide transporters	In goblet cells
Monocarboxylate transporter	In the intestine
CD44 receptor	In the intestine
Neonatel Fc Receptor (FcRn)	In the intestine

3. Ways to increase bioavailability of oral peptides

In order to increase peptide bioavailability and overcome the physical and enzymatic barrier of the GI tract, the formulation of peptides drugs in oral delivery systems has been approached from different angles, i.e. chemical modification of peptides, special drug delivery systems (nanoparticles), targeted delivery, co-administration of enzyme inhibitors and absorption enhancers, and devices. A dual focus is necessary early in development: optimizing the molecule and the formulation. Reviews of oral peptide delivery systems in clinical trials as well

as promising candidates in preclinical stages are written by Aguirre *et al.* [12] and Lakkiredy *et al.* focusing on diabetes peptides [4].

3.1 Direct modifications of peptide structure

3.1.1 Cyclization

Cyclization is an option to obtain higher bioavailability after oral administration as evidenced by the undecapeptide cyclosporine A, and its stable cyclic backbone formulated in an enteric coated microemulsion (Sandimmune®, Novartis, Switzerland) [80]. Somatostatin and encephalin have also improved oral absorption after cyclization [81]. In general, cyclization is carried out between side chains or ends of the peptide sequences through disulfide bonds, lanthionine, hydrazine or lactam bridges. Its widespread use is limited when larger peptides and proteins are needed for therapy [82].

3.1.2 PEGylation

PEGylation of therapeutic peptides is a modification strategy used when cyclization is not possible. It consists in grafting a polyethylene glycol (PEG) residue to a protein or peptide drug, covalently or not in the case of PEG prodrugs [83]. PEG comprises a group of non-toxic polymers approved by the FDA for human intravenous, oral and dermal applications [84]. For oral delivery, peptides conjugated to branched chain PEGs display increased pH and thermal stability and higher resistance to intestinal proteolytic digestion compared to linear PEGs [85]. A PEG-conjugated insulin known as hexyl-insulin monoconjugate-2 (HIM2, Nobex Corporation, USA) acquired by Biocon (USA) to become IN-105 was the first successful orally delivered PEGylated insulin [86]. In a Phase II trial (CTRI/2009/091/000479) pre -prandial administration of IN-105 to T2D patients reduced post-prandial glycaemic excursions, although there was considerable intra-patient variability [87]. In a Phase III trial it did not adequately reduce glycated haemoglobin (HbA1c) levels and failed to meet its primary endpoint (NCT03430856). PEGylation of sCT also resulted in resistance to intestinal enzymes and a 6-fold increase in intestinal absorption in a rat model [88]. Gong *et al.* replaced cysteine at position 39 of exenatide sequence with PEG and an improved biological half-life and efficacy

was obtained in diabetic mice [89]. Neither PEGyated sCT nor exenatide have progressed to clinical evaluation in oral formats.

3.1.3 Peptide-targeted ligand conjugates

An alternative modification approach is to conjugate the peptide to an intestinal epithelial receptor-targeted ligand that can shuttle the peptide across the epithelium (Table 1 Section 2.3.4). A number of potential receptor targets have been identified including transferrin, vitamin B_{12} [90], PepT1, folate, biotin and FcRn [91,92]. Biorexis Technology Inc. (USA) synthesized a peptide conjugated with transferrin that obtained more favourable PK in preclinical studies [93]. An insulin-transferrin conjugate in a hydrogel format demonstrated higher resistance to enzymatic degradation [94]. With a biotinylation approach, results showed that Lys26,34-biotin-GLP-1 had an oral hypoglycemic efficacy 9 fold greater than the native GLP-1 [95]. Another study showed the best stability efficacy against intestinal enzymes for Lys12-27-biotin-Exendin-4 [96].

3.1.4 Lipidization

The addition of a long fatty acid chains has been used to improve peptide uptake by membrane by increasing its lipophilicity and enhancing its stability. Although there are many reports on the oral administration of lipidized peptides, including insulin [97,98], calcitonin [99] and enkephalin [100] none of them has been further developed into an advanced development stage. Many factors such as the linker used in lipid-conjugation, the formulations for oral administration and other excipients can influence the bioavailability of a lipidized peptide.

3.1.5 Peptidomimetics

The formation of a peptidomimetics is based on the substitution of natural amino acids with unnatural ones to create a peptide sequence more resistant to enzymatic degradation (D-conformation, N-methylation, tetra-substitution, side chains methylations(s). As an oral example, desmopressin contains a deaminated amino terminal and contains a more stable D-arg at position eight, which increases stability and lipophilicity. Replacement of ala2 with D-ala2 improved stability, prolonged half-life and increased activity of GLP-1 in microspheres

after oral gavage in mice [101]. However, by changing the amino acids sequence, the activity of the drug can be compromised

3.2 Formulation technologies

3.2.1 Dosage form design

Experience from conventional formulations shows that the peptide-degrading acidic environment in the stomach can be successfully avoided by enteric-coated formulations. The solid dosage form is covered with a weakly acidic polymer film that delays release by dissolving above the pKa in a pH-dependent fashion. Frequently used polymers are cellulose acetate phthalate, polyvinyl acetate phthalate, cellulose derivatives and methacrylic acid copolymers (Eudragits®) [102]. The oral peptide formulation, Peptelligence™ acquired by Enteris BioPharma (USA) uses an enteric coated solid dosage form with other pH modifiers (citric acid, tartaric acid or vitamin C). However, the other excipients are contained in vesicles without contacting the Eudragit®-enteric coating, thereby avoiding undesirable interactions and enabling dissolution at the designated duodenal pH value. One way to ensure the peptide and other additives reach the epithelial surface at the same time for a more effective absorption is to formulate as liquid-filled or semi-solid oily dispersions (e.g. Chiasma Pharmaceutical, Israel). Some patents also disclose stability and oral bioavailability of peptides in solution formats with polyprotic alcohols (Novo-Nordisk, Denmark). Another strategy involves inclusion of a disintegrant that facilitates more rapid dissolution of the peptide and enhancers (e.g. Peptelligence™ technology, Unigene Laboratories, USA).

3.2.2 Enzyme inhibitors and pH modifiers

Enzyme inhibitors protect peptides from luminal degradation by binding to the target enzyme to reduce its activity. Inclusion of an enzyme inhibitor like aprotinin which is effective against trypsin and chemotrypsin, soybean trypsin inhibitor (SBTI), and Bowman-Birk inhibitor which inhibit endopeptidases can improve oral peptide delivery [103]. However, the efficacy of peptidase inhibitors is often limited due to low potency, rapid dilution, digestion, and absorption in the GI tract. On one hand, in a small short-term clinical study, aprotinin was co-administered

with human calcitonin in the colon, and failed to increase the bioavailability of human calcitonin [104]. On the other hand, Liu *et al.* demonstrated that the co-administration of various enzyme inhibitors with insulin improved insulin bioavailability in rats [105]. As high doses are needed to generate an effect, care must be taken with the use of inhibitors in long-term therapy because of their possible toxic effects [106]. Disturbance of the digestion of nutritive proteins and stimulation of protease secretion can be a result of feedback regulation [107]. Acidifying organic acids including citric acid and tartaric acid can also locally modulate the pH away from the optimum value for peptidases. Citric acid inhibits intestinal serine proteases by creating a low pH environment and is used in some oral peptide dosage forms, notably by Enteris Pharma (NJ, USA) [108].

3.2.3 Muco adhesive systems or mucolytics

Bioadhesive drug delivery systems are developed to extend the residence time at a localized site of drug absorption, intensify contact with the mucosa to increase the drug concentration gradient and ensure immediate absorption without dilution or degradation by luminal fluids. Various polymers (polyacrylates, cellulose derivatives, chitosan derivatives) modified with a thiol moiety improved the mucoadhesion by formation of covalent bonds with the cysteine-rich sub-domains of mucus glycoproteins [109]. A significant reduction in the glucose levels of diabetic mice was achieved by oral administration of insulin minitablets based on a thiolated polymer [110]. Thiomatrix GmbH (Austria) developed an enteric-coated dosage forms containing superporous hydrogels composed of thiolated chitosan that improved intestinal residence time by 45-60 min in man [111].

Despite N-acetylcysteine (NAC) having established safety in man, with approval for use in respiratory and abdominal conditions, there is little interest in combining NAC or other mucolytics with other approaches. In part, this relates to high variability in mucous production, the requirement for high concentrations of mucolytics in the formulation, and because disulphide bond reduction can also degrade certain peptides [112]. However, mucolytic enzymes such as papain or bromelain can cleave specific protein substructures within the

mucus gel layer and might be a better option [113]. *In vivo* results obtained by Muller reported that papain-functionalized poly(acrylic acid) nanoparticles (NPs) have an increased capacity to cross the mucus layer, [114]. Other particles decorated with different mucolytic proteases showed a mucus permeation behavior that corelated with *in vivo* results [115]. In another study, negatively charged nanoparticles, such as the silica and silver nanoparticles could better permeate the pores of porcine intestinal mucus with the addition of trehalose [116].

3.3 Novel devices for oral delivery of peptides

Modern advances in electronics and materials has led to a renewed focus on devices for oral drug delivery. They resemble more conventional oral solid dosage forms (e.g capsule) but carry small electronic and/or mechanical elements. Preclinical studies utilizing microneedles capsule, ultrasound, intestinal patches and particulate systems show promise for further increasing oral bioavailability of therapeutic agents [117].

3.3.1 Microneedle capsules

A prototype microneedle capsule for oral delivery of peptide is based on increasing the penetration by piercing the mucosa directly with hollow or solid microneedles [118]. Rani Therapeutics (USA) developed a capsule reported as a “robotic pill” and claimed to have more than 50% bioavailability for insulin in preclinical studies and have completed Phase I studies with an unloaded capsule. A gaseous reaction provides momentum to let the drug coated degradable sugar-based micro-needles penetrate the epithelium. An unrelated recent study by Traverso *et al.* showed that improved insulin bioavailability was obtained compared to the subcutaneous administration with their particular stainless-steel microneedle system in pigs [119].

Abramson *et al.* recently proposed a device, consisting of a self-orientation millimeter-scale applicator (SOMA) for drug delivery in the stomach [120] (Figure 9). Thanks to the tortoise’s shell shape, the device could self-orient its bottom part in contact with the stomach mucosa allowing the injection of the drug into the tissue via a millipost system. In swine, blood glucose

level was similarly decreased with the SOMA-loaded insulin device and s.c injections. The safety aspects of these new technologies are yet to be evaluated.

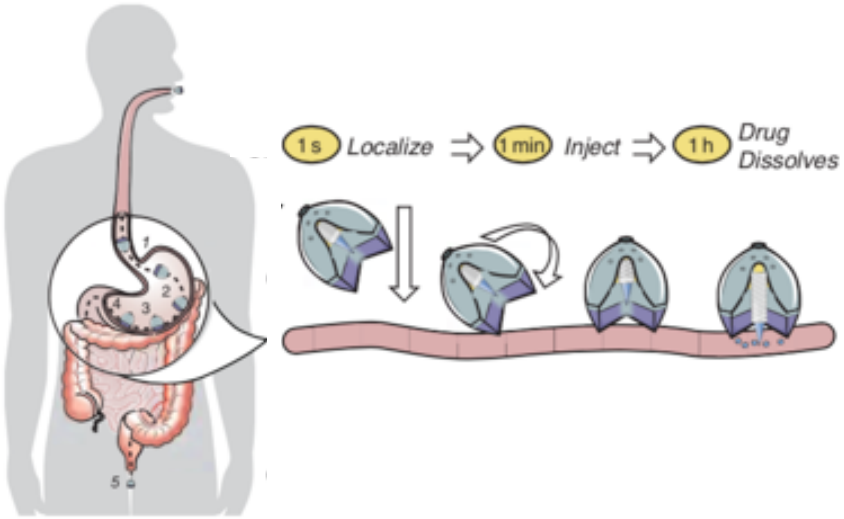

Figure 9: Mechanical API localization and injection for oral gastric delivery of macromolecules based on SOMA device. Adapted with permission from [120].

3.3.2 Ultrasound and Intestinal patch systems

Schoellhammer *et al.* examined the use of one-minute ultrasound treatments localized at low-frequency in porcine GI tissue *ex vivo* and *in vivo* [121]. Penetration of 3- and 70-kD dextran throughout the colonic tissue *ex vivo* was possible with ultrasound application. Intestinal patch systems are based on a unidirectional drug release depot from a microdevice adhered to the intestinal wall [118,122]. Intestinal patch-based devices are being developed for oral delivery of insulin, exenatide, calcitonin, interferon-alpha, erythropoietin and human granulocyte colony-stimulating factor [123]. Gupta *et al.* evaluated mucoadhesive devices for the delivery of exenatide and insulin by placing them in rat jejunum. They obtained a relative bioavailability increase of 13 and 80-fold respectively compared to intestinal injections [124]. Oral delivery of capsules containing micropatches (50 U/kg insulin and 0.2 mg dimethyl palmitoyl ammonion propanesulfonate (PPS) admixed with citric acid (15 mg) decreased plasma glucose in rats by 22% compared to a drop of insulin (1 U/kg, s.c). The main inconvenience is the need for strong binding with the mucus to avoid being washed away by gastric juice or digested food.

3.3.3 Particulate carrier systems

Nanotechnology applied to the oral delivery field could have potential application i.e protecting payload from pre-systemic degradation, targeting epithelial receptors in GI regions and improving permeability [125]. The use of nano-sized delivery vehicles (100-1000 nm) has been investigated for oral delivery of antibiotics, vaccines, cancer therapeutics and biopharmaceuticals [19]. The actual nanocarriers in clinical trials are represented by calcium nanoparticles, silica nanoparticles and liver targeted liposomes for oral delivery of insulin (Table 2). Homayun *et al.* give a comprehensive review of other advanced particulate carriers for oral drug delivery in preclinical studies [126]. A vitamin-B_{12} NP oral delivery system (CobOral, Access Pharmaceuticals, USA) is also in preclinical research with insulin and human growth hormone as payloads. Nanocomplexes of chitosan with anionic polymers (i.e alginate) or peptides (poly-gamma-glutamic acid) have also demonstrated enhanced oral delivery of insulin in animal models [127].

Table 2: Nanocarriers in clinical and preclinical trials for oral delivery of peptides

Company	Product	Strategy	Clinical phase
NOD Pharmaceuticals, Inc (China)	NodlinTM	Np with a calcium phosphate core and PEGylated salts of fatty acids, coated with carbomer and cellulose acetate phthalate	I
Oshadi Drug Administration Ltd. (Israel)	Oshadi Icp	Silica-based Np	II
Diasome Pharma (USA)	HDV-I	Liver-targeted liposomes	III
NanoMega Medical Corp. (USA)	Nanomega's nanoparticulate system	Insulin exendin-4 nanoparticules	Pre-clinical

3.4 Strategies in clinical trials

Major challenges, both physicochemical and physiological, exist for an efficient oral delivery of peptides. Investigators attempted to address pre-systemic degradation and poor permeation in the same formulation. A common approach is to combine peptidase inhibitors with absorption-modifying excipients (AMEs) or chemical PEs. These are usually formulated in

enteric-coated dosage forms [12], although those formulated with salcaprozate sodium (SNAC), the leading candidate PE of the Eligen® technology (Emisphere, NJ, USA), do not seem to require coating. In addition to avoiding degradation by gastric enzymes and low pH, enteric-coated capsules and tablets avoid dilution and premature release of both PE and the macromolecule in the stomach. Furthermore, coatings can assist in promoting co-release of both in high concentrations at the same region to maximize intestinal permeability [128], a formulation goal to maximize payload delivery.

Incorporation of PEs in conventional oral dosage forms is considered a relatively basic technology approach to address macromolecule permeability [129]. The ease with which PEs can be blended with the API using standard pharmaceutical processes makes manufacturing simple, economic and easy to scale. The technology appears to be suitable for a range of dosage forms: tablets and capsules, as well as solutions and suspensions [130]. Without the need for sophisticated and costly formulation, PEs are commercially attractive compared to, for example, nanotechnology [131] and device-based systems [123]. The majority of formulations currently in clinical trials for oral peptides are, therefore, based on PEs, whereas most nanotechnology and device-based systems remain in preclinical research [12]. This scenario may change if PE-based formulations prove efficacious and commercially viable for only very few peptides: highly potent, stable, long-$t_{½}$ molecules of relatively low MW, and with a large therapeutic index (TI).

4. Intestinal Permeation Enhancers

4.1 Overview

One of the simplest approaches to increasing oral bioavailability of peptides is the use of intestinal PEs. They are typically excipients that transiently increase permeability of co-administered payloads across the small intestinal epithelium. Study of absorption promoters began in the 1960s when ethylenediaminetetraacetic acid (EDTA) was shown to increase absorption of heparin in rats and dogs [132]. Since then, numerous compounds proved to be

effective PEs for poorly permeable molecules in *in vitro* and *in vivo* studies [133,134]. A comprehensive analysis of the majority of synthetic chemical PEs from these classes that are used with peptides is available [129] and some of them are summarized in Table 3. Permeation enhancers of natural origin called bioenhancers are summarized by Peterson *et al.* [135].

Fundamentally, drug permeation is promoted either by paracellular PEs via the opening of TJs or transcellular PEs via an increase in plasma membrane permeability (Figure 10). Paracellular PEs can be subcategorized as either 1st generation or 2nd generation [136]. 1st generation comprised the more clinically advanced TJ openers, they act through intracellular signaling mechanisms that modulate the TJs such as EDTA, oleic acid, nitric oxide or C_{10}. The 2nd generation PEs (typically peptides themselves) have been designed to be more targeted with a specific mechanism of action via direct disruption of TJ proteins and have not reached clinical trials yet. They included *zonula occludens* toxin (ZOT), the C-terminal fragment of *Clostridium perfringens enterotoxin* (C-CPE), mellitin, follicle stimulating hormone-fused occludin peptide and claudin peptide (Table 3).

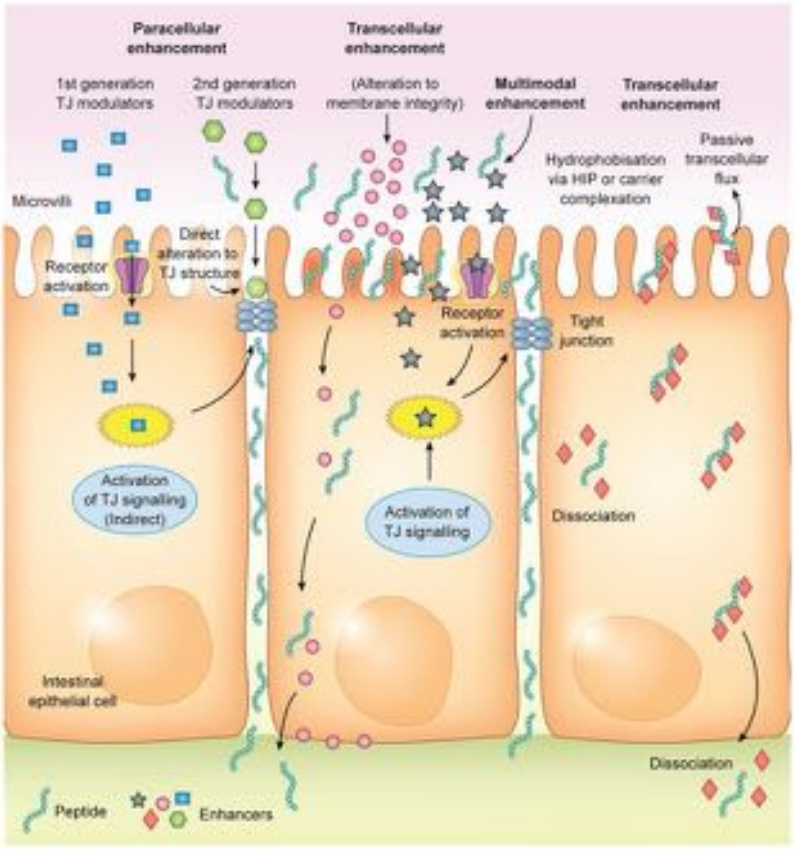

Figure 10: Modes of PE action. From [129] with permission.

Transcellular PEs alter epithelial permeability by two mechanisms (i) reversible perturbation of the epithelial plasma membrane [129] or (ii) physical interaction with the active to improve passive transcellular permeation (hydrophobization via ion-pairing (HIP) [137]. Most surfactant-type PEs alter the natural anatomy of intestinal membrane by increasing intestinal membrane fluidity and modifying the structural integrity of the plasma membrane through a detergent action. This mechanism of action explains why when using PEs, it is important to maintain a balance between increased permeation of the peptide and toxicity. Any effects of the PEs should be local and transient.

Table 3: A summary of intestinal permeation enhancers and their mechanisms of action. Adapted from [129].

Absorption enhancer	**Mechanism of action**		**References**
Fatty acids Medium chain glycerides / C_{10}	Multimodal	PLC, MLCK, Membrane fluidity	[138]
Long chain fatty acid esters Lauroyl carnitine chloride (LCC) / Palmitoyl carnitine chloride (PCC)	Multimodal	Ca^{2+} and ATP levels, Membrane fluidity, Claudin modulation	[139], [140]
Bile salts Sodium taurocholate / Sodium taurodeoxycholate	Multimodal	Membrane fluidity, Tight junction modulation	[141]
Cationic polymers Chitosan salts / N-trimethylated chitosan	Multimodal	Membrane fluidity TJ alteration via PKC	[142]
Toxins and venom extracts Melittin (bee venom extract)	Multimodal	Membrane fluidity	[143]
Zonula occludens toxin (ZOT)	Paracellular	Activation of PKC	[144]
C-terminal fragment of *Clostridium perfringens* enterotoxin (C-CPE)	Paracellular	Claudin modulation	[145]
Chelating agents EDTA, EGTA	Paracellular	Complexation of calcium and magnesium (tight junction opening), PKC activation	[146]
Permeant Inhibitor of Phosphatase (PIP) peptide Peptide 640 / CPI 17	Paracellular	Modulates MLC	[147]
Surfactants Sodium dodecyl sulfate / odium dioctyl sulfosuccinate	Transcellular	Membrane fluidity, Oxidative phosphorylation, ATP depletion	[148]
Cell penetrating peptides Human Immunodeficiency Virus (HIV)-1 Tat protein	Transcellular	Carrier	[149,150]
Polyarginine / Penetratin	Transcellular	Carrier	[151,149]
Transportan (L-penetratin)	Transcellular	Membrane fluidity	[149]
Ionic liquids Choline geranate	Transcellular	Membrane fluidity	[152]

4.2 Considerations for PEs in clinical trials for oral peptide delivery

There are currently over 50 clinical trials in which PEs were shown to increase oral absorption of poorly permeable molecules, mostly achieved using surfactants [106]. PEs that increase permeability across Caco-2 monolayers, isolated intestinal tissue mucosae, and in rodent models may also improve oral BA in humans, but this is not guaranteed since such studies are predominantly based on admixtures with payloads, not oral formulations. Furthermore, scale-up of the final formulation, PE dose, dilution, spreading, and release of both PE and payload during transit in the human GI tract, as well as the influence of enzymes, bile salts, and lipids in human intestinal fluids, must all be taken into account when attempting to make oral BA predictions for humans from preclinical studies. The most widely tested PEs in these trials include Eligen® carriers, MCFAs, acyl carnitines, bile salts, and EDTA [153] (Table 4).

The MCFA, sodium caprate (C_{10}), and the C_8 derivative, salcaprozate sodium (SNAC), are of particular interest as they have had over 20 years of development in proprietary delivery platforms and have been tested in human trials more than any other PEs. C_{10} was originally developed as the main component of an oral solid-dosage form by Elan Pharma (Dublin, Ireland), and then, following licensing, by Merrion Pharmaceuticals (Dublin, Ireland) as GIPET™, Gastro-Intestinal Permeation Enhancement Technology) for oral peptide delivery, and also following licensing from Elan by Ionis Pharmaceuticals (CA, USA) for oral delivery of antisense oligonucleotides. SNAC was developed by Emisphere (NJ, USA) as the lead agent of its Eligen® carrier technology. Novo Nordisk (Bagsværd, Denmark) eventually licensed both GIPET™ and Eligen® in 2012 to assess with their insulin and GLP-1 analogues, ultimately opting to focus on a SNAC tablet formulation with their highly potent, stable, long-$t_{½}$ (160 h) injectable GLP-1 analogue, semaglutide, for advanced clinical development.

Table 4: Examples of technologies included in solid dosage forms in clinical trials for oral systemic delivery of biological drugs adapted from [79] and [154].

Company	Technology	Indication	Drug	Phase	Strategy	ClinicalTrial.gov
Emisphere Technologies, Inc. (USA) with Novo-Nordisk (Denmark)	Eligen® NN9924/OG217SC	Diabetes	Semaglutide	Market	PE: Sodium N-[8-(2-hydroxybenzoyl) Amino] Caprylate (SNAC)	NCT03021187 NCT03015220 NCT02906930 NCT02863419 NCT02849080 NCT02773381 NCT02692716 NCT02607865
	Eligen® with Novo insulin candidate	Diabetes	Insulin	I	PE: N-acylated alpha-amino acid (undisclosed)	NCT00982254
Emisphere Technologies, Inc. (USA) with Nordic Biosciences (Denmark) and Novartis (Switzerland)	Eligen®	Osteoporosis	Salmon calcitonin	III	PE: 8-(N-2-hydroxy-5-chlorobenzoyl)- amino-caprylic acid (5-CNAC)	NCT00525798 NCT00486434 NCT00704847
Unigene/Tarsa Therapeutics (USA)	TBRIA™	Osteoporosis	Salmon calcitonin	III	Bile salts / carnitines / surfactants	NCT01292187
Chiasma, Ltd. (USA)	TPE/ Mycapssa™	Acromegaly	Octreotide	III	PE: Sodium caprate	NCT03252353 NCT02685709 NCT01412424

Oramed Pharmaceuticals, Inc. (Israel)	POD™/ ORMD 0801	Diabetes	Insulin Exenatide	II	PEs: EDTA, bile salts Enzyme inhibitors: soy bean trypsin inhibitor, aprotinin	NCT03467932
Enteris Biopharma, Inc. (USA)	Peptelligence™	Endometriosis	Ovarest (oral leuprolide tablet)	II	PE: Acyl carnitine/ pH modulator, CA/ Peptide with D-stereochemistry resistant to proteases	NCT02807363
		Chronic Kidney Disease associated pruritus, chronic pain	KORSUVA (CR845/difelikefalin)	II		NCT03617536 NCT02524197 NCT02944448
Merrion Pharmaceuticals Ltd. (Ireland) with Novo Nordisk A/S (Denmark)	Insulin 320 (NN1957)	Diabetes	Insulin	I	PE: sodium caprate	NCT02479022
	Insulin 338/ GIPET I/ OI338GT (NN 1953)		Insulin	II	PE: sodium caprate	NCT02470039
	NNC0113-0987 (NN9926) / OI338GT		GLP-1 analogue	I	PE: sodium caprate	NCT02094521
	GIPET/ ACY-7/ MER-104	Prostate cancer, male oral contraception	Acyline	I / II	PE: sodium caprate	NCT00603187
Aegis Therapeutics (USA)	Intravail technology	Diabetes	Leptin	I	PE: Alkyl maltosides	-

4.3 Introducing the permeation enhancer, C_{10}

C_{10} is the sodium salt of capric acid, an aliphatic saturated 10-carbon MCFA (Figure 11). Fatty acids are ubiquitous nutrients liberated in high quantities during digestion of glycerides in the GI tract. They are also present in low mM concentrations in various nutrient sources, including milk. C_{10} is approved as a food additive in both the USA and European Union (EU) and there are no daily limits on consumption; it was recently concluded that its presence in food should have no impact on human health [155].

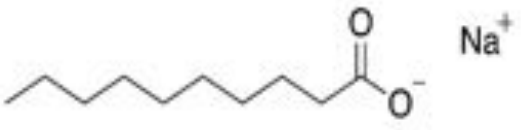

Figure 11: Structure of Sodium caprate

C_{10} is a soluble anionic surfactant, sensitive to changes in pH and ionic strength. The critical micellar concentration (CMC) value of C_{10}, like other ionizable surfactants, varies depending on the medium composition (Table 5). Micelles form at lower concentrations in higher-ionic-strength buffers because the counter-ions in media interact closely with anionic head groups. Thus, varying the ionic strength alters the free monomeric concentration of C_{10} in the small intestine.

Table 5: CMC reported for C_{10} in different buffers from [156].

Buffer	CMC (mM)	Ref
Saline	140	[157]
HEPES with NaCl and KCl	45	[158]
HBSS	28.1	[159]
HBSS with 25 mM HEPES without Ca^{2+}	13	[160]
Water	50	[161]

The capacity of C_{10} to clinically improve intestinal drug absorption was demonstrated in rectal suppositories of ampicillin, for which it gained approval in Sweden (1992) and Japan (1985). Doktacillin™ suppositories were marketed by Astra Pharma (Sweden) and contained ampicillin (250 mg), C_{10} (25 mg) and hard fat (950 mg), (Pharmasol™ B-105, NOF Corp. Japan). The

inclusion of C_{10} in this formulation improved rectal BA of ampicillin in man from 13% to 23% [162]. Doktacillin™ is now part of the portfolio of Meda (Sweden), but it is no longer marketed [162]. It was since assessed in clinical trials by Merrion Pharma as oral solid-dosage forms (GIPET™) for the delivery of a wide range of poorly permeable actives, including selected small molecules (e.g., zoledronic acid, alendronate) and macromolecules (insulin, desmopressin, acyline, and antisense oligonucleotides) [163].

4.4 Introducing the permeation enhancer, SNAC

SNAC is a synthetic *N*-acetylated amino-acid derivative of salicylic acid (Figure 12). It was discovered as part of a screen to identify carrier-based PEs that could “chaperone” poorly permeable payloads across the intestine [164].

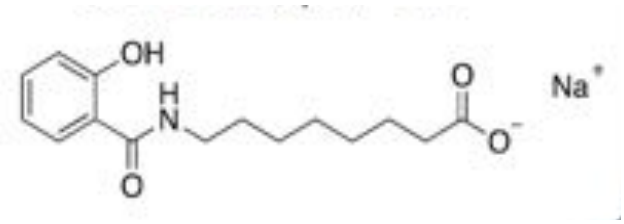

Figure 12: Structure of SNAC

The carrier library of over 1500 compounds was collectively termed Eligen®, and it formed the portfolio of Emisphere Technologies. SNAC is the most extensively tested carrier and the only PE approved in an oral formulation designed to improve oral BA, albeit with a small molecule, cyanocobalamin/SNAC [165]. It is important to note that this oral form of vitamin B_{12} was approved under the regulatory pathway for medical foods, which does not have to meet the same standards required for drug approvals, although the regulatory requirements for medical foods are still higher than those of dietary supplements [166].

Emisphere obtained generally recognized as safe (GRAS) status for SNAC, which enabled the development of cyanocobalamin/SNAC via the medical food regulatory pathway. Having GRAS status for this PE may also have mitigated some of the perceived safety risks associated with the oral semaglutide program at Novo Nordisk. In the 1990s, initial focus on SNAC was aimed at developing an oral formulation of the poorly permeable macromolecule, heparin [167].

In other preclinical studies, it also improved intestinal permeation of peptides (sCT and insulin) [168], along with poorly permeable small molecules (e.g., cromolyn) [169]).

SNAC was tested in many formats: taste-masked liquids, tablets, and soft gelatin capsules. Similar to C_{10}, SNAC can be blended with the active pharmaceutical ingredient (API) using conventional processes, which makes manufacturing uncoated oral tablet dosage forms economic and relatively easy to scale.

4.5 Intestinal absorption-promoting capacity of C_{10} and SNAC

PEs can improve permeability via a combination of mechanisms. Such mechanisms include opening tight junctions to increase paracellular permeability, decreasing mucus viscosity, inhibition of epithelial efflux pumps, complexation/hydrophobization of payload, increasing membrane fluidity, and (indirectly) via peptidase inhibition. The various mechanisms of action of C_{10} and SNAC were previously studied using cell biology and physicochemical techniques including membrane fluorescence, Western blotting, electrophoretic mobility, molecular imaging, and physical analysis. In particular, a concern is that intricate mechanisms determined in *in vitro* assays might not reflect the true mechanism, because the PE concentrations used *in vitro* are typically lower than the efficacious doses used *in vivo.* There is, therefore, uncertainty regarding the actual local concentrations of PE and payload at the small intestinal epithelial wall in a particular region due to variability in dissolution, spreading, and dilution in the human GI lumen during transit.

4.5.1 Mechanism of C_{10} -induced permeability enhancement across intestinal epithelia

The mode of action of C_{10} was studied extensively *in vitro* using different cell-based models. From those studies, Figure 13 is a composite summarizing the possible multiple effects of C_{10} on intestinal epithelia. At low concentrations, increases in permeability of hydrophilic small molecules across Caco-2 monolayers using relatively low concentrations of C_{10} (2.5 mM) can be uncoupled from loss of monolayer integrity, accompanied by reversible reductions in transepithelial electrical potential (TEER) [170,171] indicative of a paracellular mechanism.

The higher concentrations required to alter permeability in isolated rat and human intestinal tissue mucosae in Ussing chambers are associated with transcellular perturbation [172,143, 173]. Mode-of-action studies at higher concentrations (8-13 mM) in Caco-2 monolayers also allude to a paracellular mechanism involving activation of membrane-bound phospholipase C [174,175]. The resulting increase in inositol 1,4,5-triphosphate (IP_3) leads to an increase in intracellular calcium (Ca^{2+}), which in turn activates calmodulin and myosin light-chain kinase (MLCK). This event triggers the contraction of the peri-junctional actomyosin ring (PAMR) [176], permitting increased tight junction (TJ) permeability.

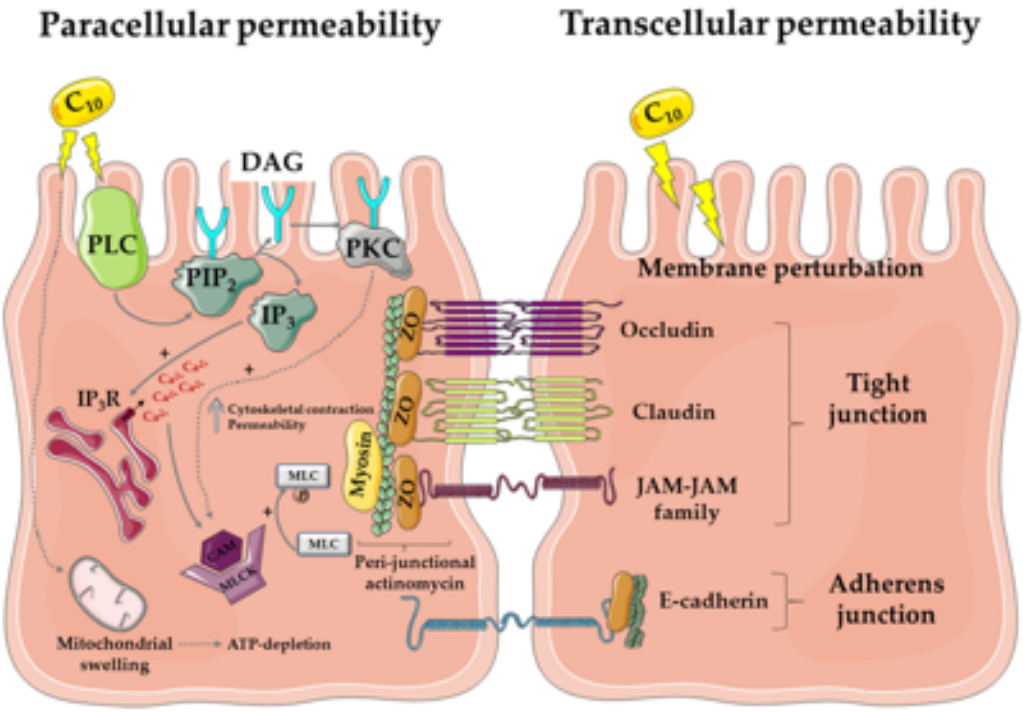

Figure 13: Mode of action of C_{10}. The diagram represents the proposed mechanism of action of C_{10} via paracellular flux (**left**) and transcellular perturbation (**right**) to induce drug permeability across the intestinal mucosa. Abbreviations: PLC: phospholipase C; PIP2: phosphatidylinositol 4,5-bisphosphate; DAG: di-acyl glycerol; PKC: protein kinase C; IP3R: inositol triphosphate receptor; MLC: myosin light chain, CAM: calmodulin; ZO: zonula occludens; JAM: junctional adhesion molecule. Image created using a template from Servier Medical Art under a Creative Commons Attribution License.

Nonetheless, those studies involving pharmacological inhibitors are not definitive proof of a discrete paracellular effect. Impedance spectroscopy in HT29/B6 human intestinal monolayers also indicates that C_{10} acts via a paracellular mechanism; this was associated with removal or redistribution claudin 5 and tricellulin [177]. However, as no assessment of transcellular perturbation was carried out, the data from this study do not provide conclusive evidence for a

paracellular mode in isolation either. Furthermore, several studies indicate that C_{10} also disrupts cell membranes at 8-13 mM. C_{10} also caused Caco-2 cell leakage of intracellular ATP from Caco-2 cells [174], a likely consequence of plasma membrane perturbation. One interpretation is that cells respond to the initial membrane perturbation challenge by C_{10} with compensating intracellular signaling processes involved in mucosal repair, beginning with disbandment of TJs, and concluded by epithelial resealing [178]. Some of the strongest evidence in favor of a mechanism driven primarily by perturbation, however, comes from high content image analysis in live Caco-2 cells. C_{10} (2.5mM) increased intracellular Ca^{2+} in Caco-2 cells prior to the plasma membrane permeability changes detected at 8.5 mM [171]. C_{10} (8.5–13 mM) altered both plasma and mitochondrial membrane integrity, indicative of perturbation; importantly, these were the minimum concentrations that were also needed to induce a permeability increase. The elucidation of the primary mode of action as membrane perturbation was clarified by the capacity of C_{10} to preferentially displace claudins 4 and 5 from lipid rafts in MDCK cells, consistent with surfactant properties [179].

Other evidence comes from a recent surfactant screen using isolated rat intestinal mucosae in Ussing chambers, where C_{10} caused a concentration-dependent increase in epithelial histology damage [180]. Given the close association between permeation enhancement and mucosal perturbation in tissue and animal models, it was, therefore, not surprising that the cytoprotectant prostaglandin analogue, misoprostol, prevented both the C_{10}-induced increase in flux of hydrophilic markers across Caco-2 monolayers and cell damage [181]. From these arguments, it is likely that the high concentrations of C_{10} used in tablets also cause a degree of mild reversible mucosal perturbation in vivo, not unlike that seen with aspirin, alcohol, and spicy foods [182]. In a study of a human rectal formulation of ampicillin with C_{10}, there was evidence of mild and reversible mucosal perturbation [170], although the data were confounded by the hyper-osmolarity of the formulation. While it is not possible to conclude that mucosal perturbation of the relatively static rectal mucosal compartment extrapolates directly to the small intestine where transit is relatively fast, it is likely that C_{10} causes mild and

reversible regional perturbation within a short period at the high concentrations exposed to the small intestinal epithelium prior to its almost complete absorption within minutes.

4.5.2 Mechanism of SNAC-induced permeability enhancement across intestinal epithelia

A different mode of action to that of C_{10} was proposed to explain how SNAC improves intestinal permeability. In the 1990s, Emisphere proposed that SNAC improves passive transcellular permeation via associating with drug molecule to create a transportable lipophilic complex via hydrophobization. The hypothesis was that dipole–dipole non-covalent interaction between the carrier and structural moieties of the payload caused a conformational change in the latter, leading to exposure of hydrophobic regions that favor transcellular permeation (Figure 14). Also, because of the weak association, carrier and drug dissociate by simple dilution on entering the blood circulation.

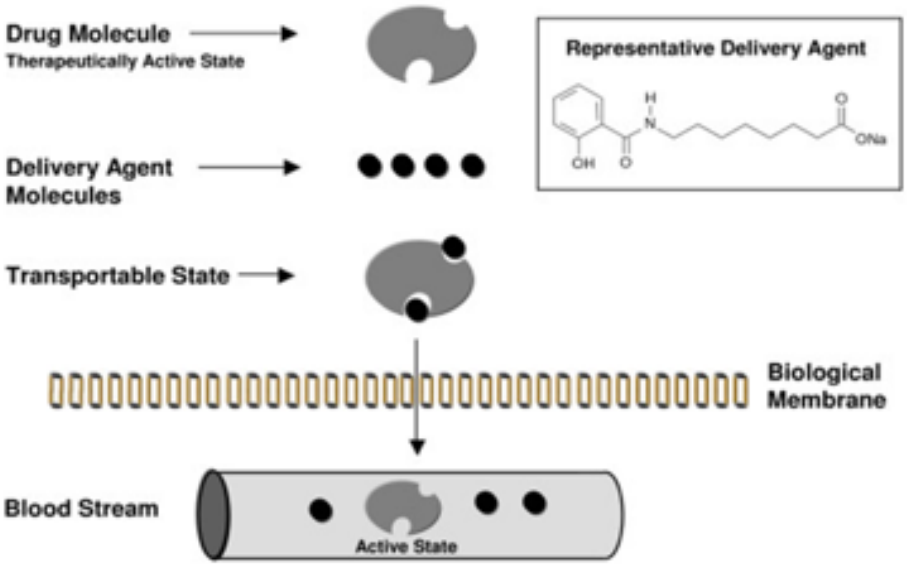

Figure 14: Schematic of Eligen® -delivery technology mechanism in intestinal epithelia, as advocated by Emisphere in 2006. Reproduced from [183] under the terms of the Creative Commons Attribution License.

The interaction between SNAC and heparin [167] and with insulin [184] was, therefore, thought to be based on increased lipophilicity through hydrogen bonding and/or hydrophobic interactions, permitting dissolution of the complex in lipid bilayers. In support of this hypothesis, SNAC at a concentration of 17 mg/ml improved the permeation of insulin, but not that of

radiolabeled mannitol across Caco-2 monolayers, suggesting that the effect was neither related to opening tight junctions nor to a decline in barrier integrity, and this interpretation was supported by confocal microscopy [184].

Higher concentrations of SNAC (50 mg/ml) more reflective of concentrations *in vivo*, however, caused complete loss of TEER and a 36-fold increase in [^{3}H]-mannitol permeability in Caco-2 monolayers [185], data that do not permit definitive conclusions to be made regarding mechanism since such high concentrations also compromised the Caco-2 model. In isolated rat jejunal mucosae mounted in Ussing chambers, SNAC (33-66 mM) boosted the flux of a polar marker molecule, 6-carboxy-fluorescein (6-CF), but not that of [^{3}H]-mannitol across the epithelium and without reducing TEER values [186]. The authors argued that SNAC was indeed exploiting a transcellular pathway and not TJs to allow permeation of the hydrophilic polar ionized molecule (6-CF) and, somewhat controversially, they suggested that SNAC was reducing the charge on CF, thereby improving the capacity to partition in the epithelium. Similar to the Caco-2 study [185], when SNAC was added to jejunal mucosae at a concentration of 165 mM, TEER dropped and the permeability coefficient (P_{app}) of [^{3}H]-mannitol was increased [186], denoting a compromising event.

Other Caco-2 studies also support a transcellular mechanism; Malkov *et al.* [187] detected intracellular signal increases ascribed to fluorescently labeled heparin and in the presence of SNAC, whereas immunohistochemistry data indicated that there were no changes of F-actin or the actinomycin ring during heparin flux. Ding *et al.* [188] used Isothermal Titration Calorimetry (ITC) and Fourier-transform infrared (FTIR) spectroscopy to study the interaction between cromolyn and SNAC, and concluded that the aromatic ring of SNAC inserted between those of cromolyn via its 2-hydroxybenzamide motif, leading to an increase in hydrophobicity of the complex and a reduction in cromolyn hydration. Lactate hydrogenase release (LDH) measurements indicated that the increased cromolyn fluxes across Caco-2 monolayers in the presence of SNAC were not associated with cell damage.

Recently, Novo Nordisk suggested a new mechanism of action for SNAC in its non-enteric coated tablet of the GLP-1 analogue, semaglutide ($t_{½}$ = 160 h). Using a ligated dog model, they found that systemic delivery was achieved solely from stomach administration of the tablet [189]. The theory is that after digestion, the tablet erodes rapidly in the stomach releasing SNAC at high concentration that transiently increase the pH of gastric fluid and inactivate pepsin. It is claimed that semaglutide is protected against pepsin by SNAC and that solubility is increased, resulting in an increased concentration-dependent flux of semaglutide across the gastric mucosa, using a transcellular mechanism as the tablet comes in intimate contact with the epithelium. Figure 15 is a composite of the possible effects that SNAC has in the stomach when formulated with semaglutide.

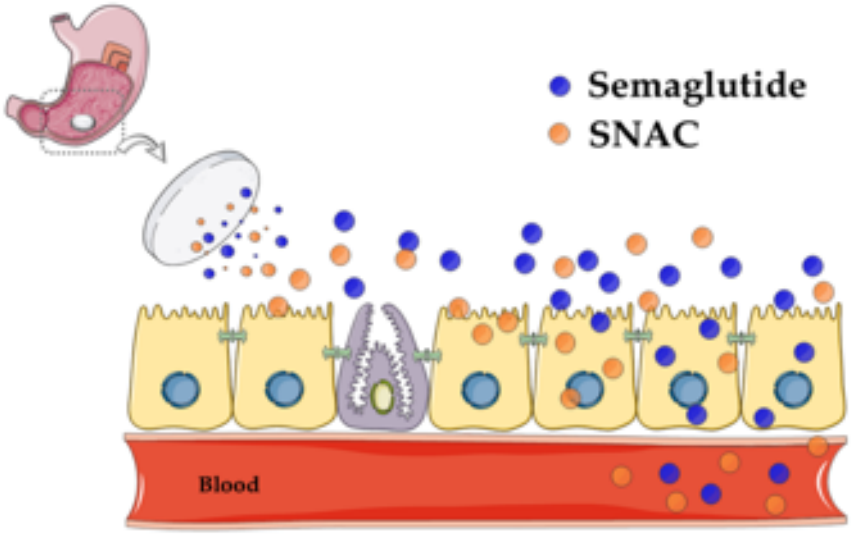

Figure 15: Theory of oral semaglutide absorption across the gastric epithelium of the stomach as advocated by Novo Nordisk. Modified with permission from Reference [189]. Blue circles = semaglutide; orange circles = SNAC. Image made using a template from Servier Medical Art under a Creative Commons Attribution License.

By shifting the emphasis toward elevation in stomach pH away from conformational changes and increased lipophilicity, the theory takes the focus away from membrane perturbation. Moreover, the authors argue that this mechanism is highly specific for semaglutide, in that similar studies with admixtures of SNAC and another GLP-1 analogue, liraglutide led to no flux increase across human gastric epithelial cell cultured monolayers [189]. Part of the role of SNAC seemed to be to convert semaglutide to a more permeable monomeric form and it seems to perform this better when formulated in a stomach-specific tablet.

4.6 C_{10} and SNAC in oral macromolecule formulations in clinical trials

4.6.1 Oral delivery of antisense oligonucleotide using C_{10}

The other arm of the original Elan licensing of C_{10}-based matrix tablets in the late 1990s continued in parallel with respect to antisense oligonucleotides. The gene medicine speciality Pharma, Ionis Pharmaceuticals (Carlsbad, CA, USA) (formerly Isis Pharma) developed a number of oral antisense oligonucleotide formulations containing C_{10} for clinical testing against RNA targets. One candidate that progressed to Phase I was ISIS 104838, a tumor necrosis factor (TNF)-α inhibitor. Oral administration of a C_{10}-based tablet to dogs resulted in average absolute oral BA of 1.4% [190]. Tissue histology of the small intestine and large intestine of the dogs indicated no changes following once-daily dosing of tablets containing ~1 g of C_{10} over seven consecutive days. A subsequent Phase I trial examined ISIS 104838 (100 or 140 mg) formulated with C_{10} (660 mg) in immediate-release mini-tablets packaged in enteric-coated gelatin capsules, with or without a second mini-tablet containing only C_{10}. The second group of mini-tablets was coated with different layers of Eudragit® RS30D to allow for subsequent further release of the C_{10} following erosion of the first tablet containing ISIS 104838 [191]. The goal was to create a greater window for absorption by prolonging the time C_{10} was in contact with the epithelium, given that it is rapidly absorbed with a T_{max} of 7 min. All formulations together from this study yielded an average oral BA of 9.5% relative to s.c. injection, with the formulation designed for additional immediate release of C_{10} giving a value of 12%; however, the intra-subject variability ranged from 2–28% [191].

4.6.2 GIPET™, oral formulations of peptide with C_{10}

GIPET™ (Merrion Pharmaceuticals, Dublin) is a solid oral dose technology that has advanced to clinical testing as enteric-coated tablets containing C_{10} with both peptide and small-molecule payloads [182]. Human studies using radiolabeled PEG revealed that the permeating enhancement effects of GIPET™ were transient and reversible in <1 h [163]. GIPET™ was tested in a range of doses with several poorly absorbed molecules in a total of 16 Phase I studies comprising over 300 subjects [163]. Overall, while oral BA values of >5% were cited

for some molecules, the most notable feature was the massive intra-subject variability across all studies, constituting an issue for safety and efficacy.

4.6.2.1 GIPET™: Low molecular-weight heparin

Pharmacokinetics analysis of human trials for GIPET™ formulations with low-molecular-weight heparin (LMWH) have been described [163]. LMWH–GIPET™ was formulated in tablets containing either 45,000 or 90,000 IU of LMWH at two dose levels of C_{10}. Oral BA was calculated relative to the standard sub-cutaneous dose of 3200 IU following administration to 14–16 subjects. Relative oral BA of 3.9–7.6% was achieved [163]. With a high dose of LMWH combined with a high dose of C_{10}, increased levels of an anti-clotting biomarker were seen in all subjects; the responses were sustained and had a similar time course to the s.c. route. This particular formulation however was not progressed clinically (Table 5).

4.6.2.2 GIPET™: Desmopressin

When desmopressin was formulated with GIPET™ and administered orally to 18 human subjects, a bioavailability of 2.4% relative to the s.c. route was detected [163], an improvement over the typical 0.2% value for Minirin® tablets. Again, this formulation was not progressed further. The GIPET™ technology was well tolerated even when repeatedly administered in these small Phase I studies [163].

4.6.2.3 GIPET™: Acyline

Other clinical trial examples include the gonadotropin-releasing hormone (GnRH) antagonist decapeptide, acyline. In a Phase I study of oral acyline, serum luteinizing hormone (LH), follicle-stimulating hormone (FSH), and testosterone were suppressed within 12 h at the 10-, 20-, and 40-mg single doses tested. However, sustained serum levels of acyline could not be detected, and there was no PK–Pharmacodynamic (PD) relationship [192].

4.6.2.4 GIPET™: Zoledronic acid

GIPET™ was also used to orally-deliver the bisphosphonate, zoledronic acid. The rationale was that an oral tablet (Orazol™) administered weekly by patients could compete with a

monthly infusion of Zometa® in a hospital setting for cancer patients with bone metastasis. In a Phase I study, urinary excretion of unchanged zoledronic acid suggested equivalent delivery via both routes [193].

4.6.2.5 GIPET™: Long-acting basal insulin and GLP-1 analogues

The licensing of GIPET™ to Novo Nordisk led to Phase I trials with respect to a proprietary insulin, NN1953, and a GLP-1 analogue; however, the resulting data were never published and, ultimately, Merrion was liquidated in 2016. Novo Nordisk in turn decided to move away from developing oral insulin to concentrate on its oral GLP-1 analogue program. Nonetheless, an important Phase II trial assessing a once-daily long-acting basal insulin (I338) with a t½ of 70 h in a GIPET™ formulation was published in 2019 [194]. In this study, a relative oral F of the daily tablet of I338 containing 550 mg of C_{10} versus the long-acting s.c.-administered insulin glargine (Lantus®, Sanofi, Paris) of 1.5–2.0% was achieved without evidence of toxicity over eight weeks. Although similar plasma glucose reduction was achieved by the oral GIPET™-based formulation to the s.c. insulin, the rationale for discontinuation was that the dose of I338 was not commercially viable. Another clinical trial explored the food effect on oral insulin 338 [195]. A 65% reduction in insulin 338 exposure was seen with immediate food ingestion after dosing and C_{10} C_{max} was slightly higher suggesting that food can increase capric acid absorption from the GI tract. However, the absorption of oral insulin 338 was not affected by food intake from 30 min after dosing. A Phase I study was published in 2018 by Biocon (India) in which a C_{10}-based formulation of their alkylated PEGylated fast-acting meal-time insulin (IN-105; Insulin Tregopil) was shown to have no effect on the PK of oral metformin in fasted conditions and it was well tolerated [196]. Therefore, C_{10} continues to be used in oral peptide formulations both in clinical trials and as a comparator for other PEs in preclinical studies. Table 6 summarizes the clinical data reported for a range of poorly permeable molecules with C_{10}.

Table 6: Summary of data from selected studies in humans reported for a range of poorly permeable molecules formulated with sodium caprate (C_{10}).

Description	Treatment	Outcome	Reference
Ampicillin with C_{10} in healthy subjects (n = 12).	Rectal suppository containing 250 mg of ampicillin and 25 mg of C_{10}.	C_{max} increased 2.6-fold compared to ampicillin alone and BA increased 1.8-fold. Some local tissue damage not ascribed to C_{10}.	[162]
Phenoxymethylpenicillin, antipyrine with C_{10} in healthy subjects (n = 6).	Rectal perfusion containing 2 g of phenoxymethylpenicillin, 8 mg of antipyrine, and 0.7 g of C_{10}. Two treatments (T), T1: pH 6 and T2: pH 7.4. Each subject received control (no C_{10}) and treatment.	C_{10} was ineffective at increasing permeability across rectal epithelium.	[197]
GIPET™: oral acyline in healthy subjects (n = 8).	3 oral tablet doses of acyline: 10, 20, and 40 mg. Subjects received all doses, 1 week apart, under fasting conditions.	Significant reduction in LH, FSH, and testosterone. No serious treatment related adverse effects.	[192]
GIPET: oral acyline in healthy subjects (n=4) ACY-7, MER-104	Oral tablet of 20 mg acyline daily for one week to determine the steady-state pharmacokinetics	Phase I / II	NCT00603187
GIPET™: oral zoledronic acid in prostate cancer patients with bone metastasis (n = 30).	Once-weekly enteric-coated Orazol™ tablets containing 20 mg of zoledronic acid versus weekly Zometa® (4 mg) i.v. infusion over 49 days.	Equivalent urine output biomarkers; claim of 5% bioavailability (BA) in patent.	[193]

GIPET™: Basal insulin in C_{10} formulation versus insulin glargine in Type 2 diabetics (s.c.) (n = 25).	Daily tablets of a long-acting insulin (I338) over 8 weeks.	1.5–2.0% bioavailability compared to s.c. Comparable reductions in plasma glucose.	[194]
Insulin tregopil (IN-105) in C_{10} tablets in healthy subjects.	Single treatments of insulin along with metformin over 4 periods of 2 days.	No effects on the pharmacokinetics (PK) of metformin; good safety.	[196]
Insulin 320 (NN1957) in C_{10} tablets in healthy subjects (n=84)	Single oral insulin 320 with 7 escalating dose levels vs insulin glargine (s.c)	-	NCT02479022
Antisense oligonucleotide with C_{10} (ISIS 104838) in healthy subjects (n = 15).	Enteric-coated tablets, four formulations, and one after a high-fat meal. Subjects received all treatments.	9.5% bioavailability compared to s.c. No study-related adverse effects.	[191]

LH, luteinizing hormone; FSH, follicle-stimulating hormone; s.c., sub-cutaneous; i.v., intravenous. The Phase II study [55] is the most comprehensive of these studies

4.6.3 Eligen carrier technology in clinical trials

In relation to other payloads and Eligen® carriers, an Eligen® formulation of insulin was assessed in a 2010 trial in 14 Type 2 diabetics where the carrier was monosodium *N*-(4-chlorosalicyloyl)-4-aminobutyrate (4-CNAB). An oral BA of 7 ± 4% was achieved from a 300-IU dose (with 200–400 mg of 4-CNAB) versus an s.c. dose of 15 IU in fasting subjects [198]. Such large variability would not be acceptable for this low-TI peptide. Another Eligen® carrier, 8-(*N*-2-hydroxy-5-chloro-benzoyl)-amino-caprylic acid (5-CNAC), was also evaluated by Novartis (Switzerland) and Nordic Biosciences (Herlev, Denmark) in three large Phase III trials for oral sCT: two for osteoarthritis [199] (NCT00486434 and NCT00704847) and one for osteoporosis [200] (NCT00525798). The dosing to several thousand patients across the three trials comprised one tablet (0.8 mg sCT with 200 mg of 5-CNAC) in a tablet administered twice a day with 50 mL of water approximately 30 min ahead of meals. These studies lasted 24 months for the osteoarthritis trials and 36 months for the osteoporosis trial. Although these trials missed their primary efficacy endpoints, interesting assessments concerning dosing formats and regimes were published with conclusions that may have relevance for future SNAC trials [201]. Differences in sCT absorption and effects on bone biomarkers occurred depending on the volume of water, proximity to a meal, and the time of day (reflecting circadian rhythms in bone turnover).

SNAC has been in a succession of clinical trials in oral formulations with poorly permeable actives since the late 1990s, culminating with approval for cyanocobalamin as a medical food for vitamin B_{12}-deficient anemic subjects in 2014 and recent approval for oral semaglutide by the FDA in September 2019 [166] [165]. Many clinical trials have been completed with oral semaglutide prior to FD4 approval for the treatment of T2D. The following is a brief overview of clinical trial data available to date.

4.6.3.1 First clinical trial with LMW heparin

The initial clinical trials were carried out using unfractionated heparin in 1998 [202]. In the first Phase I study, 2.25 g taste-masked SNAC was combined with 30,000–150,000 IU heparin and

administered to subjects via gavage; the formulation achieved increases in outputs associated with anti-coagulation efficacy: activated partial thromboplastin time and production of anti-factor Xa. This led to subsequent Phase I and II trials with taste-masked 10–15-mL liquid formulations in patients undergoing total hip replacements; oral heparin was dosed at either 60,000 or 90,000 IU with 1.5 or 2.25 g of SNAC respectively, and results were compared to s.c. administration of 5000 IU of heparin [203]. The oral dosing regimen comprised 12–16 doses over a four-day period after surgery. Data from the second Phase I study showed that the oral heparin liquid formulation induced anti-factor Xa activity similar to s.c. heparin. In the Phase II trial, major bleeding events were similar between oral and s.c. heparin groups, thereby offering encouragement on the safety front.

In 2002, the oral liquid heparin formulation ultimately missed its primary efficacy end-point in a Phase III trial (PROTECT) comparing oral heparin (either 60,000 IU/1.5 g SNAC or 90,000 IU/2.25 g SNAC three times a day) to s.c. LMWH (enoxaparin) over a 30-day period with assessment for deep vein thrombosis as the read-out. The study comprised over 2000 patients undergoing elective hip replacement, a study that was associated with poor compliance due to the bitter taste of the solution [183]. Direct leveraging from a taste-masked drink to a solid dosage form was not possible, due to the high quantities of SNAC and heparin. Subsequently, a new Phase I PK–PD study was eventually carried out in 2007 in 16 subjects receiving a 75,000 IU heparin/500 mg SNAC total dose in soft gel capsules [204]. It confirmed the effect on aPTT and the orally delivered heparin had a C_{max} of 58 min. Ultimately, a solid dose formulation of oral heparin/SNAC never reached Phase III and was abandoned, perhaps in part because of the advantages of LMWH over unfractionated heparin, as well as the advent of alternative oral anti-thrombotics. Table 7 summarizes the clinical trial performance of oral SNAC and related Emisphere carrier formulations across a range of poorly permeable molecules.

Tableau 7: Summary of data from selected studies in humans reported for a range of poorly permeable molecules formulated with Eligen carriers. T2D-type 2 diabetes; sCT—salmon calcitonin.

Description	Treatment	Outcome	Reference
Vitamin B_{12} with SNAC in tablets in healthy subjects (n = 20). Medical food clinical study.	(A) Two tablets, each with 5 mg of vitamin B_{12} with 100 mg of SNAC (B) One tablet: 5 mg of vitamin B_{12} with 100 mg of SNAC (C) One commercial tablet: 5 mg of vitamin B_{12} (D) 1 mg of vitamin B_{12} via i.v. injection.	Treatment (B) achieved 3% higher absolute BA compared to the commercial oral formulation. No adverse effects.	[165]
Heparin with SNAC in hip replacement patients, (n = 123). Phase II.	Two studies: one dose every 8 h (max 16 doses), and two doses every 8 h (max 12 doses).	Achieved anti-factor Xa activity comparable to s.c. heparin. No change in major bleeding events compared to s.c.	[203]
Insulin with 4-CNAB in untreated T2D (n = 10). Phase II.	300 mg of insulin with 400 mg of 4-CNAB, or 15 IU of insulin s.c. Performed under fasting conditions.	C_{max} was higher and was reached faster compared to s.c. Shorter duration and high subject variability. No adverse effects.	[198]
sCT with 5-CNAC in osteoarthritic patients over 24 months (n = 1176 and n = 1030). Phase III.	0.8 mg of sCT in tablets twice daily for 24 months.	No significant effect compared to placebo.	[201]
sCT with 5-CNAC in postmenopausal women with osteoporosis (n = 4665). Phase III.	0.8 mg or placebo in tablets daily, together with vitamin D and calcium for 36 months.	No beneficial effect on fractures was observed. No change in quality of life.	[12]

4.6.3.2 Oral delivery of semaglutide with SNAC: Phase III

Recent focus has shifted entirely to the clinical development of an oral semaglutide/SNAC tablet by Novo Nordisk and selected oral semaglutide clinical data are summarized in Table 8. Once-daily oral semaglutide with 300 mg of SNAC resulted in improved glycemic control and greater reductions in body weight than placebo in a 26-week Phase II dose-escalation study in doses ranging from 2.5–40 mg of semaglutide per day in over 600 patients with T2D [205]. Daily oral administration of semaglutide (20 mg and 40 mg) with SNAC lowered glycated hemoglobin (HbA1c) by over 1.4% and these data were comparable with that seen with weekly s.c. administration of semaglutide (1 mg). For oral semaglutide with SNAC, the oral BA is likely to be ~1%, although the focus of the publications was on the PD effect and biomarkers. Clues come from Beagle dog studies where tablets containing 300 mg of SNAC with 5–20 mg of semaglutide gave oral BA values of 1.22 ± 0.25% following oral administration [189,206]. Novo Nordisk completed ten Phase IIIa PIONEER (Peptide Innovation for Early Diabetes Treatment) trials in 2018 for oral semaglutide.

PIONEER 1 compared the efficacy and safety of oral semaglutide as monotherapy with placebo in patients with T2D managed by diet and exercise alone. Top-line data from PIONEER 1 achieved significance with respect to a reduction in HbA1c of 1.5% with a 14-mg semaglutide dose in T2D, along with evidence of some weight loss [207]. Recent PIONEER 5 trials also revealed that renal impairment did not affect PK parameters of 5 mg and 10 mg of semaglutide formulated with 300 mg of SNAC over a short time frame in diabetics [208]. This design was repeated in diabetic patients with hepatic impairment with the same outcome in that PK values were not altered and, therefore, no dose adjustment was needed in these patients [209]. The question of the impact of proton pump inhibitor, omeprazole, on PK was also assessed, as elevation of bulk stomach pH might have confounded the purported mechanism of SNAC. Using a 5-mg semaglutide dose in patients taking 40 mg of omeprazole over a 10-day period with a follow-up period out to 21 days, overall PK values for both semaglutide and SNAC were unchanged, leading to a conclusion that dose adjustment would

be also unnecessary in patients on concomitant omeprazole [210]. The implications of these findings would support the determination that the pH increase created by SNAC in the stomach must be at the semaglutide tablet surface [189] and does not impact bulk stomach pH; otherwise, a large effect of omeprazole on PK would have been expected. In another study, oral semaglutide (20 mg/day) or SNAC alone (300 mg) did not appear to alter the exposure of lisinopril, warfarin or digoxin [211].

Several PIONEER Phase III trials (PIONEER 2, 3, 4) compared oral semaglutide with established glucose-lowering drugs i.e empaglifozin sitagliptin, and liraglutide, respectively. At week 52, all patients receiving oral semaglutide experienced a significant reduction in HbA1c and body weight. The impact of a flexible dose adjustment of oral semaglutide was also investigated with sitagliptin in patients with uncontrolled T2D. The slower titration of the dose improved tolerability, weight reduction and HbA1c reduction.

The PIONEER 6 Phase III study enrolled diabetics with cardiovascular disease in order to examine oral semaglutide PK and PD in this cohort to see if the daily 14-mg formulation increases cardiovascular (CV) risk [212]. The results show that death from CV causes occurred in 0.9% of the oral semaglutide group and 1.9% of the placebo group. In all the PIONEER studies, oral semaglutide was well tolerated with the most common adverse event being mild to moderate nausea which diminished over time and was attributed to known effects of s.c.-administered GLP analogues. PIONEER 9 and 10 enrolled Japanese participants with T2D to meet regulatory requirements in Japan. It will be interesting to examine patient compliance with the current rather inconvenient dosing regime, especially in post-marketing studies if oral semaglutide is approved, since the daily tablet must be taken at least 30 min before meals in the morning in order to avoid food interference with formulation performance.

Table 8: Selected PIONEER Phase III data from the daily semaglutide/SNAC oral tablet formulation in T2D patients. Adapted from [213].

Description	Parameters	Comment	Reference
Oral semaglutide in healthy subjects taking omeprazole (n = 54)	5 mg for 5 days, followed by 10 mg for 5 days ± 40 mg omeprazole.	AUC and stomach pH slightly higher in semaglutide/omeprazole group, but no need to change dose regime.	[210] (NCT02249871)
Phase II dose-ranging 26-week study in patients (n = 632)	0.7-1.9% reduction in glycated hemoglobin (HbA1c); some BW reduction; mild gastro-intestinal (GI) side effects common.	The key trial which supported moving to Phase III.	[205] NCT01923181)
PIONEER 1 26-week study, n = 703 Oral semaglutide (3, 7 or 14 mg/day) vs PBO	Mean 1.5% reduction in HbA1c confirmed with 14-mg dose; 4.1-kg BW reduction; mild–moderate nausea in 16% versus 6% in PBO.	14 mg established as semaglutide dose with 300 mg of SNAC in all studies.	[207] (NCT02906930)
PIONEER 2 52-week study, n=821 Oral semaglutide (14 mg/day) vs empagliflozin (25 mg/day)	Semaglutide: 1.4% in HbA1c reduction, 4.2 kg BW reduction Empaglifozin: 0.9% in HbA1c reduction, 3.8 kg BW reduction	14 mg semaglutide betters 25 mg empagliflozin for the reduction of HbA1c in patients with T2D uncontrolled on metformin.	[214] (NCT02863328)
PIONEER 3 78-week study, n=1 864 Oral semaglutide (14 mg/day) vs sitagliptin (100 mg/day)	Semaglutide: 1.3% in HbA1c reduction, 3.5 kg BW reduction Sitagliptin: 0.8% in HbA1c reduction, 1.1 kg BW reduction	14 mg semaglutide achieved better HbA1c and BW reduction compared to sitagliptin	[215] (NCT02607865)

PIONEER 4 52-week study, n=711 Oral semaglutide (14 mg/day) vs s.c liraglutide (1.8 mg/day) vs PBO	Semaglutide: 1.2% in HbA1c reduction, 5.0 kg BW reduction Liraglutide: 0.9% in HbA1c reduction, 3.1 kg BW reduction PBO: 0.2% increase in HbA1c, 1.2 kg BW reduction	Oral semaglutide has significant reduction in BW and HbA1c compared to liraglutide and PBO with T2D patients uncontrolled on metformin	[216] (NCT02863419)
PIONEER 5 26-week study, n = 324 Oral semaglutide (14 mg/day) vs PBO in renal-impaired patients	5 mg of semaglutide for 5 days; 10 mg for 5 days, assessed up to 21 days after; no change in PK overall.	Area under curve (AUC) and half-life ($t_{½}$) similar to regular T2D patients, no need to change dose regime. eGFR unchanged in both groups	[208], [217] (NCT02827708)
Oral semaglutide in hepatic-impaired patients (n = 56)	Design as for PIONEER-5.	AUC, C_{max}, and $t_{½}$ unchanged, no need to change in dose regime.	[209] (NCT02016911)
PIONEER 6 n = 3 183 Oral semaglutide (14 mg/day) vs PBO and cardiovascular (CV) outcomes in T2D patients	Primary endpoints: reduction in major CV events over median 16-month period.	Cardiovascular outcomes not different from PBO, but suggestion of a mortality benefit of oral tablet.	[212] (NCT02692716)
PIONEER 7 52-week study, n=504 Oral semaglutide flexible dose (3,7 or 14 mg/d) adjustement vs sitagliptin (100 mg/d)	Semaglutide: HbA1c reduction1.4% and BW loss 2.9 kg Sitagliptin: HbA1c reduction 0.7%, BW loss 0.9 kg	Flexible approach of oral semaglutide has superior HbA1c and BW reduction compared to sitagliptin	[218] (NCT02849080)

PIONEER 8 26-week study, n=731 Oral semaglutide (3,7 or 14 mg/d) vs PBO in insulin-treated patients	Semaglutide: HbA1c reduction1.4% with 14mg/d and BW loss 3.3 kg	Insulin dose reduction was greater with semaglutide than with placebo	[219] (NCT03021187)
PIONEER 9 52-week study, N=243 Oral semaglutide vs PBO or liraglutide Japanese T2D patients	Oral semaglutide daily (3, 7 and 14 mg) versus PBO or liraglutide (0.9 mg s.c)	Significant reduction in HbA1c for all dose compared to PBO or liraglutide	[220] (NCT03018028)
PIONEER-10 57-week study, N=458 Oral semaglutide vs dulaglutide Japanese T2D patients	Oral semaglutide daily 3, 7 or 14 mg versus dulaglutide (0.75 mg s.c) weekly	Significant reduction in HbA1c and body weight for all dose compared to dulaglutide	[221] (NCT03015220)

BW= body weight, eGFR=estimated glomerular filtration rate, PBO=placebo, HbA1c=glycated hemoglobin A1C

4.7 Safety of SNAC and C_{10} in preclinical and clinical studies

4.7.1 Reports from preclinical studies

In terms of preclinical safety data, the experience for both molecules is extensive. Numerous studies reveal little toxicity of high doses of C_{10} in rats, dogs, and pigs following oral administration alone and in combination with payloads [156,163]. In a study of the acute effects of a C_{10}-based dosage form (Orasense™) in Beagles, Raoof *et al.* provided evidence of the safety of oral hydroxypropyl methyl cellulose-coated C_{10}/antisense tablets [190]. Several hundred milligrams of C_{10} were used in each tablet and dogs received treatment three times per day for seven days. Clinical chemistry and blood biochemistry parameters were normal; the dogs tolerated the formulation and there was normal weight gain. Canine intestinal issues were also adjudged normal following macroscopic examination *post mortem*. Five separate canine daily tolerance studies revealed encouraging safety data for selected components of the GIPET I and II technology [182]. Similar studies were also carried out on intra-intestinal catheterized pigs where C_{10} was formulated with antisense oligonucleotides at doses up to 100 mg/kg of the MCFA; it was well tolerated following multiple doses and with little evidence of intestinal epithelial damage, *post mortem* [222].

For SNAC, Riley *et al.* carried out a sub-chronic oral toxicity test of SNAC in rats and found a no observed adverse effect (NOAEL) level of 1 g/kg/day in rats for up to 13 weeks; it was only a massive dose of 2 g/kg/day that eventually caused significant mortality [223]. It was also examined for gestational toxicity in pregnant rats at oral doses up to 1 g/kg/day where slight weight loss was seen; there was no effect on growth of pups, but some evidence of a small increase in the still-birth rate was noted [224]. Some GI effects including emesis and diarrhea were observed in studies involving monkeys at a SNAC dose of ≥1.8 g/kg/day [225]. SNAC ultimately achieved provisional GRAS status as a food additive. The safety data from clinical and preclinical studies, therefore, raised no red flags for either agent in oral dosage forms at high concentrations with a wide range of actives tested to date. An important safety consideration is the high inter-subject variability typically associated with the low oral bioavailability values for low TI payloads tested with both PEs to date.

4.7.2 Reports from clinical trials

Although C_{10} was previously marketed in a rectal product, this has only a limited relevance to the safety of an orally delivered tablet formulation, similar to the approval of a SNAC/vitamin-B_{12} medical food product. Nonetheless, the clinical trial experience with both PEs in hundreds of subjects over more than 20 years indicated that few subjects experienced side-effects that caused drop out from trials. The majority of reports were related to mild GI effects including

nausea and diarrhea for GIPET™ [163,182] and SNAC [205]. The prescribing information for oral semaglutide notes that the most common side effects with use include nausea, abdominal pain, diarrhea, decreased appetite, vomiting and constipation [226]. The Phase II trial with the insulin 338 tablet with 550 mg C_{10} also provided extensive toxicity data in 25 subjects administered daily doses over a timeframe of 8 weeks [194,195]. There is no direct evidence, even from studies with a duration as long as six months, that stomach or duodenal ulcers are caused by these PEs, nor that pathogens can gain entry across a compromised intestinal epithelium. Still, post-marketing surveillance will provide more safety data in the context of daily administration over several years for SNAC with vitamin B_{12} and also with semaglutide.

4.7.3 Evaluation of epithelial damage and recovery after PE exposure

It is clear that surfactant-based PEs cause a mild degree of reversible perturbation of the intestinal mucosa. The small intestinal epithelium is entirely renewed every 72 h [227]; there is a high rate of cellular turnover and the intestine has a high capacity to replace cells, due to migrating stem cells from the intestinal crypt. There is also a reserve of stem cells that are dormant until epithelial injury occurs, at which point they are recruited to assist with restoration [228]. The capacity of the intestinal mucosa to repair is also associated with secretion of mucus, prostaglandins, and bicarbonate [225]. For a comprehensive review of repair and restoration of the intestinal barrier, see Blikslager *et al.* [178]. The capacity for epithelial repair following C_{10} exposure was investigated in rat jejunal instillations, where full restitution was seen within 60 min of exposure [229]. These data were similar to that seen in rat models with other PEs including bile salts [230] and sodium dodecyl sulfate (SDS) [231]. Since C_{10} and SNAC are rapidly and completely absorbed, one interpretation is that, following local and transient mucosal perturbation leading to a transient increase in permeability, the epithelium recovers due to gradual absorption and dilution of the PE.

Although naturally, the concentrations of bile salts and mixed micelles found in the duodenum and jejunum can lead to mucosal damage, yet repair is the typical outcome [232]. Rapid mucosal repair and regeneration are therefore normal physiological processes and hence the mucosal perturbation caused by dietary substances, endogenous secretions and absorption promoters can normally be tolerated. Reversibility studies performed with C_{10} in humans using the lactulose:mannitol urinary excretion ratio (LMER) assay showed that, following intra-jejunal administration to human subjects, the enhancer only increased permeability in a 20-min window [182]. It seems that dilution, spreading, and rapid intestinal absorption of both C_{10} and SNAC prevent prolonged exposure *in vivo.*

4.7.4 Evaluation of microbiome changes after PE exposure

Another concern over routine use of PEs is based on their potential capacity to promote microbiome changes and absorption of microorganisms, antigens, and toxins leading to local inflammation, autoimmune disease, and sepsis [233]. Surfactants may impair the protective mucus layer, facilitating the diffusion of luminal bacteria to the intestinal epithelium and ultimately disturbing the host microbiota [234]. In a recent controversial study which generated much debate, evidence was provided that the approved excipient emulsifiers, polysorbate-80 and carboxymethyl cellulose, disturb microbiota composition and induce obesity in mice [235]. Whether these data have any true significance for humans is not known at this point, but it is clear that intestinal microbiome research is going to become more relevant in toxicology profiling of oral formulations, not just those associated with peptides.

4.7.5 Evaluation of bystander molecules after PE exposure

A second concern that is continually raised is the potential increase in permeability of bystander molecules arising from tissue damage induced by PEs [19,236]. Taking into account the precise conditions required for permeation enhancement (high concentrations of payload and PE contemporaneously at the intestinal epithelium), as well as the marked difference in the MW of candidate payloads (3-10 kDa) with a molecular radii of 10-20 Ä compared to that of typical bacteria, viruses, and bacterial lipopolysaccharide (LPS) (>100 kDa), this concern may be overstated. Nonetheless, clinical pharmacology data from binge-drinking human subjects suggests that alcohol can permit absorption of endotoxins and can promote elevation of type 1 cytokines in plasma, akin to a low-grade infection [237]; thus, together with the study of relevant microbiome changes, more research is needed to filter the true toxicological risks of orally delivered PEs following chronic exposure.

4.7.6 Anti-microbial potential of C_{10}

Several studies describe an anti-microbial effect of C_{10} at high concentrations. Cox *et al.* demonstrated the bactericidal property of C_{10} against *Salmonella typhimurium,* and it also prevented its attachment to rat intestinal epithelia [238]. Moreover, there was no evidence from the same study that C_{10} promoted permeation of this gut pathogen across isolated rat intestinal mucosa. At low mM concentrations, C_{10} is also bactericidal against *Helicobacter pylori [86]*. In a screen of 13 bacterial isolates, C_{10} inhibited growth and biofilm formation at concentrations that are used to promote absorption in cell cultures and *in vivo* models (unpublished data, Rawlinson L. and Brayden D.J.).

In an *in vivo* study with chickens, incorporation of C_{10} in feed at a level of 3 g/kg protected them from colonization by *Salmonella enterica* [239]. Finally, capric acid has antifungal activities on *Microsporium gypsum* mycelia and spores *in vitro* [240]. These data are consistent with the

well-known anti-microbial actions of MCFAs [241]. Although, to our knowledge, similar data are not reported for SNAC, it would be surprising if, upon examining its structure, it did not have similar anti-microbial actions.

5. A head to head comparison between SNAC and C_{10}

5.1 Conclusions from clinical trials

The ideal intestinal permeation enhancer should be carefully studied from many different aspects including safety, effectiveness and stability in the GI tract, and the kinetics of intestinal absorption of the promoter itself. In comparing the safety and efficacy of C_{10} and SNAC as PEs in preclinical and clinical studies, examination of 20–30 years of literature would suggest that several of the key parameters are similar. Both can permit oral bioavailability of a range of macromolecular payloads of up to 5%, with mean values closer to ~1%. The SNAC clinical PK data with semaglutide seem to be on a par with previous performance, for example, with sCT; however, it is due to its formulation with a potent peptide with a long $t_{½}$ and high TI that is of particular interest. It is the long $t_{½}$ that can compensate for large intra-subject variability [189]. Aspects that tip the balance to SNAC compared to C_{10} include the following: broader clinical experience and an approved vitamin B_{12} product, more extensive toxicology studies and GRAS status, and the lack of requirement for protection against stomach acid. Finally, the main argument advanced for oral peptide delivery is improved convenience over needles leading to better compliance. Patients will, however, be required to wait 30 min before eating and drinking after taking tablets of semaglutide/SNAC each morning; thus, patients will ultimately decide if this is an inconvenience preferable to a once-a-week injection of semaglutide, assuming similar pricing.

5.2 Outstanding aspects in researching C_{10} and SNAC

5.2.1 Lack of mechanistic data for SNAC

The *in vitro* studies on the mechanism of action of the two agents on cultured intestinal epithelia suggest some common surfactant-based features as described in Section 4.5.

First, C_{10} and SNAC are weak acids that display amphiphilicity and surface activity. However, there is a structural difference between them since the structure of SNAC relates to a salicylic-acid moiety, while C_{10} comprises only 12 carbons MCFA without additional aromatic ring. As a consequence, there is a greater distribution of hydrophilic functional groups in the salicylamide region of SNAC, as evident from its higher polar surface area (89.5 $Å^2$) compared to C_{10} (40.1 $Å^2$) [242,243]. It follows that the hydrophobic region of SNAC should be less efficient at inserting into phospholipid membranes than C_{10} [171]. A non-specific

detergent/surfactant effects on the epithelium should be expected. This may be one of the reasons why higher concentrations of SNAC than C_{10} are needed to improve permeation.

Second, the theory in the 1990s claimed that SNAC is a chaperone system that increase transcellular flux of multiple payloads via hydrophobization of the payload through non-covalent linkages. There are a number of anomalies concerning the original chaperone transcellular mechanism proposed for SNAC with multiple payloads [183]. If Eligen® carriers acted solely using dipole–dipole interactions via hydrophobization (and not an electrostatic interaction), it would be difficult to envisage a significant increase in passive permeation since the retention of ionized functional groups would impede passive movement across phospholipid bilayers. SNAC forms a conjugate base at the pH of the small intestinal lumen, so it can undergo complexation via hydrophobic ion pairing (HIP) with the conjugate acid of basic amino-acid side chains in macromolecules. However, HIP cannot fully account for Eligen®-mediated hydrophobization of anionic payloads including heparin and cromolyn [169]. An alternative interpretation arises from another SNAC study with cromolyn; SNAC increased Caco-2 epithelial cell membrane fluidity as measured by fluorescence anisotropy, consistent with a surfactant-induced membrane perturbation effect, whereas in this study there was no increase in cromolyn's lipophilicity [244]. Still, the overall contribution of transcellular perturbation to the increased flux is not clear since the presence of hydrophilic functional groups in the salicylamide region of SNAC gives rise to inefficient micelle formation (CMC: 56 mM in phosphate-buffered saline (PBS)) [244], and this will not favor membrane insertion. In summary, evidence from Caco-2 studies is not yet convincing enough to solely ascribe an exclusive transcellular mechanism for SNAC. On the other hand, there are some differences between the mechanism of action of SNAC and those of PEs with mechanisms associated with tight-junction openings (e.g., EDTA). Also, the new mechanism suggested for SNAC arising from ligated dog studies argues for a local increase in stomach pH around semaglutide, a mechanism that appears to be specific for this molecule. So, how is SNAC working with other payloads and in which part of the GI?

Thirdly, a transcellular mechanism should account for epithelial endocytosis uptake pathways (e.g., via clathrin- or caveolae-mediated pathways or macropinocytosis), where a template to follow is in place for the other group of transcellular permeability-enhancing agents, the cell-penetrating peptides [245].

5.2.2 Lack of interactions studies between payload and SNAC or C_{10}

There is a lack of understanding of the physicochemical aspects of how C_{10} interacts with mixed micelles in the small intestine in the fasted and fed states and if C_{10} interacts with the

payloads. Above its CMC of 25 mM in physiological buffer [171], C_{10} forms micelles and there is a distinct ratio of monomer to micellar-bound material, as highlighted in a recent study on alkyl maltosides [246]. In simulated intestinal buffers, it is uncertain whether the payload is incorporated into or adsorbs onto colloidal structures (e.g., mixed micelles, vesicles, lipid droplets), or whether it admixes with the C_{10} monomer. There is resulting confusion over which format the payload permeates. The consensus, however, is that dissolved monomeric fatty acids perturb the enterocyte membrane whereas mixed micelles are not absorbed *per se*.

It remains unclear if the high concentrations of SNAC required to improve small intestinal epithelial permeation relate to tight junction openings, membrane perturbation, membrane fluidization or payload solubility changes. As explained in Section 4.4, the thermodynamic considerations with respect to the non-covalent linkage between SNAC and payload during epithelial flux are yet to be addressed. There is little data to directly support the chaperone hypothesis with no calculations of the affinity of SNAC to payloads to support this conclusion. With advanced biophysical methods, it is possible to obtain affinity binding to decipher the interaction between SNAC and payloads. It is likely that much of the discrepancy surrounding the mechanism of SNAC will be resolved. Is this payload-specific and region-specific theory entirely compatible with the previous data from small intestinal studies in which SNAC was paired with many payloads of differing structures?

5.2.3 Lack of uniform assays to determine permeation enhancement capacity

As explained in section 4.5, mechanistic studies for C_{10} and SNAC deals with a variety of testing systems with *in vitro/ ex situ* and *in vivo* models. However, caution must be taken in making definitive conclusions on whether a TJ modulation mechanism is or is not present using those assays. The epithelial TEER values yield information on monolayer integrity as a first indication but reveal no direct information about tight junctions. Not every decrease in TEER leads to a higher apparent permeation coefficient for a drug and it is not a direct proof of a paracellular mode of action. Also, in the literature, the evaluation of permeation enhancement for SNAC and C_{10} is based on different markers such as mannitol, inulin, polyethylene glycol or FITC-dextran. First, with comparable TEER values, P_{app} (permeability coefficient) depends on the marker used resulting in a general problem with the comparability of results obtained when using different markers [247]. Second, another concern is the capacity of a fluorescently labeled payloads to remain intact during flux, this stability needs to be assessed. Third, the selected cell lines or tissue can impact significatively the Papp values obtained for certain tracers as the expression of barrier properties is different reflected by a large range of TEER values [248]. In conclusion, many of the studies are not comparable with one another due to a variety of markers, use of different cell lines, and tissue model bioassays.

A combination of experiments is usually required to make mechanistic assessments for an enhancer (i.e immunostaining, voltage clamping, fluorescence microscopy, permeability studies). However, these techniques are often used inconsistently across laboratories and mechanistic analysis tends to be incomplete. Only one experiment such as immunostaining is not conclusive enough to discriminate the route of action of a PE. Indeed, the absence of changes in tight-junction-associated antibody imaging for associated proteins is not definitive. Similarly, cytotoxicity assays based on mitochondrial enzymes may not represent the first sign of membrane perturbation and need to be combine with techniques that directly evaluate membrane perturbation.

6. Thesis aims

The overall aims of this thesis were to:

1. Investigate the interaction between SNAC or C_{10} with a model peptide, exenatide, in a range of media from simple to complex buffers with advanced biophysical methods **(Chapter II)**

2. Assess the cytotoxicity *in vitro* of C_{10} and SNAC by determining the epithelial cellular response after exposure to the PEs using conventional cytotoxicity assays and high content analysis **(Chapter III)**

3. Establish the intestinal transport routes of paracellular markers using Caco-2 monolayers when exposed to SNAC and C_{10} as well as effects on selected TJ protein distribution **(Chapter III)**

4. Investigate permeation enhancement of paracellular markers by SNAC and C_{10} across isolated rat stomach, jejunal and colonic mucosae mounted in Ussing chambers and non-everted gut sacs **(Chapter IV)**

5. Assess the morphological changes in tissue and mucus via histological sampling following administration of SNAC and C_{10} in rat intestinal mucosae in Ussing chambers, non-everted gut sacs, and *in vivo* rat intestinal instillations (**Chapter IV).**

References

1. Fosgerau, K. and T. Hoffmann, Peptide therapeutics: current status and future directions. Drug Discov Today, 2015. 20(1): p. 122-8.
2. Usmani, S.S., et al., THPdb: Database of FDA-approved peptide and protein therapeutics. PLoS One, 2017. 12(7): p. e0181748.
3. Guerci, B., et al., Lack of Treatment Persistence and Treatment Nonadherence as Barriers to Glycaemic Control in Patients with Type 2 Diabetes. Diabetes Therapy, 2019. 10(2): p. 437-449.
4. Lakkireddy, H.R., et al., Oral delivery of diabetes peptides - Comparing standard formulations incorporating functional excipients and nanotechnologies in the translational context. Adv Drug Deliv Rev, 2016. 106(Pt B): p. 196-222.
5. Benet, L.Z., et al., The use of BDDCS in classifying the permeability of marketed drugs. Pharm Res, 2008. 25(3): p. 483-8.
6. Rasalam, R., et al., GLP-1 Receptor Agonists for Type 2 Diabetes and Their Role in Primary Care: An Australian Perspective. Diabetes Ther, 2019. **10**(4): p. 1205-1217.
7. Sharma, D., et al., Recent updates on GLP-1 agonists: Current advancements & challenges. Biomed Pharmacother, 2018. **108**: p. 952-962.
8. Cowan Report Therapeutic Categories Outlook: Comprehensive Study. 2014.
9. Abramson, A., et al., Quantifying the Value of Orally Delivered Biologic Therapies: A Cost-Effectiveness Analysis of Oral Semaglutide. J Pharm Sci, 2019. **108**(9): p. 3138-3145.
10. Lipska, K.J., et al., Trends in Drug Utilization, Glycemic Control, and Rates of Severe Hypoglycemia, 2006–2013. Diabetes Care, 2017. **40**(4): p. 468.
11. Lewis, A.L. and J. Richard, Challenges in the delivery of peptide drugs: an industry perspective. Ther Deliv, 2015. **6**(2): p. 149-63.
12. Aguirre, T.A., et al., Current status of selected oral peptide technologies in advanced preclinical development and in clinical trials. Adv Drug Deliv Rev, 2016. **106**(Pt B): p. 223-241.
13. Richard, J., Challenges in oral peptide delivery: lessons learnt from the clinic and future prospects. Ther Deliv, 2017. **8**(8): p. 663-684.
14. O'Driscoll, C.M., et al., Oral delivery of non-viral nucleic acid-based therapeutics - do we have the guts for this? European Journal of Pharmaceutical Sciences, 2019. **133**: p. 190-204.
15. Amidon, G.L., et al., A theoretical basis for a biopharmaceutic drug classification: the correlation of in vitro drug product dissolution and in vivo bioavailability. Pharm Res, 1995. **12**(3): p. 413-20.
16. Larregieu, C.A. and L.Z. Benet, Distinguishing between the permeability relationships with absorption and metabolism to improve BCS and BDDCS predictions in early drug discovery. Mol Pharm, 2014. **11**(4): p. 1335-44.
17. Smart, A.L., S. Gaisford, and A.W. Basit, Oral peptide and protein delivery: intestinal obstacles and commercial prospects. Expert Opin Drug Deliv, 2014. **11**(8): p. 1323-35.
18. Renukuntla, J., et al., Approaches for enhancing oral bioavailability of peptides and proteins. Int J Pharm, 2013. **447**(1-2): p. 75-93.
19. Choonara, B.F., et al., A review of advanced oral drug delivery technologies facilitating the protection and absorption of protein and peptide molecules. Biotechnol Adv, 2014. **32**(7): p. 1269-1282.
20. Muheem, A., et al., A review on the strategies for oral delivery of proteins and peptides and their clinical perspectives. Saudi Pharmaceutical Journal, 2016. **24**(4): p. 413-428.
21. Fuhrmann, G. and J.C. Leroux, Improving the stability and activity of oral therapeutic enzymes-recent advances and perspectives. Pharm Res, 2014. **31**(5): p. 1099-105.
22. Wang, J., et al., Toward oral delivery of biopharmaceuticals: an assessment of the gastrointestinal stability of 17 peptide drugs. Mol Pharm, 2015. **12**(3): p. 966-73.

23. Moroz, E., S. Matoori, and J.C. Leroux, Oral delivery of macromolecular drugs: Where we are after almost 100years of attempts. Adv Drug Deliv Rev, 2016. **101**: p. 108-121.
24. Abuhelwa, A.Y., et al., Food, gastrointestinal pH, and models of oral drug absorption. European Journal of Pharmaceutics and Biopharmaceutics, 2017. **112**: p. 234-248.
25. Dressman, J.B., et al., Upper gastrointestinal (GI) pH in young, healthy men and women. Pharm Res, 1990. **7**(7): p. 756-61.
26. Russell, T.L., et al., Upper gastrointestinal pH in seventy-nine healthy, elderly, North American men and women. Pharm Res, 1993. **10**(2): p. 187-96.
27. Youngberg, C.A., et al., Comparison of gastrointestinal pH in cystic fibrosis and healthy subjects. Dig Dis Sci, 1987. **32**(5): p. 472-80.
28. Ensign, L.M., R. Cone, and J. Hanes, Oral drug delivery with polymeric nanoparticles: the gastrointestinal mucus barriers. Adv Drug Deliv Rev, 2012. **64**(6): p. 557-70.
29. Taherali, F., F. Varum, and A.W. Basit, A slippery slope: On the origin, role and physiology of mucus. Adv Drug Deliv Rev, 2018. **124**: p. 16-33.
30. Pearson, J.P., P.I. Chater, and M.D. Wilcox, The properties of the mucus barrier, a unique gel--how can nanoparticles cross it? Ther Deliv, 2016. **7**(4): p. 229-44.
31. Dahlgren, D., et al., The effects of three absorption-modifying critical excipients on the in vivo intestinal absorption of six model compounds in rats and dogs. Int J Pharm, 2018. **547**(1-2): p. 158-168.
32. Johansson, M.E., J.M. Larsson, and G.C. Hansson, The two mucus layers of colon are organized by the MUC2 mucin, whereas the outer layer is a legislator of host-microbial interactions. Proc Natl Acad Sci U S A, 2011. **108 Suppl 1**: p. 4659-65.
33. Boegh, M. and H.M. Nielsen, Mucus as a barrier to drug delivery - understanding and mimicking the barrier properties. Basic Clin Pharmacol Toxicol, 2015. **116**(3): p. 179-86.
34. Cone, R.A., Barrier properties of mucus. Adv Drug Deliv Rev, 2009. **61**(2): p. 75-85.
35. Johansson, M.E., H. Sjovall, and G.C. Hansson, The gastrointestinal mucus system in health and disease. Nat Rev Gastroenterol Hepatol, 2013. **10**(6): p. 352-61.
36. Falavigna, M., et al., Mucus-PVPA (mucus Phospholipid Vesicle-based Permeation Assay): An artificial permeability tool for drug screening and formulation development. Int J Pharm, 2018. **537**(1-2): p. 213-222.
37. Varum, F.J., et al., Mucoadhesion and the gastrointestinal tract. Crit Rev Ther Drug Carrier Syst, 2008. **25**(3): p. 207-58.
38. Hatton, G.B., et al., Animal Farm: Considerations in Animal Gastrointestinal Physiology and Relevance to Drug Delivery in Humans. Journal of Pharmaceutical Sciences, 2015. **104**(9): p. 2747-2776.
39. Netsomboon, K. and A. Bernkop-Schnurch, Mucoadhesive vs. mucopenetrating particulate drug delivery. Eur J Pharm Biopharm, 2016. **98**: p. 76-89.
40. Griesser, J., et al., Self-emulsifying peptide drug delivery systems: How to make them highly mucus permeating. Int J Pharm, 2018. **538**(1-2): p. 159-166.
41. Yun, Y., Y.W. Cho, and K. Park, Nanoparticles for oral delivery: targeted nanoparticles with peptidic ligands for oral protein delivery. Adv Drug Deliv Rev, 2013. **65**(6): p. 822-32.
42. Fabiano, A., Y. Zambito, and A. Bernkop-Schnürch, About the impact of water movement on the permeation behaviour of nanoparticles in mucus. International Journal of Pharmaceutics, 2017. **517**(1): p. 279-285.
43. Boegh, M., et al., Steric and interactive barrier properties of intestinal mucus elucidated by particle diffusion and peptide permeation. Eur J Pharm Biopharm, 2015. **95**(Pt A): p. 136-43.
44. Abreu, M.T., Toll-like receptor signalling in the intestinal epithelium: how bacterial recognition shapes intestinal function. Nature Reviews Immunology, 2010. **10**: p. 131.

45. Bennett, K.M., S.L. Walker, and D.D. Lo, Epithelial microvilli establish an electrostatic barrier to microbial adhesion. Infect Immun, 2014. **82**(7): p. 2860-71.
46. Veiseh, O., et al., Managing diabetes with nanomedicine: challenges and opportunities. Nat Rev Drug Discov, 2015. **14**(1): p. 45-57.
47. Freeman, H.J., Clinical relevance of intestinal peptide uptake. World J Gastrointest Pharmacol Ther, 2015. **6**(2): p. 22-7.
48. Peters, S.A., et al., Predicting Drug Extraction in the Human Gut Wall: Assessing Contributions from Drug Metabolizing Enzymes and Transporter Proteins using Preclinical Models. Clin Pharmacokinet, 2016. **55**(6): p. 673-96.
49. Drozdzik, M., et al., Protein abundance of clinically relevant multidrug transporters along the entire length of the human intestine. Mol Pharm, 2014. **11**(10): p. 3547-55.
50. Li, M., et al., The consequence of regional gradients of P-gp and CYP3A4 for drug-drug interactions by P-gp inhibitors and the P-gp/CYP3A4 interplay in the human intestine ex vivo. Toxicol In Vitro, 2017. **40**: p. 26-33.
51. Benet, L.Z., The drug transporter-metabolism alliance: uncovering and defining the interplay. Mol Pharm, 2009. **6**(6): p. 1631-43.
52. Mahato, R.I., et al., Emerging trends in oral delivery of peptide and protein drugs. Crit Rev Ther Drug Carrier Syst, 2003. **20**(2-3): p. 153-214.
53. Ekins, S., et al., Application of three-dimensional quantitative structure-activity relationships of P-glycoprotein inhibitors and substrates. Mol Pharmacol, 2002. **61**(5): p. 974-81.
54. Shin, K., V.C. Fogg, and B. Margolis, Tight junctions and cell polarity. Annu Rev Cell Dev Biol, 2006. **22**: p. 207-35.
55. Matter, K. and M.S. Balda, Functional analysis of tight junctions. Methods, 2003. **30**(3): p. 228-34.
56. Powell, D.W., Barrier function of epithelia. Am J Physiol, 1981. **241**(4): p. G275-88.
57. Takenaka, T., et al., Human small intestinal epithelial cells differentiated from adult intestinal stem cells as a novel system for predicting oral drug absorption in humans. Drug Metab Dispos, 2014. **42**(11): p. 1947-54.
58. Lu, Z., et al., Claudins in intestines: Distribution and functional significance in health and diseases. Tissue Barriers, 2013. **1**(3): p. e24978.
59. Clarke, L.L., A guide to Ussing chamber studies of mouse intestine. Am J Physiol Gastrointest Liver Physiol, 2009. **296**(6): p. G1151-66.
60. Tomita, M., et al., Enhancement of Colonic Drug Absorption by the Paracellular Permeation Route. Pharmaceutical Research, 1988. **5**(6): p. 341-346.
61. Snoeck, V., B. Goddeeris, and E. Cox, The role of enterocytes in the intestinal barrier function and antigen uptake. Microbes Infect, 2005. **7**(7-8): p. 997-1004.
62. Zihni, C., et al., Tight junctions: from simple barriers to multifunctional molecular gates. Nat Rev Mol Cell Biol, 2016. **17**(9): p. 564-80.
63. Niessen, C.M., Tight junctions/adherens junctions: basic structure and function. J Invest Dermatol, 2007. **127**(11): p. 2525-32.
64. Feldman, G.J., J.M. Mullin, and M.P. Ryan, Occludin: structure, function and regulation. Adv Drug Deliv Rev, 2005. **57**(6): p. 883-917.
65. Saitou, M., et al., Complex phenotype of mice lacking occludin, a component of tight junction strands. Mol Biol Cell, 2000. **11**(12): p. 4131-42.
66. Schulzke, J.D., et al., Epithelial transport and barrier function in occludin-deficient mice. Biochim Biophys Acta, 2005. **1669**(1): p. 34-42.
67. Al-Sadi, R., et al., Occludin regulates macromolecule flux across the intestinal epithelial tight junction barrier. Am J Physiol Gastrointest Liver Physiol, 2011. **300**(6): p. G1054-64.
68. Gonzalez-Mariscal, L., et al., Tight junction proteins. Prog Biophys Mol Biol, 2003. **81**(1): p. 1-44.

69. Barmeyer, C., J.D. Schulzke, and M. Fromm, Claudin-related intestinal diseases. Semin Cell Dev Biol, 2015. **42**: p. 30-8.
70. Furuse, M., et al., Claudin-based tight junctions are crucial for the mammalian epidermal barrier: a lesson from claudin-1-deficient mice. J Cell Biol, 2002. **156**(6): p. 1099-111.
71. Rosenthal, R., et al., Claudin-2-mediated cation and water transport share a common pore. Acta Physiol (Oxf), 2017. **219**(2): p. 521-536.
72. Landy, J., et al., Tight junctions in inflammatory bowel diseases and inflammatory bowel disease associated colorectal cancer. World J Gastroenterol, 2016. **22**(11): p. 3117-26.
73. Hu, C.-A.A., et al., Autophagy and tight junction proteins in the intestine and intestinal diseases. Animal Nutrition, 2015. **1**(3): p. 123-127.
74. Turner, J.R., et al., The role of molecular remodeling in differential regulation of tight junction permeability. Semin Cell Dev Biol, 2014. **36**: p. 204-12.
75. Amasheh, S., et al., Claudin-2 expression induces cation-selective channels in tight junctions of epithelial cells. J Cell Sci, 2002. **115**(Pt 24): p. 4969-76.
76. Van Itallie, C.M. and J.M. Anderson, Architecture of tight junctions and principles of molecular composition. Semin Cell Dev Biol, 2014. **36**: p. 157-65.
77. Lee, S.H., Intestinal permeability regulation by tight junction: implication on inflammatory bowel diseases. Intest Res, 2015. **13**(1): p. 11-8.
78. Lin, L., et al., SLC transporters as therapeutic targets: emerging opportunities. Nat Rev Drug Discov, 2015. **14**(8): p. 543-60.
79. Han, Y., et al., Multifunctional oral delivery systems for enhanced bioavailability of therapeutic peptides/proteins. Acta Pharmaceutica Sinica B, 2019.
80. Craik, D.J., et al., The future of peptide-based drugs. Chem Biol Drug Des, 2013. **81**(1): p. 136-47.
81. Vlieghe, P., et al., Synthetic therapeutic peptides: science and market. Drug Discov Today, 2010. **15**(1-2): p. 40-56.
82. Nielsen, D.S., et al., Orally Absorbed Cyclic Peptides. Chem Rev, 2017. **117**(12): p. 8094-8128.
83. Pisal, D.S., M.P. Kosloski, and S.V. Balu-Iyer, Delivery of therapeutic proteins. J Pharm Sci, 2010. **99**(6): p. 2557-75.
84. Dozier, J.K. and M.D. Distefano, Site-Specific PEGylation of Therapeutic Proteins. International journal of molecular sciences, 2015. **16**(10): p. 25831-25864.
85. Ryan, S.M., et al., Conjugation of salmon calcitonin to a combed-shaped end functionalized poly(poly(ethylene glycol) methyl ether methacrylate) yields a bioactive stable conjugate. J Control Release, 2009. **135**(1): p. 51-9.
86. Clement, S., et al., Oral modified insulin (HIM2) in patients with type 1 diabetes mellitus: results from a phase I/II clinical trial. Metabolism, 2004. **53**(1): p. 54-8.
87. Khedkar, A., et al., A dose range finding study of novel oral insulin (IN-105) under fed conditions in type 2 diabetes mellitus subjects. Diabetes Obes Metab, 2010. **12**(8): p. 659-64.
88. Youn, Y.S., et al., Improved intestinal delivery of salmon calcitonin by Lys18-amine specific PEGylation: stability, permeability, pharmacokinetic behavior and in vivo hypocalcemic efficacy. J Control Release, 2006. **114**(3): p. 334-42.
89. Gong, N., et al., Site-specific PEGylation of exenatide analogues markedly improved their glucoregulatory activity. Br J Pharmacol, 2011. **163**(2): p. 399-412.
90. Chalasani, K.B., et al., A novel vitamin B12-nanosphere conjugate carrier system for peroral delivery of insulin. J Control Release, 2007. **117**(3): p. 421-9.
91. Pridgen, E.M., et al., Transepithelial transport of Fc-targeted nanoparticles by the neonatal fc receptor for oral delivery. Sci Transl Med, 2013. **5**(213): p. 213ra167.
92. Petrus, A.K., T.J. Fairchild, and R.P. Doyle, Traveling the vitamin B12 pathway: oral delivery of protein and peptide drugs. Angew Chem Int Ed Engl, 2009. **48**(6): p. 1022-8.

93. Kim, B.-J., et al., *Transferrin Fusion Technology: A Novel Approach to Prolonging Biological Half-Life of Insulinotropic Peptides.* The Journal of pharmacology and experimental therapeutics, 2010. **334**: p. 682-92.
94. Kavimandan, N.J., et al., Synthesis and characterization of insulin-transferrin conjugates. Bioconjug Chem, 2006. **17**(6): p. 1376-84.
95. Youn, Y.S., et al., Improved peroral delivery of glucagon-like peptide-1 by site-specific biotin modification: design, preparation, and biological evaluation. Eur J Pharm Biopharm, 2008. **68**(3): p. 667-75.
96. Jin, C.H., et al., A new orally available glucagon-like peptide-1 receptor agonist, biotinylated exendin-4, displays improved hypoglycemic effects in db/db mice. J Control Release, 2009. **133**(3): p. 172-7.
97. Wang, Y., et al., Proinsulin-transferrin fusion protein as a novel long-acting insulin analog for the inhibition of hepatic glucose production. Diabetes, 2014. **63**(5): p. 1779-88.
98. Asada, H., et al., Absorption characteristics of chemically modified-insulin derivatives with various fatty acids in the small and large intestine. J Pharm Sci, 1995. **84**(6): p. 682-7.
99. Wang, J., et al., Reversible lipidization for the oral delivery of salmon calcitonin. J Control Release, 2003. **88**(3): p. 369-80.
100. Wang, J., et al., Reversible lipidization for the oral delivery of leu-enkephalin. J Drug Target, 2006. **14**(3): p. 127-36.
101. Joseph, J.W., et al., Oral delivery of glucagon-like peptide-1 in a modified polymer preparation normalizes basal glycaemia in diabetic db/db mice. Diabetologia, 2000. **43**(10): p. 1319-1328.
102. Mrsny, R.J., Oral drug delivery research in Europe. J Control Release, 2012. **161**(2): p. 247-53.
103. Maroni, A., et al., Oral colon delivery of insulin with the aid of functional adjuvants. Adv Drug Deliv Rev, 2012. **64**(6): p. 540-56.
104. Hastewell, J., et al., The colonic absorption of human calcitonin: the effects of increasing local concentration and co-administration with a protease inhibitor. International Journal of Pharmaceutics, 1995. **126**(1): p. 245-251.
105. Liu, H., et al., Potential utility of various protease inhibitors for improving the intestinal absorption of insulin in rats. J Pharm Pharmacol, 2003. **55**(11): p. 1523-9.
106. Maher, S., et al., Formulation strategies to improve oral peptide delivery. Pharm Pat Anal, 2014. **3**(3): p. 313-36.
107. Bernkop-Schnurch, A., The use of inhibitory agents to overcome the enzymatic barrier to perorally administered therapeutic peptides and proteins. J Control Release, 1998. **52**(1-2): p. 1-16.
108. Welling, S.H., et al., The role of citric acid in oral peptide and protein formulations: Relationship between calcium chelation and proteolysis inhibition. European Journal of Pharmaceutics and Biopharmaceutics, 2014. **86**(3): p. 544-551.
109. Asane, G.S., et al., Polymers for mucoadhesive drug delivery system: a current status. Drug Dev Ind Pharm, 2008. **34**(11): p. 1246-66.
110. Millotti, G., et al., In vivo evaluation of thiolated chitosan tablets for oral insulin delivery. J Pharm Sci, 2014. **103**(10): p. 3165-70.
111. Dorkoosh, F.A., et al., Feasibility study on the retention of superporous hydrogel composite polymer in the intestinal tract of man using scintigraphy. J Control Release, 2004. **99**(2): p. 199-206.
112. Bernkop-Schnurch, A., C. Valenta, and S.M. Daee, Peroral polypeptide delivery. A comparative in vitro study of mucolytic agents. Arzneimittelforschung, 1999. **49**(9): p. 799-803.
113. Müller C, L.K., Hauptstein S, Hintzen F, Salvenmoser W, Bernkop-Schnürch A. , Preparation and characterization of mucus-penetrating papain/poly(acrylic acid) nanoparticles for oral drug delivery applications. An Interdisciplinary Forum for Nanoscale Science and Technology, 2013. **15:1–13**
114. Muller, C., et al., Development and in vivo evaluation of papain-functionalized nanoparticles. Eur J Pharm Biopharm, 2014. **87**(1): p. 125-31.

115. Mahmood, A., et al., Protease-functionalized mucus penetrating microparticles: In-vivo evidence for their potential. Int J Pharm, 2017. **532**(1): p. 177-184.

116. Siddhanta, S., et al., Shedding Light on the Trehalose-Enabled Mucopermeation of Nanoparticles with Label-Free Raman Spectroscopy. Small, 2019. **0**(0): p. 1901679.

117. Vllasaliu, D., et al., Recent advances in oral delivery of biologics: nanomedicine and physical modes of delivery. Expert Opin Drug Deliv, 2018. **15**(8): p. 759-770.

118. Rzhevskiy, A.S., et al., Microneedles as the technique of drug delivery enhancement in diverse organs and tissues. J Control Release, 2018. **270**: p. 184-202.

119. Traverso, G., et al., Microneedles for drug delivery via the gastrointestinal tract. Journal of pharmaceutical sciences, 2015. **104**(2): p. 362-367.

120. Abramson, A., et al., An ingestible self-orienting system for oral delivery of macromolecules. Science, 2019. **363**(6427): p. 611-615.

121. Schoellhammer, C.M., et al., Defining optimal permeant characteristics for ultrasound-mediated gastrointestinal delivery. J Control Release, 2017. **268**: p. 113-119.

122. Tao, S.L. and T.A. Desai, Micromachined devices: the impact of controlled geometry from cell-targeting to bioavailability. J Control Release, 2005. **109**(1-3): p. 127-38.

123. Banerjee, A. and S. Mitragotri, Intestinal patch systems for oral drug delivery. Curr Opin Pharmacol, 2017. **36**: p. 58-65.

124. Gupta, V., et al., Delivery of Exenatide and Insulin Using Mucoadhesive Intestinal Devices. Ann Biomed Eng, 2016. **44**(6): p. 1993-2007.

125. Berardi, A. and L. Bisharat, Nanotechnology systems for oral drug delivery: challenges and opportunities. 2016. p. 52-84.

126. Homayun, B., X. Lin, and H.J. Choi, Challenges and Recent Progress in Oral Drug Delivery Systems for Biopharmaceuticals. Pharmaceutics, 2019. **11**(3).

127. Sonaje, K., et al., In vivo evaluation of safety and efficacy of self-assembled nanoparticles for oral insulin delivery. Biomaterials, 2009. **30**(12): p. 2329-39.

128. Baluom, M., et al., Synchronized release of sulpiride and sodium decanoate from HPMC matrices: a rational approach to enhance sulpiride absorption in the rat intestine. Pharm Res, 2000. **17**(9): p. 1071-6.

129. Maher, S., R.J. Mrsny, and D.J. Brayden, Intestinal permeation enhancers for oral peptide delivery. Adv Drug Deliv Rev, 2016. **106**(Pt B): p. 277-319.

130. Park, K., I.C. Kwon, and K. Park, Oral protein delivery: Current status and future prospect. Reactive and Functional Polymers, 2011. **71**(3): p. 280-287.

131. Card, J.W. and B.A. Magnuson, A review of the efficacy and safety of nanoparticle-based oral insulin delivery systems. Am J Physiol Gastrointest Liver Physiol, 2011. **301**(6): p. G956-67.

132. Windsor, E. and G.E. Cronheim, Gastro-intestinal absorption of heparin and synthetic heparinoids. Nature, 1961. **190**: p. 263-4.

133. Whitehead, K., N. Karr, and S. Mitragotri, Safe and effective permeation enhancers for oral drug delivery. Pharm Res, 2008. **25**(8): p. 1782-8.

134. Hamman, J.H., G.M. Enslin, and A.F. Kotze, Oral delivery of peptide drugs: barriers and developments. BioDrugs, 2005. **19**(3): p. 165-77.

135. Peterson, B., et al., Drug Bioavailability Enhancing Agents of Natural Origin (Bioenhancers) that Modulate Drug Membrane Permeation and Pre-Systemic Metabolism. Pharmaceutics, 2019. **11**(1).

136. Kondoh, M., et al., Targeting tight junction proteins-significance for drug development. Drug Discov Today, 2008. **13**(3-4): p. 180-6.

137. Zupancic, O. and A. Bernkop-Schnurch, Lipophilic peptide character - What oral barriers fear the most. J Control Release, 2017. **255**: p. 242-257.

138. Brayden, D.J. and E. Walsh, Efficacious intestinal permeation enhancement induced by the sodium salt of 10-undecylenic acid, a medium chain fatty acid derivative. Aaps j, 2014. **16**(5): p. 1064-76.

139. W. Stern, N.M., S. Carl, Oral delivery of peptides by Peptelligence technology. Drug Dev. Deliv., 2013. **13**: p. 36–42.

140. Hochman, J.H., J.A. Fix, and E.L. LeCluyse, In vitro and in vivo analysis of the mechanism of absorption enhancement by palmitoylcarnitine. J Pharmacol Exp Ther, 1994. **269**(2): p. 813-22.

141. Sharma, P., et al., Absorption enhancement, mechanistic and toxicity studies of medium chain fatty acids, cyclodextrins and bile salts as peroral absorption enhancers. Farmaco, 2005. **60**(11-12): p. 884-93.

142. Van der Merwe, S.M., et al., Trimethylated chitosan as polymeric absorption enhancer for improved peroral delivery of peptide drugs. Eur J Pharm Biopharm, 2004. **58**(2): p. 225-35.

143. Maher, S., et al., Evaluation of intestinal absorption enhancement and local mucosal toxicity of two promoters. I. Studies in isolated rat and human colonic mucosae. Eur J Pharm Sci, 2009. **38**(4): p. 291-300.

144. Fasano, A. and S. Uzzau, Modulation of intestinal tight junctions by Zonula occludens toxin permits enteral administration of insulin and other macromolecules in an animal model. J Clin Invest, 1997. **99**(6): p. 1158-64.

145. Salama, N.N., N.D. Eddington, and A. Fasano, Tight junction modulation and its relationship to drug delivery. Adv Drug Deliv Rev, 2006. **58**(1): p. 15-28.

146. Dos Santos, I., et al., Improvement of norfloxacin oral bioavailability by EDTA and sodium caprate. Int J Pharm, 2003. **260**(1): p. 1-4.

147. Taverner, A., et al., Enhanced paracellular transport of insulin can be achieved via transient induction of myosin light chain phosphorylation. Journal of Controlled Release, 2015. **210**: p. 189-197.

148. Takatsuka, S., et al., Enhancement of intestinal absorption of poorly absorbed hydrophilic compounds by simultaneous use of mucolytic agent and non-ionic surfactant. Eur J Pharm Biopharm, 2006. **62**(1): p. 52-8.

149. Nielsen, E.J., et al., In vivo proof of concept of oral insulin delivery based on a co-administration strategy with the cell-penetrating peptide penetratin. J Control Release, 2014. **189**: p. 19-24.

150. Liang, J.F. and V.C. Yang, Insulin-cell penetrating peptide hybrids with improved intestinal absorption efficiency. Biochem Biophys Res Commun, 2005. **335**(3): p. 734-8.

151. Morishita, M., et al., A novel approach using functional peptides for efficient intestinal absorption of insulin. J Control Release, 2007. **118**(2): p. 177-84.

152. Banerjee, A., et al., Ionic liquids for oral insulin delivery. Proc Natl Acad Sci U S A, 2018. **115**(28): p. 7296-7301.

153. Aungst, B.J., Absorption enhancers: applications and advances. Aaps j, 2012. **14**(1): p. 10-8.

154. Durán-Lobato, M., Z. Niu, and M.J. Alonso, Oral Delivery of Biologics for Precision Medicine. Advanced Materials, 2019. **0**(0): p. 1901935.

155. Younes, M., Aggett, P., Aguilar, F., Crebelli, R., Re-evaluation of sodium, potassium and calcium salts of fatty acids (E 470a) and magnesium salts of fatty acids (E 470b) as food additives. EFSA J., 2018.

156. Maher, S., et al., Safety and efficacy of sodium caprate in promoting oral drug absorption: from in vitro to the clinic. Adv Drug Deliv Rev, 2009. **61**(15): p. 1427-49.

157. Van Hoogdalem, E.J., et al., Absorption enhancement of rectally infused cefoxitin sodium by medium-chain fatty acids in conscious rats: concentration-effect relationship. Pharm Res, 1988. **5**(7): p. 453-6.

158. Lapre, J.A., et al., Lytic effects of mixed micelles of fatty acids and bile acids. Am J Physiol, 1992. **263**(3 Pt 1): p. G333-7.

159. Shima, M., et al., Effects of medium-chain fatty acids and their acylglycerols on the transport of penicillin V across Caco-2 cell monolayers. Biosci Biotechnol Biochem, 1997. **61**(7): p. 1150-5.

160. Lindmark, T., Y. Kimura, and P. Artursson, Absorption enhancement through intracellular regulation of tight junction permeability by medium chain fatty acids in Caco-2 cells. J Pharmacol Exp Ther, 1998. **284**(1): p. 362-9.

161. Namani, T. and P. Walde, From Decanoate Micelles to Decanoic Acid/Dodecylbenzenesulfonate Vesicles. Langmuir, 2005. **21**(14): p. 6210-6219.

162. Lindmark, T., et al., Mechanism of absorption enhancement in humans after rectal administration of ampicillin in suppositories containing sodium caprate. Pharm Res, 1997. **14**(7): p. 930-5.

163. Walsh, E.G., et al., Oral delivery of macromolecules: rationale underpinning Gastrointestinal Permeation Enhancement Technology (GIPET). Ther Deliv, 2011. **2**(12): p. 1595-610.

164. Leone-Bay, A., et al., N-Acylated .alpha.-Amino Acids as Novel Oral Delivery Agents for Proteins. Journal of Medicinal Chemistry, 1995. **38**(21): p. 4263-4269.

165. Castelli, M.C., et al., Pharmacokinetics of oral cyanocobalamin formulated with sodium N-[8-(2-hydroxybenzoyl)amino]caprylate (SNAC): an open-label, randomized, single-dose, parallel-group study in healthy male subjects. Clin Ther, 2011. **33**(7): p. 934-45.

166. Smith, L., Mosley, J, Ford, M., & Courtney, J., Cyanocobalamin/Salcaprozate Sodium: A novel way to treat vitamin B12 deficiency and anemia. J. Hematol. Oncol. Pharm., 2016.

167. Leone-Bay, A., et al., Acylated non-alpha-amino acids as novel agents for the oral delivery of heparin sodium, USP. J Control Release, 1998. **50**(1-3): p. 41-9.

168. Goldberg, M. and I. Gomez-Orellana, Challenges for the oral delivery of macromolecules. Nat Rev Drug Discov, 2003. **2**(4): p. 289-95.

169. Leone-Bay, A., et al., Oral delivery of sodium cromolyn: preliminary studies in vivo and in vitro. Pharm Res, 1996. **13**(2): p. 222-6.

170. Lindmark, T., T. Nikkila, and P. Artursson, Mechanisms of absorption enhancement by medium chain fatty acids in intestinal epithelial Caco-2 cell monolayers. J Pharmacol Exp Ther, 1995. **275**(2): p. 958-64.

171. Brayden, D.J., J. Gleeson, and E.G. Walsh, A head-to-head multi-parametric high content analysis of a series of medium chain fatty acid intestinal permeation enhancers in Caco-2 cells. Eur J Pharm Biopharm, 2014. **88**(3): p. 830-39.

172. Sawada, T., et al., Role of paracellular pathway in nonelectrolyte permeation across rat colon epithelium enhanced by sodium caprate and sodium caprylate. Pharm Res, 1991. **8**(11): p. 1365-71.

173. Maher, S., et al., Evaluation of intestinal absorption and mucosal toxicity using two promoters. II. Rat instillation and perfusion studies. Eur J Pharm Sci, 2009. **38**(4): p. 301-11.

174. Tomita, M., M. Hayashi, and S. Awazu, Absorption-enhancing mechanism of EDTA, caprate, and decanoylcarnitine in Caco-2 cells. J Pharm Sci, 1996. **85**(6): p. 608-11.

175. Feighery, L.M., et al., Myosin light chain kinase inhibition: correction of increased intestinal epithelial permeability in vitro. Pharm Res, 2008. **25**(6): p. 1377-86.

176. Shimazaki, T., et al., Absorption-enhancing effects of sodium caprate and palmitoyl carnitine in rat and human colons. Dig Dis Sci, 1998. **43**(3): p. 641-5.

177. Krug, S.M., et al., Sodium caprate as an enhancer of macromolecule permeation across tricellular tight junctions of intestinal cells. Biomaterials, 2013. **34**(1): p. 275-282.

178. Blikslager, A.T., et al., Restoration of barrier function in injured intestinal mucosa. Physiol Rev, 2007. **87**(2): p. 545-64.

179. Sugibayashi, K., Y. Onuki, and K. Takayama, Displacement of tight junction proteins from detergent-resistant membrane domains by treatment with sodium caprate. European journal of pharmaceutical sciences : official journal of the European Federation for Pharmaceutical Sciences, 2009. **36**(2-3): p. 246-253.

180. Maher, S., et al., Effects of surfactant-based permeation enhancers on mannitol permeability, histology, and electrogenic ion transport responses in excised rat colonic mucosae. Int J Pharm, 2018. **539**(1-2): p. 11-22.

181. Brayden, D.J., et al., Sodium caprate-induced increases in intestinal permeability and epithelial damage are prevented by misoprostol. Eur J Pharm Biopharm, 2015. **94**: p. 194-206.

182. Leonard, T.W., et al., Promoting absorption of drugs in humans using medium-chain fatty acid-based solid dosage forms: GIPET. Expert Opin Drug Deliv, 2006. **3**(5): p. 685-92.

183. Arbit, E., et al., Oral heparin: status review. Thrombosis journal, 2006. **4**: p. 6-6.

184. Malkov, D., et al., Oral delivery of insulin with the eligen technology: mechanistic studies. Curr Drug Deliv, 2005. **2**(2): p. 191-7.

185. Brayden, D., et al., Heparin absorption across the intestine: effects of sodium N-[8-(2-hydroxybenzoyl)amino]caprylate in rat in situ intestinal instillations and in Caco-2 monolayers. Pharm Res, 1997. **14**(12): p. 1772-9.

186. Hess, S., V. Rotshild, and A. Hoffman, Investigation of the enhancing mechanism of sodium N-[8-(2-hydroxybenzoyl)amino]caprylate effect on the intestinal permeability of polar molecules utilizing a voltage clamp method. Eur J Pharm Sci, 2005. **25**(2-3): p. 307-12.

187. Malkov, D., et al., Pathway of oral absorption of heparin with sodium N-[8-(2-hydroxybenzoyl)amino] caprylate. Pharm Res, 2002. **19**(8): p. 1180-4.

188. Ding, X., et al., Oral absorption enhancement of cromolyn sodium through noncovalent complexation. Pharm Res, 2004. **21**(12): p. 2196-206.

189. Buckley, S.T., et al., Transcellular stomach absorption of a derivatized glucagon-like peptide-1 receptor agonist. Sci Transl Med, 2018. **10**(467).

190. Raoof, A.A., et al., Oral bioavailability and multiple dose tolerability of an antisense oligonucleotide tablet formulated with sodium caprate. J Pharm Sci, 2004. **93**(6): p. 1431-9.

191. Tillman, L.G., R.S. Geary, and G.E. Hardee, Oral delivery of antisense oligonucleotides in man. J Pharm Sci, 2008. **97**(1): p. 225-36.

192. Amory, J.K., et al., Oral administration of the GnRH antagonist acyline, in a GIPET-enhanced tablet form, acutely suppresses serum testosterone in normal men: single-dose pharmacokinetics and pharmacodynamics. Cancer Chemother Pharmacol, 2009. **64**(3): p. 641-5.

193. Leonard, T.W., Composition and drug delivery of bisphosphonates. . 2010.

194. Halberg, I.B., et al., Efficacy and safety of oral basal insulin versus subcutaneous insulin glargine in type 2 diabetes: a randomised, double-blind, phase 2 trial. The Lancet Diabetes & Endocrinology, 2019. **7**(3): p. 179-188.

195. Halberg, I.B., et al., The Effect of Food Intake on the Pharmacokinetics of Oral Basal Insulin: A Randomised Crossover Trial in Healthy Male Subjects. Clin Pharmacokinet, 2019.

196. Khedkar, A., et al., Impact of Insulin Tregopil and Its Permeation Enhancer on Pharmacokinetics of Metformin in Healthy Volunteers: Randomized, Open-Label, Placebo-Controlled, Crossover Study. Clin Transl Sci, 2019. **12**(3): p. 276-282.

197. Lennernas, H., et al., The influence of caprate on rectal absorption of phenoxymethylpenicillin: experience from an in-vivo perfusion in humans. J Pharm Pharmacol, 2002. **54**(4): p. 499-508.

198. Kapitza, C., et al., Oral insulin: a comparison with subcutaneous regular human insulin in patients with type 2 diabetes. Diabetes care, 2010. **33**(6): p. 1288-1290.

199. Karsdal, M.A., et al., Treatment of symptomatic knee osteoarthritis with oral salmon calcitonin: results from two phase 3 trials. Osteoarthritis Cartilage, 2015. **23**(4): p. 532-43.

200. Henriksen, K., et al., A randomized, double-blind, multicenter, placebo-controlled study to evaluate the efficacy and safety of oral salmon calcitonin in the treatment of osteoporosis in postmenopausal women taking calcium and vitamin D. Bone, 2016. **91**: p. 122-9.

201. Karsdal, M.A., et al., Lessons learned from the development of oral calcitonin: the first tablet formulation of a protein in phase III clinical trials. J Clin Pharmacol, 2011. **51**(4): p. 460-71.

202. Baughman, R.A., et al., Oral delivery of anticoagulant doses of heparin. A randomized, double-blind, controlled study in humans. Circulation, 1998. **98**(16): p. 1610-5.

203. Berkowitz, S.D., et al., Oral heparin administration with a novel drug delivery agent (SNAC) in healthy volunteers and patients undergoing elective total hip arthroplasty. J Thromb Haemost, 2003. **1**(9): p. 1914-9.

204. Mousa, S.A., et al., Pharmacokinetics and pharmacodynamics of oral heparin solid dosage form in healthy human subjects. J Clin Pharmacol, 2007. **47**(12): p. 1508-20.

205. Davies, M., et al., Effect of Oral Semaglutide Compared With Placebo and Subcutaneous Semaglutide on Glycemic Control in Patients With Type 2 Diabetes: A Randomized Clinical Trial. Jama, 2017. **318**(15): p. 1460-1470.

206. Bjerregaard, S., Nielsen, F. S., Sauerberg, P, Solid compositions comprising a GLP-1 agonist and a salt of n-(8-(2-hydroxybenzoyl)amino)caprylic acid. 2012.

207. Aroda, V.R., et al., PIONEER 1: Randomized Clinical Trial of the Efficacy and Safety of Oral Semaglutide Monotherapy in Comparison With Placebo in Patients With Type 2 Diabetes. Diabetes Care, 2019. **42**(9): p. 1724-1732.

208. Granhall, C., et al., Pharmacokinetics, Safety and Tolerability of Oral Semaglutide in Subjects with Renal Impairment. Clin Pharmacokinet, 2018. **57**(12): p. 1571-1580.

209. Baekdal, T.A., et al., Pharmacokinetics, Safety, and Tolerability of Oral Semaglutide in Subjects With Hepatic Impairment. J Clin Pharmacol, 2018. **58**(10): p. 1314-1323.

210. Baekdal, T.A., et al., A randomized study investigating the effect of omeprazole on the pharmacokinetics of oral semaglutide. Expert Opin Drug Metab Toxicol, 2018. **14**(8): p. 869-877.

211. Baekdal, T.A., et al., Effect of Oral Semaglutide on the Pharmacokinetics of Lisinopril, Warfarin, Digoxin, and Metformin in Healthy Subjects. Clin Pharmacokinet, 2019. **58**(9): p. 1193-1203.

212. Bain, S.C., et al., Cardiovascular safety of oral semaglutide in patients with type 2 diabetes: Rationale, design and patient baseline characteristics for the PIONEER 6 trial. Diabetes Obes Metab, 2019. **21**(3): p. 499-508.

213. Drucker, D.J., Advances in oral peptide therapeutics. Nature Reviews Drug Discovery, 2019.

214. Rodbard, H.W., et al., Oral Semaglutide Versus Empagliflozin in Patients With Type 2 Diabetes Uncontrolled on Metformin: The PIONEER 2 Trial. Diabetes Care, 2019. **42**(12): p. 2272-2281.

215. Rosenstock, J., et al., Effect of Additional Oral Semaglutide vs Sitagliptin on Glycated Hemoglobin in Adults With Type 2 Diabetes Uncontrolled With Metformin Alone or With Sulfonylurea: The PIONEER 3 Randomized Clinical Trial. Jama, 2019.

216. Pratley, R., et al., Oral semaglutide versus subcutaneous liraglutide and placebo in type 2 diabetes (PIONEER 4): a randomised, double-blind, phase 3a trial. Lancet, 2019.

217. Mosenzon, O., et al., Efficacy and safety of oral semaglutide in patients with type 2 diabetes and moderate renal impairment (PIONEER 5): a placebo-controlled, randomised, phase 3a trial. Lancet Diabetes Endocrinol, 2019. **7**(7): p. 515-527.

218. Pieber, T.R., et al., Efficacy and safety of oral semaglutide with flexible dose adjustment versus sitagliptin in type 2 diabetes (PIONEER 7): a multicentre, open-label, randomised, phase 3a trial. Lancet Diabetes Endocrinol, 2019. **7**(7): p. 528-539.

219. Zinman B, A.V., Buse JB, et al, Oral semaglutide as add-on to insulin in T2DM: PIONEER 8. June 7-11, 2019, American Diabetes Association 79th Scientific Sessions: San Francisco, CA.

220. Dose-response, safety and efficacy of oral semaglutide versus placebo and versus liraglutide, all as monotherapy in Japanese subjects with type 2 diabetes (PIONEER 9). Available from: ttps://clinicaltrials.gov/ct2/show/NCT03018028?term=oral+semaglutide &phase=2&rank=6.

221. Safety and efficacy of oral semaglutide versus dulaglutide both in combination with one OAD (oral antidiabetic drug) in Japanese subjects with type 2 diabetes (PIONEER10). Available from: https://clinicaltrials.gov/ct2/show/NCT03015220?term=oral+semagl utide&phase=2&rank=5.

222. Raoof, A.A., et al., Effect of sodium caprate on the intestinal absorption of two modified antisense oligonucleotides in pigs. Eur J Pharm Sci, 2002. **17**(3): p. 131-8.

223. Riley, M.G., M.C. Castelli, and E.A. Paehler, Subchronic oral toxicity of salcaprozate sodium (SNAC) in Sprague-Dawley and Wistar rats. Int J Toxicol, 2009. **28**(4): p. 278-93.

224. Riley, M.G. and R.G. York, Peri- and postnatal developmental toxicity of salcaprozate sodium (SNAC) in Sprague-Dawley rats. Int J Toxicol, 2009. **28**(4): p. 266-77.

225. McCartney, F., J.P. Gleeson, and D.J. Brayden, Safety concerns over the use of intestinal permeation enhancers: A mini-review. Tissue Barriers, 2016. **4**(2): p. e1176822.

226. Nordisk, N., Rybelsus (semaglutide tablets) prescribing information. September 2018: Plainsboro, NJ.

227. van der Flier, L.G. and H. Clevers, Stem cells, self-renewal, and differentiation in the intestinal epithelium. Annu Rev Physiol, 2009. **71**: p. 241-60.

228. Laine, L., K. Takeuchi, and A. Tarnawski, Gastric mucosal defense and cytoprotection: bench to bedside. Gastroenterology, 2008. **135**(1): p. 41-60.

229. Wang, X., S. Maher, and D.J. Brayden, Restoration of rat colonic epithelium after in situ intestinal instillation of the absorption promoter, sodium caprate. Ther Deliv, 2010. **1**(1): p. 75-82.

230. Gookin, J.L., et al., PG-mediated closure of paracellular pathway and not restitution is the primary determinant of barrier recovery in acutely injured porcine ileum. Am J Physiol Gastrointest Liver Physiol, 2003. **285**(5): p. G967-79.

231. Narkar, Y., et al., Evaluation of mucosal damage and recovery in the gastrointestinal tract of rats by a penetration enhancer. Pharm Res, 2008. **25**(1): p. 25-38.

232. Scott Swenson, E. and W.J. Curatolo, (C) Means to enhance penetration: (2) Intestinal permeability enhancement for proteins, peptides and other polar drugs: mechanisms and potential toxicity. Advanced Drug Delivery Reviews, 1992. **8**(1): p. 39-92.

233. Konig, J., et al., Human Intestinal Barrier Function in Health and Disease. Clin Transl Gastroenterol, 2016. **7**(10): p. e196.

234. Cani, P.D., Human gut microbiome: hopes, threats and promises. Gut, 2018. **67**(9): p. 1716-1725.

235. Chassaing, B., et al., Dietary emulsifiers impact the mouse gut microbiota promoting colitis and metabolic syndrome. Nature, 2015. **519**(7541): p. 92-6.

236. Tscheik, C., I.E. Blasig, and L. Winkler, Trends in drug delivery through tissue barriers containing tight junctions. Tissue Barriers, 2013. **1**(2): p. e24565.

237. Bala, S., et al., Acute binge drinking increases serum endotoxin and bacterial DNA levels in healthy individuals. PLoS One, 2014. **9**(5): p. e96864.

238. Cox, A.B., et al., In vitro interactions between the oral absorption promoter, sodium caprate (C(10)) and S. typhimurium in rat intestinal ileal mucosae. Pharm Res, 2008. **25**(1): p. 114-22.

239. Van Immerseel, F., et al., Medium-chain fatty acids decrease colonization and invasion through hilA suppression shortly after infection of chickens with Salmonella enterica serovar Enteritidis. Appl Environ Microbiol, 2004. **70**(6): p. 3582-7.

240. Chadeganipour, M. and A. Haims, Antifungal activities of pelargonic and capric acid on Microsporum gypseum. Mycoses, 2001. **44**(3-4): p. 109-12.

241. Huang, C.B., et al., Short- and medium-chain fatty acids exhibit antimicrobial activity for oral microorganisms. Arch Oral Biol, 2011. **56**(7): p. 650-4.

242. Sodium decanoate, PubChem ID 16211937. Available from: https://pubchem.ncbi.nlm.nih.gov/compound/16211937.

243. Sodium caprozate PubChem ID 22669833. Available from: https://pubchem.ncbi.nlm.nih.gov/compound/23669833.

244. Alani, A.W. and J.R. Robinson, Mechanistic understanding of oral drug absorption enhancement of cromolyn sodium by an amino acid derivative. Pharm Res, 2008. **25**(1): p. 48-54.

245. Rehmani, S. and J.E. Dixon, Oral delivery of anti-diabetes therapeutics using cell penetrating and transcytosing peptide strategies. Peptides, 2018. **100**: p. 24-35.

246. Gradauer, K., et al., Interaction with Mixed Micelles in the Intestine Attenuates the Permeation Enhancing Potential of Alkyl-Maltosides. Molecular Pharmaceutics, 2015. **12**(7): p. 2245-2253.

247. Gaillard, P.J. and A.G. de Boer, Relationship between permeability status of the blood-brain barrier and in vitro permeability coefficient of a drug. Eur J Pharm Sci, 2000. **12**(2): p. 95-102.

248. Van Itallie, C.M., et al., The density of small tight junction pores varies among cell types and is increased by expression of claudin-2. J Cell Sci, 2008. **121**(Pt 3): p. 298-305.

Chapter 2

Characterization of the physico-chemical interactions between exenatide and SNAC or C_{10}

Chapitre 2 : Caractérisation des interactions physico-chimiques entre exenatide et SNAC ou C_{10}

Résumé

L'une des principales approches d'amélioration de la perméabilité intestinale des peptides administrés par voie orale consiste à les associer à des promoteurs d'absorption. En effet, une biodisponibilité améliorée de peptides a été décrite pour de nombreux essais cliniques lorsque le salcaprozate de sodium (SNAC) ou le caprate de sodium (C_{10}) étaient incorporés dans la formulation. Cependant, peu d'informations sont disponibles sur la façon dont les promoteurs d'absorption interagissent avec la macromolécule thérapeutique. L'objectif de notre étude était de comparer les interactions biophysiques entre un peptide modèle analogue de GLP-1, l'exénatide (Byetta®, Lilly) et les deux promoteurs d'absorption SNAC et C_{10} en utilisant une variété de techniques analytiques complémentaires. La concentration micellaire critique a été mesurée autour de 40 mM pour les deux promoteurs dans différents tampons. L'organisation en structures polydisperses des promoteurs seuls a été déterminée par une méthode de diffusion dynamique de la lumière dans différents milieux. La formation de complexes d'interactions avec l'exénatide à des ratios spécifiques a été observé avec C_{10}. Le profil qualitatif de l'interaction exénatide/promoteur obtenue par résonance plasmonique de surface indique une cinétique d'association/dissociation rapide et de faibles affinités. La signature thermodynamique de l'interaction, suivie dans l'eau par titration calorimétrique isotherme, indique une contribution enthalpique défavorable compensée par des contributions entropiques élevées. Une faible affinité a pu être quantifiée avec une constante de dissociation de l'ordre 10-100 µM. L'électrophorèse capillaire d'affinité a permis de confirmer la faible interaction entre SNAC ou C_{10} et l'exénatide en milieu salin. En milieux biopharmaceutiques gastro-intestinaux représentatifs FaSSIF/FeSSIF, la présence de sels biliaires a réduit l'affinité d'interaction entre exénatide et C_{10}. En conclusion, cette étude suggère que l'interaction entre exénatide et SNAC ou C_{10} présente un niveau d'affinité relativement faible, influencée par l'organisation supramoléculaire des promoteurs, peu sélective et comparable entre les deux promoteurs.

Mots clés : Interactions biophysiques, affinité, milieux simulés, caprate de sodium, SNAC

Chapter 2: Characterization of the physico-chemical interactions between exenatide and SNAC or C_{10}

Abstract

A common approach to tackle the poor intestinal membrane permeability of peptides after oral administration is to formulate them with a permeation enhancer (PE). Increased oral bioavailability for oral peptide candidates has been reported from clinical trials when either salcaprozate sodium (SNAC) or sodium caprate (C_{10}) are incorporated in the formulation. However, little is known about how they physically interact with peptides. Our objective was to compare the biophysical interactions between the GLP-1 analogue, exenatide (Byetta®, Lilly), and C_{10} or SNAC using a variety of advanced analytical techniques. First, critical micelle concentration was measured to be around 40 mM in different buffers for both PEs. Dynamic light scattering (DLS) measurements revealed polydisperse particulate structures for SNAC and C_{10}. C_{10} formed supramolecular structures with exenatide at specific ratios suggesting possible interaction. Surface plasmon resonance (SPR) indicated the formation of exenatide/PE complexes with a high contribution of non-specific interactions and rapid binding kinetics, resulting in overall low affinities. DLS and isothermal titration calorimetry (ITC) were used to examine the supramolecular organization of the PEs, and revealed thermodynamic signatures characterized by unfavorable enthalpic contributions compensated by favorable entropic ones, but with low-affinity estimates in water (K_D in the 10-100 µM range). With affinity capillary electrophoresis (ACE), weak interactions between exenatide and SNAC or C_{10} were confirmed in saline, with a dissociation constant around 10 µM and 30 µM respectively. In bio-relevant intestinal media, the bile salts in FaSSIF/FeSSIF further reduced the binding of both agents to exenatide ($K_D \approx 100$ µM), indicating that the interaction between the PEs and exenatide might be inhibited by bile salts in the GI lumen. This study suggests that the interactions of these PEs with exenatide follow a similar non-covalent mechanism and are of low affinity.

Keywords: Biophysical interactions, affinity, biorelevant buffers, sodium caprate, SNAC.

1. Introduction

A common approach to tackle the poor peptide permeability after oral administration is the incorporation of permeation enhancers (PEs) in conventional enteric-coated oral dosage forms [1]. PEs can increase fluxes of poorly absorbed macromolecules by modulating either the transcellular route by disrupting plasma membranes or the paracellular route by modulating tight junctions (TJs) [2]. There are currently over 50 clinical trials in which PEs have been shown to increase oral absorption of poorly permeable molecules, mostly achieved using surfactant-type molecules [3]. The medium-chain fatty acids (MCFAs), sodium caprate (C_{10}), and the C_8 derivative salcaprozate sodium (SNAC), are of particular interest as they have had over 20 years of development in proprietary delivery platforms in human trials for oral peptides [4,5] (Figure 1). Also, oral semaglutide co-formulated with SNAC was recently approved by US Food and Drug Administration (FDA) in 2019 as the first oral peptide formulation for the treatment of type 2 diabetes (Rybelsus®, Novo-Nordisk, Denmark).

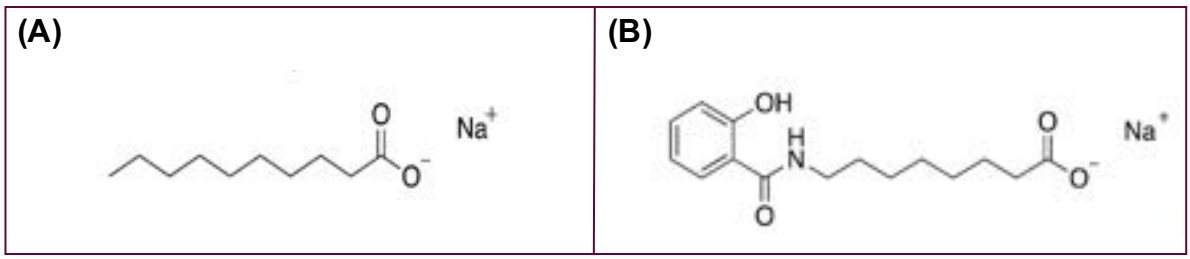

Figure 1: Structure of **(A)** C_{10} and **(B)** SNAC

Sodium caprate (C_{10}) is the sodium salt of capric acid, an aliphatic saturated 10-carbon MCFA with a molecular weight of 194 Da (Figure 1A). C_{10} is a soluble anionic surfactant with a critical micellar concentration (CMC) value of ~20-25 mM in aqueous buffers [6]. Anionic micelles form at lower concentrations in higher ionic strength buffers because the counter-ions in media interact closely with anionic head groups. Thus, varying the ionic strength alters the free monomeric concentration of C_{10} in the small intestine. At pH values 1-3 units below its pKa (~5) in gastric fluid, it exists in the non-ionized, insoluble capric acid form. At such acidic pH values, the surfactant can reduce surface tension, but does not exhibit detergent action. At pH values 1-3 units above its pKa (i.e. values that typically occur in the upper small intestine), capric acid converts to its ionizable soluble salt with detergent capacity, C_{10}. Like many other detergents, it does not form micelles efficiently owing to repulsion between the charged hydrophilic head groups. This feature enables its interaction with epithelial plasma membrane and confers a transcellular contribution to its mode of action. Both the US and EU have approved C_{10} as a food additive with no upper safety limit; it has a long history of safe use in humans [7]. C_{10} was the main component of the GIPET™ (Merrion Pharmaceuticals, Dublin,

Ireland) oral peptide formulations, which was tested in a phase II trial of a long t½ basal insulin from Novo-Nordisk [8]. Mechanistic data suggest that C_{10} combines a tight junction-opening mechanism mediated by intracellular pathways with initial mild plasma membrane perturbation [9]. No studies have yet been described the interaction between C_{10} and payloads.

There is a structural difference between C_{10} and SNAC, which is a synthetic *N*-acetylated amino acid derivative of salicylic acid with a molecular weight (Mw) of 301 Da (Figure 1B). SNAC is thought to primarily act via a non-covalent chaperone mechanism for payloads involving the transcellular lipophilic pathway across small intestinal epithelia [10]. SNAC was synthesized by Emisphere (NJ, USA) as the lead prototype of its Eligen® carrier technology: PEs that could "chaperone" macromolecules across the intestine [11]. Emisphere controversially contended that SNAC enhances permeability by forming a weak and non-covalent reversible complex with the active macromolecule, which dissociated at some stage during epithelial flux (Figure 2). The mechanism may involve a reversible change in protein conformation and protection against degradation prior to absorption.

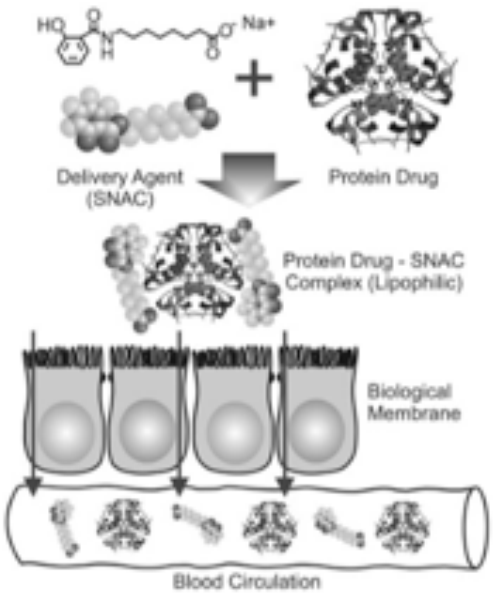

Figure 2: The formed lipophilic complex between SNAC and payload as proposed by Emisphere [12].

Since 1990, SNAC has been tested in many formats, combined with poorly permeable macromolecules or small molecules (heparin [13], salmon calcitonin [14], insulin [15], cromolyn [16]) aimed at developing oral formulations. SNAC is a component of Novo-Nordisk's oral semaglutide, a long half-life fatty acid-acylated GLP-1 analogue, which has completed 10 Phase III trials and was approved by FDA in 2019 (Rybelsus®) [17]. When SNAC is co-formulated with semaglutide in a non-enteric-coated tablet, they form a complex with high lipophilic properties facilitating semaglutide absorption through the gastric mucosa [18, 19].

The thermodynamic considerations in respect of the non-covalent linkage between SNAC or C_{10} and payload during epithelial flux have not been addressed. Neither were there any calculations on the affinity of SNAC to payloads to confirm this complex mechanism. As there is still debate over the creation of a transportable complex between SNAC and payload, it was of central importance to characterize the actual interaction of SNAC to a relevant macromolecule in a rigorous and quantitative manner. Better insight on the binding mechanism could lead to better understanding of the phenomena of permeation enhancement for SNAC. In this study, exenatide (Mw 4.2 kDa), an amphiphilic negatively-charged GLP-1 analogue was used as a model peptide to investigate if an interaction occurs when mixed with SNAC [20]. Bindings were also measured in the presence of C_{10} in order to compare with SNAC, since more is known about its mechanism of action on the plasma membrane and at TJs.

Complementary methods were used to assess changes that occur both at the level of the peptide and the complexed PEs in terms of affinity [21] (Figure 3). Dynamic light scattering (DLS) was first used to specify the colloidal behavior of PEs alone and to explore the complexation with exenatide (Figure 3A). The exenatide/PE interaction was then studied with Surface Plasmon Resonance (SPR) (Figure 3B). This biosensor-based reaction requires immobilization of the peptide on a thin gold surface of a chip. Then, ligands (i.e. PEs) are injected by means of a microfluidic system and made to flow over the peptide. The SPR method detects the peptide mass change upon complex formation and kinetic constants of the non-covalent binding process along with affinity constants can be determined from the sensorgrams. Isothermal Titration Calorimetry (ITC) was then used as a non-separative approach to measure the complete thermodynamic profiles for the exenatide/PEs interactions in solution (Figure 3C). It is the only technique that can measure heat changes associated with biomolecular interaction in solution [22]. Previous studies have shown that it is an extremely valuable tool for studying binding efficiencies between molecules [23], as well as enzymatic kinetics [24]. ITC simultaneously provides a complete thermodynamic profile for molecular-level interactions in a single experiment [25]. Also, there is no requirement for modification or labelling molecules since the heat exchange during these interactions is a natural property. Lastly, Affinity Capillary Electrophoresis (ACE) was used to monitor complex formation in free solution with buffers mimicking physiological conditions (FaSSIF/FeSSIF biorelevant media) (Figure 3D) [26]. With this separative approach, a capillary is filled with buffer containing the PE and a small amount of peptide is injected into the capillary [26,27]. Binding constants can be calculated from the change in the electrophoretic mobility of the peptide upon complexation [28].

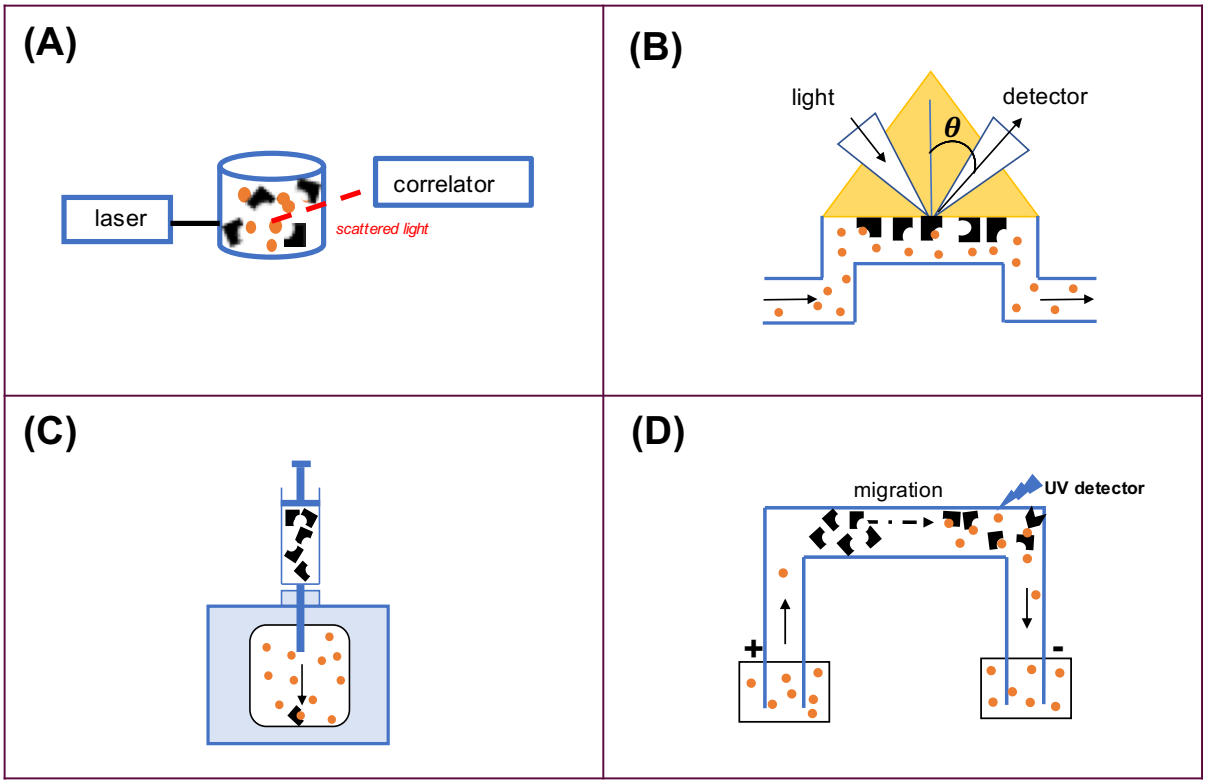

Figure 3: Schematics of the biophysical techniques studied. The interactions of either C_{10} or SNAC with exenatide were analyzed by **(A)** Dynamic Light Scattering (DLS), **(B)** Surface Plasmon Resonance (SPR), **(C)** Isothermal Titration Calorimetry (ITC) and **(D)** Affinity Capillary Electrophoresis (ACE). In each assay, the PEs are denoted as orange circles and the peptide is indicated as a black shape.

2. Materials and methods

2.1 Reagents

Exenatide acetate (Mw = 4 246.6 kDa; lyophilized powder with purity > 98%) was purchased from CarboSynth Limited (Berkshire,UK). Biotinylated exenatide (Mw = 4 414 kDa) was purchased from Anaspec Inc. (Fremont, CA). C_{10} was purchased from Sigma (Missouri, USA) and SNAC was from AstaTech Inc. (Bristol, USA). Media 199 was supplied by Sigma. The reagent N-ethyl-N'-(3-dimethylaminopropyl)-carbodiimide (EDC) and N-hydroxysuccinimide (NHS), ethanolamine HCl, 10% v/v surfactant P20 solution, 10X HBS-P+ (0.01 M HEPES pH 7.4, 0.15 M NaCl, 0.005% v/v surfactant P20), sensor chip CM5 (29149603), sensor chip SA (29104992), as the Biotin CAPture Kit (28920234) containing CAP chip, Conjugate Biotin CAPture [CAP] solution and regeneration reagents (8 M guanidine-HCl and 1 M NaOH) were purchased from Biacore (GE Healthcare Life Sciences, France). Hank's Balanced Salt Solution (HBSS) buffer was prepared with 10mM HEPES and 150mM NaCl. pH was adjusted at 7.4 with a solution of 1M NaOH. Boric acid (99.5%), phosphoric acid (100%), DMSO (99.5%), polybrene (>94%) (M_r 4 000-6 000), dextran sulphate (200 000 g/mol) were provided by Sigma (St. Louis, USA). Sodium taurocholate and Lipoid S100 were purchased from Thermo Fisher

scientific (Waltham, USA). All buffers were prepared using water and were filtered through a 0.22 µm nylon membrane (Millex, Millipore) before use. Unless otherwise noted, water refers to deionized water prepared with a Direct-QR 3 Water Purification System from Millipore (Billerica, USA), with a resistivity ≥ 18.2 MΩ.cm. All other common chemicals were reagent-grade.

2.2 Dynamic light scattering

CMC values for C_{10} and SNAC were measured by DLS in either water or PBS with a DynaPro®NanoStar apparatus (Wyatt Technology, USA) configured with a 90° scattering angle. All measurements were made at 25°C, SNAC and C_{10} concentration stock solution were between 45 - 90mM after passing through a 0.1 mm filter. The CMC was estimated using the Dynamics software package version 7.6.1.9 fitting the hydrodynamic radius as a function of PEs concentration curves. Particle size was determined with a Zetasizer Nano-ZS (Malvern Instrument, UK) based on quasi-elastic light scattering. Each measurement was performed in triplicate at an angle of 173° at 25°C. Hydrodynamic diameter and polydispersity index (PdI) were recorded for C_{10} and SNAC solutions, and mixtures of exenatide/PEs at various ratios in water, PBS and HBSS buffers.

2.3 Tensiometry

The CMC of SNAC was determined using an Attension Theta Optical Tensiometer (Biolin Scientific AB). Four buffers commonly used for permeability assays were screened: deionized water, Krebs-Henseleit buffer (KH), HBSS as well as Medium 199. The pendant drop method was used, and the surface tension was measured using freshly prepared solutions of 0-100 mM SNAC. Experimental parameters for the instrument were set using a drop size of 10 µl for a 10 s measurement. The camera was then adjusted to provide clear images with a good focus and a subsequent calibration of the instrument using a titanium sphere of known dimensions followed. For each concentration, the image of the drop was taken from a charge couple device camera and the shape of the drop was analyzed with the software to determine the surface tension. An average of the surface tension of each concentration was calculated and plotted against concentration of SNAC. Finally, the CMC was determined by extrapolation of the two straight trendlines at low and high concentration regions of surface tension. The intersection point represents the CMC.

2.4 Surface plasmon resonance

SPR measurements were performed on a Biacore T100 instrument at 25°C (GE healthcare Life Sciences, France). Three types of chip were used in the experiments: carboxymethylated dextran (CM5), streptavidin (SA) and the CAPture kit sensor chips.
Exenatide was first immobilized covalently through its primary amine groups on a CM5 sensor chip. Briefly, the carboxymethyl dextran matrix of the sensor chip surface was activated for 7 min by injection of a 1:1 mixture of 0.4 M EDC and 0.1 M NHS at 5 µl/min. Exenatide (42.5 µg/ml in 0.01 M acetate, pH 4.5) was injected for a period of 600 s at 5 µl/min. Unreacted sites on the chip surface were blocked by injection of 1 M ethanolamine-HCl (pH 8.5) for a period of 7 min. Non-specific binding (NSB) was assessed on a blank channel, also called reference channel, which follows the same coupling procedure without the peptide injection. Binding experiments were carried out by injecting C_{10} or SNAC in HBSS using a flow of 30 µl/min for 1 min and observing the dissociation over a 2 min period.

The SA sensor chip consists of streptavidin covalently immobilized on a carboxymethylated dextran matrix. Biotinylated exenatide was captured onto this chip by injecting biotin-exenatide 50 µg/ml HBS during 5 min at 5 µl/min. Free biotin (30 µg/ml) was injected in reference channels. C_{10} or SNAC in HBSS were injected during 2 min at 30 µl/min and dissociation was recorded during 10 min. To regenerate the surface, a 50 mM NaOH solution was injected for 1 min at a rate 30 µl/min.

The Biotin CAPture kit contains reagents and sensor chip for reversible capture of biotinylated molecules. The chip consists of DNA single strand attached to the matrix. Streptavidin coupled to the complementary DNA single strand is provided in the kit. The sensor chip was coated by the oligo-streptavidin solution (biotin CAPture reagent) by a 5 min injection at 2 µl / min. A solution of biotinylated exenatide (50 µg/ml in 1X HBN-N) was captured by 2 min injection at 5 µl/min flow rate, whereas the reference channel did not receive the peptide injection. A regeneration step consisting of a 2 min injection of a standard regeneration solution (3/1 v/v freshly made mixture of 8 M guanidine-HCl and 1 M NaOH) was performed at 10 µl / min between each biotin-exenatide capture. During the binding cycle, C_{10} or SNAC in HBSS were injected for 2 min at 30 µl / min and dissociation was recorded over a 4 min period. To analyze the data, the assay channel was subtracted by the control channel to eliminate nonspecific interaction with the BIAevaluation 3.1 software. Multiple sensorgrams from different concentrations of analyte were overlaid and aligned.

2.5 Isothermal titration calorimetry

ITC experiments were performed at 37°C using a Microcal VP-ITC (Malvern Panalytical, France) with a 1.441 ml sample cell. PE concentrations solutions were in excess compared to exenatide. The reference cell was filled with distilled water. The sample cell was filled with 2-30 mM C_{10} solutions or 20-60 mM SNAC solutions. The sample solution was titrated with the exenatide solution placed in the syringe at a concentration 1 or 2 mM to obtain the raw heat flow generated by the interactions between exenatide and PEs. 28 successive injections of 10 µl of 30 sec duration were carried out following an initial 2 µl first injection. The spacing between injections was set at 240 sec. To allow a homogeneous mixing in the cell during the titration, the stirring speed of the syringe was kept constant at 502 rpm. A dilution experiment was performed by injecting the exenatide solution into the buffer solution, using the same protocol as the titration experiment. In some cases, the reverse dilution can also be measured by injecting the buffer solution into the PE solution. The dilution and reverse dilution heats should stay negligible. Raw heat data was recorded for the dilution and titration experiments. They were plotted as the total heat generated per second as a function of time. The area under individual peaks (heat generated per injection) was integrated using MicroCal LLC Origin 7® into enthalpograms. The result of integrated dilution experiment was subtracted from each integrated titration experiment to take into account the heat of dilution. To avoid the contribution of heat of dilution, the exenatide and PE solutions were prepared in exactly the same buffer. The stoichiometry (n), binding constant (K_a) and enthalpy change (ΔH) were extracted from the integrated experimental data using the fit model of "one set of sites". The Gibbs free energy (ΔG) and entropy change (ΔS) were calculated from Equations 1 and 2, where R is the ideal gas constant and T is the absolute temperature.

Equation 1: $\Delta G = -RT * \ln(K_a)$, Equation 2: $\Delta G = \Delta H - T\Delta S$

2.6 Affinity capillary electrophoresis

A capillary zone electrophoresis (CZE) method was first developed to measure accurately exenatide electrophoretic mobility alone first using a bare fused silica (Section 2.6.1). Then, ACE studies were performed on coated capillaries by injecting exenatide and successively increasing the amount of PEs in the background electrolyte (BGE). The exenatide mobility was shifted to the mobility of the formed complex and the dissociation constant of the interaction was calculated (Section 2.6.2). A Sciex PA 800 plus system (Sciex Separation, CA) controlled by Karat 9.1 software (Sciex Separation, CA) was used to carry out CZE and ACE experiments. Detection were performed at 214 nm with a constant temperature (T = 25°C). Conductivity and pH values of buffer solutions and samples were acquired with a Seven Compact pH meter

(Mettler Toledo, Switzerland). Preparation of background electrolyte (BGE) and buffer ionic strength calculations were based on simulations with the computer program PhoeBus (Analis, Belgium).

2.6.1 Exenatide analysis by CZE

Bare fused silica capillaries were 60 cm total length (49.8 cm to the detector) with an internal diameter (ID) of 50 µm. The optimized BGE was 120 mM sodium phosphate pH 7.0, preferentially selected as it reflects the pH of the small intestine and ensures complete ionisation of both exenatide and PEs [66]. It was prepared as follows: 2.79 ml of the stock solution of 1 M phosphoric acid was mixed with 4.39 ml of 1 M NaOH. Deionized water was added to a total volume of 50 ml. The pH was checked and adjusted with 1 M NaOH. Pre-conditioning of fused silica capillaries procedure was similar for CZE and ACE: flushing at 50 psi for 5 min with 1 M NaOH, 5 min with 0.1 M NaOH, 5 min with water followed by 5 min with the BGE. The capillary was then equilibrated with the BGE by applying 30 kV twice for 15 min. Between runs, capillaries were rinsed by flushing 5 min with 0.1 M NaOH (50 psi), 5 min with water (50 psi), and 5 min with the BGE (50 psi). All experiments were carried out with normal polarity (cathode at the outlet). Exenatide was dissolved in PBS (0.1 or 1.2 mg/ml). Co-injection of 0.03% v/v DMSO (electroosmotic flow marker) in PBS and exenatide was made by applying a pressure of 0.5 psi for 3 sec and 10 sec respectively. 30 kV was applied during the run and samples were renewed every three runs to avoid depletion or evaporation. The electrophoretic mobility of the exenatide peak (μ_{ep}) was estimated from the apparent mobility ($\mu_{app)}$ by deducing the electroosmotic mobility (μ_{eo}).

2.6.2 Analyses of exenatide-PEs interaction in PB-DS coated capillaries by ACE

As some adsorption of exenatide and other components (like PEs or components of biorelevant media) to silica wall could render binding constants estimates inaccurate, we decided to use a coated capillary to perform ACE experiments. A double-layer, anionic-coating was used to modify the capillary using the method of Katayama *et al.* [29]. Stock solutions of cationic polybrene (PB) and dextran sulphate (DS) were prepared by dissolving solid either PB or DS in water under heating at 50°C. Bare fused silica capillary was pre-conditioned similarly to CZE. The capillary was then coated with the 10% (w/v) PB solution for 10 min at 10 psi; after 5 min the capillary was flushed with water for 5 min at 10 psi and then 3% (w/v) DS solution for 10 min at 10 psi; then again with water for 5 min under 10 psi. Electro-osmotic flow was measured using 0.03% v/v DMSO in PBS after the coating procedure to confirm proper formation of layers. The capillary was then equilibrated with the BGE by applying 20 kV for 15 min. No regeneration between runs was necessary. Overall, co-injection of 0.03% v/v DMSO marker in PBS and exenatide was made allowing the peptide to migrate in the buffer that

contained increasing concentration of PEs. Between runs, the capillary was flushed with deionized water at 10 psi for 5 min and the BGE at 10 psi for 5 min.

ACE studies with exenatide and both SNAC or C_{10} were performed in different buffers using specific conditions described in Table 1. The exenatide-C_{10} and exenatide-SNAC interactions were studied in saline buffers and also in FaSSIF and FeSSIF buffers in the case of exenatide-C_{10} (Table S2) [30]. Those biorelevant buffers use the same sodium taurocholate (NaTC) / lecithin mixture at either low or high concentrations to reflect the ratio of bile salt/phospholipids in fasted and fed states, respectively. The exenatide-SNAC interaction could not be monitored with those buffers as it directly led to a precipitation. PE stock solutions were prepared daily by adding the buffer to a weighed amount of PEs and were subsequently diluted with the BGE.

Table 1: Separation conditions for ACE studies.

System of interaction	Exenatide-C_{10}	Exenatide-C_{10}	Exenatide-SNAC
Saline buffer	-	120 mM phosphate pH 7.0	
Biorelevant buffer	FeSSIF	FaSSIF	-
[Exenatide] (mM)	1.2 mg/ml		
[C_{10}] (mM)	0-100	0-60	-
[SNAC] (mM)	-	-	0-100
Capillary ID (µm)	25	50	
Voltage (kV)	-15	-15	30
Polarity	reverse	reverse	normal
DMSO injection	1 psi for 10 sec	0.5 psi for 3 sec	
Exenatide injection	2 psi for 15 sec	0.5 psi for 10 sec	

The relative viscosity of BGE containing PEs was measured using CZE. Bare fused silica capillary was prepared as described in Section 2.6.1 and filled with the BGE containing the enhancers at 10 psi over a 2 min period. Then, 0.3% v/v DMSO in PBS was loaded at a pressure of 0.5 psi for 10 sec and a constant pressure (5 psi) was applied to the system for 3 min. The DMSO migration time was then converted into the viscosity by applying the Hagen-Poiseuille's law Equation 3 [32].

Equation 3: $\eta = t\ x\ \frac{\Delta P D^2}{32l^2}$ with ΔP the applied pressure (Pa), D the inner capillary diameter (m), l the capillary length (m) and *t* the DMSO migration time.

Consequently, exenatide electrophoretic mobilities were multiplied by a viscosity correction factor (*f*) (Equation 4):

Equation 4: $f = \frac{\eta}{\eta_0}$, with η and η_0 the viscosity of the BGE with and without PE respectively.

The electrophoretic mobility of the free exenatide (with no enhancers in the running buffer) was measured independently. Assuming a 1:1 dynamic equilibrium, binding constant determinations were based on exenatide mobility variations upon addition of increasing concentrations of PEs to the running buffer. Data were treated by direct non-linear regression based on the following Equation 5 [33]:

Equation 5: $\mu_{ep} = \frac{\mu_0 + \mu_c K[L]}{1+K[L]}$, where μ_{ep} is the experimentally determined electrophoretic mobility of exenatide (running buffer containing PE), μ_0 the electrophoretic mobility of the free exenatide (analysed without PE), μ_c that of the complexed form of exenatide with enhancer and [L] the PE concentration in the BGE. The Origin® software (version 7.0) (Microcal Software) was used to assess the agreement with the theoretical model and to determine K_D values (calculation by iterations). The K_D values was also determined using linear transformations [34]: (i) double-reciprocal, (ii) x-reciprocal and (iii) y-reciprocal.

3. Results and discussion

3.1 Colloidal characterization

3.1.1 Evaluation of the CMC of SNAC and C_{10}

SNAC and C_{10} are both anionic amphiphilic surfactants, as they contain hydrophilic (polar) and hydrophobic (non-polar) moieties. Physicochemical properties of SNAC or C_{10} including the CMC value and hydrophilic-lipophilic balance (HLB) play an important role in their permeation enhancement efficacy as they give an insight on how they behave in solution and interact with biological membranes [35]. First, we used DLS to determine the CMC of C_{10} and SNAC in different media. Plots of the hydrodynamic radius as a function of PE concentration were obtained (Figure S1). In general, at low concentrations, the intensity of scattered light detected from each PE concentration was low and similar to that obtained in buffer alone, reflecting the dissolution of SNAC or C_{10} molecules as unimers. At higher concentrations, the scattering intensity revealed a linear increase with PE concentration due to the presence of colloidal structure, indicating that the CMC was reached The intersection between the two lines at a specific concentration corresponded to the CMC of PEs. Experimental CMC values were in good agreement with those from the literature and are summarized in Table 2. The CMC of C_{10} was twice as high in deionized water compared to in PBS, whereas the CMC of SNAC was 6.5 times lower in deionized water than in PBS (6 mM compared to 39 mM). Those differences in CMC values highlight the importance of the ionic strength of the buffer and of pH, because close packing of the carboxyl head groups is strongly opposed by electrostatic repulsion unless this is offset by sufficient salt (counter ion) or acid protonation.

Table 2: CMC values for C_{10} and SNAC determined by DLS in deionized water and PBS and compared with literature when available.

	C_{10}		SNAC	
	Literature	DLS	Literature	DLS
De-ionized water	50 mM [36]	45 mM	No data	6 mM
PBS	25 mM [9]	23 mM	56 mM [10]	39 mM

As CMC values are seldom reported in the literature for SNAC, further investigations were made by tensiometry to determine the CMC values of SNAC in buffers commonly used for permeability assays: HBSS buffer (Caco-2 assays), KH buffer (isolated rat tissue assays), Medium 199 (non-everted gut sacs assays). With all buffers, the surface tension versus concentration relationship was characterized by two regions: one at a lower concentrations range, characterized by a fast decrease in the surface tension, and the other at higher concentrations at which the surface tension values remained almost constant (Figure 4). The concentration at the intercept of these two regions indicates the CMC by extrapolation. The results are presented in Table 3. A good correlation was obtained between the CMC value determined by DLS (6 mM) and by tensiometry (8 mM) in deionized water. In other buffers, CMC values of SNAC varied only slightly, ranging between 33.5 mM and 37.4 mM.

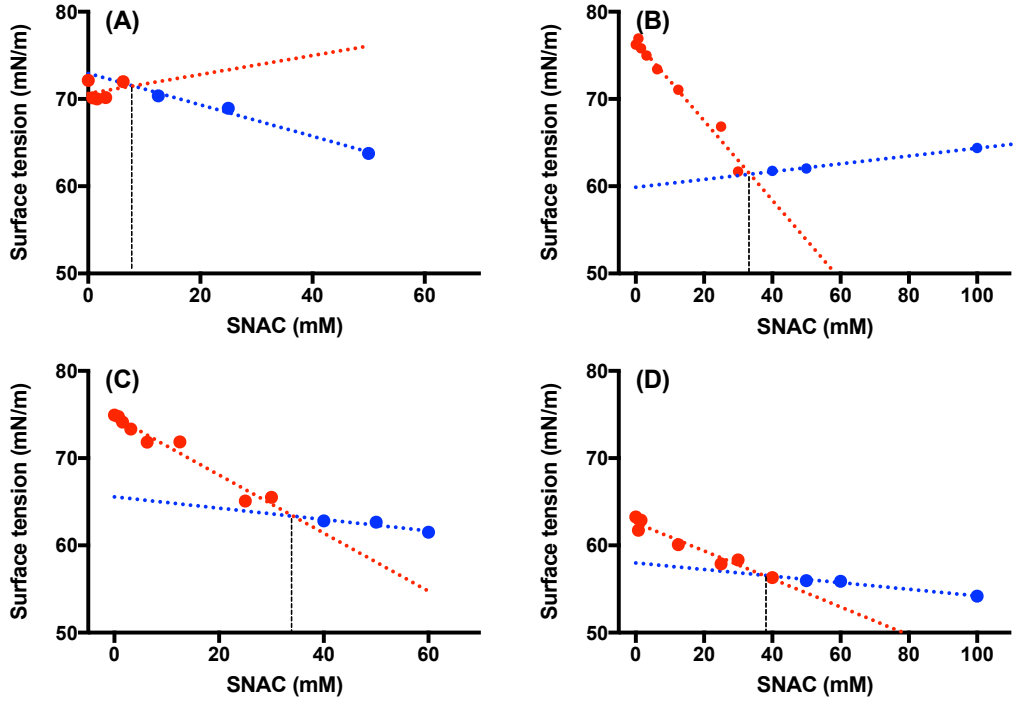

Figure 4: Effect of SNAC concentrations on the surface tension in **(A)** deionized water, **(B)** HBSS, **(C)** KH buffer and **(D)** Medium 199. Red points: described a fast decrease in surface tension, Blue points: described a stable surface tension, Red dotted line: extrapolation of the red points fit, Blue dotted line: extrapolation of the blue points fit.

Table 3: CMC values and interfacial properties of SNAC in various buffers measured by tensiometry.

Buffer	CMC (mM)	Surface tension at CMC (mN/m)
De-ionized water	8.0	71.5
HBSS	33.5	61.4
KH	34.2	63.4
Medium 199	37.4	56.6

Overall, we measured CMC values for SNAC and C_{10} in relatively simple buffers, as this threshold concentration value is closely related to permeation enhancement capacity of PEs to enhance absorption. We show that depending on the buffer, CMC values changed, so a single overall CMC value cannot be established. This variability makes it difficult to extrapolate CMC values from *in vitro* to *in vivo* where pH, temperature and solution tonicity vary to a far greater extent. In the case of C_{10}, numerous CMC values are reported in the literature and range between 10 and 100 mM [7] (Table S1). Differences among reported CMCs for C_{10} relate to buffer selection, the presence of additional surfactants, incubation temperature, and methods of measurement. For example, the CMC value for C_{10} in water at 25°C was 5-fold higher than in HBSS-without Ca^{2+} (50 mM compared to 13 mM respectively) [35]. When the temperature was set at 50°C, the CMC value in water was twice as high as at 25°C (106 mM compared to 50 mM) [36]. Walsh *et al.* determined the CMC value of C_8-C_{12} in Ca^{2+}-free Dulbecco's modified Eagle's medium (DMEM) by high resolution ultrasonic spectroscopy [37]. The CMC values for C_{10} in Ca^{2+}-free DMEM (26 mM) obtained by the method closely matched those in the literature for HBSS (28.8 mM) by Shima *et al* [38] and our own data in PBS (23 mM). Walsh *et al.* showed that as the C-chain length for MCFAs increases, CMC decreases in the aqueous medium due to the increased hydrophobicity of the alkyl chain. With CMC values of ~30 mM for both SNAC and C_{10}, similar local concentrations should be targeted under *in vivo* conditions to achieve increases in drug permeation as higher concentrations will likely cause partitioning of the PE and payload into micelles and mixed micelles.

3.1.2 Exploration of exenatide/PE complexation

DLS measurements were also used to explore the formation of macromolecular structures resulting from the interaction between PEs and exenatide in deionized water, PBS, and HBSS. To do so, size distribution profiles of exenatide alone and each PE alone were measured beforehand. For exenatide alone, high concentrations of 2 mM were required to obtain a good signal-to-noise ratio. A monodisperse distribution was observed in the 2-6 nm range, consistent with exenatide oligomer formation [39] (Table 4). The greater hydrodynamic diameter of exenatide in PBS and HBSS (6 nm and 5 nm respectively) may be attributed to the presence of large oligomeric chains compared to those obtained in de-ionized water (3

nm). The self-association number of exenatide at 2 mM in water has been previously estimated by Wang et al. and was approximated to be trimers [40]. Lee *et al.* found the particle size of native exenatide (23.5 µM) in PBS to be 3.6 ± 0.4 nm [41].

Table 4: DLS measurements for 2 mM exenatide solution. Results are expressed as mean ± SEM, with n=3.

Buffers	Size (nm)	Pdi
De-ionized water	3 ± 0.5	0.18 ± 0.02
PBS	6 ± 0.1	0.21 ± 0.05
HBSS	5 ± 0.8	0.17 ± 0.07

DLS measurements on PEs alone were performed at high concentrations (above the CMC values). For a 400 mM C_{10} solution, two peaks were present on the intensity-weighted size distribution profile for all three buffers tested. Table 5A gives the mean hydrodynamic diameters measured for the two peaks of around 2 nm and 450 nm respectively. Our results are in good agreement with previous evidence of polydisperse particulate structures of C_{10} in saline at a concentration of 200 mM using nanotracking analysis [7]. These authors indicate that C_{10} formed heterogenic-sized particles at pH 6.4-7.8. Namani *et al.* discovered using differential scanning calorimetry (DSC), that in a pH region between 6.4-7.8, the octanoic acid/sodium octanoate/water system gave rise to vesicle formation [36]. Along with the narrow pH range of vesicle formation, they noticed that a high concentration of non-associated decanoate was present with the vesicles. Similarly, in our study, we observed that C_{10} formed heterogenic-sized particles, as indicated by the presence of a small population that could correspond to C_{10} monomers/micelles and a larger population that could be vesicles. The size distribution of a SNAC solution at 100 mM in PBS or HBSS buffer presented two peaks with mean hydrodynamic diameters of around 2 nm and 200 nm respectively, as shown in Table 5B. This polydisperse structure was not fully present in water, with only a large population around 300 nm.

Table 5: Peak sizes and Pdi values of **(A)** 400 mM C_{10} solution and **(B)** 100 mM SNAC solution, measured by DLS in various media. Results are expressed as mean ± SEM, with n=3.

(A)

Buffer	Size peak 1	Size peak 2	Pdi
De-ionized water	427 ± 106	2 ± 0.1	0.6 ± 0.1
PBS	535 ± 14	3 ± 0.1	0.6 ± 0.1
HBSS	458 ± 10	3 ± 0.1	0.2 ± 0.1

(B)

Buffers	Size peak 1	Size peak 2	Pdi
De-ionized water	269 ± 26	-	0.5 ±0.1
PBS	187 ± 6	2 ± 0.1	0.3 ±0.1
HBSS	158 ± 79	1 ± 0.1	0.5 ±0.2

DLS experiments on exenatide/PE associations were then performed at a fixed exenatide concentration (1 mM) and increasing PE concentrations. Figure 5 gives the typical intensity-weighted distribution functions obtained in the case of C_{10} in various buffers. In PBS, the peak of exenatide alone at around 6 nm was hardly changed in the presence of 20 mM C_{10} (Figure 5C). However, as the concentration of C_{10} reached 50 mM (i.e above its CMC in PBS) in the presence of exenatide, a well-defined peak with a mean hydrodynamic diameter of approximately 120 nm appeared, distinct from the peak of C_{10} alone, which may indicate the formation of distinct colloidal objects resulting from the exenatide/C_{10} complexation. Visually, the solution had a colloidal aspect, consistent with the formation of supramolecular structures, as shown in Figure 5D in images (c) and (d) for 50 mM and 80 mM respectively. When higher C_{10} concentrations were used (80 mM and above) in the presence of exenatide, the size profiles in 1 mM exenatide solution were comparable with those of C_{10} alone, likely due to an excess of the latter. As a consequence, the formation of complexes between exenatide and C_{10} in PBS likely occurs at high C_{10} concentrations above the CMC. In water and HBSS, similar size distribution profiles were obtained using similar C_{10} concentrations (Figure 5A and B respectively). The colloidal aspect of the solution could also be observed at 80 mM C_{10} in water and 50 mM C_{10} in HBSS, although a macroscopic precipitation was observed from 150 mM C_{10} in HBSS. We conclude that the interaction between exenatide and C_{10} in these three media is dependent on the C_{10} concentration, which must be in a specific high range to allow formation of a supramolecular structure with exenatide.

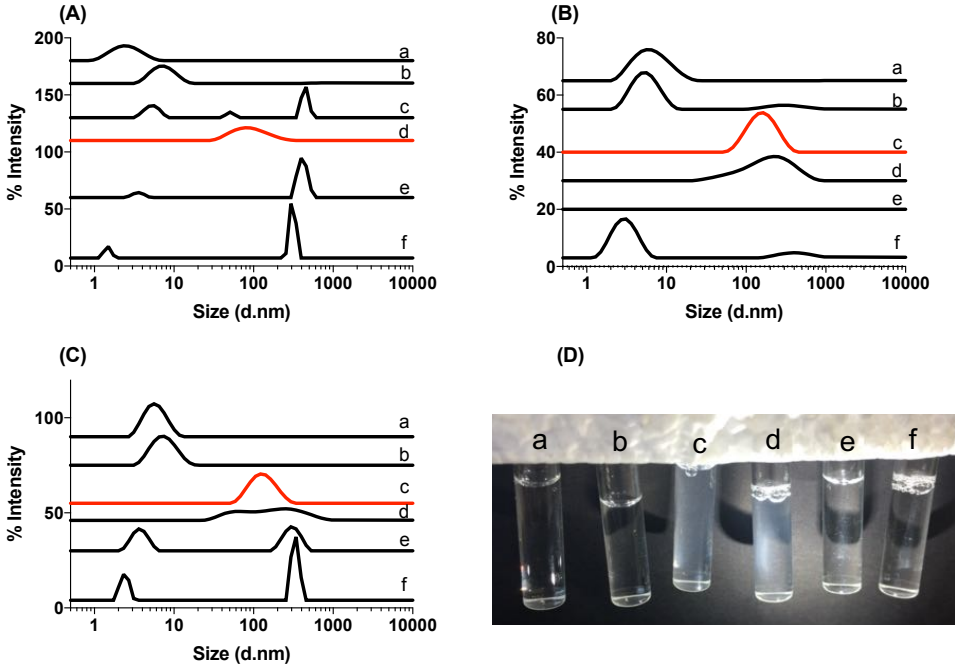

Figure 5: Intensity-weighted size distribution obtained by dynamic light scattering of exenatide and C_{10} solutions, and exenatide-C_{10} mixtures in **(A)** de-ionized water, **(B)** HBSS and **(C)** PBS. In red, highlight of a profile attributed to a complex between exenatide and C_{10}. **(D)** Visual observation of the samples in PBS. The compositions were **(a)** exenatide alone at 1 mM; **(b-e)** exenatide-C_{10} mixtures with 1 mM exenatide and (b) 20, (c) 50, **(d)** 80 and **(e)** 150 mM C_{10}. **(f)** C_{10} alone et 400 mM.

The variation in size of exenatide in the solution when adding SNAC was also studied with the same methodology. For all mixtures of 1 mM exenatide and 10-100 mM SNAC, cloudy suspensions were observed, revealing some interaction between the peptide and the PE (Figure 6). However, the hydrodynamic size of the complexes could not be measured directly by DLS in the same conditions as with C_{10}.

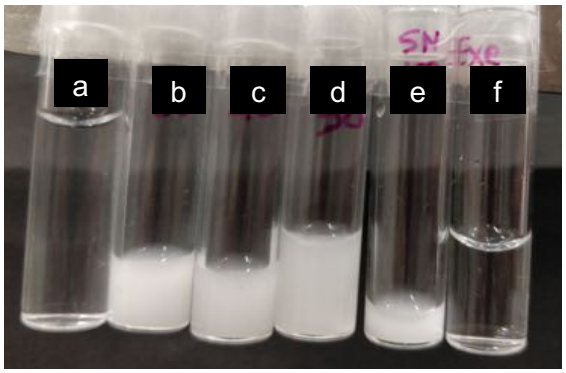

Figure 6: Visual observation of the solutions of exenatide and SNAC solutions, and exenatide-SNAC mixtures. The compositions were: (a) exenatide alone at 1 mM, (b-e) exenatide-SNAC mixtures with 1 mM exenatide and **(b)** 10, **(c)** 40, **(d)** 50, **(e)** 100 mM SNAC; and **(f)** SNAC alone at 100 mM.

In previous studies, the anionic surfactant, sodium dodecyl sulfate (SDS), when mixed with a peptide caused formation of mixed micelles and, with increasing concentration, led to peptide aggregation. The authors claimed that this phenomenon was due to charge neutralization [42]. Similar charge neutralization might occur when monomeric SNAC is mixed with exenatide to cause precipitation. Other studies showed that SDS aggregated proteins above their pI [43]. In our studies, the pH of the buffers was always higher than the exenatide pI (4.8). C_{10} shows a very closed structure compared to SDS and it could also cause aggregation, that could explain the presence of a monodisperse population detected at specific C_{10}/exenatide ratios.

3.2 Affinity measurement using SPR

3.2.1 Immobilization of exenatide on SPR sensor chips

We compared three different techniques of immobilization of exenatide on SPR sensor chips for further interaction studies (Figure 7): covalent amine coupling onto a carboxymethylated dextran (CM5)-coated sensor chip (Figure 7A); capture of biotinylated exenatide on a streptavidin (SA)-based chip (Figure 7B); a refinement of the latter technique with the streptavidin group reversely bound to the chip via DNA hybridization (Figure 7C). The purpose was to get enough signal when measuring the interaction to allow quantification of the affinity constants. Also, another challenge was to use the same sensor chip during multiple cycles involving the two different PEs with reproducible regeneration of the surface. This becomes crucial in studying interactions that are based on supramolecular construction such as micelle or complex formation, which do not display a specific character compared to a classical protein/peptide interaction for example.

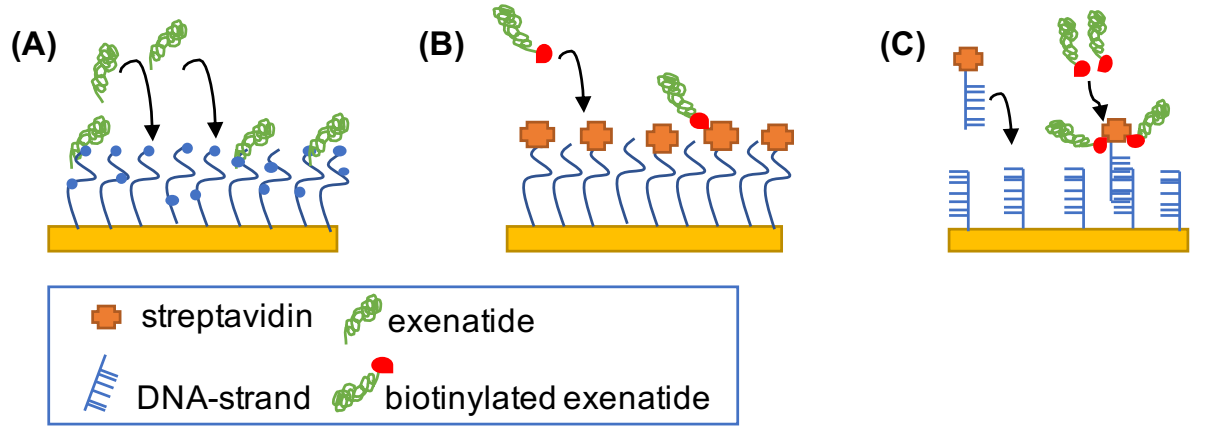

Figure 7: Schematic illustration of the three sensor chips screened for optimal interaction studies between exenatide and PEs composed of **(A)** dextran-, **(B)** streptavidin-, **(C)** DNA-based capturing surface.

The CM5 chip is composed of carboxymethylated dextran matrix covalently attached to a gold surface [44]. Exenatide immobilization should be favored when the carboxylic groups of the carboxymethyl dextran and primary amine groups of the peptide are highly ionized. A pre-concentration step induced on a CM5 chip by electrostatic interaction, promoted coupling. It was necessary to study the pH influence on the pre-concentration step to maximize the yield of covalently linked exenatide. Solutions containing exenatide at 42.5 µg/ml in 0.01 M acetate buffers at pH values of 3.5, 4, 4.5 or 5 were injected for 2 min on the CM5 chip at a rate of 5 µl/min to determine the optimal pH for immobilization. An acetate buffer (0.01 M) at pH 4.5 exhibited the highest electrostatic response in response units (RU) for exenatide. The pI of exenatide is 4.8, which therefore confers a net positive charge on it in this buffer, which facilitates electrostatic interaction between exenatide and the surface of the chip. The immobilized densities of exenatide were ~700 RU, corresponding to a theoretical maximal detection of 1700 RU of C_{10} with a stoichiometry of 50, and 4110 RU of SNAC with a stoichiometry of 80. However, the method of covalent immobilization of exenatide on the CM5 chip was based on the reaction of the primary amine groups. With exenatide, a heterogeneous surface may have been obtained due to the presence of several primary amino groups in the sequence (His, Lys, Lys, Arg). A random immobilization of exenatide might have blocked the interaction with PEs. To prepare a homogeneous sensor surface, site-directed coupling or orientation-controlled immobilization of the peptide is preferable to random covalent coupling [45].

An alternative approach to produce active surfaces is to immobilize biotinylated exenatide on a streptavidin surface on a chip [46]. This is based on the high-affinity and noncovalent interaction between biotin and streptavidin on the sensor chip ($K_D \approx 10^{-15}$ M). Advantages include reassurance that all immobilized exenatide will be in the same orientation on the

surface, as the biotin is specifically linked to a single lysine residue of the exenatide sequence. A high density of captured exenatide was obtained with a response of approximately 1200 RU. However, biotinylated exenatide was irreversibly bound to the streptavidin chip surface, preventing surface regeneration and further capture. After injection of either C_{10} or SNAC at high concentration on the surface, the baseline level was lower than the starting level just after immobilization of exenatide. Detergent-like action of the PEs could also have compromised the surface. Those reasons caused difficulties in optimization and repeatable use of this chip. Li *et al.* [47] investigated the use of a SA chip with streptavidin affinity tags fused to a protein to allow a repeated regeneration without loss of activity. However, this method involved an individualized tag for each protein.

The CAP chip is built on a carboxymethylated dextran matrix to which a ss-DNA molecule is pre-immobilized [48]. To generate the surface, a reagent composed of streptavidin conjugated with the complementary ss-DNA molecule was injected and hybridized to the surface of the sensor chip with the ss-DNA [49]. Biotinylated exenatide was then injected and captured on the streptavidin at a level of 700 RU, similar to the CM5 chip. After injecting C_{10} or SNAC, the surface was successfully regenerated and rebuilt in each cycle (as long as high PE concentrations were avoided). Because of the nature of the oligonucleotide interaction, injection of mild solutions (6 M Guanidine-HCl in 0.25 M NaOH) are able to break this interaction, leaving the surface clean for the next capture of CAP-reagent. This configuration was therefore selected. A deactivated flow cell was used as a reference where no exenatide was immobilized but was functionalized with the CAPture reagent and free biotin. In these conditions, the PE solutions prepared in HBSS at 10-80 mM were injected to flow for 1 min at 30 µl/min on the biotinylated exenatide surface to allow equilibrium to be obtained.

3.2.2 Interactions of exenatide with PEs

For both PEs, sensorgrams show a clear discernible change in RU during both association and dissociation phases, with concentration-dependency (Figure 8). For C_{10}, the association phase showed a curvature of typical specific interaction and tended to reach the equilibrium plateau. The curvature can also be seen on the dissociation phase, particularly at 40 mM C_{10}. For other concentrations, a return to baseline was observed during the dissociation, typical of weak interaction with the surface-bound exenatide. For SNAC, the kinetics differed: the association was slower as the curvature is less important. The signal was low even if the molecule is bigger in MW (the SPR signal is proportional to the MW), while the dissociation was flat. From these data, an interaction between exenatide and both PEs was observed.

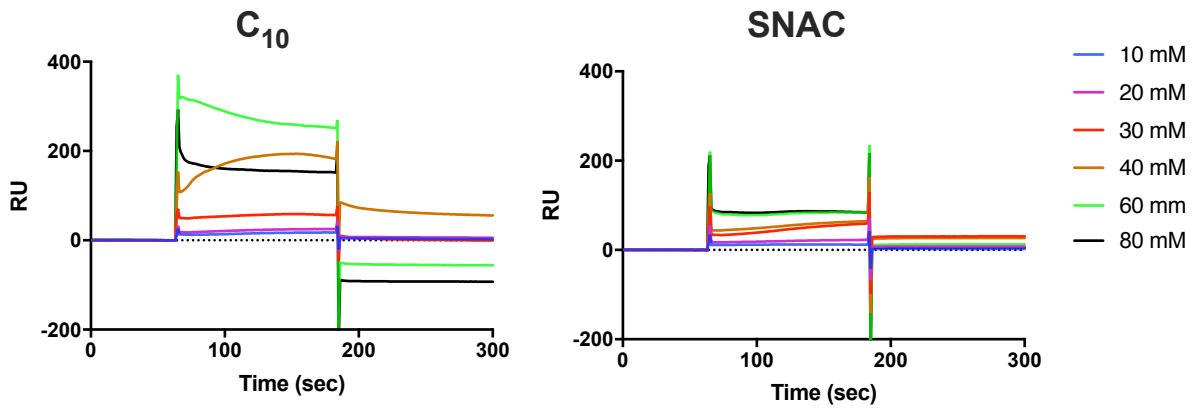

Figure 8: Overlaid sensorgrams showing the binding of C_{10} and SNAC to immobilized exenatide.

Both PEs bound weakly to the exenatide surface, as indicated by a low signal even at very high PE concentration, with a fast return to baseline during dissociation. A low specific binding of 4-14% was found between exenatide and PEs, due to the high non-specific binding on the reference cell (Figure S2). Affinity constants could not be extracted from steady state data fitting, as the interaction of PEs with exenatide could not be described by a simple 1:1 interaction model. Studies of weak-affinity interactions involving ligands with a Mw < 1000 Da usually requires both high ligand and analyte concentrations to obtain a measurable signal, as was the case here. These conditions have a major drawback with apparent loss in specific binding at high ligand concentration. Strategies to reduce non-specific binding in specific interaction studies include addition of bovine serum albumin as a blocking protein, the addition of a surfactant such as Tween 20, or addition of salt or free dextran chains to samples [50]. However, those additives could still interfere with the interaction between the peptide and the PEs.

Taken together, the SPR results revealed that C_{10} and SNAC physically interact with exenatide, however with a low specificity. Detailed quantification of the interaction was limited by the low Mw of the PEs used and the need for high concentrations. Another important limitation was the need to immobilize one of the interaction partners onto a surface, which may not fully represent the exenatide/PE association in the colloidal state.

3.3 Affinity measurements using ITC

3.3.1 System configuration and influence of the buffer

Routine ITC measurements are performed by injecting small molecule ligands into a macromolecule solution. In our case, a reverse configuration was used, with exenatide injected into the sample cell containing the PE. This configuration limits PE dilution to prevent changes in its supramolecular organisation. An additional advantage arising from this configuration was that high PE/exenatide ratios could be screened, reflecting similar predicted parameters when

formulated together in a tablet [8,52]. The titration and dilution signals were recorded in water and buffers (PBS, HBSS) (Figure 9A). In all cases, the dilution signals measured were small or negligible, supporting the choice of this configuration. Heat titration signals measured in buffers provided insufficient amplitude compared to the dilution ones, preventing further analysis of the interaction signal in these conditions (Figure 9B). In contrast, titrations in water led to significant interaction signals and were selected for further investigation.

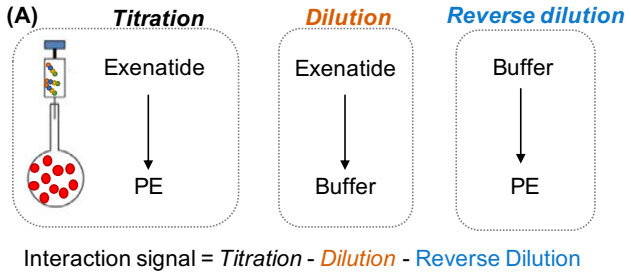

(B)

Buffer	Water	HBSS, PBS
Dilution signal	-	+
Titration signal	+++	+
Interaction signal	+++	-

Figure 9: (A) Selected ITC configurations and **(B)** Determination of the interaction signal from the recorded titration and dilution signals in various buffers.

3.3.2 Binding of exenatide to C_{10} in de-ionized water

Typical calorimetric analyses of exenatide binding to C_{10} are shown in Figure 10. The upper panel shows the rate of heat released as a function of time from 10 µl aliquots of exenatide titrated into a cell containing C_{10} solution measured at 37°C in water. The lower panel shows the integrated areas under the respective peaks from the top panel plotted against the molar ratio of exenatide added into the C_{10} solution. In the case of 4 mM C_{10}, the enthalpogram gave a large endothermic pattern, which decreased in magnitude with subsequent injections, showing saturation ($\Delta H = 20.6 \pm 0.3$ kcal.mol^{-1}). The data are best fitted by a non-linear least squares approach to the one-set-of-sites binding ("1:1 interaction model") as shown by the binding isotherms in Figure 10 (lower panel). The K_D value obtained for exenatide binding to 4 mM C_{10} was 7 ± 1 µM, and the ΔG, i.e. the free energy associated to this binding interaction, was around -7 kcal.mol^{-1} (a negative ΔG confirms that the interaction takes place spontaneously). The calculated enthalpy was around 21 cal.mol^{-1} and the entropic contribution $T\Delta S$ around 29 cal.mol^{-1}. Thus, the binding of exenatide to C_{10} is an entropy-driven process with a positive $T\Delta S$ that counteracts a positive binding enthalpy (ΔH) (see Table 6 for compiled thermodynamic data). The associated stoichiometry in these conditions was around 60 C_{10} molecules per exenatide molecule.

However, the total concentration of C_{10} in the reaction cell had a pronounced influence on this interaction, as the enthalpy profiles do not overlap (Figure 10, lower panel). In particular, the stoichiometry strongly depended on the total C_{10} concentration. The data presented in Table 6 show that the number of C_{10} molecules associated with each molecule of exenatide increased with increasing C_{10} concentration. For all three concentrations, the endothermic

binding enthalpy varied only modestly, and the negative free energy of binding also remained relatively constant. The relatively large but invariant positive binding entropies, along with positive enthalpies, indicates that exenatide binding to C_{10} remains primarily entropy driven. Such entropic control of the binding process indicates that hydrophobic interactions play a predominant role in the association between exenatide and C_{10}. The supramolecular organization of C_{10} also affects the interaction, even though it is not directly related to the CMC (above 12 mM, the interaction seems independent of the C_{10} concentration). These data also confirm that electrostatic interactions make only small contributions in the binding equilibrium of C_{10} with exenatide.

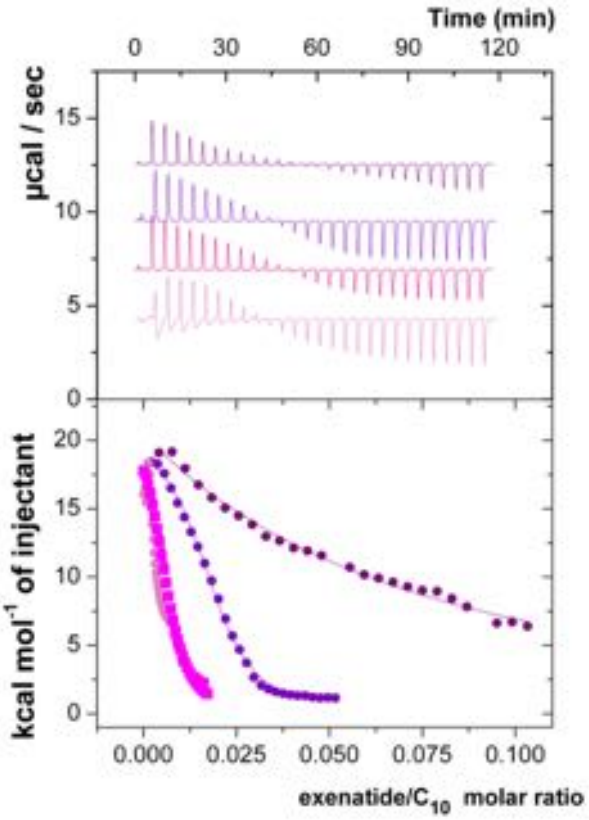

Figure 10: ITC profiles corresponding to the repeated injections of 1 mM exenatide into (●) 2 mM, (●) 4 mM, (●) 12 mM or (●) 30 mM C_{10} solution. Upper panel shows the raw data for the titration of C_{10} with exenatide. Lower panel shows the integrated heats of binding obtained from the raw data, after subtracting the heat of dilution. The solid lines represent the best curve fits to the experimental data using the one set of sites model from MicroCal Origin®.

Table 6: ITC parameters determined for the interaction of exenatide with C_{10}. (The isotherm with 2 mM C_{10} could not be analysed satisfactorily with the binding models available in the ITC analysis software).

[C_{10}] mM	n (C_{10}/exe)	K_D (µM)	ΔG (kcal.mol^{-1})	ΔH (kcal.mol^{-1})	TΔS (kcal.mol^{-1})
2	*> 10^4*	*nd*	*nd*	*nd*	*nd*
4	59 ± 6	7 ± 1	-7.21 ± 0.14	20.6 ± 0.3	27.8 ± 0.2
12	148 ± 4	21 ± 2	-6.64 ± 0.19	22.4 ± 0.9	29.0 ± 0.7
30	200 ± 15	70 ± 33	-6.06 ± 0.95	25.0 ± 4.2	31.1 ± 3.2

3.3.3 Binding of exenatide to SNAC in deionized water

The data obtained for the binding of exenatide to SNAC reveal more complex interactions than seen for C_{10}. The standard 1:1 interaction model was insufficient to fit all the data. This model was therefore used on restricted ranges of molar ratios in order to fit the main slope and then to compare the results with those obtained for C_{10}. The heat resulting from the first few additions of exenatide to SNAC were exothermic, increased in magnitude with subsequent injections, and eventually reached a plateau allowing interpretation of integrated signals (Figure 11, upper panel). The K_D values were the same order of magnitude as C_{10}, with entropic contributions counteracting positive enthalpies. As with C_{10}, the profiles obtained for different total SNAC concentration did not overlap, showing the importance of the self-organisation of SNAC. Here also, higher total concentrations of SNAC resulted in higher PE/exe stoichiometries (Table 7). The concentration ranges investigated with SNAC were higher than with C_{10} due to differences in the signal amplitude between the two PEs; unlike C_{10}, SNAC concentrations were all above its CMC in water. These observations are consistent with hypothesis that SNAC molecules form micelle-like clusters upon binding to exenatide. Further interpretations are however hampered by variations in ΔH, which may be related to the limited aqueous solubility of SNAC in water, and a tendency of dissolved SNAC to aggregate in the sample cell during the experiment.

In summary, for both PEs, some general characteristics were observed: binding to exenatide occurred with unfavourable (positive) enthalpy and highly favourable (positive) entropic changes, resulting in low affinities (K_D values in the 10-100 µM range). Those thermodynamic profiles are consistent with unfavourable electrostatic forces and can be related to hydrophobic interactions and/or water removal during exenatide association to PEs.

Feng *et al.* investigated the interaction between PAMAM dendrimers and heparin using ITC and concluded that dendrimers formed aggregates with a necklace structure on the heparin chain [53]. Also, further addition of heparin to the dendrimer solutions led to precipitation of aggregates. Similarly, Bhuyan *et al* emphasized the interaction between SDS (in the range of 0-100 mM) and ferrocytochrome c using far-UV circular dichroism [54]. These authors showed that, below its CMC, SDS monomers bind to proteins by predominantly hydrophobic interactions. At higher concentrations than the CMC, the necklace model was proposed where the micelles nucleate on the hydrophobic patches of the protein chain driving it to expand. In our study, the stoichiometry recorded by ITC indicated that more than 60 molecules of PEs interacted with exenatide thus a similar “necklace” organisation of PEs could exist along the exenatide chain. Ding *et al.* also investigated molecular interaction between SNAC and cromolyn using ITC, NMR, and FTIR spectroscopy. With ITC, injection of C_{10} into cromolyn

solution did not produce a heat of titration, indicating no interaction. Injection of SNAC into cromolyn solution indicated a weak interaction binding constant which could not be determined. As the 2-hydroxybenzamide moiety on SNAC is the only difference with C_{10} structure, the authors concluded that the existence of an interaction between SNAC and cromolyn is based on this group promoting ring stacking between the two compounds [55]. This difference could explain the more complex interaction detected with ITC in our study compared to C_{10}. In addition, the alkyl chains of SNAC and C_{10} might interact with exposed hydrophobic regions of exenatide. In both cases, a notable feature is the importance of the supramolecular organisation of the PEs (even though not strictly correlated to CMC) showing that the interaction of exenatide with the PEs is not merely micellar solubilization.

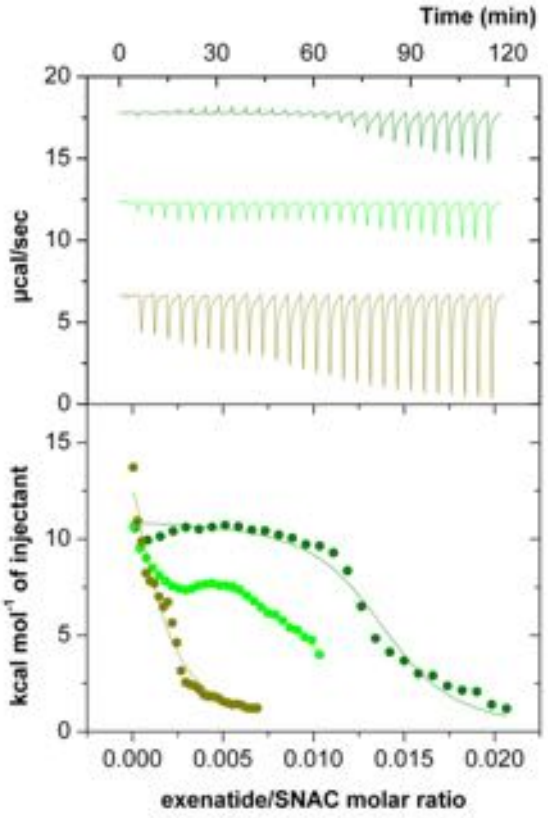

Figure 11: Integrated heat data after 2 mM exenatide injection into (●) 20 mM, (●) 40 mM, (●) 60 mM of SNAC solution. Upper panel shows the raw data for the titration of SNAC with exenatide. Lower panel shows the integrated heat of binding obtained from the raw data after subtracting the heat of dilution. The solid lines represent the best curve fits to the experimental data using the one set of sites model from MicroCal Origin®.

Table 7: Thermodynamic parameters determined for the interactions of exenatide (2 mM) with increasing SNAC concentration.

[SNAC] mM	n (SNAC/exe)	K_D (µM)	ΔG (kcal.mol^{-1})	ΔH (kcal.mol^{-1})	TΔS (kcal.mol^{-1})
20	75 ± 1	5 ± 0.8	-7.6 ± 0.2	10.4 ± 0.2	18.0 ± 0.1
40	127 ± 1	7 ± 1.1	-7.3 ± 0.2	4.0 ± 0.1	11.3 ± 0.1
60	910 ± 230	98 ± 25	-6.1 ± 0.3	14.3 ± 4.3	20.2 ± 4.0

3.4 Affinity measurement using ACE

3.4.1 Optimization of ACE conditions

In order to quantify the interaction between exenatide and PEs, we initially focused on optimization of electrophoretic conditions for the analysis of exenatide in a fast and reproducible way using CZE. Care was taken to limit exenatide and also PE adsorption to the capillary, as that could lead to artefacts when measuring affinities. The composition (sodium phosphate, sodium borate), ionic strength (from 40 to 120mM) and pH (from 7.0 to 9.0) of the background electrolyte were investigated using bare fused silica capillaries (Table 8). BGE pHs above the pI of exenatide were selected to ensure electrostatic repulsion between the anionic exenatide and negatively charged silanols [56]. Indeed, exenatide has a poly-cationic nature at pH = 7, with six positively charged amino acids present. These moieties could provide a multi-point attachment to the capillary wall. Inclusion of additives in the buffer was not explored, as they could compete with ligands during affinity measurements. Separation with sodium borate buffer gave a high variation in peak areas (RSD> 8.0%). Using phosphate buffer pH 7.4, a decrease in RSD for migration time and area was observed as the ionic strength was increased. The best separation conditions were obtained with 120 mM phosphate buffer pH 7.0.

In order to further minimize the adsorption of exenatide to the capillary wall, we evaluated the impact of a polybrene-dextran sulphate (PB-DS) double-layer coating (DL) on the repeatability of exenatide migration time (Tm) and peak area using this phosphate buffer. After 6 consecutive analyses of exenatide, repeatability of migration time was very satisfactory (RSD = 1.2 %) with a marked improvement in repeatability for peak areas (RSD = 1.6%) (Table 8). Over several days, the inter-day repeatability evaluated from different batches of capillaries (n=6), was less than 1.5% and 4.5% for Tm and peak areas respectively. As a conclusion, the PB-DS coating and the 120mM phosphate buffer were therefore found to be suitable for ACE studies.

Table 8: Reproducibility of exenatide analysis performed in different BGEs on a bare fused silica capillary and DL-coated capillary.

Capillary	Silica				DL-silica
Buffers	Borate	Phosphate			Phosphate
	pH 9.0	pH 7.4		pH 7.0	pH 7.0
	40 mM	40 mM	80 mM	120 mM	120 mM
RSD of migration times (%)	0.3	2.2	0.6	1.4	1.2
RSD of peak areas (%)	8.7	6.4	6.7	3.7	1.6

To quantify the binding of exenatide to PEs, PE was added to the BGE (up to 100 mM SNAC and 60 mM C_{10}). Thus, prior to the estimation of affinity constants, separate viscosity measurements were performed on each different BGE by CZE to determine the viscosity correction factor (f) (Section 2.6.2) to be applied to the electrophoretic mobilities estimation [57]. C_{10} or SNAC increased the viscosity of the phosphate buffer dependent on concentration as denoted by an increase in the viscosity correction factor (Figure 12A and 12B respectively). The effect was moderate with SNAC, where f increased to 1.10 for 100 mM SNAC but was more pronounced for C_{10}. Indeed, from 0 to 20 mM C_{10}, the viscosity remained stable, but a clear increase was noted from 20 to 60 mM reaching a value of 1.30 at 60 mM. At concentration above 20 mM C_{10} also increased the viscosity of FaSSIF and FeSSIF buffers. The exenatide electrophoretic mobilities were corrected accordingly with the viscosity correction factor to determine the binding constants [32].

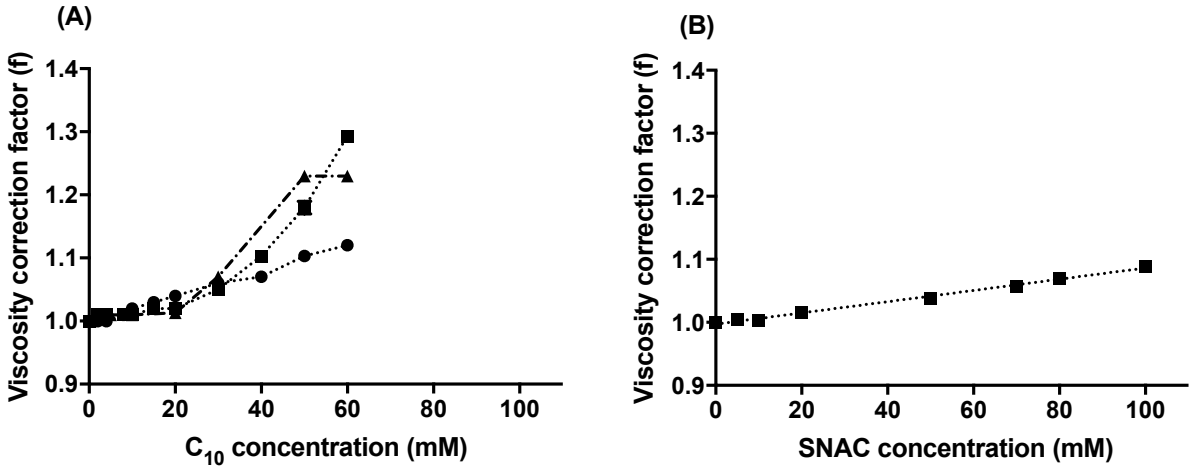

Figure 12: Viscosity correction factor determined by CE in (■)120mM phosphate buffer pH 7.0, (●) FaSSIF or (▲) FeSSIF buffer as a function of the added **(A)** C_{10} and **(B)** SNAC concentration.

3.4.2 Binding of exenatide to C_{10} in saline and biorelevant buffers

A representative series of electropherograms of exenatide in the presence of C_{10} is illustrated in Figure 13. Above 10 mM C_{10}, the exenatide peak was sharper and shifted towards the electro-osmotic flow peak with an accelerated electrophoretic mobility. With 30, 40 and 50 mM C_{10}, two peaks were observable, whereas only one remained for 60 mM C_{10}. This difference of behavior may be ascribable to difference of mobility in the exenatide/C_{10} complex or to a higher affinity of exenatide to C_{10}. Similar decrease in migration time of the negatively charged proteins (ovalbumin) by anion binding (salicylate) was previously observed [58].

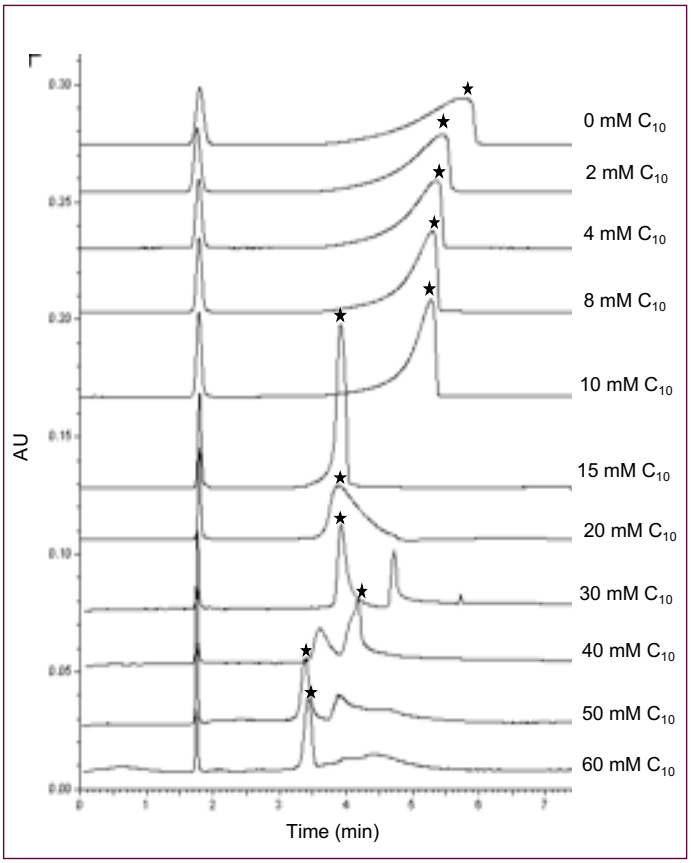

Figure 13: Electropherograms of exenatide in presence of C_{10}. Conditions: BGE, 120 mM phosphate buffer, pH 7.0; UV detection: 214 nm; temperature, 25°C; voltage -15 kV; PB-DS coated capillary 50 cm x 50 µm; hydrodynamic injection of 10 sec under 0.5 psi. Sample: exenatide at 1.2 mg/ml. Concentrations of C_{10} added to the BGE are indicated on the respective electropherograms. Black star indicates exenatide peak.

The influence of C_{10} concentration on the electrophoretic mobility of exenatide reveals a sigmoid curve as binding isotherm, with a plateau from around 30 mM C_{10} that couldn't be fitted with a nonlinear regression model (Figure 14A). The three linear regression models showed the interest of considering two regimens, below and above 20 mM C_{10} (Figure 14B, 14C and 14D). From these models, the K_D values were obtained with a correlation coefficient (r^2) > 0.99 for the first regimen and were all in the 30-45 µM range (Table 9), which confirms a low affinity. These values are in the same order of magnitude as those obtained with ITC (actually in the middle of the range of K_D values obtained in ITC for 2 mM ≤ C_{10} ≤ 40 mM). The impact of the total C_{10} concentration also confirms the importance of its supramolecular organization on its interaction with exenatide, as the 30 mM pivot point is close to its CMC value. Binding constants from the second regimens (C_{10} concentration > 20 mM) could not be properly estimated as indicated by the low correlation coefficient values.

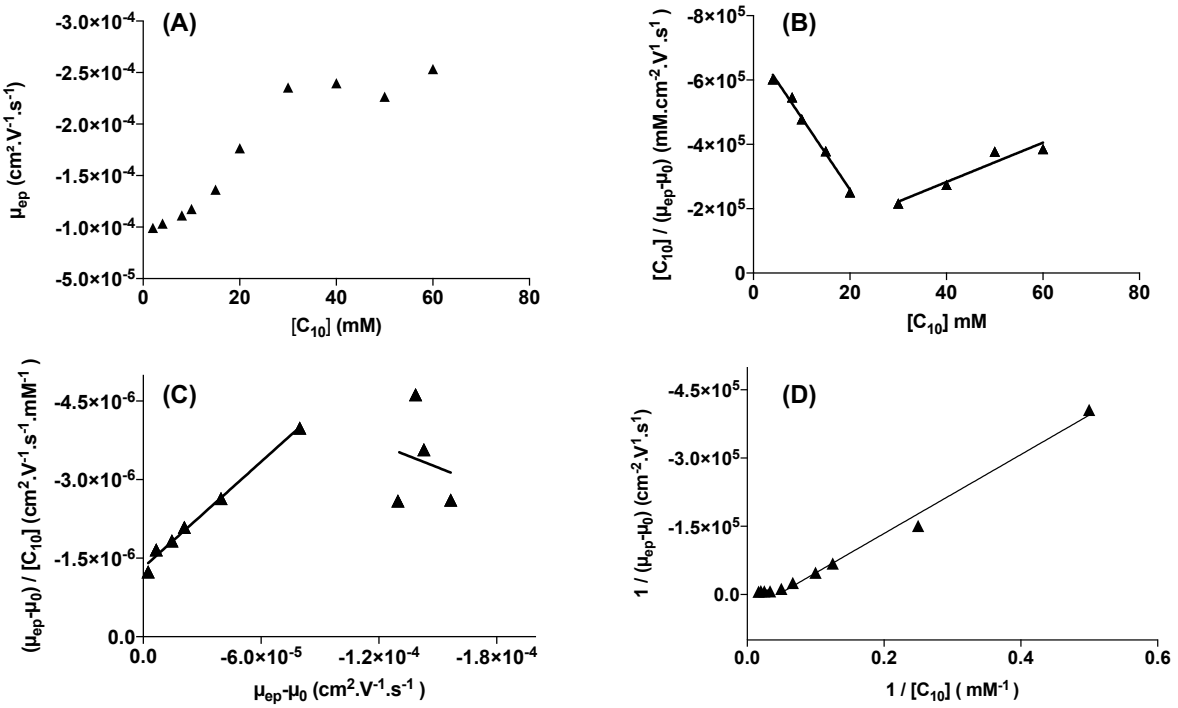

Figure 14: Binding isotherms for the exenatide-C_{10} interaction in 120 mM phosphate buffer pH 7.0. **(A)** Binding curve**; (B)** double-reciprocal plot; **(C)** x-reciprocal plot**; (D)** y-reciprocal plot. Each point represents n=3.

Table 9: Estimation of the binding constants for exenatide with C_{10} in phosphate buffer (first regimen for $C_{10} \leq 20$ mM and second regimen for $C_{10} > 30$ mM) and r^2 for each linearization method.

	First regimen K_D (µM)	r^2	Second regimen K_D (µM)	r^2
Nonlinear regression	10.2 ± 5.5	0.8995		
double reciprocal	45.3 ± 10.0	0.9914	286.9 ± 210.3	0.0883
x-reciprocal	33.6 ± 0.8	0.9904	14.8 ± 26.8	0.0296
y-reciprocal	31.6 ± 78.8	0.9906	159.0 ± 21.6	0.9203

The characteristics of exenatide-C_{10} binding was then tested similarly in the presence of FaSSIF and FeSSIF buffers. In FaSSIF buffer, the exenatide peak was only slightly shifted at low C_{10} concentrations (2-10 mM), as typically seen with weak interactions when the concentration of ligand is not high enough (Figure 15A). In contrast, a clear shift towards longer migration times was seen in FeSSIF buffer with similar C_{10} concentrations (Figure 15B). At concentrations $C_{10} > 15$ mM, broadening of the exenatide peak occurred and peaks eluted more slowly with increasing C_{10} concentration in FaSSIF buffer. It could indicate the conformational changes of exenatide upon binding with C_{10} [60]. On the contrary, in FeSSIF buffer, C_{10} binding was less influence on the exenatide migration as its elution remained stable.

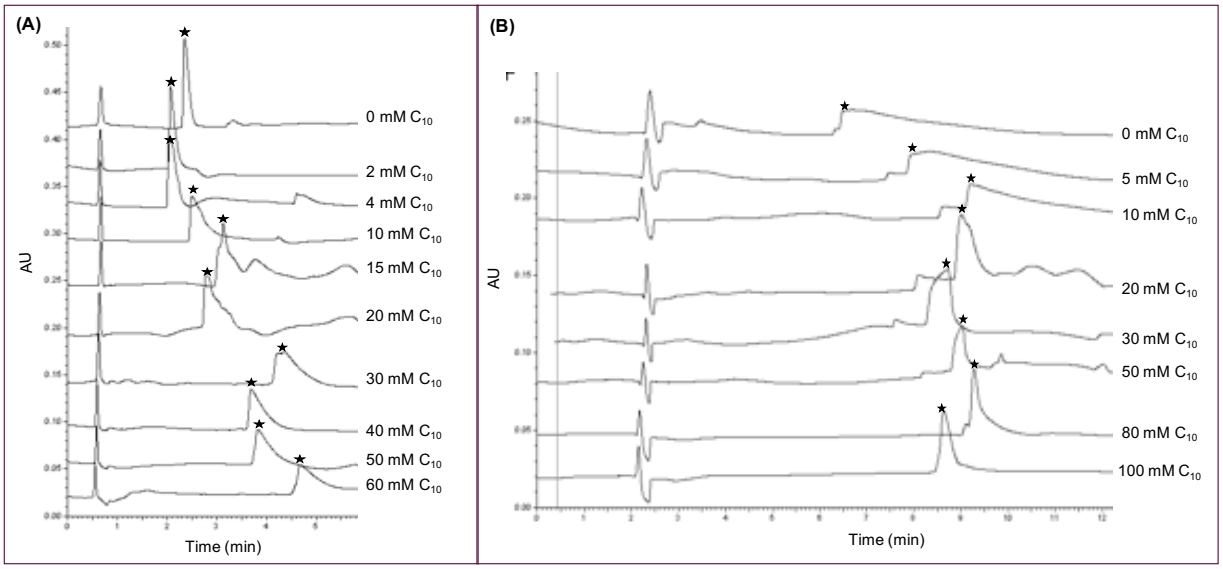

Figure 15: ACE profiles of exenatide in presence of C_{10} in a **(A)** FaSSIF and **(B)** FeSSIF buffer. Sample: exenatide at 1.2 mg/ml. Concentrations of C_{10} added to the BGE are indicated on the respective electropherograms. Conditions as described in Figure 14. Black star indicates exenatide peak.

When exenatide-C_{10} affinity was measured in biorelevant buffers, FaSSIF and FeSSIF, the binding models reveal a similar two-regimen pattern as above (Figure S3 and S4 respectively). The pivot concentration that divided the two regimens was 10 mM and 20 mM C_{10} in FaSSIF and FeSSIF respectively. Estimation of binding constants were acceptable for both regimens in FaSSIF buffer but were less precise in FeSSIF buffer (lower r^2) (Table 10). A slightly decreased affinity was estimated in biorelevant buffer compared to phosphate buffer (K_D~90 µM versus K_D~40 mM respectively). This may be explained by a change in C_{10} supramolecular organization induced by FaSSIF or FeSSIF components, as well as by a new interaction occurring between exenatide and the latter.

Table 10: Estimation of the binding constants for exenatide with C_{10} in **(A)** FaSSIF buffer (first regimen for $C_{10} \leq 10$ mM and second regimen for $C_{10} > 15$ mM) and **(B)** in FeSSIF buffer (first regimen for $C_{10} \leq 20$ mM and second regimen for $C_{10} \geqq 30$ mM) with and r^2 for each linearization method.

		First regimen K_D (µM)	r^2	Second regimen K_D (µM)	r^2
(A)	Nonlinear regression	Not applicable		-	
	double reciprocal	90.1 ± 5.8	0.9985	92.3 ± 15.9	0.9346
	x-reciprocal	87.1 ± 2.7	0.9908	84.6 ± 7.5	0.8885
	y-reciprocal	90.1 ± 14.4	0.9755	90.9 ± 25.5	0.9947
(B)	Non-linear regression	Not applicable		-	
	double reciprocal	8.2 ± 8.8	0.9453	90.1 ± 24.0	0.8901
	x-reciprocal	12.9 ± 5.2	0.4644	76.1 ± 12.7	0.7819
	y-reciprocal	10.4 ± 5.6	0.2154	92.2 ± 14.2	0.9911

3.4.3 Binding of exenatide to SNAC in saline buffer

Unlike what was observed for C_{10}, the binding curve indicated that the complexation between exenatide and SNAC did not reach saturation in the tested conditions (Figure 16). Also, all the exenatide-SNAC binding isotherms can be distinguished from the exenatide-C_{10} profiles by the presence of a unique regimen corresponding to a single equilibrium in the same 120 mM phosphate buffer (pH 7.0). However, the interaction is still weak, as indicated by the estimated K_D at around 10 µM (Table 11). This value is in the same order of magnitude as those determined by ITC for SNAC concentrations of 20-40 mM. Further studies were however limited by the lower solubility of SNAC, especially in the presence of FaSSIF and FeSSIF components.

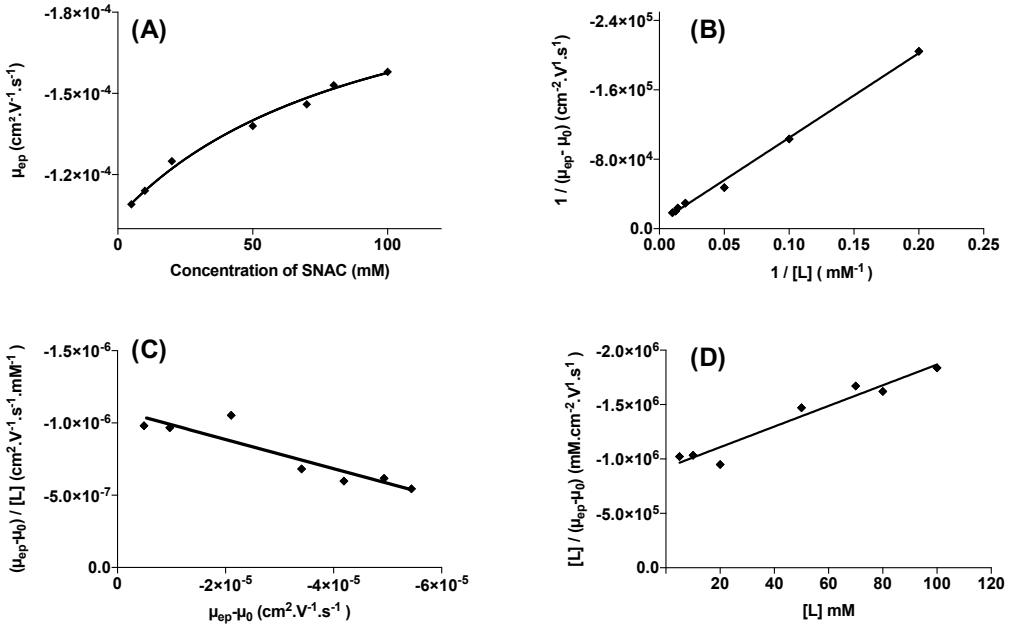

Figure 16: Binding isotherms for the exenatide-SNAC interaction in 120 mM phosphate buffer pH 7.0 **(A)** Binding curve**; (B)** double-reciprocal plot; **(C)** x-reciprocal plot**; (D)** y-reciprocal plot. Each point represents n=3.

Table 11: Estimation of the binding constants for exenatide with SNAC in phosphate buffer and r^2 for each linearization method.

	K_D (µM)	r^2
Nonlinear regression	10.4 ± 2.5	0.989
double-reciprocal	7.4 ± 2.6	0.996
x-reciprocal	10.1 ± 1.0	0.837
y-reciprocal	10.1 ± 1.0	0.941

Overall, ACE experiments confirmed the low affinity associated with the exenatide-C_{10} and -SNAC interactions. With C_{10}, despite the successful analysis conditions of exenatide including in complex media, the presence of multiple components and the supramolecular organization

of C_{10}, limit a precise quantification of the interaction but reveal the existence of several interaction regimens [61]. Progent *et al.* also emphasized the existence of several binding equilibria (multiple class binding) between polymers and peptides [62]. With SNAC, binding isotherms indicated a simpler interaction assuming a valid equilibrium with stoichiometry 1:1. Finally care must be taken in interpreting ACE data as numerous parameters other than the interaction could affect exenatide mobilities such as ionic strength [64], or conductivity [65] changes between the different BGEs used.

4. Conclusions

Four biophysical methods were used to determine the interactions between exenatide and two different PEs, C_{10} and SNAC. They provided complementary data that could enlighten understanding of the PEs/exenatide interactions as well as providing methodological insights (Figure 17). With SPR, the study of exenatide immobilization on the chip surface showed the importance of controlling exenatide orientation and regeneration for an interaction study. Exenatide/PE complexes formed, but with a high contribution of non-specific interactions, rapid binding kinetics, and overall low affinities. Supramolecular organization of the PEs was confirmed by DLS. ITC revealed that the thermodynamic signatures obtained heavily depended on total PE concentration, with unfavorable enthalpies compensated by favorable entropies upon titration with exenatide. The dominant forces driving exenatide/PE association are thought to be mainly hydrophobic ones. While low affinities of exenatide for PEs were semi-quantified in water (K_D in the 10-100 µM range), use of complex media confounded this technique. With ACE, the optimization of the separation media and capillary coating allowed successful monitoring of exenatide complexation with the PEs. Consistent affinity values were determined in saline media (K_D in the 10-30 µM range). They were also determined in the presence of simulated intestinal fluids, which were found to decrease the exenatide/C_{10} interaction strength (K_D ~ 100 µM), thereby indicating that bile salts weaken exenatide/PE association. Above the CMC, interactions are complex and are difficult to measure with advanced biophysical techniques. It is even more difficult to predict under changing pH, temperature, and solution tonicity encountered *in vivo*.

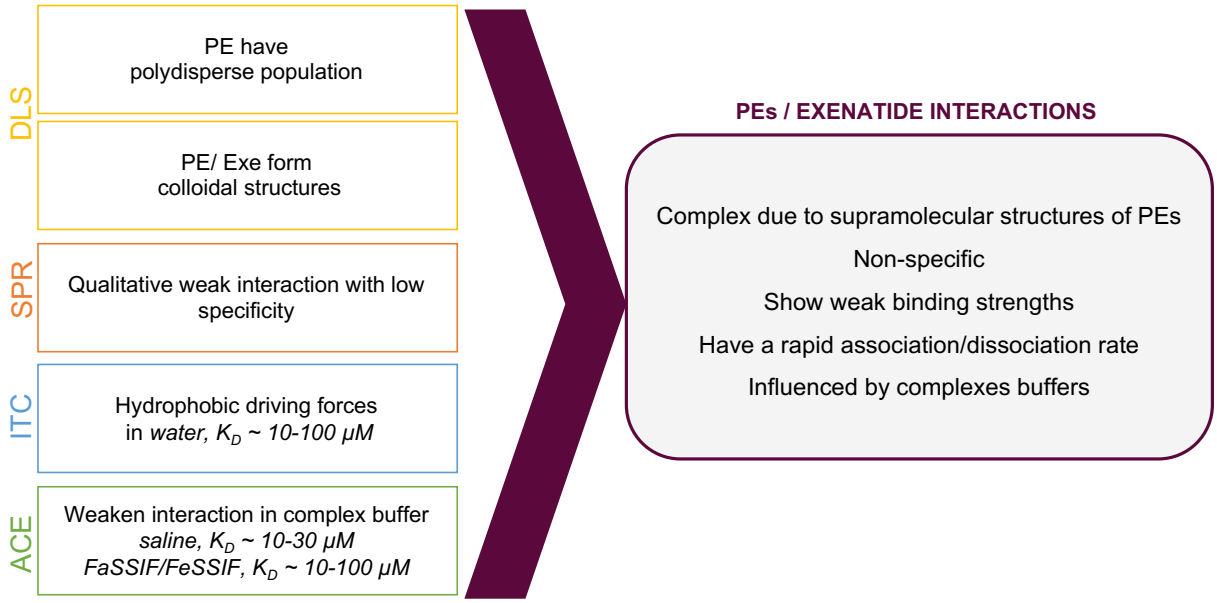

Figure 17: Summary of interaction studies between exenatide and PEs.

Acknowledgments

The authors wish to thank Prof. Myriam Taverna for her guidance in the electrophoresis experiments, Mme Magali Noiray for her help in the ITC and SPR experiment. Also Dr. Sarinj Fattah (UCD) and Dr. Waleed Faisal (University College Cork) for their help in the tensiometry experiments. Thank you to Mr. Loic Villemet from Sanofi who performed the experiments for CMC determination of PEs using DLS in water and PBS.

Supplementary data

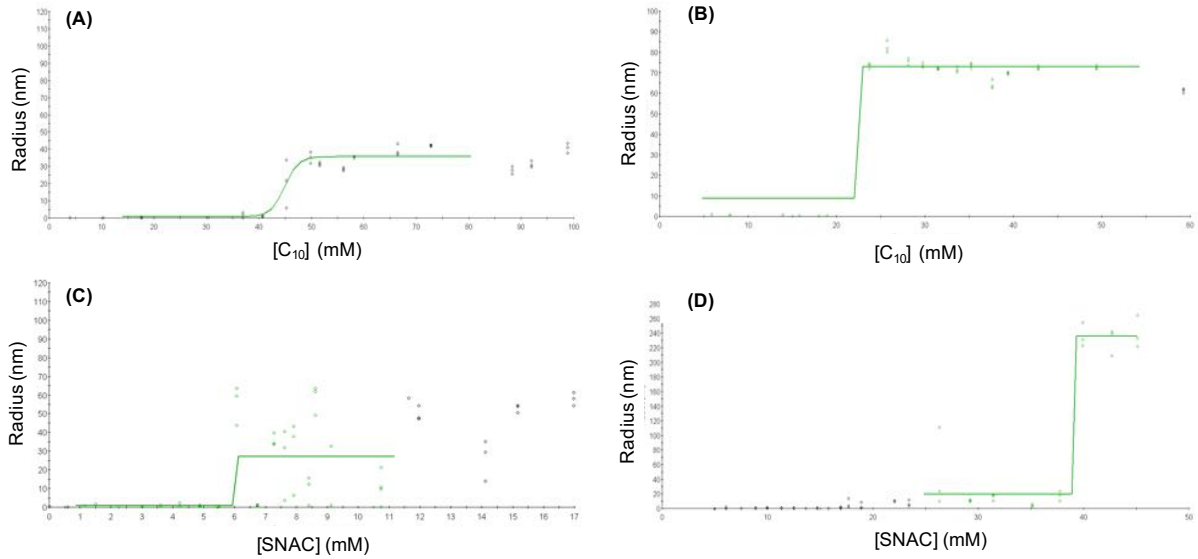

Figure S1: Variation of hydrodynamic radius as a function of permeations enhancers concentration determined by DLS with C_{10} in **(A)** deionized water and in **(B)** PBS and with SNAC in **(C)** deionized water and in **(D)** PBS.

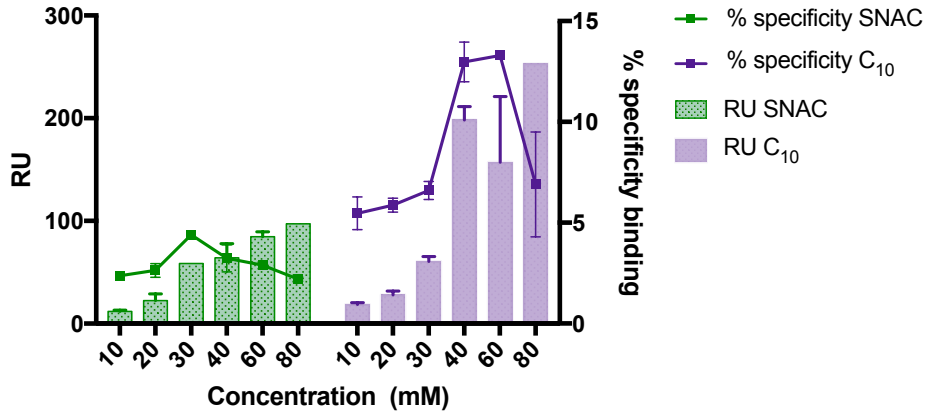

Figure S2: Binding of SNAC or C_{10} to immobilized biotinylated exenatide determined by SPR using a CAP chip with RU represented as histograms and percentage of specific binding as curves. Equilibrium responses were corrected by the reference signal from a flow cell with no immobilized peptide.

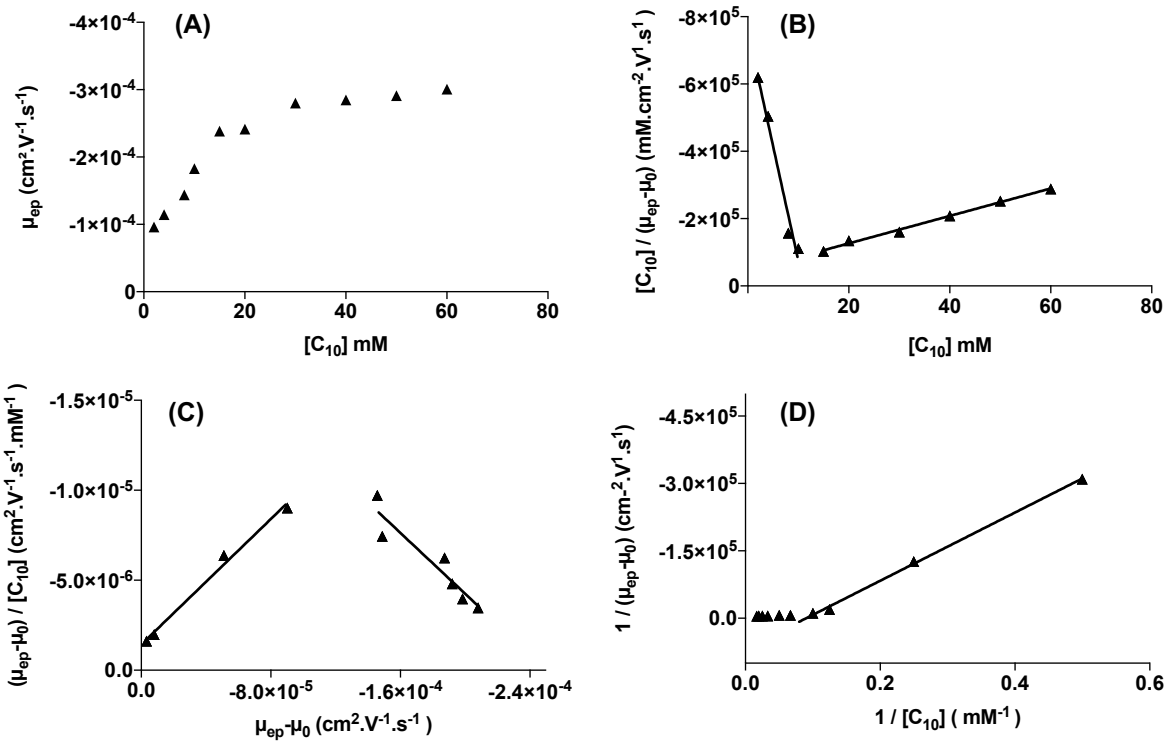

Figure S3: Binding isotherms for the exenatide-C_{10} interaction in FaSSIF. (**A)** Binding curve; **(B)** double-reciprocal plot; **(C)** x-reciprocal plot; **(D)** y-reciprocal plot. Each point represents n=3.

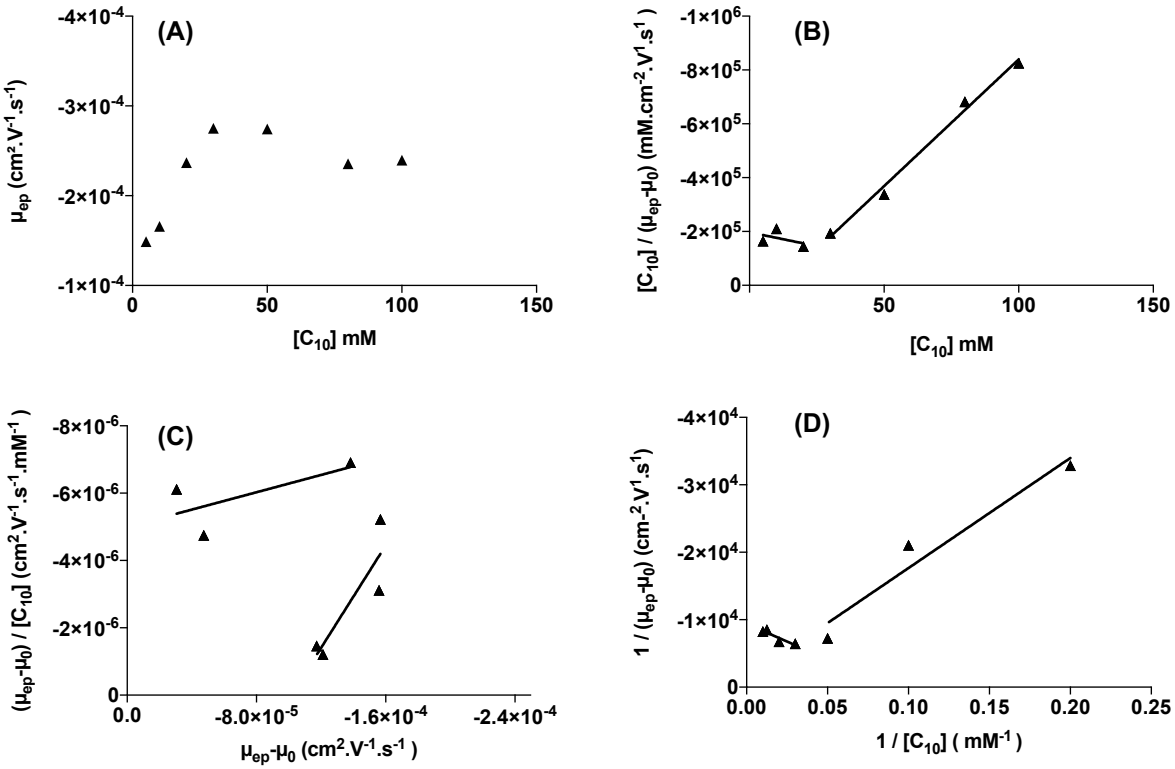

Figure S4: Binding isotherms for the exenatide-C_{10} interaction in FeSSIF **(A)** Binding curve; **(B)** double-reciprocal plot; **(C)** x-reciprocal plot; **(D)** y-reciprocal plot. Each point represents n=3.

Table S1: CMC values reported for capric acid or C_{10} in different buffers and by different methods of measurement, summarized by Maher *et al.* [7].

Buffer	CMC (mM)	Temperature (°C)	Ref.
Saline	140	20	[66]
Saline (0.9% w/v)	25-30	25-37	Unpublished data
HEPES with NaCl and KCl	45	Not specified	[67]
HEPES with NaCl, KCl and cholate (5 mM)	5	Not specified	[67]
HBSS with 25 mM HEPES without Ca2+	13	22	[68]
HBSS without Ca2+ or Mg2+	13	Room temperature	[35]
HBSS without Ca2+ or Mg2+	51	Not specified	[69]
HBSS without CaCl2	28.8	37	[70]
HBSS	28.1	Not specified	[38]
Borate buffer (50 mM) pH9	80-100	25	[71]
Water	95.5-106	25-50	[72]
Water	50	22-25	[36]

Table S2: Compositions of FaSSIF and FeSSIF biorelevant media used as BGE for ACE experiments (from [31]).

	FaSSIF	FeSSIF
Acetic acid	-	144 mM
Sodium chloride	105.9 mM	204 mM
Sodium taurocholate	3 mM	15 mM
Phosphatidylcholine	0.75 mM	3.7 mM
NaH_2PO_4, $2H_2O$	33 mM	-
Sodium hydroxide 1N	q.s. ad pH 6.5	q.s. ad pH 5.0

References

1. Aguirre, T.A., et al., *Current status of selected oral peptide technologies in advanced preclinical development and in clinical trials.* Adv Drug Deliv Rev, 2016. **106**(Pt B): p. 223-241.
2. Maher, S., R.J. Mrsny, and D.J. Brayden, *Intestinal permeation enhancers for oral peptide delivery.* Adv Drug Deliv Rev, 2016. **106**(Pt B): p. 277-319.
3. Maher, S., et al., *Formulation strategies to improve oral peptide delivery.* Pharm Pat Anal, 2014. **3**(3): p. 313-36.
4. Davies, M., et al., *Effect of Oral Semaglutide Compared With Placebo and Subcutaneous Semaglutide on Glycemic Control in Patients With Type 2 Diabetes: A Randomized Clinical Trial.* Jama, 2017. **318**(15): p. 1460-1470.
5. Halberg, I.B., et al., *Efficacy and safety of oral basal insulin versus subcutaneous insulin glargine in type 2 diabetes: a randomised, double-blind, phase 2 trial.* The Lancet Diabetes & Endocrinology, 2019. **7**(3): p. 179-188.
6. Lichtenberg, D., R.J. Robson, and E.A. Dennis, *Solubilization of phospholipids by detergents. Structural and kinetic aspects.* Biochim Biophys Acta, 1983. **737**(2): p. 285-304.
7. Maher, S., et al., *Safety and efficacy of sodium caprate in promoting oral drug absorption: from in vitro to the clinic.* Adv Drug Deliv Rev, 2009. **61**(15): p. 1427-49.
8. Halberg, I.B., et al., *The Effect of Food Intake on the Pharmacokinetics of Oral Basal Insulin: A Randomised Crossover Trial in Healthy Male Subjects.* Clin Pharmacokinet, 2019.
9. Brayden, D.J., J. Gleeson, and E.G. Walsh, *A head-to-head multi-parametric high content analysis of a series of medium chain fatty acid intestinal permeation enhancers in Caco-2 cells.* Eur J Pharm Biopharm, 2014. **88**(3): p. 830-39.
10. Alani, A.W. and J.R. Robinson, *Mechanistic understanding of oral drug absorption enhancement of cromolyn sodium by an amino acid derivative.* Pharm Res, 2008. **25**(1): p. 48-54.
11. Leone-Bay, A., et al., *N-Acylated .alpha.-Amino Acids as Novel Oral Delivery Agents for Proteins.* Journal of Medicinal Chemistry, 1995. **38**(21): p. 4263-4269.
12. Neves, J. and B. Sarmento, *Mucosal Delivery of Biopharmaceuticals: Biology, Challenges and Strategies*. 2014.
13. Mousa, S.A., et al., *Pharmacokinetics and pharmacodynamics of oral heparin solid dosage form in healthy human subjects.* J Clin Pharmacol, 2007. **47**(12): p. 1508-20.
14. Buclin, T., et al., *Bioavailability and biological efficacy of a new oral formulation of salmon calcitonin in healthy volunteers.* J Bone Miner Res, 2002. **17**(8): p. 1478-85.
15. Malkov, D., et al., *Oral delivery of insulin with the eligen technology: mechanistic studies.* Curr Drug Deliv, 2005. **2**(2): p. 191-7.
16. Leone-Bay, A., et al., *Oral delivery of sodium cromolyn: preliminary studies in vivo and in vitro.* Pharm Res, 1996. **13**(2): p. 222-6.
17. Bucheit, J.D., et al., *Oral Semaglutide: A Review of the First Oral Glucagon-Like Peptide-1 Receptor Agonist.* Diabetes Technol Ther, 2019.
18. Lorenz, M., A. Evers, and M. Wagner, *Recent progress and future options in the development of GLP-1 receptor agonists for the treatment of diabesity.* Bioorg Med Chem Lett, 2013. **23**(14): p. 4011-8.
19. Antza, C., et al., *The development of an oral GLP-1 receptor agonist for the management of type 2 diabetes: evidence to date.* Drug Des Devel Ther, 2019. **13**: p. 2985-2996.
20. Gentilella, R., et al., *Glucagon-like peptide-1 receptor agonists in type 2 diabetes treatment: are they all the same?* Diabetes Metab Res Rev, 2019. **35**(1): p. e3070.
21. Vuignier, K., et al., *Drug-protein binding: a critical review of analytical tools.* Anal Bioanal Chem, 2010. **398**(1): p. 53-66.

22. Ladbury, J.E.D., M. L., *Biocalorimetry 2: Applications of Calorimetry in the Biological Sciences*. 2004, West Sussex, England: John Wiley & Sons: Chichester.
23. Haq, I., *Thermodynamics of drug-DNA interactions.* Arch Biochem Biophys, 2002. **403**(1): p. 1-15.
24. Cliff, M.J., A. Gutierrez, and J.E. Ladbury, *A survey of the year 2003 literature on applications of isothermal titration calorimetry.* J Mol Recognit, 2004. **17**(6): p. 513-23.
25. Thanassoulas, A. and G. Nounesis, *Isothermal Titration Calorimetry: A Powerful Tool for the Characterization of Molecular Interactions*, in *Thermodynamics and Biophysics of Biomedical Nanosystems: Applications and Practical Considerations*, C. Demetzos and N. Pippa, Editors. 2019, Springer Singapore: Singapore. p. 63-103.
26. Jiang, C. and D.W. Armstrong, *Use of CE for the determination of binding constants.* Electrophoresis, 2010. **31**(1): p. 17-27.
27. Olabi, M., M. Stein, and H. Watzig, *Affinity capillary electrophoresis for studying interactions in life sciences.* Methods, 2018. **146**: p. 76-92.
28. Albishri, H.M., et al., *Recent advances in affinity capillary electrophoresis for binding studies.* Bioanalysis, 2014. **6**(24): p. 3369-92.
29. Katayama, H., Y. Ishihama, and N. Asakawa, *Development of Novel Capillary Coating Based on Physical Adsorption for Capillary Electrophoresis.* Analytical Sciences, 1998. **14**(2): p. 407-408.
30. Klein, S., *The use of biorelevant dissolution media to forecast the in vivo performance of a drug.* Aaps j, 2010. **12**(3): p. 397-406.
31. Klein, S., *The use of biorelevant dissolution media to forecast the in vivo performance of a drug.* The AAPS journal, 2010. **12**(3): p. 397-406.
32. Allmendinger, A., et al., *High-throughput viscosity measurement using capillary electrophoresis instrumentation and its application to protein formulation.* J Pharm Biomed Anal, 2014. **99**: p. 51-8.
33. Ehala, S., et al., *Affinity capillary electrophoretic study of K+/Na+ selectivity of hexaarylbenzene-based polyaromatic receptor.* Procedia Chemistry, 2010. **2**(1): p. 14-19.
34. Tanaka, Y. and S. Terabe, *Estimation of binding constants by capillary electrophoresis.* J Chromatogr B Analyt Technol Biomed Life Sci, 2002. **768**(1): p. 81-92.
35. Lindmark, T., T. Nikkila, and P. Artursson, *Mechanisms of absorption enhancement by medium chain fatty acids in intestinal epithelial Caco-2 cell monolayers.* J Pharmacol Exp Ther, 1995. **275**(2): p. 958-64.
36. Namani, T. and P. Walde, *From Decanoate Micelles to Decanoic Acid/Dodecylbenzenesulfonate Vesicles.* Langmuir, 2005. **21**(14): p. 6210-6219.
37. Brayden, D.J. and E. Walsh, *Efficacious intestinal permeation enhancement induced by the sodium salt of 10-undecylenic acid, a medium chain fatty acid derivative.* Aaps j, 2014. **16**(5): p. 1064-76.
38. Shima, M., et al., *Effects of medium-chain fatty acids and their acylglycerols on the transport of penicillin V across Caco-2 cell monolayers.* Biosci Biotechnol Biochem, 1997. **61**(7): p. 1150-5.
39. Hudson, F.M. and N.H. Andersen, *Exenatide: NMR/CD evaluation of the medium dependence of conformation and aggregation state.* Biopolymers, 2004. **76**(4): p. 298-308.
40. Wang, S., et al., *Structural study of an active analog of EX-4 in solution and micelle associated states.* Biopolymers, 2011. **96**(3): p. 348-57.
41. Lee, J., et al., *Preparation and evaluation of palmitic acid-conjugated exendin-4 with delayed absorption and prolonged circulation for longer hypoglycemia.* Int J Pharm, 2012. **424**(1-2): p. 50-7.
42. Otzen, D.E., et al., *Aggregation of S6 in a quasi-native state by sub-micellar SDS.* Biochim Biophys Acta, 2008. **1784**(2): p. 400-14.
43. Gitlin, I., J.D. Carbeck, and G.M. Whitesides, *Why are proteins charged? Networks of charge-charge interactions in proteins measured by charge ladders and capillary electrophoresis.* Angew Chem Int Ed Engl, 2006. **45**(19): p. 3022-60.

44. Johnsson, B., S. Lofas, and G. Lindquist, *Immobilization of proteins to a carboxymethyldextran-modified gold surface for biospecific interaction analysis in surface plasmon resonance sensors.* Anal Biochem, 1991. **198**(2): p. 268-77.
45. Shi, J.-X., et al., *Improvement of Homogeneity of Analytical Biodevices by Gene Manipulation.* Analytical Chemistry, 2004. **76**(3): p. 632-638.
46. Liu, Y. and W.D. Wilson, *Quantitative analysis of small molecule-nucleic acid interactions with a biosensor surface and surface plasmon resonance detection.* Methods Mol Biol, 2010. **613**: p. 1-23.
47. Li, Y.J., et al., *Reversible immobilization of proteins with streptavidin affinity tags on a surface plasmon resonance biosensor chip.* Anal Bioanal Chem, 2006. **386**(5): p. 1321-6.
48. Rogez-Florent, T., et al., *Amine coupling versus biotin capture for the assessment of sulfonamide as ligands of hCA isoforms.* Anal Biochem, 2016. **511**: p. 42-51.
49. Hutsell, S.Q., et al., *High-affinity immobilization of proteins using biotin- and GST-based coupling strategies.* Methods Mol Biol, 2010. **627**: p. 75-90.
50. Drescher, D.G., N.A. Ramakrishnan, and M.J. Drescher, *Surface plasmon resonance (SPR) analysis of binding interactions of proteins in inner-ear sensory epithelia.* Methods Mol Biol, 2009. **493**: p. 323-43.
51. Hearty, S., et al., *Measuring Antibody-Antigen Binding Kinetics Using Surface Plasmon Resonance.* Methods Mol Biol, 2018. **1827**: p. 421-455.
52. Tillman, L.G., R.S. Geary, and G.E. Hardee, *Oral delivery of antisense oligonucleotides in man.* J Pharm Sci, 2008. **97**(1): p. 225-36.
53. Feng, X., et al., *Host-guest chemistry of dendrimer-drug complexes. 5. Insights into the design of formulations for noninvasive delivery of heparin revealed by isothermal titration calorimetry and NMR studies.* J Phys Chem B, 2010. **114**(34): p. 11017-26.
54. Bhuyan, A.K., *On the mechanism of SDS-induced protein denaturation.* Biopolymers, 2010. **93**(2): p. 186-99.
55. Ding, X., et al., *Oral absorption enhancement of cromolyn sodium through noncovalent complexation.* Pharm Res, 2004. **21**(12): p. 2196-206.
56. Stutz, H., *Protein attachment onto silica surfaces--a survey of molecular fundamentals, resulting effects and novel preventive strategies in CE.* Electrophoresis, 2009. **30**(12): p. 2032-61.
57. Ostergaard, J., H. Jensen, and R. Holm, *Use of correction factors in mobility shift affinity capillary electrophoresis for weak analyte-ligand interactions.* J Sep Sci, 2009. **32**(10): p. 1712-21.
58. Xu, Y., et al., *Precise, fast, and flexible determination of protein interactions by affinity capillary electrophoresis: part 3: anions.* Electrophoresis, 2014. **35**(15): p. 2203-12.
59. Holm, R., et al., *Complexation of tauro- and glyco-conjugated bile salts with alpha-cyclodextrin and hydroxypropyl-alpha-cyclodextrin studied by affinity capillary electrophoresis and molecular modelling.* J Sep Sci, 2011. **34**(22): p. 3221-30.
60. Chu, Y.H. and C.C. Cheng, *Affinity capillary electrophoresis in biomolecular recognition.* Cell Mol Life Sci, 1998. **54**(7): p. 663-83.
61. Sun, P., A. Hoops, and R.A. Hartwick, *Enhanced albumin protein separations and protein-drug binding constant measurements using anti-inflammatory drugs as run buffer additives in affinity capillary electrophoresis.* J Chromatogr B Biomed Appl, 1994. **661**(2): p. 335-40.
62. Progent, F., et al., *A study of the binding between polymers and peptides, using affinity capillary electrophoresis, applied to polymeric drug delivery systems.* Electrophoresis, 2002. **23**(6): p. 938-44.
63. Redweik, S., Y. Xu, and H. Wätzig, *Precise, fast, and flexible determination of protein interactions by affinity capillary electrophoresis: Part 1: Performance.* ELECTROPHORESIS, 2012. **33**(22): p. 3316-3322.
64. Sazelova, P., et al., *Determination of binding constants of multiple charged cyclodextrin complexes by ACE using uncorrected and ionic strength corrected actual mobilities of the species involved.* Electrophoresis, 2019.

65. Ouadah, N., et al., *Mobility Shift Affinity Capillary Electrophoresis at High Ligand Concentrations: Application to Aluminum Chlorohydrate–Protein Interactions.* ACS Omega, 2018. **3**(12): p. 17547-17554.

66. Van Hoogdalem, E.J., et al., *Absorption enhancement of rectally infused cefoxitin sodium by medium-chain fatty acids in conscious rats: concentration-effect relationship.* Pharm Res, 1988. **5**(7): p. 453-6.

67. Lapre, J.A., et al., *Lytic effects of mixed micelles of fatty acids and bile acids.* Am J Physiol, 1992. **263**(3 Pt 1): p. G333-7.

68. Lindmark, T., Y. Kimura, and P. Artursson, *Absorption enhancement through intracellular regulation of tight junction permeability by medium chain fatty acids in Caco-2 cells.* J Pharmacol Exp Ther, 1998. **284**(1): p. 362-9.

69. Sakai, M., et al., *Cytotoxicity of absorption enhancers in Caco-2 cell monolayers.* J Pharm Pharmacol, 1998. **50**(10): p. 1101-8.

70. Kimura, Y., et al., *Physico-chemical Properties of Fatty Acids for Assessing the Threshold Concentration to Enhance the Absorption of a Hydrophilic Substance.* Biosci Biotechnol Biochem, 1998. **62**(3): p. 443-7.

71. Morigaki, K., et al., *Thermodynamic and kinetic stability. Properties of micelles and vesicles formed by the decanoic acid/decanoate system.* Colloids and Surfaces A: Physicochemical and Engineering Aspects, 2003. **213**(1): p. 37-44.

72. Campbell, A. and G. Lakshminarayanan, *Conductances and surface tensions of aqueous solutions of sodium decanoate, sodium laurate, and sodium myristate, at 25 and 35.* Canadian Journal of Chemistry, 2011. **43**: p. 1729-1737.

Chapter 3

Comparison of the mechanisms of action of SNAC and C_{10} in Caco-2 assays

Chapitre 3 : Comparaison des mécanismes d'actions de SNAC et C_{10} sur cellules Caco-2

Résumé

Le salcaprozate de sodium (SNAC) et le caprate de sodium (C_{10}) sont les principaux promoteurs d'absorption utilisés dans les formulations orales pour la délivrance de peptides. Cependant leur mécanisme d'action fait toujours débat. Le but de cette étude était de (i) comparer leur effet promoteur par mesure de la résistance électrique transépithéliale (TEER) et la perméabilité du FITC-dextran 4000 (FD4) au travers de monocouches différenciées de Caco-2, et évaluer la localisation des protéines associées aux jonctions serrées par immunohistochimie, et (ii) de comparer leur impact sur les paramètres cellulaires en utilisant des essais de cytotoxicité conventionnels et quantifier ces multiples paramètres par *high content analysis* (HCA) dans les cellules Caco-2. Le C_{10} (8.5 mM) réduit la TEER de façon réversible et augmente la perméabilité du marqueur FD4 au travers des monocouches de Caco-2 alors que le SNAC n'a aucun effet sur les deux paramètres exceptés à des concentrations excessives. L'immunomarquage a confirmé que le C_{10} a entrainé la réorganisation de trois protéines des jonctions serrées alors que SNAC n'a affecté que la localisation de la claudine-5. Les tests de cytotoxicité ont indiqué que le SNAC était moins actif que le C_{10} dans l'induction de déstabilisation des lysosomes, des noyaux et de la membrane plasmique. D'après les analyses par HCA (*High Content Analysis*), le potentiel de la membrane mitochondriale et le calcium intracellulaire des cellules Caco-2 ont été altérés suite à une exposition au C_{10} et au SNAC mais suivant des schémas d'altération différents. Dans l'ensemble, de fortes concentrations de C_{10} et SNAC ont été nécessaires pour provoquer des changements sublétaux à l'échelle cellulaire, ce qui correspond à leur absence connue de toxicité *in vivo*. Les expériences par HCA ont confirmé que les deux surfactants présentent des caractéristiques semblables à celle d'un détergent qui reflète la fluidisation initiale de la membrane plasmique suivie de perturbation de l'homéostasie cellulaire. En conclusion, les augmentations de perméabilité de FD4 dans les monocouches Caco-2 en réponse au C_{10} se sont produites à des concentrations similaires à celles qui ont modifié les paramètres cellulaires. Pour le SNAC, une altération de la cellule a été confirmé même en l'absence d'augmentation du flux paracellulaire.

Mots clés : Délivrance orale de peptide, promoteurs d'absorption intestinale, jonctions serrées, cytotoxicité d'excipient, caprate de sodium, SNAC.

Chapter 3: Comparison of the mechanisms of action of SNAC and C_{10} in Caco-2 assays

Abstract

Salcaprozate sodium (SNAC) and sodium caprate (C_{10}) are two leading intestinal permeation enhancers (PEs) in advanced oral peptide formulations. There is debate over their mechanism of action on intestinal epithelia. The aims were: (i) to compare their effects on the barrier function by measuring transepithelial electrical resistance (TEER) and permeability of FITC-labelled dextran 4000 (FD4) across Caco-2 monolayers, along with immunohistochemistry of tight junction (TJ)-associated proteins; and (ii) to compare cellular parameters using conventional end-point cytotoxicity assays and quantitative high content analysis (HCA) of multiple sub-lethal parameters in Caco-2 cells. C_{10} (8.5 mM) reversibly reduced TEER and increased FD4 permeability across monolayers, whereas SNAC had no effect on either except at very high concentrations. Immunostaining confirmed that C_{10} exposure led to reorganization of three TJ proteins, whereas SNAC only affected claudin-5 localization. End-point toxicology assays indicated that SNAC was less potent than C_{10} at inducing lysosomal and nuclear changes and plasma membrane perturbation. According to HCA, mitochondrial membrane potential and intracellular calcium in Caco-2 cells were altered by both C_{10} and SNAC exposure after 2h, but with different patterns. Overall, high concentrations of C_{10} and SNAC were required to cause sub-lethal changes, consistent with their known lack of toxicity *in vivo*. HCA confirmed that both surfactants display detergent-like features that reflect initial membrane fluidization followed by changes in intracellular parameters. In conclusion, FD4 permeability increased in monolayers in response to C_{10} and occurred at similar concentrations as those that altered HCA parameters. For SNAC, HCA parameters were altered, even in the absence of paracellular flux increases.

Keywords: Oral peptide delivery, intestinal permeation enhancers, tight junctions, excipient cytotoxicity, sodium caprate, SNAC

1. Introduction

Cell-based cytotoxicity assays are used to measure parameters involved in differentiation, apoptosis and necrosis. Mechanistic parameters can be monitored to probe cytotoxicity including lysosomal function, release of intracellular contents, chromatin condensation, metabolite content, mitochondrial function, and apoptosis [1]. Common endpoints assays involve direct measurements of cellular changes after a short- or long-term exposure to a chemical [2]. 96-well readouts on cells have advantages in being straightforward, and of sufficient throughput to generate statistical metrics on assay performance. However, with traditional cell-based screens, a limitation is that only average responses over cell populations are obtained and the full diversity and asynchronicity of individual cellular changes are summated [3]. The development of quantitative microscopic technologies to explore mechanisms of cytotoxicity at individual sub-cellular level has been a major advance.

High content analysis (HCA) is an automated technology that combines the accuracy of fluorescent microscopy with the throughput of flow cytometry [4]. Compared to conventional assays, HCA encompasses multi-parametric monitoring and simultaneously detects molecular and cellular effects at single cell scale [3,5]. A cocktail of fluorescent markers enables contemporaneous imaging and detection of organelle health in live cells [6]. Over a wide range of time points and concentrations, the intensities and kinetics of multiple fluorescent dye signals can record intracellular activities in parallel [7]. Following image acquisition, HCA software can perform object segmentation of the subcellular structures from which the intensities originate allowing quantitative morphometric analysis [5]. Parameters can therefore calculate changes in cell number (CN), nuclear area (NA), nuclear intensity (NI), mitochondrial membrane potential (MMP), plasma membrane permeability (PMP), and intracellular calcium (IC). This yields information on the number, shape, and size of individual cells, assessment of their nuclei and other membrane organelles, as well as mitochondrial and plasma membrane barrier function [6, 8, 9].

A HCA human hepatocytes model demonstrated high sensitivity for detecting potential human toxicity as part of an analysis of 250 marketed drugs compared to conventional cytotoxicity assays [10]. O'Brien *et al.* found out that concordance with liver human toxicity was an order of magnitude higher for the HCA assay compared to conventional assays. False negatives typically exceeded 80% for conventional assays, but they were less than 10% for HCA. HCA has been widely used in discovery by the pharmaceutical industry for optimization and prioritization of lead molecules [11-13], and HCA has been successfully applied in pre-clinical assessment of toxicity using a wide range of substances for numerous cell types [14]. HCA

allows a rapid and low-cost screening for toxicity potential which may reduce and refine preclinical animal studies. Tomida *et al.* used manual methods for cytotoxicity assays and demonstrated that, even without the use of automated HCA, multiple assays were more effective than single assays at predicting toxicity [15]. However, such manual and single-signal assays are substantially more labour intensive, time consuming, and costly, as well as being less precise than those of an automated assay. No single cell parameter will definitively detect adverse effects and accurately predict toxicity potential *in vivo*.

Increasing oral absorption of peptides via perturbation of the intestinal mucosa has been achieved using surfactant-based permeation enhancers (PEs) in over 50 clinical studies [16]. The leading PE candidates in these trials include medium chain fatty acids (MCFAs), acyl carnitines, bile salts, and ethylenediaminetetraacetic acid (EDTA) [17]. The MCFA, sodium caprate (C_{10}), and the C_8 derivative, salcaprozate sodium (SNAC), are of particular interest as there are the key components of advanced solid-dose oral peptide formulations and have over 20 years of clinical trials behind them. SNAC (Emisphere, NJ, USA) was assessed in multiple Phase III PIONEER trials in tablets with the Glucagon-like-1 peptide analogue, semaglutide [18, 19]. Consequently, Rybelsus® (Novo-Nordisk, Copenhagen, Denmark) was approved by FDA in 2019 as the first daily oral peptide formulation for the treatment of type 2 diabetes. SNAC was previously approved as an oral vitamin B_{12} under Medical Food regulations [20], so it has had extensive preclinical and clinical toxicology assessment in oral dosage forms.

In parallel, C_{10} was the main component of the GIPET™ (Merrion Pharmaceuticals, Dublin, Ireland) oral peptide formulations, including a Phase II trial of a long t½ basal insulin [21]. Current data suggests that C_{10} combines a tight junction-opening mediated by intracellular pathways associated with an initial mild plasma membrane perturbation *in vitro* [22]. In contrast, SNAC is thought to primarily act via a non-covalent chaperone mechanism for payloads involving the transcellular lipophilic pathway across small intestinal epithelia [23]. Recently, a new mechanism for SNAC specifically in respect of oral delivery of semaglutide was demonstrated. It increased stomach pH immediately around the tablet thereby rendering pepsin inactive [24]. This latter mechanism might still be consistent with the chaperone theory, albeit in the gastric epithelium. HCA can therefore allow conclusions to be made on mechanistic differences between effects of SNAC and C_{10} on Caco-2 cells.

It is necessary to better understand potential intestinal epithelial toxicity that might be caused by surfactant-based PEs since there is usually a close association of mucosal perturbation with increases in drug permeability [25]. Previous HCA studies revealed that when Caco-2 cells on 96 well plates were exposed to 8.5 mM C_{10} for 60 min, NI, IC, NA, PMP, MMP, and

CN were all increased [22]. Higher concentrations of C_{10} and longer exposure times caused cell death as determined by the MTT assay, so these HCA data reflect reversible sub-lethal effects that yield insights into the mechanisms of action of C_{10}. Overall, these data [22] provided rank-order data on the parameters for the sodium salts of a series of MCFAs. C_{10} was not the the most effective MCFA, but had more favourable parameters and better solubility than the higher chain length MCFA, C_{12}. SNAC has never been assessed by HCA in any cell type.

The first aim of this study was to investigate the individual effects of SNAC and C_{10} on intestinal permeability and tight junction (TJ) localization in Caco-2 monolayers. Secondly, we compared cellular changes on Caco-2 cells exposed to either C_{10} or SNAC by performing a series of conventional cytotoxicity assays. Finally, we used HCA to provide comparative data into the epithelial mechanism of action and sub-lethal cytotoxicity of SNAC and C_{10} in Caco-2 cells by assessing six parameters. We also confirmed if actions of C_{10} on parameters in Caco-2 cells were in line with those previously published [22]. In the current study, a reduction in transepithelial electrical resistance (TEER) and an increase in fluorescein isothiocyanate-dextran 4,000 Da (FD4) permeability across monolayers was confirmed for C_{10}, accompanied by changes in three tight junction proteins. However, SNAC had no effect on TEER or FD4 fluxes except at excessive concentrations. SNAC was less potent compared to C_{10} in respect of causing lysosomal and nuclear changes and plasma membrane perturbation. For both PEs, HCA indicated that they induced calcium deregulation, plasma membrane permeabilization, and mitochondrial perturbation.

2. Materials and Methods

2.1 Materials

FD4, poly-lysine, sodium salt of capric acid (C_{10}), Neutral Red (NR) reagent (Assay Kit Neutral Red Based TOX4-1KT), carbonylcyanide-p-trifluoromethoxyphenylhydrazone (FCCP), ionomycin, and Triton™ X-100 were obtained from Sigma (Ireland). SNAC was from AstaTech, Inc. (Bristol, USA). MTS reagent (CellTiter 96® Aqueous Cell Proliferation Assay), LDH-Glo™ Assay (J2380), CellTox Green Assay were supplied by Promega (Ireland). JC-1 dye (ab141387) was supplied by Abcam (UK). Valinomycin was supplied by Cayman Chemical (USA). Hoechst 33342, Fluo-4 AM, tetramethyl rhodamine methyl ester (TMRM), TOTO-3 iodide 642 / 660 dyes were obtained from Invitrogen™, Biosciences (Ireland). Alexa Fluor® 594 mouse monoclonal antibody against occludin (1:400), Alexa Fluor® 594 mouse monoclonal antibody against ZO-1 (1:400), and Alexa Fluor® 488 mouse monoclonal antibody against claudin-5 (1:500) were sourced from Thermo Fisher Scientific (USA). Dako fluorescence-mounting media was obtained from Dako Diagnostics (Ireland). Caco-2 cells (passage 56-66)

were obtained from European Collection of Cell Cultures (UK). All other reagents/materials were standard laboratory grade. All solvents used were HPLC grade.

2.2 Cell culture

Caco-2 cells were cultured in 75 cm^2 cell culture flasks in a 95% O_2/5% CO_2 atmosphere at 37°C and 95% relative humidity. Caco-2 cells were cultured in Dulbecco's Modified Eagle Medium (DMEM) media supplemented with 10% foetal bovine serum, 1% penicillin/streptomycin, 1% non-essential amino acids, 1% L-glutamine. 0.025% trypsin EDTA solution was used to dissociate the adherent cells from the flask prior to staining with trypan blue for cell counting and for a viability check using a Countess® automated cell counter.

2.3 FD4 flux across Caco-2 monolayers: C_{10} and SNAC exposure

Caco-2 cells were cultured on plastic until confluent and then seeded at a density of 3 x 10^5 cells/well on 1.12 cm^2 area Transwell® filters (polyester, pore size 0.4 µm, diameter 12 mm) (Corning Costar Corp., USA) and grown for 21-28 days in DMEM [26]. TEER ($\Omega.cm^2$) was monitored throughout the culture period as a measure of monolayer differentiation and integrity using an EVOM™ voltohmmeter with a chopstick electrode (World Precision Instruments (WPI), UK). Apical-to-basolateral transport of the paracellular flux marker, FD4, was examined. Transport buffer consisted of Hank's Balanced Salt Solution (HBSS) supplemented with glucose (12.5 mM) and 4-(2-hydroxyethyl)-1-piperazineethanesulfonic acid (HEPES, 25 mM). In this and subsequent *in vitro* assays, calcium-free buffers were used on the apical side of monolayers exposed to C_{10} in order to avoid precipitation. Before flux initiation, DMEM was replaced with the relevant HBSS buffer on the apical side and HBSS on the basolateral side and equilibrated for 30 min at pH 7.4. TEER measurements were made before and after HBSS replacement to ensure monolayer integrity.

FD4 solution was also prepared in HBSS. At time zero, 250 µg / ml FD4 was added to the apical side in the presence and absence of C_{10} (2.5, 5, 8.5, 10 mM) or SNAC (10, 20, 30, 40 mM). The apparent permeability coefficient (P_{app}) of FD4 across monolayers was measured by taking basolateral samples every 20 min for 120 min, followed by replacement with fresh HBSS, while apical samples were taken at 0 and 120 min. In recovery studies to see whether TEER values could be re-established, the HBSS containing the PE was removed from both sides and replaced with fresh DMEM, with the TEER read at $T_{24\,h}$ to determine recovery. TEER was expressed as the percentage TEER relative to the untreated monolayer before media replacement, (% initial TEER). FD4 containing samples were transferred onto a Nunc 96 well white Maxisorp® plate (Thermo Scientific, MA, USA). The T_0 apical sample was diluted to 1:10

(20 µl in 180 µl HBSS) and then to 1:100 on the plate. The FITC signal intensity was measured at excitation / emission wavelengths of 490 nm / 525 nm respectively using a Spectra Max Gemini fluorescence intensity microplate reader (Molecular Devices, CA, USA). The P_{app} values for FD4 with each PE were calculated according to the following equation:

$$\mathbf{P_{app}} = \frac{\mathbf{dQ}}{\mathbf{dt}} \frac{\mathbf{1}}{\mathbf{A \cdot C_0}}$$

where dQ/dt is the transport rate across the epithelium (mol.s^{-1}), A is the surface area of the cell monolayer (1.12 cm^2), and C_0 is the initial concentration of flux marker in the donor compartment (mol / ml) [26]. Transport experiments were run in triplicate with three independent replicates.

2.4 Immunofluorescence of tight junction proteins in Caco-2 monolayers exposed to PEs

The effect of SNAC and C_{10} on localization of junctional proteins was assessed with immunofluorescent staining of occludin, ZO-1 and claudin-5 [27]. Confluent Caco-2 cells grown on 8 well Nunc™ Lab-Tek II chamber slides (Fischer) were exposed to C_{10} (2.5, 5.0 and 10 mM) or SNAC (10, 20 and 40 mM) in serum-free DMEM for 120 min. Following exposure, media was removed and cells were washed gently with ice cold PBS. Cells were fixed in ice-cold methanol for 15 min and washed with PBS. Non-specific binding sites were blocked with 1% (w/v) BSA in PBS for 45 min at room temperature. Cells were washed with PBS and permeabilized with Triton™ X-100 (0.1% w/v) in PBS for 10 min. Cells were probed with Alexa Fluor® 594 mouse monoclonal antibody against occludin (1:400), Alexa Fluor® 594 mouse monoclonal antibody against ZO-1 (1:400), and Alexa Fluor® 488 mouse monoclonal antibody against claudin-5 (1:500) for 120 min in the dark at room temperature. Cells were counterstained with Hoescht (1µM) to visualize the nuclear DNA. The slides were washed with PBS and mounted in Dako fluorescence mounting media. Images were examined using a Zeiss Axiovert 200 M inverted fluorescence microscope (Carl Zeiss, Germany) with Zeiss AxioVision Rel. 4.8 software for controlling the image recording, microscope stage and image merge. Images were processed using ImageJ®.

2.5 Cytotoxicity assessment using conventional assays

2.5.1 MTS for cell viability proliferation assay

Caco-2 cells were cultured on 96 well plates at a density of 2 x 10^4 cells per well in supplemented DMEM (Section 2.2) and incubated for 24 h before treatment to allow the cells to adhere. At 24 h, 200 µl of SNAC or C_{10} diluted in DMEM was added to wells, with Triton®-X-100 (0.1 % v/v) used as a positive control. The assay was carried out at 1, 2, 4 or 24 h

exposure times according to previous descriptions [28]. Treatments were removed, 100 µl media was added to each well and cells were treated with 20 µl of MTS (3-(4, 5-dimethylthiazol-2-yl)-5-(3-carboxymethoxyphenyl)-2-(4-sulfophenyl)-2H-tetrazolium. Plates were incubated for a further 4 h, after which the absorbance was measured at 490 nm using a UVM 340 plate reader (ASYS Hitech Gmbh, Austria). Each value presented was normalized against untreated control and calculated from three separate experiments, each of which included triplicates.

2.5.2 LDH Glo™ assay for plasma membrane permeability

The LDH-Glo™ assay was used to quantify LDH release from Caco-2 cells when exposed to C_{10} and SNAC for 2 h [29]. Cells were seeded onto 96-well white plates and incubated overnight. Media was removed, replaced with 100 µl PE diluted in HBSS (Ca^{2+}-free HBSS with C_{10}) per well. Cells incubated with HBSS were used as negative control while positive controls contained 0.1 % (w/v) Triton®-X-100. 2 µl media was removed from each well and mixed with a 198 µl of storage buffer (200 mM Tris-HCl (pH 7.3), 10% glycerol, 1% BSA). 50 µl of this mixture was then added to 50 µl of LDH detection reagent (containing Lactate, NAD+, Reductase, Reductase Substrate and Ultra-Glo™ rLuciferase). The plate was placed on an Orbital shaker (500 rpm) in the dark for 60 min at room temperature. Luminescence was measured using the plate reader CLARIOstar (BMG Labtech, Germany) and is proportional to the amount of LDH in the sample. LDH release (%) was calculated by setting the positive control to 100 % membrane permeability.

2.5.3 CellTox Green™ assay for nuclear membrane permeability

Integrity of the nuclear membrane was carried out on Caco-2 cells using the CellTox Green™ assay [30]. Cells were seeded in a white 96 well plate and incubated overnight. Media was removed and the cells washed using PBS (x 2). 50 µL (2 X) CellTox Green™ reagent (1:500 dilution of CellTox™ Green dye in DMEM) was added along with 100 µl SNAC- or C_{10}-diluted DMEM per well. Plates were incubated for 15 min on an Orbital shaker shielded from light. The assay was then carried out using 2 h exposure times for PEs at 37 ºC. Cells incubated with DMEM and dye in the absences of PEs were used as negative control while positive control wells contained Triton®-X-100 (0.1 % v/v). Fluorescence was recorded at 485/520 ($\lambda_{ex}/\lambda_{em}$) using the plate reader CLARIOstar (BMG Labtech, Germany). CellTox Green™ binding DNA (%) was calculated by setting the positive control to 100 % permeabilization of cell nuclei.

2.5.4 JC-1 assay for mitochondrial membrane potential

Mitochondria physiology was also monitored by examining the variation of the MMP ($\Delta\Psi_m$) following SNAC or C_{10} exposure to Caco-2 cells using the JC-1 dye assay [31]. Cell were seeded as for MTS assay in a white 96 well plate incubated overnight. Media was removed

and 20 µM JC-1 solution in HBSS was added to each well. Plates were incubated for a further 10 min at 37°C to allow uptake of the JC-1 dye into viable cells. Dye solution was removed, and cells washed with PBS. 100 µl of PE treatment diluted HBSS (Ca^{2+}-free HBSS for C_{10}) were added per well. Treatments included SNAC and C_{10} at concentrations up to 40 mM. Negative control wells contained HBSS, while positive control wells contained 1 µM valinomycin, a depolarizing agent [32]. The assay was carried out using 2 h exposure times for C_{10} and SNAC on Caco-2 cells at 37 ºC. Fluorescence was recorded at 535/590 ($\lambda_{ex}/\lambda_{em}$) for detection of JC-1 aggregates, and at 475/530 for detection of JC-1 monomers using the plate reader CLARIOstar (BMG Labtech, Germany). JC-1 probe accumulates in active mitochondria forming red-fluorescent aggregates whereas monomeric dye stays in the cytoplasm if mitochondria are compromised. A ratio between JC-1 aggregates and JC-1 monomer signals indicates the variation of MMP, which was then calculated, with data normalized by setting the untreated control to 1.0.

2.5.5 NR assay to assess lysosomal integrity

Caco-2 were seeded and treated with C_{10}, SNAC, or Triton-X-100 (0.1 % v/v, positive control) on a 96 well plate over 2 h, similar to the MTS assay. Treatments were removed and 20 µl of NR solution 33 µg/ml v/v in PBS was added to each well with 180 µl HBSS supplemented with 12.5 mM D-glucose and buffered with 25 mM HEPES buffer. Plates were incubated for a further 3 h at 37°C to allow uptake of the vital dye into viable cells [33]. The dye-media was then completely removed from the wells and cells were washed with PBS. Cells were then quickly rinsed for 2 min with 150 µl of NR assay fixative solution to remove unincorporated dye. 150 µl of NR assay solubilisation solution was added to each well to aid the release of the intracellular dye into the solution. The plate was then left at 37 °C with 5% CO_2 for further 20 min and shaken for 10 min. The background absorbance was measured at 690 nm and corrected for background absorbance at 540 nm using a UVM 340 plate reader (ASYS Hitech Gmbh, Austria). Each value presented was normalised against untreated control and calculated from three separate experiments, each of which included triplicates.

2.6 HCA on Caco-2 cells exposed to SNAC or C_{10}

Imaging plates were coated and cells seeded at low density to prevent overgrowth [5], [34]. Nunclon® 96 well plates were coated with a poly-lysine solution as follows: 20 µl aqueous poly-lysine solution (0.1 mg/ml) was added to wells and incubated for 10 min at 20 ºC. Plates were washed with 150 µl PBS twice and dried for 2 h before seeding cells. Caco-2 cells were transferred to coated well plates at a density of 6 x10 ^{3} cells in DMEM per well and incubated for 24 h before PE exposure. 24 h post-seeding, medium was replaced with either Ca^{2+}-free DMEM for C_{10} or DMEM for SNAC for either 2 h or 24 h. After exposure, medium was removed

and a dye mix (150 µl of 2 x stock in Ca^{2+}-free medium) was added. It contained final concentrations of 0.8 µM Hoechst 33342 (blue dye to measure CN, NA and NI); 1 µM Fluo-4 AM (green dye to measure IC); 20 nM TMRM (red dye to measure MMP); and 1 µM TOTO-3 (dark red dye to measure PMP). Cells were incubated with dyes for 50 min before positive controls were added for each non-nucleus-related parameter: 100 µM mitochondrial uncoupler, FCCP, for MMP, 20 µM calcium ionophore, ionomycin, for IC, and 0.05% (w/v) Triton™ X-100 for PMP. 50 µl medium was removed from each positive control well and replaced with 50 µl of the positive control agent. The plate was incubated for a further 10 min before image acquisition [35]. Each PE treatment or control was added in duplicate to each plate and each experiment was run on three separate occasions.

The automated epi-fluorescence Zeiss microscope was used to analyze the plates and the system was equipped with an incubator to maintain constant temperature, CO_2, and humidity during analysis. A Cellomics ArrayScan VTI HCS Reader was used to acquire images with automated focusing. A custom-made algorithm was used so that the Cell Health Profiling bioapplication reported field view details (average intensity per cell using a fixed threshold in each field acquired). Cell count, nuclear size and nuclear intensity were determined by number and area of regions identified based on Hoechst 33342 and its fluorescence intensity. MMP was defined as total TMRM fluorescence intensity, IC by the intensity of Fluo-4 AM, and PMP by Toto-3 intensity. The excitation/emission wavelengths used were Hoechst 33342: 365/515 nm, Fluo-4: 475/515 nm, TMRM: 549/600 nm and Toto-3: 655/730 nm. Optimal exposure times were 50 ms for Hoechst 33342, 200 ms for Fluo-4, 50 ms for TMRM and 100 ms for Toto-3. The nuclei fluorescence of Hoechst was used for focusing and cell counts and 10 random fields per well were imaged using a 10 X objective magnification. For each other parameter, 10 random fields per well were imaged using a 20 X objective magnification. The incubator was set to 37°C but no extra CO_2 was admitted to the plate. Lids were left on the 96-well plates to prevent evaporation.

2.7 Statistical analysis

Statistical analysis was carried out using Prism-5® software (GraphPad, San Diego, USA). Statistical significance was measured by one-way ANOVA with Dunnett *post-hoc* tests for *in vitro* calculations of P_{app} and *in vitro* conventional toxicity assays. For HCA study, variations in PE concentration induced changes were normalized to the untreated control and each treatment time was analysed by one-way ANOVA with Dunnett's *post-test* to compare treatment groups to the untreated controls. Results are presented as the mean ± standard error of the mean (SEM). A significant difference was considered if $p < 0.05$. IC_{50} values were extrapolated from the concentration-response graph by plotting triplicate data points over a concentration range and calculating values using regression analysis.

3. Results

3.1 Effects of C_{10} and SNAC on TEER and the P_{app} of FD4 across Caco-2 monolayers

Basal TEER for Caco-2 monolayers was 2605 ± 48 Ω. cm^2 (n=19) within the range of TEER values typically reported by this lab [36] and others [37]. The effects of SNAC and C_{10} on the permeability of FD4 was determined. Monolayers were exposed to C_{10} (2.5-10 mM) and SNAC (10-40 mM) and TEER values were assessed over 120 min. Concentrations were comparable to those previously used in Caco-2 monolayer studies with C_{10} [38] and with SNAC [39]. A concentration-dependent decrease in TEER was observed after exposure to C_{10} leading to a nadir of 12 % of the initial basal TEER (Fig. 1A). The induced reduction in TEER following exposure to 2.5 and 5 mM C_{10} was reversed by 50% in fresh media after 24 h. Monolayers exposed to 8.5 and 10 mM C_{10} however, did not recover TEER, indicating an irreversible effect. The mean basal P_{app} of FD4 across monolayers was 0.3 x 10^{-8} cm. s^{-1}, in agreement with previous data [26]. Following exposure to 2.5 mM C_{10} the P_{app} was unchanged, and only slightly increased with 5 mM C_{10}. However, a 25-fold increase was obtained in the presence of 8.5 mM C_{10} (P_{app} = 7.3 x 10^{-8} cm. s^{-1}), while a 60-fold increase was seen with 10 mM C_{10} (P_{app} = 17.4 x10^{-8} cm. s^{-1}) (Fig. 1C). The reversible reduction in TEER at concentrations of 2.5 and 5 mM C_{10} and large increases in enhancement ratios in the P_{app} at 8.5 mM and 10 mM C_{10} is suggestive of epithelial tight junction opening. These results confirm effects of C_{10} on paracellular flux markers in Caco-2 monolayers [22].

In contrast to C_{10}, decreases in TEER values were not observed for monolayers exposed to SNAC at 10, 20 and 30 mM compared to controls. Monolayer exposure to a very high concentration of SNAC (40 mM) however, reduced TEER values to a nadir of 26% of the initial value and not even partial restoration was observed after 24 h incubation in fresh media (Fig. 1B). Following apical addition of FD4 with SNAC (10, 20 and 30 mM), no increases in the P_{app} of FD4 were seen. With 40 mM SNAC however, a 96-fold increase over basal P_{app} was obtained (Fig. 1D), but this was likely to be a toxicity artefact at this excessive concentration, as suggested by both the TEER data and cytotoxicity indications. The P_{app} changes with regard to fold increases in FD4 are summarised in Fig. 1E.

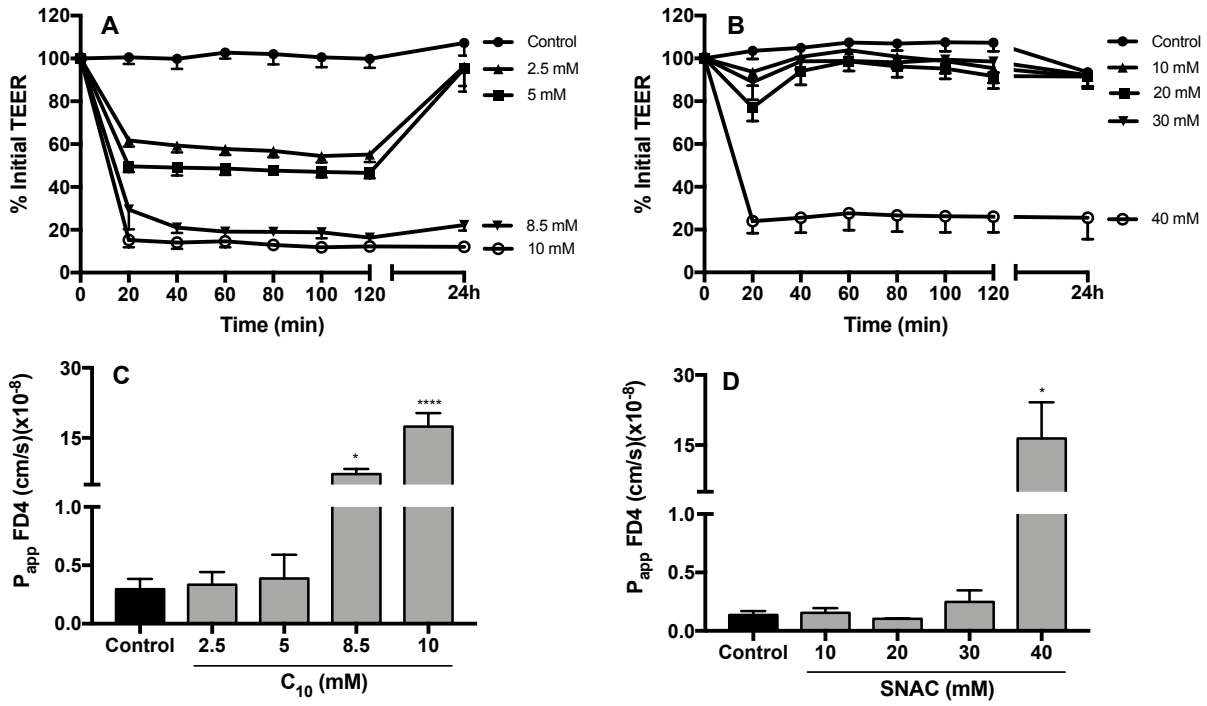

E

C_{10}		SNAC	
Concentration (mM)	Fold increase	Concentration (mM)	Fold increase
0	-	0	-
2.5	1.1	10	1.1
5.0	1.3	20	0.8
8.5	24.6	30	1.2
10.0	58.9	40	95.7

Figure 1: Effects of C_{10} and SNAC on Caco-2 monolayers. **(A)** % Change in TEER in response to C_{10} and recovery from 120 min, **(B)** % Change in TEER in response to SNAC and recovery from 120 min, **(C)** P_{app} of FD4 in response to C_{10}, **(D)** P_{app} of FD4 in response to SNAC, **(E)** Enhancement ratios in the presence of C_{10} or SNAC. Mean ± SEM; n=4 per group. ***P<0.001, *P<0.05 compared to untreated controls.

3.2 Effects of C_{10} and SNAC on TJ protein localization in Caco-2 monolayers

To assess the effects of C_{10} and SNAC on tight junction proteins, immunofluorescent staining was used. In untreated control Caco-2 monolayers, claudin-5, ZO-1 and occludin localized at the plasma membrane in a continuous manner and resembled a cobblestone pattern (Fig. 2A) [40]. There was no difference in the localization of any of the three proteins in cells exposed to the 2.5 mM C_{10} concentration that induced TEER reduction followed by recovery in fresh buffer in monolayers (Fig. 2B). However 5 mM C_{10} caused internalization of ZO-1, leading to poor membrane definition and with cell sloughing, indicative of membrane perturbation. Claudin-5 and occludin were also relocated and internalised in the presence of 5 mM C_{10} (Fig. 2C). 10 mM C_{10} also altered claudin-5 and ZO-1 localization with a disruption of the immunostaining

(Fig. 2D). Claudin-5 immunostaining was hardly detected in cells exposed to 10 mM C_{10}, and there was minimal membrane staining for occludin and ZO-1, suggesting some loss of cell membrane integrity. This data indicates that increasing concentrations of C_{10} leads to reorganization of TJ proteins and is consistent with the concentration-dependent induced decreases in TEER and increases in the P_{app} of FD4.

For SNAC concentrations that did not alter Caco-2 monolayer TEERs (10 and 20 mM), there was no difference in the localization of occludin and ZO-1 compared to controls on Caco-2 cells (Fig. 2E, F). However, disruption of the continuous cobblestone pattern with claudin-5 was present, as indicated by a faint immunofluorescent signal and discontinuous membrane definition, unlike in control cells. At 40 mM SNAC however, claudin-5 was almost undetectable and accumulated at some regions (Fig. 2G). In summary, C_{10} induced internalisation and re-organisation of TJ proteins on Caco-2 cells, consistent with increased transepithelial flux of FD4 across monolayers via the paracellular route at concentrations < 10 mM. SNAC also caused some reorganisation of claudin-5 at concentrations that neither reduced TEER nor increased FD4 flux. One interpretation is that this effect of SNAC on claudin-5 could be initial perturbation, but perhaps it was not sufficient enough to open tight junction to the degree needed to increase FD4 permeability.

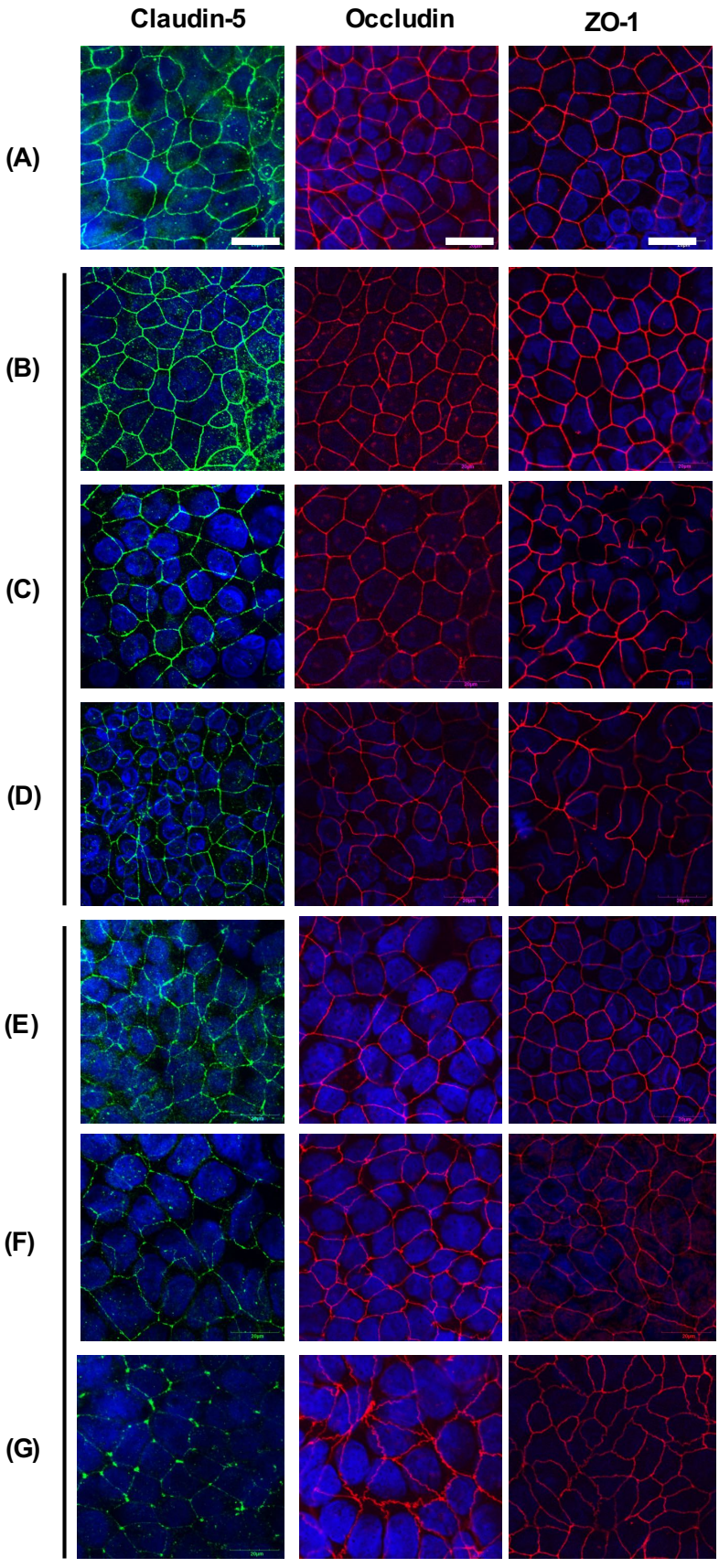

Figure 2: Representative immuno-fluorescence analysis of the localization of selected tight junction proteins on Caco-2 cells on chamber slides exposed to PEs for 2 h. **(A)** untreated; **(B)** 2.5 mM C_{10}; **(C)** 5 mM C_{10}; **(D)** 10 mM C_{10}; **(E)** 10 mM SNAC; **(F)** 20 mM SNAC; **(G)** 40 mM SNAC. Marker bar indicates 20 µm.

3.3 Assessment of C_{10} and SNAC cytotoxicity on Caco-2 cells: conventional assays

3.3.1 MTS assay

The viability of Caco-2 cells exposed to either C_{10} or SNAC for 1, 2, 4, and 24 h was determined. The most relevant exposure times for intestinal epithelia is likely to be < 4 h, as the gut wall will only temporarily be exposed to transiting oral formulations [41]. Decreases in cell viability at all time points were related to concentrations and exposure times for both agents (Fig. 3). Significant decreases in mitochondrial activity were seen only at very high concentrations of SNAC: at 40 mM following 1 h exposure and 20 mM after 4 h. The assay was more sensitive to lower concentrations of C_{10} than SNAC where decreases in viability were produced by 20 mM C_{10} (at 1 h), and 10 mM C_{10} (at 4 h). At 2 h exposures to concentrations of 20 mM and above, C_{10} caused greater reductions in the percentage of viable cells (36 % remaining) than SNAC (77 % remaining). Importantly, only the excessive concentrations of 20 mM and 40 mM C_{10} were as cytotoxic as the positive control, Triton-X-100 (0.1% v/v), at 1 h and 2 h exposures respectively, whereas no concentration of SNAC reached such equivalence. Effects on the MTS signal were therefore more pronounced with chronic exposure and slightly more prevalent with C_{10} compared to SNAC. However, the MTS assay gives no information on mechanism of action and is not based on a specific mitochondrial property.

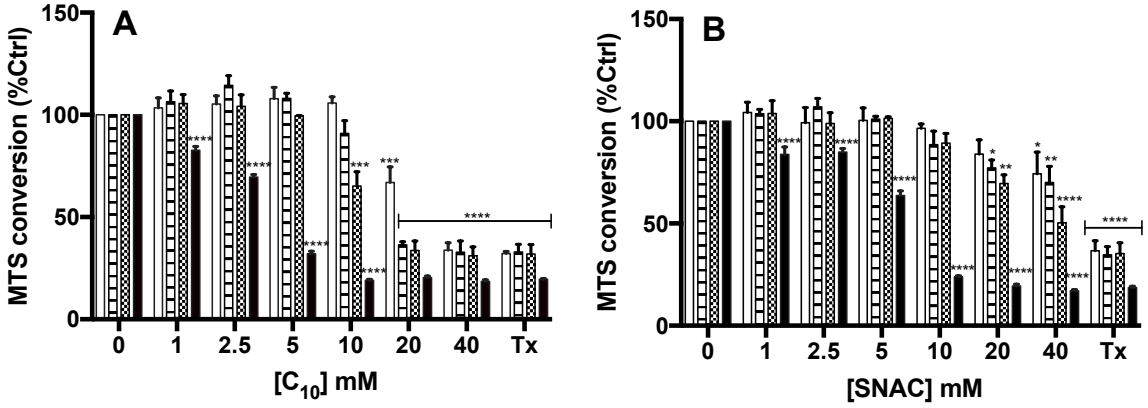

Figure 3: MTS results for **(A)** C_{10} and **(B)** SNAC on Caco-2 cells grown on wells over time 1 h; 2 h; 4 h; 24 h. Triton®-X-100 (Tx, 0.1% v/v) was used as a positive control. Results presented as percentage of MTS converted compared to untreated medium control. Mean ± SEM; n=3. *P < 0.05, **P < 0.01, ***P < 0.001.

3.3.2 LDH Glo™ assay

Evaluation of cell viability was also assessed using the LDH Glo™ assay. The release of LDH enzyme from the cytoplasm of the cells into the cell medium is an indicator of plasma membrane integrity. Fig. 4A summarize the effects of C_{10} and SNAC on Caco-2 cells. At

concentrations of < 5 mM for 2 h, neither agent altered LDH release. There was a trend for increase in release at C_{10} concentrations above that, reaching significance at 20 mM, whereas SNAC did not induce release even at 40 mM. The LDH assay indicates that C_{10} but not SNAC induced concentration-dependent reductions in plasma membrane integrity.

3.3.3 CellTox Green™ assay

Nuclear membrane integrity was studied by the CellTox Green™ assay. Fluorescence is emitted when the dye binds DNA by permeating compromised plasma- and nuclear membranes. As shown by Fig. 4B, a concentration-dependent increase in signal was seen following 2 h exposures to C_{10} above 5 mM, which reached significance at 40 mM. Similarity between data from the LDH release and the CellTox Green™ assays indicate linkage between compromised plasma membrane integrity and increased nuclear membrane permeability. On the contrary, SNAC did not alter the CellTox Green™ signal at any concentration, in keeping with its lack of effect on LDH release.

3.3.4 JC-1 assay

The effect of SNAC and C_{10} on MMP is reported in Fig. 4C. Fluctuations in the $\Delta\Psi_m$ was affected by both agents compared to untreated cells following exposure to the PEs for 2 h. For concentrations < 5 mM, the largest reduction in ratio was observed with C_{10} compared to SNAC at the same concentration. $\Delta\Psi_m$ was also significantly decreased at lower C_{10} concentrations (1 mM) compared to SNAC (5 mM). Above those concentrations, the $\Delta\Psi_m$ was decreased for both PE to the same extent as the positive control, valinomycin. Mitochondrial perturbation therefore occurred at lower concentrations for both agents compared to other parameters measured by conventional cytotoxicity assays. It should be noted that the total fluorescence of probes accumulating in mitochondria might be increased if the PMP was increased in parallel.

3.3.5 NR assay

Indirect effects of SNAC and C_{10} on Caco-2 cell lysosomal membranes were investigated using the NR assay on Caco-2 cells and was visualized by light microscopy after 2 h exposures. The dye accumulates in the lysosomes of healthy cells following passive diffusion across the plasma cell membrane. For both PEs, a bi-phasic response was obtained [42]. An initial concentration-dependent increase of signal was seen for SNAC (1-10 mM) and C_{10} (1-5 mM). This higher dye accumulation compared to controls could indicate hormesis ahead of loss in integrity (Fig. 4D). Similar to the MTS assay, loss of signal indicative of unstable lysosomal membranes was only significant with 20 mM C_{10} and 40 mM SNAC.

Microscopic observations confirmed the loss of NR colour in Caco-2 cells at high concentrations (Fig. 4E). The capacity of viable cells to retain NR began to reduce at 10 mM C_{10}, accompanied by a decrease in cell number (Fig. 4E (vii)). The dye was still retained however, even at 20 mM SNAC (Fig. 4E (IV)). Possible destabilization of the lysosomal membrane to inhibit retention of NR seems to occur at lower C_{10} concentrations than SNAC.

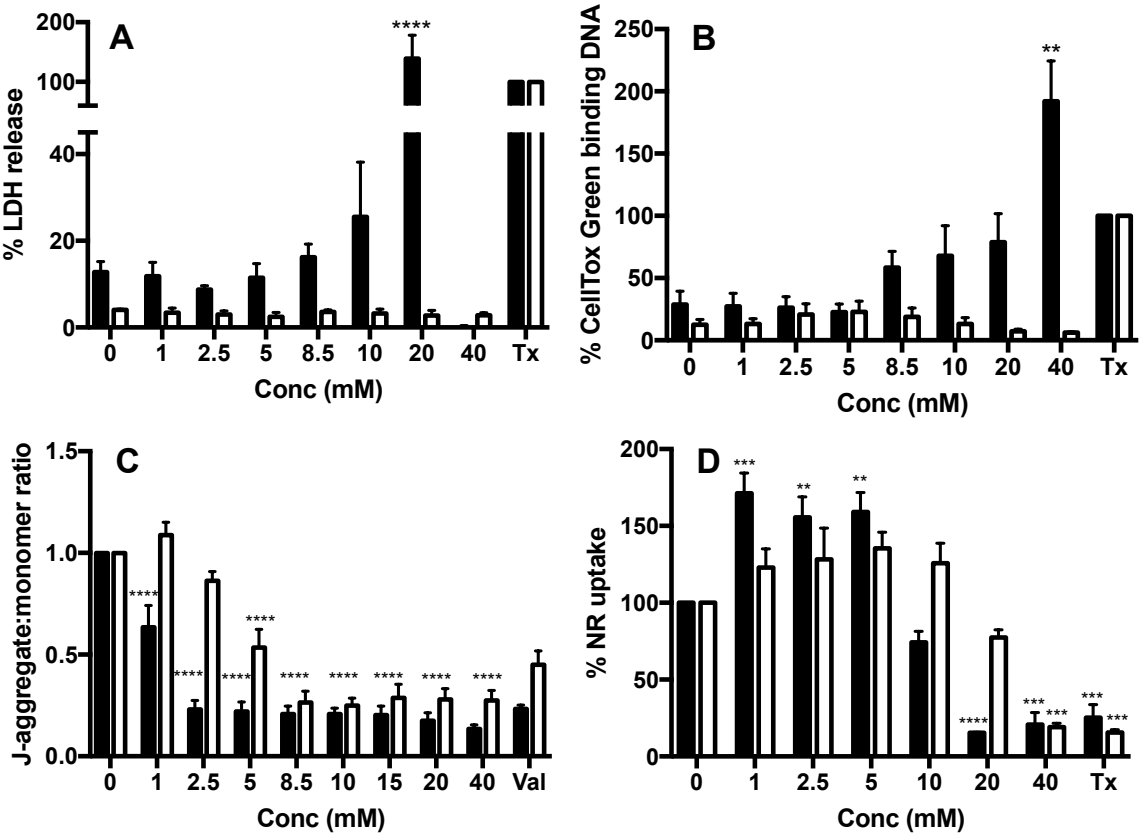

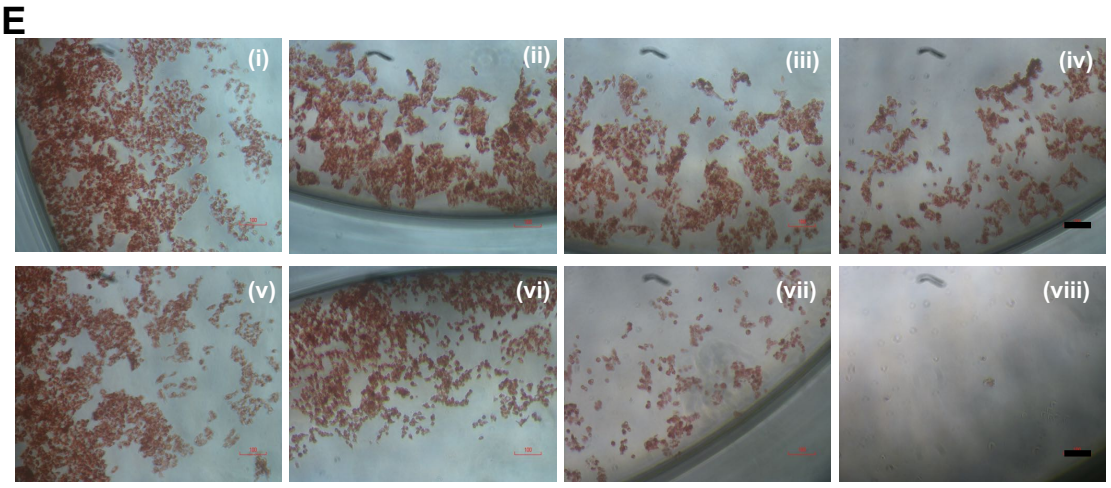

Figure 4: Effect of ■ C_{10} and □ SNAC on Caco-2 cells following 2 h exposures. Triton®-X-100 (Tx, 0.1 % v/v) was the positive control in (A) (B), (D). **(A)** LDH release; **(B)** CellTox Green™, **(C)** JC-1 assay, where valinomycin (Val, 1 µM) was the positive control. **(D)** NR uptake. Results expressed as percentage uptake compared to untreated media control. Mean ± SEM (n = 3- 4). *P < 0.05, **P < 0.01, ***P < 0.001. **(E)** Light microscopy of Caco-2 cells with NR after 2 h exposures to **(i)** SNAC vehicle, **(ii)** 5 mM SNAC, **(iii)** 10 mM SNAC, **(iv)** 20 mM SNAC, **(v)** C_{10} vehicle; **(vi)** 5 mM C_{10}; **(vii)** 10 mM C_{10} **(viii)** 20 mM C_{10}. Horizontal bar=100 µm.

3.3.6 Summary of conventional cytotoxicity assay data

The decline in the cell viability indicated by the MTS assay in response to both agents at very high concentrations is likely caused by an interference with mitochondrial respiration. Over 2 h, results indicated a lower *in vitro* cytotoxicity profile for SNAC compared to C_{10} in Caco-2 cells using these five end-point assays. When comparing the IC_{50} of C_{10} and SNAC across the assays (Table 1), a trend was observed for both agents of initial MMP perturbation at low concentrations, followed by an increased nuclear, lysosomal, and plasma membrane permeability at excessively high concentrations. Mitochondrial metabolic activity as measured by MTS was associated with the highest IC_{50} for each PE.

Table 1: IC_{50} values for five standard cytotoxicity assays following 2 h exposures to C_{10} and SNAC in Caco-2 cells on 96-well plates. Results expressed as mean IC_{50} ± SEM; n=3 for all assays.

IC_{50} (mM)	**C_{10}**	**SNAC**
MTS	20.5 ± 2.4	> 40
LDH-Glo™	11.0 ± 2.8	> 40
CellTox Green™	7.1 ± 2.6	>40
Neutral Red	13.3 ± 4.2	27.9 ± 5.4
JC-1	1.2 ± 0.4	6.4 ± 1.4

3.4 HCA for C_{10} and SNAC on Caco-2 cells

HCA was used to evaluate acute C_{10} and SNAC mechanisms in live undifferentiated Caco-2 cells following 2 h and 24 h exposures. A 2 h exposure is physiologically more relevant as oral absorption of both PEs is rapid *in vivo* with a T_{max} seen typically within an hour of dosing [21, 43]. A 24 h exposure nonetheless allowed assessment of the chronology of responses and is common in HCA protocols of cell exposure. Maximal responses to the four fluorescent dyes were obtained in cells using positive controls (Suppl. Fig. 1).

Figure 5 shows representative fluorescence images of C_{10}- and SNAC-induced changes in the six parameters on Caco-2 cells following 24 h exposures. Morphological changes in cell shape and reductions in cell number were evident over several concentrations for both agents. An IC increase was detectable with 2.5 mM C_{10} (Fig. 5B), but it decreased at 5 mM C_{10} and was not observed at 8.5 mM C_{10} (Fig. 5C, 5D). With C_{10}, MMP perturbation was reflected by an increase in fluorescence intensity of the red TMRM dye at 2.5 mM, followed by a decrease at 5 mM, and a complete loss of signal at 8.5 mM. At 8.5 mM C_{10}, cells exhibited an increase of PMP, as indicated by nuclear fluorescent changes from blue to dark red as the Toto-3 dye permeated leaky membranes to stain DNA (Fig. 5D). The dark red colour correlated with net CN reduction.

Following exposure to SNAC for 24 h there was a noticeable rise in IC concentration at 2.5 mM (Fig. 5F), which was further intensified at 5 mM (Fig. 5G) and maintained at 8.5 mM (Fig. 5H) compared to controls (Fig. 5E). MMP signal was maintained at each SNAC concentration and was still visible at 8.5 mM (Fig. 5H). Caco-2 exposure to SNAC at equimolar concentrations compared to C_{10} did not alter PMP. In summary, these data suggest that sub-lethal actions of both C_{10} and SNAC following 24 h exposures to Caco-2 cells are due to multiple mechanisms ranging from membrane perturbation to intracellular calcium concentration increases, changes consistent with mild surfactant actions at relatively high concentrations.

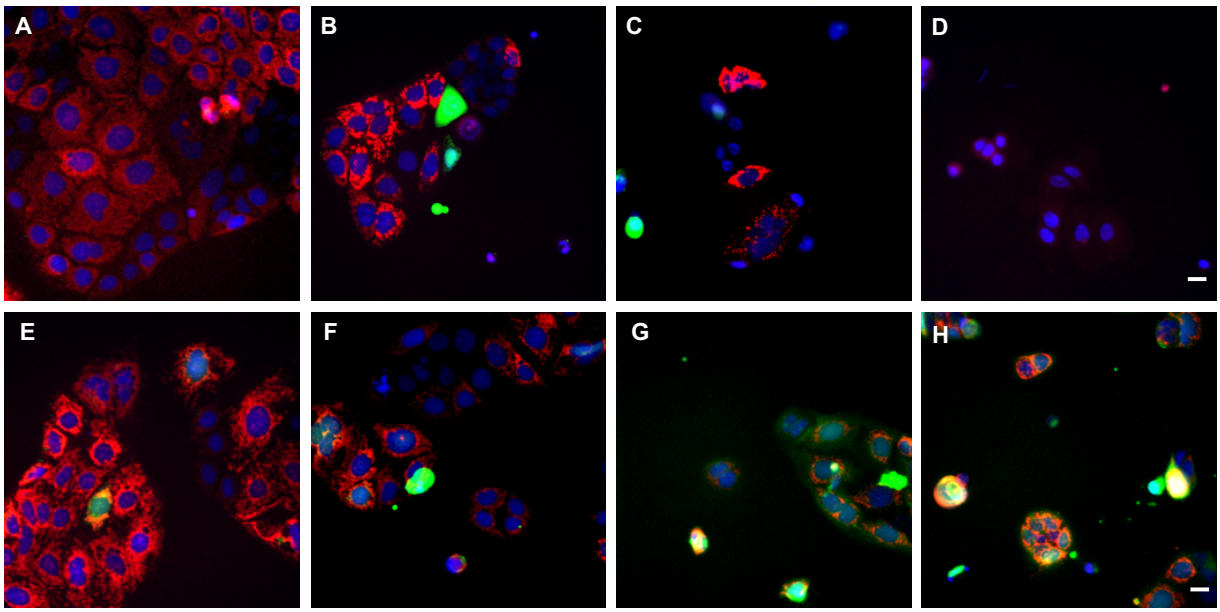

Figure 5: Representative HCA images of Caco-2 cells after 24 h exposures. (A) untreated; (B) 2.5 mM C_{10}; (C) 5 mM C_{10}; (D) 8.5 mM C_{10}; (E) Untreated; (F) 2.5 mM SNAC; (G) 5 mM SNAC; (H) 8.5 mM SNAC. Each fused fluorescent image was acquired at 20 x objective magnification and pseudo-coloured accordingly; Hoechst® (blue; nuclear staining), Fluo-4 AM (green; measure of IC), TOTO®-3 iodine (dark red; measure of PMP) and TMRM (red; measure of MMP). Horizontal bars = 20 µm.

The effect of C_{10} and SNAC after 2 h exposure on Caco-2 cell parameters by HCA are shown in Fig. 6, with representative images shown in Suppl. Fig. 2. Table 2 provides the values representing the minimum concentration that produced significant changes in each parameter compared to untreated controls following 2 h and 24 h exposures.

For both agents, the initial metric affected following 2 h exposures to 5 mM C_{10} and 1 mM SNAC was the MMP (Fig. 6A). 5 mM C_{10} led to a mitochondrial hyperpolarization, a likely hormetic stress response to perturbation, followed by subsequent loss of MMP at 20 mM, which was the concentration that showed significance in the MTS assay after 2 h. Only a reduction in MMP was recorded with SNAC from concentrations of 1 mM upwards and with no hyperpolarization detected. Additional effects of on cell homeostasis was detected with increased NA with 5 mM C_{10} (Fig. 6B). NI was significantly increased at a threshold

concentration of 8.5 mM C_{10} (Fig. 6C), which correlated with the IC_{50} of 7.1 mM calculated for the increased nuclear permeability to CellTox Green™. The intensity of fluorescence from nuclei is higher when cells undergo apoptosis as nuclei condense. Incubation with SNAC had no effect on the nuclei as no changes were recorded for either NA or NI (Fig. 6B, C). Changes in PMP were found for each agent at similar concentrations (15 mM) and preceded changes in IC (20 mM) (Fig. 6D). After 2 h exposure, only a minor increase in IC was observed with at 8.5 mM C_{10} and with 20 mM SNAC (Fig. 6E). 20 mM C_{10} significantly reduced CN (Fig. 6F), but NA and NI were already altered in surviving cells at 5 mM and 8.5 mM C_{10}. Reductions in CN may be due to sloughing of cells from the substrate. CN was not reduced by SNAC even at a concentration as high as 20 mM. After 2 h exposure, significant changes in IC, PMP and MMP were seen at the same concentrations of C_{10} that promote increased P_{app} of FD4 across monolayers and it seems that IC changes are the main triggering event for flux. For SNAC, even though HCA detected changes in PMP at 15 mM in undifferentiated Caco-2 cells, no enhancement of FD4 flux was present in Caco-2 monolayers at < 30 mM SNAC.

Table 2: Effects of PEs on HCA cell parameters in Caco-2 cells on 96-well plates following 2 h or 24 h exposure to and SNAC.

	C_{10}		**SNAC**	
	2h	24h	2h	24h
IC	8.5 mM*	0.75 mM*	20 mM*	5 mM*
	20 mM*	8.5 mM		
MMP	5 mM***	0.75 mM*	1 mM*	10 mM*
	20 mM*	5 mM*		
PMP	15 mM***	5 mM**	15 mM*	10 mM*
NI	8.5 mM*	5 mM*	> 20 mM	8.5 mM*
NA	5 mM**	15 mM **	> 20 mM	> 20 mM
CN	20mM*	2.5 mM *	> 20 mM	5 mM *

Values are minimum concentrations that produced a significant change in a parameter. White box = increase in parameter value. Grey box = decrease in value. IC, intracellular calcium; MMP, mitochondrial membrane potential; PMP, plasma membrane permeability; NI, nuclear intensity; NA, nuclear area; CN, cell number. *P<0.05 compared to controls. **P<0.01 compared to controls. ***P<0.001 compared to untreated controls. n = 3 per group.

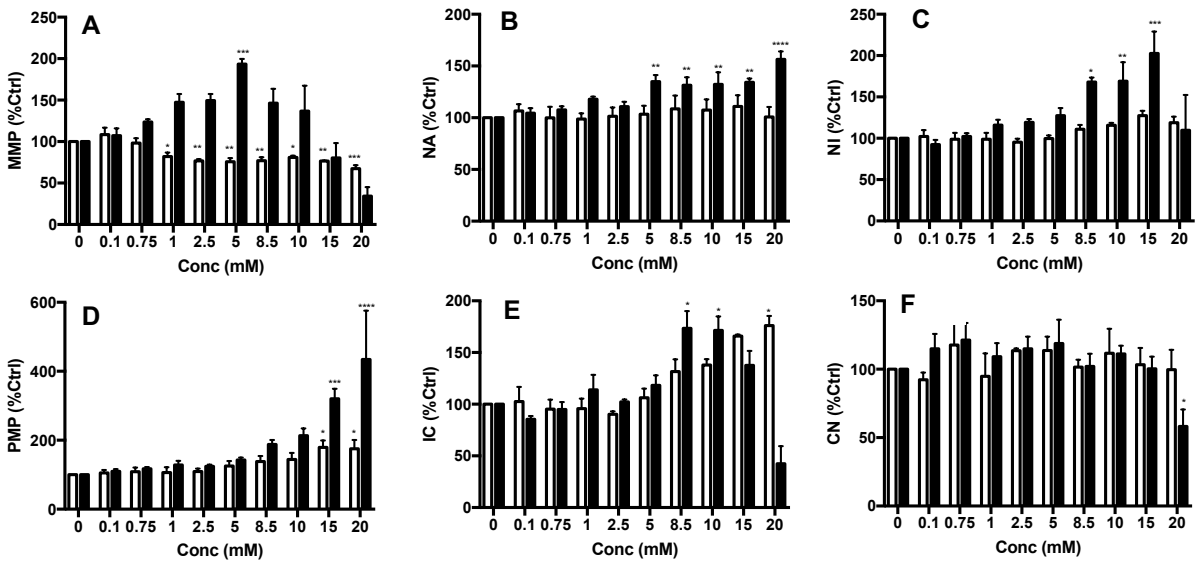

Figure 6: Caco-2 cell parameter responses on 96 well plates to C_{10} and SNAC over 2 h. Bar code: ■ C_{10}; □ SNAC. Abbreviations: mitochondrial membrane potential (MMP), nuclear area (NA), nuclear intensity (NI), plasma membrane potential (PMP), intracellular calcium (IC), cell number (CN). *P < 0.05, **P < 0.01, ***P < 0.001 compared to untreated controls (n = 3).

We then compared responses in Caco-2 cells to the two agents following exposure for 24 h (Table 2, Fig. 7). Increasing the exposure time to 24 h in Caco-2 cells resulted in a reduction in CN at lower concentrations of C_{10} and SNAC than at 2 h (Fig. 7F). C_{10} caused a reduction in CN at 2.5 mM whereas SNAC did so at 5 mM (Fig. 7F). The data for 24 h exposure confirms that C_{10} and SNAC altered each cell metric in a concentration-dependent fashion, except for NA which was not altered by SNAC (Fig. 7B). In response to C_{10} exposure, nuclear condensation (Fig. 7C) (5 mM), MMP reduction (5 mM) (Fig. 7A), and increases in PMP (5 mM) (Fig. 7D) were detected in Caco-2 cells at concentrations below those that caused reductions in IC (Fig. 7E) (8.5 mM). However, in the presence of SNAC, the initial stress response to membrane perturbation was manifested by an increase in IC at 5 mM, which was more evident at higher SNAC concentrations (Fig. 7E). At 5 mM SNAC, a decrease in CN (Fig. 7F) was recorded, followed by a decrease in NI (at 8.5 mM), but without affecting NA (Fig. 7B). Importantly, reductions in MMP (Fig. 7A) and increases in PMP (Fig. 7D) were detected for SNAC at 10 mM and for C_{10} at 5 mM following 24 h exposures.

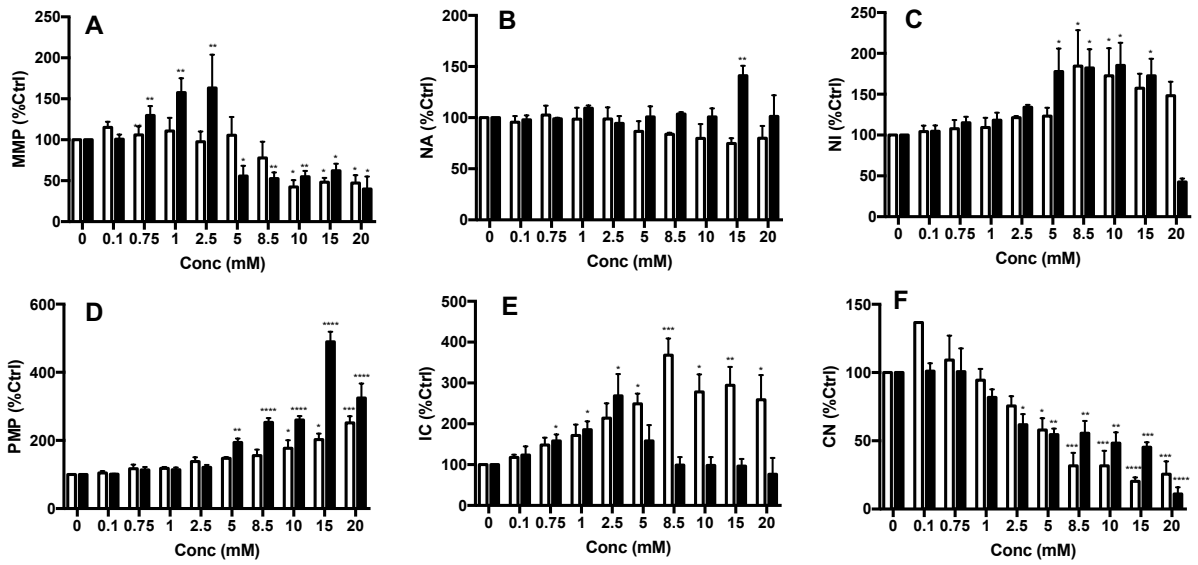

Figure 7: Caco-2 cell parameter responses on 96 well plates to and SNAC over 24 h. Bar code: ■ C_{10}; □ SNAC. Abbreviations: mitochondrial membrane potential (MMP), nuclear area (NA), nuclear intensity (NI), plasma membrane potential (PMP), intracellular calcium (IC), cell number (CN) *P < 0.05, **P < 0.01, ***P < 0.001 compared to untreated controls (n = 3).

4. Discussion

The aim of this study was to compare the intestinal permeation-enhancing capacity and cytotoxicity potential of C_{10} and SNAC on Caco-2 monolayers. Their effects on cytotoxicity were compared using *in vitro* conventional assays and HCA on undifferentiated Caco-2 cells. Paracellular permeability of C_{10} and SNAC was assessed across Caco-2 monolayers by assessing FD4 permeability and TEER. Then, fluorescent immunostaining of TJs proteins allowed to further study the effects on tight junctions. With C_{10}, FD4 fluxes increased at low concentrations accompanied by reversible reductions in TEER, consistent with the paracellular mechanism first outlined for in Caco-2 monolayers over 20 years ago [44-46]. Reductions in TEER after 24h exposure (only partially recoverable) were found with 8.5 mM C_{10}, which were associated with increased transepithelial flux. Moreover, immunostaining of TJs proteins revealed perturbations with ZO-1 internalization, and redistribution of claudin-5 and occludin. Those data are in agreement with previous findings confirming that C_{10} permeation enhancement in Caco-2 monolayers is primarily due to transport via the paracellular route associated with TJ dilation [45, 46]. Krug *et al.* also confirmed a marked reduction of tricellulin and claudin-5 expression in tight junctions in the HT-29/B6 cells when exposed to C_{10} [47].

Incubation with SNAC did not decrease in TEER nor increase in the permeability of the paracellular pathway of Caco-2 monolayers at < 40 mM. The permeability barrier was intact at < 30 mM SNAC. Despite the lack of induction of flux of FD4, a progressive removal of claudin-

5 from the TJ at high concentrations of SNAC was observed, although expression of ZO-1 and occludin were maintained. Claudin-5 is classically regarded as a sealing claudin, since it increases barrier properties as denoted by effects on TEER [48, 49]. Normal expression of ZO-1 and occludin might have compensated for the loss of claudin-5 and may have contributed in keeping TJs sealed in the presence of SNAC, in accordance with the detection of stable TEER and the absence of a FD4 P_{app} increase [49]. Those data showed the differential contribution of individual TJ proteins to TEER and the permeability of FD4. Indeed, ZO-1 and occludin regulate the paracellular permeability of marker molecules, whereas claudin-5 primarily affects the passage of ions. At 40 mM SNAC, permeation enhancement of FD4 was seen as a likely consequence of toxicity and do not allow a conclusion on the mechanism of action in this model at such high concentrations. Indeed, we observed gaps in differentiated monolayers grown on Transwell®-Clears in the presence of 40 mM SNAC (data not shown). This reflects limitations of testing PEs in Caco-2 monolayers, where it is difficult to discriminate concentrations of a true PE effect from cytotoxicity. It is important to note a limitation of the current study in that exposing monolayers to PEs for periods of as long as 120 min is questionable since enhancement seen with C_{10} and SNAC is rapid and reversible *in vivo*. This is possibly because both are rapidly absorbed with a T_{max} < 10 min for each.

In the literature, some have argued that changes in membrane fluidity due to SNAC exposure does not lead to a compromise of the barrier of epithelial monolayers. For example, Ding *et al.* [50] concluded that SNAC increased cromolyn's permeation across Caco-2 cell monolayers in a concentration-dependent manner: remarkably, 67 mM SNAC did not increase permeability whereas 83 mM did so. Similarly, in another study by Malkov *et al.* the permeability of radiolabeled mannitol, another paracellular marker, was surprisingly not increased even in the presence of 55 mM SNAC on Caco-2 monolayers [51]. According to our data for FD4 with SNAC in Caco-2 monolayers, such concentrations impair the barrier and remove cells from the filter, and therefore conclusions on mechanistic effects of the PE cannot be made from those studies.

Alternatively, Alani *et al.* confirmed that SNAC induced membrane fluidity increases in Caco-2 monolayers in a concentration-dependent manner and concluded that membrane perturbation was the main mechanism of action of SNAC in promoting permeation enhancement for cromolyn [23]. Similarly, Wu *et al*. [52] demonstrated that a supra-maximal concentration of 124 mM SNAC enhanced the transcellular passive diffusion of human growth hormone (hGH) across the Caco-2 cell monolayer, but this was almost certainly an artifact. The same concentration of 124 mM also caused a decrease in Caco-2 cell mitochondrial dehydrogenase activity after 60 min incubation as measured by the MTT assay, indicative of

membrane perturbation. An increase in LDH leakage from the Caco-2 monolayer was also observed after 2 h (but not 1 h) treatment with SNAC in the current study, an indication of membrane disruption. Still, these authors were of the opinion that SNAC did not cause significant damage to cell membranes compared to 1 mM oleic acid, which caused a 3-fold increase in fluorescence anisotropy [52]. In another study, FITC-heparin was detected in the cytoplasm of Caco-2 monolayers when SNAC was added (33-66 mM) after only 10 min exposure and 30 min, highlighting a cellular internalization mechanism [48]. Compared to our study, the TEER for Caco-2 monolayers exposed to 66 mM SNAC remained similar to initial values following 30 min exposure [51], but it is difficult to see how the monolayers remained intact at this concentration. Overall, very high concentrations of SNAC were used in these historical studies, which would inevitably lead to the loss of TEER arising from non-specific epithelial damage.

With both conventional cytotoxicity and HCA assays, MMP changes in Caco-2 cells was the first metric to be affected by low concentrations of C_{10} and SNAC over 2 h. Mitochondrial physiology is a particularly sensitive parameter to chemical challenge [53]. HCA revealed a subsequent hyperpolarization and depolarization of MMP after 2 h and 24 h exposures. High-contents readouts were therefore more sensitive for detection of this sub-lethal change prior to the onset of general mitochondrial collapse, as detected by the JC-1 assay. Conventional cytotoxicity assays were confirmed here as having lower sensitivity than HCA. With regard to interpreting the HCA data, the MMP hyperpolarization obtained for C_{10} was likely due to compensatory hormesis before its collapse [54]. However, only depolarization of MMP was confirmed for SNAC using the JC-1 assay, which was in agreement with HCA.
One explanation for the hormesis in MMP caused by C_{10} could be that at low C_{10} concentration the initial insertion of molecule into the plasma membrane structure is likely to occur as part of its fluidization mechanism partitions into lipid bilayers and can promote influx of extracellular calcium. As the cytoplasmic Ca^{2+} concentration rises, mitochondria adapt by accumulating more Ca^{2+} ions to buffer the cytosolic loading and consequently become hyperpolarized [55]. In healthy mitochondria, the MMP is generated by reduced NADH, and it arises from the electrochemical potential across the inner mitochondrial membrane, with the energy released forming ATP [56]. In hyperpolarized mitochondria, ATP production is increased and promotes Ca^{2+} cell efflux by the plasma membrane Ca^{2+}-ATPase. Excessive production of protons combines with oxygen lead to leakage of free electrons thereby increasing harmful reactive oxygen species (ROS) production [57]. Accumulation of ROS into mitochondria may lead to the damage of the mitochondrial lipids and proteins, as well as effects on the mitochondrial genome. At moderate C_{10} concentrations, an overload of calcium inside mitochondria increases the inner mitochondrial membrane permeability via opening of the mitochondrial

permeability transition pore [58]. This releases pro-apoptotic factors into the cytosol and activates caspases leading to apoptosis and irreversible cellular damage. In addition, the rapid loss of the proton gradient across the inner mitochondrial membrane leads to depolarization of the MMP. As a consequence, the outflow of Ca^{2+} released into the cytoplasm increases IC levels. With C_{10}, IC was maintained at high levels before loss of MMP and PMP, indicating that disruption of Ca^{2+} homeostasis is a primary consequence of cellular exposure to high C_{10}. This conclusion is in keeping with the mechanism of action initially proposed for C_{10} from HCA data [22]. Calcium efflux may be due to disruption of membrane bound, energy-dependent Ca^{2+} efflux transporters, or may occur by increased passive diffusion across the perturbed membrane into the Ca^{2+}-free extracellular medium [59]. To fully address the mechanisms implicated in mitochondrial impairment other parameters could be screened such as pre-lethal changes in mitochondrial superoxide production, mitochondrial permeability transition, or mitochondrial mass [53].

HCA also identified overall differences between C_{10} and SNAC with respect to IC levels in Caco-2 cells. At low concentrations of both PEs, IC levels increased due to initial depolarization of MMP, which led to release of mitochondrial calcium into the cytoplasm. However, at high SNAC concentrations, maintenance of high IC was observed, whereas for C_{10} the level of IC was decreased (Fig. 8). Although it might not be specific of a particular mechanism, sustained elevation of intracellular calcium might indicate of deleterious effects [60].

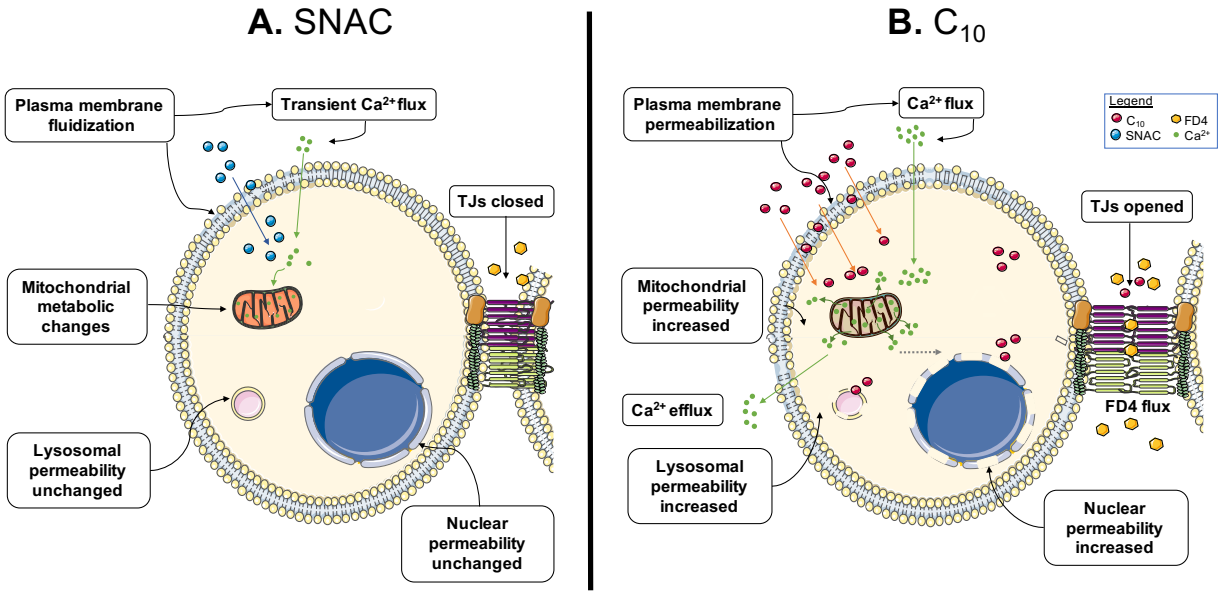

Figure 8: Putative mechanisms of **(A)** SNAC and **(B)** C_{10} on Caco-2 cells.

For both PEs at low concentrations, plasma membrane fluidization in the initial stages does not impair plasma membrane integrity, stimulate LDH release, or increase PMP. At high C_{10} concentrations, changes in cell membrane barrier function were manifested: increased PMP,

loss of MMP, increased LDH release, as well as impaired nuclear- and lysosomal membrane permeability and TJs relocalization. Those data confirm that C_{10} induced membrane perturbation at the same concentrations as those that increased FD4 flux across monolayers. Furthermore, the decrease seen in MMP at 20 mM C_{10} at 2 h correlated with MTS data. Specific monitoring of plasma membrane fluidization using the Laurdan probe after exposure to C_{10} or SNAC could account for differences in calcium retention [61].

Multiple processes occur simultaneously according to HCA when cells are exposed to SNAC or C_{10}. Reduction in MMP was evident for both agents at low concentrations, but association with membrane permeability was unclear, as the conventional assays indicated no LDH leakage, NR release, or increase of DNA staining at concentrations <20 mM. Perhaps the MMP reduction is a first step towards altered membrane permeability. Surfactant-induced membrane perturbation as associated with membrane permeabilization was more pronounced at low C_{10} concentrations whereas higher SNAC concentrations were required to induce similar effects. In a previous study, Malkov *et al.* found no signs of DNA staining in response to 33 mM SNAC in Caco-2 [51]. This confirms that very high SNAC concentrations are required to permit even a weak detergent action based on a non-specific mechanism of action. Even though SNAC caused a reduction in the PMP in Caco-2 cells, this effect might still not be enough to permit either IC efflux or flux of FD4. With HCA, CN is also used to monitor cell proliferation. The MTS assay gave a good correlation for cell viability, matched to reductions in CN. Conflicting reports are found in the literature regarding the comparison of CN with the MTT assay. One group found high concordance between the two methods [62]. Since the MTS assay indirectly measures mitochondrial activity, comparing the HCA mitochondrial parameter is imperative. However, MTS assay is far less sensitive at detecting mitochondrial impairment compared to HCA [63].

In this study exposure to low concentrations of C_{10} allowed complete recovery of TEER after 2h on Caco-2 monolayers but not at high concentrations (> 8.5 mM C_{10}). Damage that occurs *in vitro* upon exposure to PEs can be overestimated due to a reduced capacity for regeneration and turnover compared to the small intestinal mucosa *in vivo* [64]. Since cells are more sensitive to cytotoxic effects of PEs than whole tissue, the risk of toxicity for these surfactants is still considered low. SNAC and C_{10} have been assessed extensively assessed in hundreds of subjects in clinical trials over the last 20 years and no major adverse events have been reported, except for mild GI issues in some subjects [65]. That is not say that there should be any complacency over the possibility of side-effects from chronic administration beyond periods that can be typically be tested in trials.

5. Conclusions

By combining HCA and conventional assays on Caco-2 cells, the mechanisms in SNAC and C_{10} permeation enhancement across Caco-2 monolayers have been clarified. Even though cell-based assays cannot yet predict PE human cytotoxicity, they allow inference of mechanisms of action *in vivo* if concentrations can be related. Overall, the HCA and flux data showed that the minimum concentrations required to induce flux across Caco-2 monolayers are lower for C_{10} than SNAC, indicating a higher potency for the former. Cytotoxicity was detected at multiple levels with alteration in calcium homeostasis and mitochondria function occurring for both PEs, but only at high concentrations. Similar efficacy, low cytotoxicity, and common features in the surfactant mechanism of action of SNAC and C_{10} *in vitro* indicate that a valid case can be made for using either in clinical development of oral macromolecule formulations.

Acknowledgments

Authors would like to thank Pr. Jeremy Simpson (UCD) for his assistance with the confocal microscope. Pr. Peter O'Brien, Pr. Kenneth Dawson and Dr. Kai Liu are thanked for their assistance in the HCA study.

Supplementary

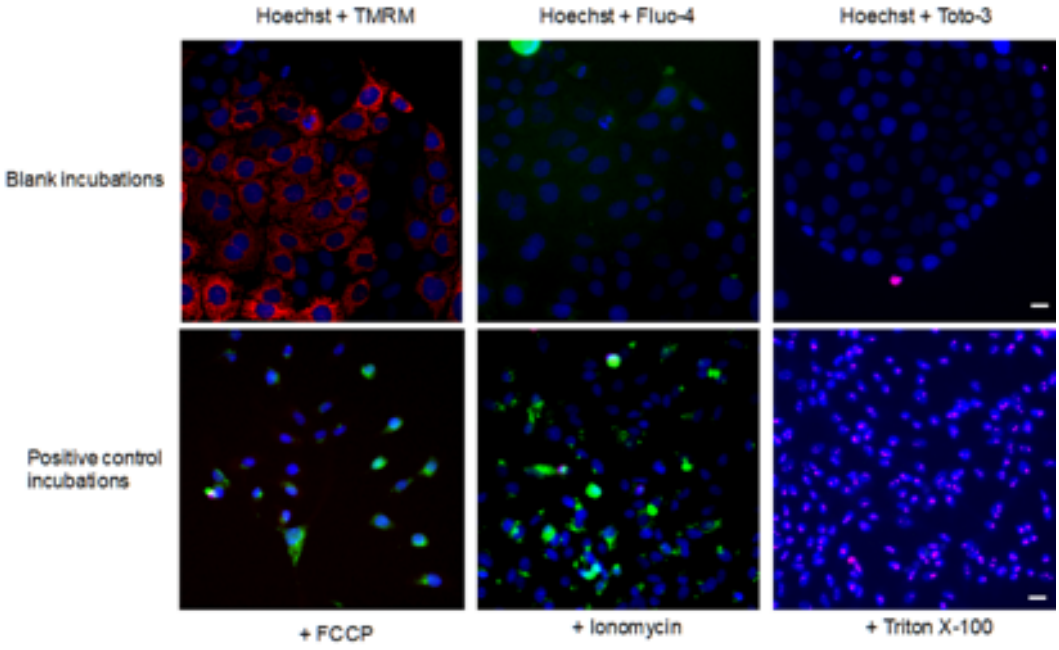

Suppl. Fig.1: HCA images of Caco-2 cells in the presence and absence of three positive controls for parameters. The dyes, Hoechst 33342 (blue-stained nuclei to measure CN, NA, NI), TMRM (red to measure MMP), fluo-4-AM (green to measure IC), Toto-3 (dark red to measure PMP) were incubated with Caco-2 cells in negative control buffer (upper panels) or with positive control agents in lower panels. Concentrations of positive controls: 100 µM FCCP, 20 µM ionomycin, 0.05 % w/v Triton® X-100. Nuclei are stained blue. Exposure times for the three positive control agents was 10 min. Horizontal bars = 20 µm.

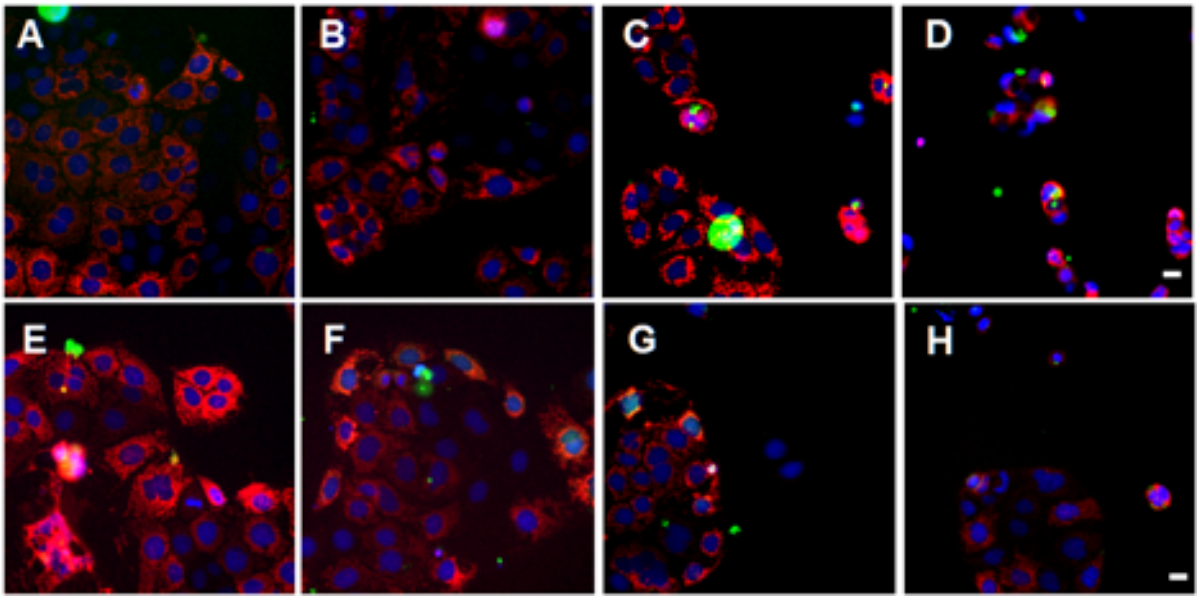

Suppl. Fig. 2. Representative HCA images of Caco-2 cells after 2 h exposures to C_{10} or SNAC. (A) Vehicle control for C_{10}; (B) 2.5 mM C_{10}; (C) 5 mM C_{10}; (D) 8.5 mM C_{10}; (E) Vehicle control for SNAC; (F) 2.5 mM SNAC; (G) 5 mM SNAC; (H) 8.5 mM SNAC. Each fused fluorescent image was acquired at 20x objective magnification and pseudo-coloured: Hoechst® (blue), Fluo-4 AM (green), TOTO®-3 (dark red) and TMRM (red). Horizontal bars = 20 µm.

References

[1] A. Adan, Y. Kiraz, Y. Baran, Cell proliferation and cytotoxicity assays, Current Pharmaceutical Biotechnology. 17 (2016) 1213-1221.

[2] Aslantürk, *In vitro* cytotoxicity and cell viability assays: principles, advantages, and disadvantages, (2019). Chapter from the Edited Volume, Genotoxicity, A Predictable Risk to Our Actual World, Ed. M. L. Larramendy, S. Soloneski. http://dx.doi.org/10.5772/intechopen.71923.

[3] P. O'Brien, J.R. Haskins, *In vitro* cytotoxicity assessment, Methods Mol. Biol. (Clifton, N.J.). 356 (2007) 415-425.

[4] D.J. Brayden, S.A. Cryan, K.A. Dawson, P.J. O'Brien, J.C. Simpson, High-content analysis for drug delivery and nanoparticle applications, Drug Discov. Today, 20 (2015) 942-957.

[5] P.J. O'Brien, A. Edvardsson, Validation of a multiparametric, high-content-screening assay for predictive/investigative cytotoxicity: evidence from technology transfer studies and literature review, Chemical Res. Toxicol. 30 (2017) 804-829.

[6] L. Tolosa, M.J. Gomez-Lechon, M.T. Donato, High-content screening technology for studying drug-induced hepatotoxicity in cell models, Arch. Toxicol. 89 (2015) 1007-1022.

[7] L.H.J. Richter, A. Beck, V. Flockerzi, H.H. Maurer, M.R. Meyer, Cytotoxicity of new psychoactive substances and other drugs of abuse studied in human HepG2 cells using an adopted high content screening assay, Toxicology Letters. 301 (2019) 79-89.

[8] N.T.T. Tham, S.R. Hwang, J.H. Bang, H. Yi, Y.I. Park, S.J. Kang, H.G. Kang, Y.S. Kim, H.O. Ku, High-content analysis of in vitro hepatocyte injury induced by various hepatotoxicants, J. Veterinary Science. 20 (2019) 34-42.

[9] J. Chiaravalli, J.F. Glickman, A high-content live-cell viability assay and its validation on a diverse 12K compound screen. SLAS Discovery: Advancing Life Sciences R & D. (2017) https://doi.org/10.1177/2472555217724745.

[10] P.J. O'Brien, W. Irwin, D. Diaz, E. Howard-Cofield, C.M. Krejsa, M.R. Slaughter, B. Gao, N. Kaludercic, A. Angeline, P. Bernardi, P. Brain, C. Hougham, High concordance of drug-induced human hepatotoxicity with in vitro cytotoxicity measured in a novel cell-based model using high content screening, Arch. Toxicology. 80 (2006) 580-604.

[11] A. Pradip, D. Steel, S. Jacobsson, G. Holmgren, M. Ingelman-Sundberg, P. Sartipy, P. Björquist, I. Johansson, J. Edsbagge, High content analysis of human pluripotent stem cell-derived hepatocytes reveals drug-induced steatosis and phospholipidosis, Stem Cells Int. (2016) 2475631-2475631. doi: 10.1155/2016/2475631.

[12] V.C. Abraham, D.L. Towne, J.F. Waring, U. Warrior, D.J. Burns, Application of a high-content multiparameter cytotoxicity assay to prioritize compounds based on toxicity potential in humans, J. Biomolecular Screening. 13 (2008) 527-537.

[13] J. Saito, A. Okamura, K. Takeuchi, K. Hanioka, A. Okada, T. Ohata, High content analysis assay for prediction of human hepatotoxicity in HepaRG and HepG2 cells, Toxicology In Vitro. 33 (2016) 63-70.

[14] M. Chen, C.W. Tung, Q. Shi, L. Guo, L. Shi, H. Fang, J. Borlak, W. Tong, A testing strategy to predict risk for drug-induced liver injury in humans using high-content screen assays and the 'rule-of-two' model, Arch. Toxicol. 88 (2014) 1439-1449.

[15] T. Tomida, H. Okamura, T. Yokoi, Y. Konno, A modified multiparametric assay using HepaRG cells for predicting the degree of drug-induced liver injury risk, J. Applied Toxicology. 37 (2017) 382-390.

[16] T.A. Aguirre, D. Teijeiro-Osorio, M. Rosa, I.S. Coulter, M.J. Alonso, D.J. Brayden, Current status of selected oral peptide technologies in advanced preclinical development and in clinical trials, Adv. Drug Deliv. Rev, 106 (2016) 223-241.

[17] B.J. Aungst, Absorption enhancers: applications and advances, AAPS Journal, 14 (2012) 10-18.

[18] J. D. Bucheit, L. G. Pamulapati, N. Carter, K. Malloy, D. L. Dixon, E. M. Sisson, Oral semaglutide: a review of the first oral Glucagon-like Peptide-1 receptor agonist. Diabetes Technol. Ther. 2019 Oct 1. doi: 10.1089/dia.2019.0185

[19] V. R. Aroda, T. Saugstrup, J. B. Buse, M. Donsmark, J. Zacho, M. J. Davies, Incorporating and interpreting regulatory guidance on estimands in diabetes clinical trials: The PIONEER 1 randomized clinical trial as an example. Diabetes Obes. Metab. 21 (2019) 2203-2210. doi: 10.1111/dom.13804.

[20] L. Smith, J. Mosley, M. Ford, J. Courtney, Cyanocobalamin/Salcaprozate Sodium: A novel way to treat vitamin B12 deficiency and anemia, J. Hematol. Oncol. Pharm. 6 (2016) 42-45.

[21] I.B. Halberg, K. Lyby, K. Wassermann, T. Heise, L. Plum-Morschel, E. Zijlstra, The effect of food intake on the pharmacokinetics of oral basal insulin: a randomised crossover trial in healthy male subjects, Clinical Pharmacokinetics. 58 (2019) 1497-1504. doi: 10.1007/s40262-019-00772-2.

[22] D.J. Brayden, J. Gleeson, E.G. Walsh, A head-to-head multi-parametric high content analysis of a series of medium chain fatty acid intestinal permeation enhancers in Caco-2 cells, Eur. J. Pharm. Biopharm. 88 (2014) 830-839.

[23] A.W. Alani, J.R. Robinson, Mechanistic understanding of oral drug absorption enhancement of cromolyn sodium by an amino acid derivative, Pharm. Res. 25 (2008) 48-54.

[24] S.T. Buckley, T.A. Baekdal, A. Vegge, S.J. Maarbjerg, C. Pyke, J. Ahnfelt-Ronne, K.G. Madsen, S.G. Scheele, T. Alanentalo, R.K. Kirk, B.L. Pedersen, R.B. Skyggebjerg, A.J. Benie, H.M. Strauss, P.O. Wahlund, S. Bjerregaard, E. Farkas, C. Fekete, F.L. Sondergaard, J. Borregaard, M.L. Hartoft-Nielsen, L.B. Knudsen, Transcellular stomach absorption of a derivatized glucagon-like peptide-1 receptor agonist, Science Trans. Med. 10 (2018). doi: 10.1126/scitranslmed.aar7047.

[25] X. Wang, S. Maher, D.J. Brayden, Restoration of rat colonic epithelium after in situ intestinal instillation of the absorption promoter, sodium caprate, Ther. Del. 1 (2010) 75-82.

[26] I. Hubatsch, E.G. Ragnarsson, P. Artursson, Determination of drug permeability and prediction of drug absorption in Caco-2 monolayers, Nature Protocols. 2 (2007) 2111-2119.

[27] Y. Ma, S. Semba, R.I. Khan, H. Bochimoto, T. Watanabe, M. Fujiya, Y. Kohgo, Y. Liu, T. Taniguchi, Focal adhesion kinase regulates intestinal epithelial barrier function via redistribution of tight junction, Biochimica et Biophysica Acta. 1832 (2013) 151-159.

[28] J.P. Gleeson, J. Heade, S.M. Ryan, D.J. Brayden, Stability, toxicity and intestinal permeation enhancement of two food-derived antihypertensive tripeptides, Ile-Pro-Pro and Leu-Lys-Pro, Peptides. 71 (2015) 1-7.

[29] Promega, Determining LDH Cytotoxicity in 3D Microtissues with the GloMax® Discover System, http://worldwide.promega.com/resources/pubhub/applications-notes/an300/an345-determining-ldh-cytotoxicity-in-3d-microtissues/ Updated 9/19. Accessed November 20th, 2019.

[30] R. Carpentier, A. Platel, H. Maiz-Gregores, F. Nesslany, D. Betbeder, Vectorization by nanoparticles decreases the overall toxicity of airborne pollutants, PloS One.12 (2017) e0183243.

[31] M. Reers, T.W. Smith, L.B. Chen, J-aggregate formation of a carbocyanine as a quantitative fluorescent indicator of membrane potential, Biochemistry. 30 (1991) 4480-4486.

[32] A. Perelman, C. Wachtel, M. Cohen, S. Haupt, H. Shapiro, A. Tzur, JC-1: alternative excitation wavelengths facilitate mitochondrial membrane potential cytometry, Cell Death & Disease. 3 (2012) e430.

[33] G. Repetto, A. del Peso, J.L. Zurita, Neutral red uptake assay for the estimation of cell viability/cytotoxicity, Nature Protocols. 3 (2008) 1125-1131.

[34] M. Persson, A.F. Loye, T. Mow, J.J. Hornberg, A high content screening assay to predict human drug-induced liver injury during drug discovery, J. Pharmacological Toxicological Methods. 68 (2013) 302-313.

[35] L.-A.B. Rawlinson, P.J. O'Brien, D.J. Brayden, High content analysis of cytotoxic effects of pDMAEMA on human intestinal epithelial and monocyte cultures, J. Controlled Release. 146 (2010) 84-92.

[36] J.P. Gleeson, D.J. Brayden, S.M. Ryan, Evaluation of PepT1 transport of food-derived antihypertensive peptides, Ile-Pro-Pro and Leu-Lys-Pro using in vitro, *ex vivo* and in vivo transport models, Eur. J. Pharm. Biopharm. 115 (2017) 276-284.

[37] M. Marusic, T. Zupancic, G. Hribar, R. Komel, G. Anderluh, S. Caserman, The Caco-2 cell culture model enables sensitive detection of enhanced protein permeability in the presence of N-decyl-beta-d-maltopyranoside, New Biotechnology. 30 (2013) 507-515.

[38] D.J. Brayden, E. Walsh, Efficacious intestinal permeation enhancement induced by the sodium salt of 10-undecylenic acid, a medium chain fatty acid derivative, AAPS J, 16 (2014) 1064-1076.

[39] D. Malkov, R. Angelo, H.Z. Wang, E. Flanders, H. Tang, I. Gomez-Orellana, Oral delivery of insulin with the eligen technology: mechanistic studies, Current Drug Delivery, 2 (2005) 191-197.

[40] S.C. Chen-Quay, K.T. Eiting, A.W. Li, N. Lamharzi, S.C. Quay, Identification of tight junction modulating lipids, J. Pharm. Sci. 98 (2009) 606-619.

[41] K.H. Yuen, The transit of dosage forms through the small intestine, Int. J. Pharm. 395 (2010) 9-16.

[42] G. Cudazzo, D.J. Smart, D. McHugh, P. Vanscheeuwijck, Lysosomotropic-related limitations of the BALB/c 3T3 cell-based neutral red uptake assay and an alternative testing approach for assessing e-liquid cytotoxicity, Toxicology In Vitro. 61 (2019) 104647.

[43] T.A. Baekdal, M. Thomsen, V. Kupcova, C.W. Hansen, T.W. Anderson, Pharmacokinetics, safety, and tolerability of oral semaglutide in subjects with hepatic impairment, J. Clin. Pharmacology, 58 (2018) 1314-1323.

[44] M. Tomita, M. Hayashi, S. Awazu, Absorption-enhancing mechanism of EDTA, caprate, and decanoylcarnitine in Caco-2 cells, J. Pharm. Sci. 85 (1996) 608-611.

[45] T. Lindmark, T. Nikkila, P. Artursson, Mechanisms of absorption enhancement by medium chain fatty acids in intestinal epithelial Caco-2 cell monolayers, J. Pharm. Exp. Ther. 275 (1995) 958-964.

[46] E.K. Anderberg, T. Lindmark, P. Artursson, Sodium caprate elicits dilatations in human intestinal tight junctions and enhances drug absorption by the paracellular route, Pharm. Res. 10 (1993) 857-864.

[47] S.M. Krug, M. Amasheh, I. Dittmann, I. Christoffel, M. Fromm, S. Amasheh, Sodium caprate as an enhancer of macromolecule permeation across tricellular tight junctions of intestinal cells, Biomaterials. 34 (2013) 275-282.

[48] H. Wen, D.D. Watry, M.C. Marcondes, H.S. Fox, Selective decrease in paracellular conductance of tight junctions: role of the first extracellular domain of claudin-5, Mol. Cellular Biol. 24 (2004) 8408-8417.

[49] S. Amasheh, T. Schmidt, M. Mahn, P. Florian, J. Mankertz, S. Tavalali, A.H. Gitter, J.D. Schulzke, M. Fromm, Contribution of claudin-5 to barrier properties in tight junctions of epithelial cells, Cell Tissue Res. 321 (2005) 89-96.

[50] X. Ding, P. Rath, R. Angelo, T. Stringfellow, E. Flanders, S. Dinh, I. Gomez-Orellana, J.R. Robinson, Oral absorption enhancement of cromolyn sodium through noncovalent complexation, Pharm. Res. 21 (2004) 2196-2206.

[51] D. Malkov, H.Z. Wang, S. Dinh, I. Gomez-Orellana, Pathway of oral absorption of heparin with sodium N-[8-(2-hydroxybenzoyl)amino] caprylate, Pharm. Res. 19 (2002) 1180-1184.

[52] S.J. Wu, J.R. Robinson, Transcellular and lipophilic complex-enhanced intestinal absorption of human growth hormone, Pharm. Res. 16 (1999) 1266-1272.

[53] L. Tolosa, A. Carmona, J.V. Castell, M.J. Gomez-Lechon, M.T. Donato, High-content screening of drug-induced mitochondrial impairment in hepatic cells: effects of statins, Arch. Toxicol. 89 (2015) 1847-1860.

[54] P.J. O'Brien, High-content analysis in toxicology: screening substances for human toxicity potential, elucidating subcellular mechanisms and in vivo use as translational safety biomarkers, Basic & Clinical Pharmacology & Toxicology, 115 (2014) 4-17.

[55] R. Rizzuto, D. De Stefani, A. Raffaello, C. Mammucari, Mitochondria as sensors and regulators of calcium signalling, Nature reviews. Molecular Cell Biology, 13 (2012) 566-578.

[56] A. Szewczyk, L. Wojtczak, Mitochondria as a pharmacological target, Pharmacological Rev. 54 (2002) 101-127.

[57] S.P. Pereira, G.C. Pereira, A.J. Moreno, P.J. Oliveira, Can drug safety be predicted and animal experiments reduced by using isolated mitochondrial fractions? ATLA. 37 (2009) 355-365.

[58] P. Bernardi, A. Rasola, Calcium and cell death: the mitochondrial connection, Sub-Cellular biochemistry, 45 (2007) 481-506.

[59] E.G. Walsh, S. Maher, M. Devocelle, P.J. O'Brien, A.W. Baird, D.J. Brayden, High content analysis to determine cytotoxicity of the antimicrobial peptide, melittin and selected structural analogs, Peptides. 32 (2011) 1764-1773.

[60] Z. Dong, P. Saikumar, J.M. Weinberg, M.A. Venkatachalam, Calcium in cell injury and death, Ann. Rev. Pathol. 1 (2006) 405-434.

[61] R.J. Cavanagh, P.A. Smith, S. Stolnik, Exposure to a non-ionic surfactant induces a response akin to heat-shock apoptosis in intestinal epithelial cells: implications for excipients safety, Mol. Pharm. 16 (2019) 618-631.

[62] J.P. Meneely, J. Hajslova, R. Krska, C.T. Elliott, Assessing the combined toxicity of the natural toxins, aflatoxin B1, fumonisin B1 and microcystin-LR by high content analysis, Food Chem. Toxicology. 121 (2018) 527-540.

[63] J. Wilson, H.F. Berntsen, K.E. Zimmer, C. Frizzell, S. Verhaegen, E. Ropstad, L. Connolly, Effects of defined mixtures of persistent organic pollutants (POPs) on multiple cellular responses in the human hepatocarcinoma cell line, HepG2, using high content analysis screening, Toxicology Applied Pharmacology, 294 (2016) 21-31.

[64] A.T. Blikslager, A.J. Moeser, J.L. Gookin, S.L. Jones, J. Odle, Restoration of barrier function in injured intestinal mucosa, Physiological Rev. 87 (2007) 545-564.

[65] C. Twarog, S. Fattah, J. Heade, S. Maher, E. Fattal, D.J. Brayden, Intestinal permeation enhancers for oral delivery of macromolecules: a comparison between salcaprozate sodium (SNAC) and sodium caprate (), Pharmaceutics. 11 (2019). 11. pii: E78. doi: 10.3390/pharmaceutics110200

Chapter 4

Effect of SNAC and C_{10} on properties of isolated rat intestinal tissue mucosae and intestinal sacs

Chapitre 4 : Effets de SNAC et C_{10} sur les propriétés de tissues intestinaux isolés et sacs intestinaux de rats

Résumé

Le but de cette étude était de : (i) étudier leur mécanisme d'action sur des muqueuses intestinales isolées de rat et montées sur des chambres de Ussing ou au travers de sacs intestinaux non inversés ; (ii) étudier leur impact sur les tissus issus de trois modèles intestinaux (chambres de Ussing, sacs intestinaux, instillations intra-jéjunales *in situ*) par une évaluation histologique et (iii) explorer leur interaction avec du mucus intestinal de porc. Les propriétés d'amélioration de la perméabilité du SNAC et du C_{10} ont été confirmées sur muqueuses jéjunales et coliques isolées, car elles augmentent le coefficient de perméabilité apparent (P_{app}) des marqueurs paracellulaires, le [^{14}C]-mannitol et le FITC-dextran 4000 (FD4). L'ajout de C_{10} au niveau apical a rapidement réduit la résistance électrique transepithéliale (TEER) dans les tissus jéjunaux et coliques isolés, mais le SNAC n'a pas réduit cette résistance. Une concentration seuil plus élevée, > 20 mM, était nécessaire pour que le SNAC atteigne une efficacité d'amélioration similaire à celle du C_{10} (10 mM). Le SNAC a augmenté les flux de FD4 dans les muqueuses gastriques isolées en fonction de la concentration, alors que le C_{10} ne l'a pas fait. Dans les sacs intestinaux, des augmentations du flux de FD4 ont été observées en présence des deux PE. L'histologie a révélé que les deux promoteurs ont induit des lésions épithéliales mineures et avec un maintien adéquat de la fonction de transport d'ions électrogénique. Le tissu jéjunal pourrait mieux résister aux dommages épithéliaux dans l'ordre suivant : instillations intra-jéjunales *in situ* > sacs jéjunaux > muqueuses jéjunales isolées. Les deux PE ont modulé les propriétés viscoélastiques du mucus isolé intestinal de porc jéjunale sans en altérer les propriétés rhéologiques. Par conséquent, la structure type gel du mucus a été préservée et a conservé la capacité intacte de récupération lors d'un challenge avec une forte contrainte. Ces résultats indiquent que le SNAC et le C_{10} sont des promoteurs d'absorption efficaces qui présentent des caractéristiques mécanistiques communes. Les données sont en bon accord avec leurs profils de toxicité actuels dans les essais cliniques.

Mot clés : Délivrance orale de peptide, promoteurs d'absorption intestinaux, Rhéologie, étude de perméabilité, C_{10}, SNAC

Chapter 4: Effects of SNAC and C_{10} on properties of isolated rat intestinal tissue mucosae and intestinal sacs

Abstract

SNAC and C_{10} are anionic surfactant excipients used as permeation enhancers in advanced oral peptide formulations. The aims of this study were to: (i) investigate their mechanism of action in isolated rat intestinal mucosae mounted in Ussing chambers and in non-everted gut sacs, (ii) study their effects on mucosa integrity through histological assessment following exposure to three intestinal models (Ussing chambers, gut sacs, *in situ* intra jejunal instillations) and (iii) explore their interactions with a native porcine intestinal mucus. Permeability-enhancing properties of SNAC and C_{10} were confirmed in isolated jejunal and colonic mucosae, as they enhanced the apparent permeability coefficient (P_{app}) of the paracellular markers, [^{14}C]-mannitol and FITC-dextran 4000 (FD4). Apical addition of C_{10} rapidly reduced the transepithelial electrical resistance (TEER) in isolated jejunal and colonic tissue, but SNAC did not. A higher threshold concentration of > 20 mM was necessary for SNAC to achieve similar efficacy in enhancement compared to C_{10} (10 mM). SNAC increased FD4 fluxes across isolated gastric mucosae in a concentration-dependent fashion, whereas C_{10} did not. In non-everted jejunal and colonics sacs, FD4 flux increases were observed in the presence of both PEs. The histology revealed that both PEs induced minor epithelial damage to the mucosa at the concentrations required to increase marker fluxes and with adequate maintenance of electrogenic ion transport function. Jejunal tissue could better withstand epithelial damage in the following order: intra jejunal *in situ* instillations > jejunal sacs > isolated jejunal mucosae. Both PEs modulated viscoelastic properties of porcine jejunal mucus without altering rheological properties. Consequently, the gel-like structure of mucus was preserved and retained the intact capacity to recover when challenged with high strain. These results indicate that SNAC and C_{10} are effective permeation enhancers with more common mechanistic features than differences. The data are in good agreement with their current toxicity profiles in clinical trials.

Key words: Oral peptide delivery, intestinal permeation enhancers, mucus rheology, permeability studies, C_{10}, SNAC

1. Introduction

The human intestinal epithelium is primarily composed of six cell epithelial types that are arranged in a crypt-villus structure [1]. As Caco-2 monolayers are derived from epithelial colorectal adenocarcinoma epithelial enterocytes, emerging models such as co-cultures expressing different types of intestinal epithelial cells [2] [3], organoids [4], and microfluidic organ chip systems [5] have been developed to better reflect *in vivo* small intestine physiology and predict drug permeability in humans [6]. Caco-2 monolayers are useful tools in preliminary assessment of permeations enhancers (PE), but they do not reflect complex *in vivo* situations [7]. Indeed, cultured cells are homogeneously composed of fully differentiated cells that are transformed, whereas the intestine expresses different levels of maturity in epithelial cells from the base of the crypts to the tip of the villus. Also, as Caco-2 over-express TJs proteins [8] and lack mucus production and a blood supply [7], the efficacy and cytotoxicity and of PEs may not correlate with *in vivo*. In the previous chapter, Caco-2 cell and monolayer models yielded useful information on the mechanism of action for SNAC and C_{10} at low concentrations, but they were overly sensitive to cytotoxic effects at higher concentrations. Similarly, a correlation was found by Quan *et al.* between the permeability-enhancing effects of various PEs and cytotoxicity in Caco-2 cells [9]. On the other hand, others concluded that PEs can enhance permeability without inducing significant toxicity in Caco-2 monolayers [10], so this is a controversial point.

To bridge the gap between cell-based assays and *in vivo* studies, several *ex vivo* and *in situ* intestinal epithelial tissue models have been used to screen the permeation enhancement capacity of PEs [11]. *Ex vivo* isolated tissue models are composed of a multicellular epithelial organization, a mucus layer, lamina propria, and contain epithelial transporters and TJ structure that reflects the complex *in vivo* morphology. As an example, isolated *ex vivo* intestinal tissue mucosae from rat and human has been tested with PEs in Ussing chambers [12], [13], [14]. C_{10} has been intensively tested in Ussing chambers as a PE for macromolecule enhancement across isolated muscle-stripped rat jejunal and colonic mucosae [15]. However, no studies have yet focused on its potential permeation enhancing effects through the gastric mucosa. Recent research has established the stomach as the major site of oral semaglutide absorptions formulated with SNAC in dogs and humans [16]. As part of the evidence, Buckley *et al.* concluded that SNAC promoted semaglutide absorption across rat gastric mucosa in Ussing chambers in a concentration-dependent manner via effects on transcellular pathways. One other study showed a predominant effect of SNAC on the transcellular pathway transport on isolated rat intestinal mucosae [17].

Therefore, to further assess mechanistic data about SNAC and C_{10} on *ex vivo* models we performed a head- to-head comparison of their permeation enhancement effects across the three intestinal regions of isolated rat mucosae in Ussing chambers. Secondly, another *ex vivo* model, the everted / non-everted gut sac is considered a quick and inexpensive bioassay and provides an opportunity to provide initial examination of the effect of PEs before proceeding into *in vivo* animal models [18], [19]. Intestinal sacs offer the contribution of a more intact mucous gel layer and maintenance of the tube-like intestinal structure compared to dissected muscle-stripped tissue mucosae mounted as sheets in Ussing chambers [20]. To our knowledge, C_{10} and SNAC enhancing effects have not been studied in non-everted gut sacs. Therefore, we investigated their effect on jejunal and colonic non-everted gut sacs. Thirdly, the *in-situ* intestinal instillation model has been widely used to test intestinal PEs [21], [22], [23] and is considered as a pre-screen before testing PEs by oral gavage. With the animal under anesthesia, a closed intestinal loop with intact blood supply is created. The loop is filled with PE solution mixed with the drug and blood samples are taken to measure the rate of drug absorption in the presence of PE. This method by-passes the effects from stomach such as pH, gastric emptying time, and dilution, so ad-mixtures of PEs and drug can be tested [11]. The PE and drug are presented to the lumen, close to the gut wall with intact blood flow and mucus layer, so this is a best-case scenario that, if successful, can then justify gavage studies with oral dose formulations. Differences in regional absorption can also be investigated [24]. In this study, we were limited to just performing histological comparisons of the effects of SNAC and C_{10} after intra jejunal instillations with the emphasis on cytotoxicity.

The narrow window between concentrations of PEs that induce efficacy and cytotoxicity in cell culture models has raised concerns that surfactant-based PEs might lead to GI damage *in vivo* [25]. A close association between permeation enhancement and mucosal perturbation has been demonstrated on isolated rat intestinal mucosae in Ussing chambers based on gross histology changes [12] and the induced release of intracellular markers of viability [26]. However, to test PE intestinal damage more deeply, *in situ*-intestinal loop instillations are preferred as they contain intact tissue with a mesenteric blood supply allowing normal epithelial repair mechanisms to be expressed [27]. *In situ* rat colonic instillations of C_{10} caused mild mucosal damage when the tissue was histologically assessed at the T_{max} for absorption-promotion [28]. Other *in situ* and *in vivo* rat studies show barely discernable-induced mucosal damage at later time points, likely masked by the intestinal epithelium's capacity to recover as the agent is absorbed. The capacity for epithelial repair following C_{10} exposure was also investigated in rat jejunal instillations, where full restitution was seen within 60 min of exposure [29]. Similarly, Swenson *et al.* investigated the toxicity of selected surfactants using an intestinal single pass perfusion model in rats and saw rapid repair of the mucosa within 1-3 h

after removal of surfactants [30] [31]. SNAC has been intensively tested in clinical trials but *ex vivo* permeability enhancement investigations are scarce in the literature. Hess *et al.* tested SNAC on isolated rat jejunal mucosae in Ussing chambers but no histology was presented in this study [17]. *In situ* jejunal and colonic instillations of 35 mg SNAC (116 mM) over 5 hours increased heparin transport without damaging the mucosa in another study [32]. In this chapter, intra jejunal instillations of SNAC and C_{10} solution were carried out as part of a qualitative histological assessment of the jejunal mucosa and to make a comparison with isolated mucosae and non-everted sacs exposed to the agents.

Intestinal goblet cells normally secrete mucus, a complex hydrogel biopolymer [33]. The carbohydrate moiety (70-80%) of the intestinal mucins creates a viscous gel barrier that protect the luminal surface from digestion, physical friction, and colonization with bacteria [34]. Two mucus layers line the stomach and colon (outer layer, loosely adherent, and an underlying layer, firmly adherent) whereas a single mucus layer protects the small intestine [35]. However, the structure of mucus can be affected when exposed to external challenges including surfactants [36]. It has been shown that disruption of the mucous layer with the mucolytic, N-acetyl cysteine (NAC), increased intestinal permeability in rats [37]. After a chronic long-term oral exposure to two FDA-approved emulsifiers, carboxymethylcellulose (CMC) and polysorbate-80 (a non-ionic surfactant), the thickness of mouse intestinal mucus was also decreased [38]. In another study, CMC decreased the mucus gel pore size and thickness in *in situ* intestinal loops and mucus-producing cell cultures. Polysorbate-80 had minimal effects on isolated porcine mucus structure, but it caused depletion of the mucus layer in cell culture and *ex vivo* tissue models, as well as changes in mucus content after exposure to rodents *in vivo* [39]. A recently discovered PE, the ionic liquid, choline geranate, also decreased viscosity of simulated mucus [40]. Zhang *et al.* reported that, in contrast, the viscosity of native pig mucus was increased with sodium dodecyl sulfate (SDS), an anionic surfactant, implying that SDS may induce denaturation and aggregation. However, nonionic surfactants, polysorbate-80 and poloxamers 188 and 407 slightly decreased the viscosity of the mucus retaining the original mucus rheology and morphology properties [41]. A safe enhancer should be able to promote peptide absorption through the intestinal mucosa without compromising the mucus layer. A permeabilization or total removal of the mucus layer could expose unprotected mucosa to microbes, viruses, and lipopolysaccharide fragments until a new layer is secreted [36]. As surfactants, we hypothesized that SNAC and C_{10} may also disrupt mucous and alter its viscosity and this might be a safety issue for chronic administration.

In this Chapter, the aim was first to investigate the permeation enhancing capacity of SNAC in comparison to C_{10} on freshly excised rat intestinal mucosae mounted in Ussing chambers.

Tissue from three distinct regions were investigated (rat gastric, jejunal, and colonic mucosae) to screen for differences in the permeability of the paracellular markers ([^{14}C]-mannitol and FD4). Second, the rat non-everted sac model was also tested to further compare SNAC and C_{10} permeation enhancement. Third, tissues from Ussing chambers, non-everted gut sacs and *in situ* jejunal instillations were then histologically assessed to compare potential damage of SNAC or C_{10}. Finally, we also investigated the effect of SNAC and C_{10} on mucus properties by investigating if they caused mucin removal from isolated tissue in the Ussing chamber and if they modulated porcine mucus rheology.

2. Materials and Methods

2.1 Reagents and Chemicals

Fluorescein isothiocyanate (FITC) labelled dextran (FD4), sodium salt of capric acid (C_{10}), N-acetyl cysteine) and Medium 199 were obtained from Sigma (Ireland). SNAC was from AstaTech, Inc. (Bristol, USA). [^{3}H]-exenatide was obtained from RC Tritec (Switzerland). Carbachol (CCh) (Merck Biosciences, UK), [^{14}C]-mannitol (Perkin Elmer, UK) were obtained from these respective suppliers. General chemicals and reagents used were of analytical grade and were obtained from Sigma–Aldrich, Dublin, Ireland.

2.2 Transport studies using isolated rat tissue mucosae in Ussing chambers

2.2.1 Tissue preparation

Ussing chamber methodology was carried out as previously described [42] [43]. Male Wistar rats (250-350g) were obtained from the UCD Biomedical Facility. All work was carried out in accordance with UCD Animal Research Ethics Committee protocol (AREC) protocol #14–28, approved in 2014 and in adherence with the “Principles of Laboratory Animal Care” (NIH Publication #85-23, revised in 1985). The animals were housed in environmentally controlled conditions of humidity and temperature under a 12:12 hour light/dark cycle with access to laboratory chow and filtered water *ad lib*. Rats were euthanized by stunning and cervical dislocation. A midline laparotomy was performed and the colon and stomach were excised and placed directly in warm Krebs-Henseleit buffer (KH) (composition in mM; NaCl 118, KCl 4.7, $CaCl_2$ 2.5, $MgSO_4$ 1.2, KH_2PO_4 1.2, $NaHCO_3$ 25, and D-glucose 11.1, at pH 7.4), which had been bubbled with 95% O_2/5% CO_2. A 5 cm piece of jejunum was removed and placed in KH solution in ice for 10 min. The seromuscular layer was then stripped to minimise the influence of the intrinsic neuromuscular system and to allow for stretching over the chamber pins by different methods depending on the organ.

- Gastric mucosae isolation from rats: KH Solution was injected with a 1 ml 27G ½'' needle directly under the seromuscular layer around the sides of the organ causing a blistering effect, with careful consideration not to place the needle near the centre [44]. A cut was made from the duodenum opening to the oesophageal opening exposing the interior. The stomach was washed several times with KH buffer until all contents were removed. The stomach was then stretched and pinned on a wax board with the mucosal side facing down. Pins were applied around the edge of the tissue and the seromuscular layer was slowly stripped with a Dumont #5 forceps and a scalpel blade.
- Jejunal mucosae isolation from rats: 15 cm of jejunum was excised at a point 10-12 cm proximal to the stomach and rinsed with KH to remove intestinal contents. A dissection was made along the mesentery exposing the mucosal side, which was faced downwards. Pins were placed through the edge of the jejunal sheet into the wax, spreading the tissue. Stripping was done under a ZEISS Stemi DV4 microscope due to the size of the seromuscular layer with blunted #5 tweezers.
- Colonic mucosae isolation from rats: The colon was opened along the mesentery and fecal matter was removed. Tissue was orientated so that the basolateral side was facing up and mucosal side facing down. The muscle layer was removed and a similar dissection was made as with the jejunum; however, the microscope was not required.

2.2.2 Mounting mucosae in the Ussing chamber

The tissue was mounted in the Ussing chamber cylindrical tissue holder with a circular diameter of 0.63 cm^2 [21] (World Precision Instruments, WPI, UK) (Figure 1). Then the tissue was bathed bilaterally with 5 ml of KH solution at pH 7.4. The system was maintained at 37°C and gassed with 95% O_2/5% CO_2, since high oxygenation levels are required to overcome the lack of blood supply [45]. The apical membrane faced one chamber half, with the basolateral membrane facing the other half. For both distal and proximal intestinal sheets, Peyer patches were avoided during mounting [46].

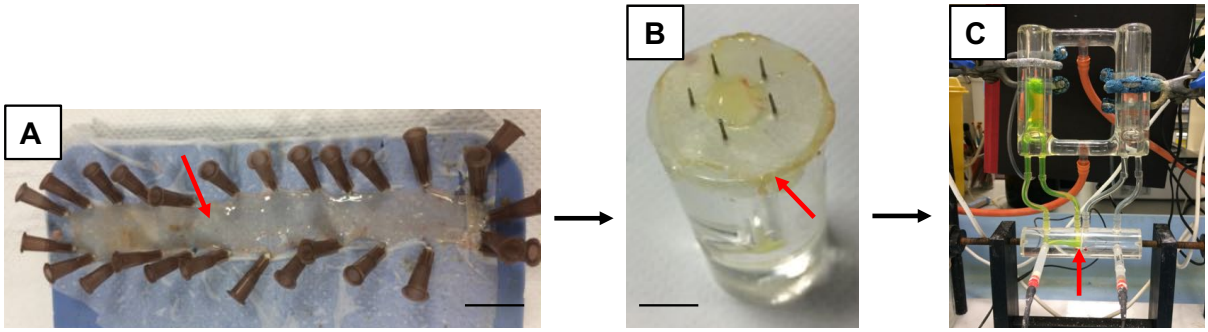

Figure 1: Ussing chamber methodology showing **(A)** A muscle-stripped jejunal mucosae with apical side up, **(B)** Mucosae mounted in the Ussing chamber cylindrical tissue holder and **(C)** Mucosa placed in Ussing chamber. Red arrows indicate mucosae. Bar=0.9 cm.

2.2.3 Measurement of electrical parameters

To determine tissue viability in chambers over time, electrical parameters were recorded. Each chamber half had a voltage (V) and current (I) electrode that was connected to a pre-amplifier (Pre-Amp), and all 4 Pre-Amps were connected to the automatic voltage clamp apparatus (EVD-4000 amplifier, World Precision Instruments, UK). The silver/silver chloride (Ag/AgCl) electrodes were freshly prepared before the start of each experiment by adding salt bridges composed of 3% agar melted in 3M KCl filled in plastic casing, while avoiding any bubbles.

The transepithelial potential difference (PD, mV) of the mounted tissue was equilibrated in an open circuit configuration for a period of 10 min (jejunum) or 15 min (colon and stomach). The tissue was voltage-clamped to 0 mV potential difference by insertion of a short circuit current (I_{sc}, $\mu A.cm^{-2}$) using the voltage clamp apparatus [47]. The I_{sc} was corrected for fluid resistance and represents the sum of the net electrogenic ion fluxes transported across the epithelium in the absence of an electrochemical gradient (mainly Na^+ absorption and Cl^-, and HCO_3^- secretion). I_{sc} and PD were measured across gastric, jejunal and colonic mucosae by switching from voltage clamp to open circuit respectively for 3 sec every 30 sec using a Pro-4 timer device (WPI, UK). Analogue signals were digitized with a Powerlab® data acquisition unit and analyzed with LabChart® (v8.1.8 2017) software from AD Instruments (UK). The tissue was equilibrated for a further 30 min (jejunum) and 45 min (colon and stomach) before commencement of transport studies to achieve a basal steady state condition.

2.2.4 Transepithelial fluxes of markers across rat tissue mucosae

After the tissue equilibration period, the paracellular flux markers, [^{14}C]-mannitol (Mw 182 Da), with a final concentration 0.1 µCi /ml (56.5 mCi/mol), or 4 kDa FD4 (2.5 mg/ml) were added apically [12]. Transepithelial flux of both markers was monitored from the apical to the basolateral chambers over 2 h. T_0 samples (100 µl) were taken from the apical and basolateral immediately prior to addition of the test PE. Basolateral samples (100 µl) were collected every 20 min for 2 h. The sampled basolateral volumes were replaced with pre-warmed KH buffer in order to maintain sink conditions and equal volumes on each side. C_{10} (10-30 mM) or SNAC (5-100 mM) were added apically to jejunal, colonic and stomach mucosae. Concentrations of PEs were based on previous studies [48] [43] [17]. Apical additions for C_{10} were carried out in calcium-free KH to prevent precipitation. Samples containing [^{14}C]-mannitol were mixed with 3 ml scintillation fluid (Ecoscint A; National Diagnostics, USA) and disintegrations per minute (DPM) were assayed in a scintillation analyser (Packard Tricarb 2900 TR). The FITC signal intensity was measured using a Spectra Max Gemini with an excitation wavelength of 490 nm and an emission wavelength of 525 nm. The P_{app} values for FD4 and [^{14}C]-mannitol were calculated as:

Eq. 1 $$P_{app} = \frac{dQ}{dt}\frac{1}{A \times C0}$$

Where dQ/dt is the transport rate across the tissue sample (slope of the time vs cumulative amount of marker), A is the surface area of mucosae (0.63 cm^2), and C_0 is the initial concentration of the flux marker in the donor compartment [42]. TEER measurements were also measured at the timepoints -30, -15, 0, 5, 10, 15, 30, 60, 90 and 120 min via the LabChart® program. TEER measurements were calculated according to Ohm's Law which follows the following formula:

Eq. 2 $$TEER\ (\Omega.\,cm^2) = R \cdot A$$

Where R = resistance (Ω) and A = tissue surface area in the Ussing chamber cylindrical holder (0.63 cm^2).

2.2.5 Electrogenic ion transport capacity of rat mucosae in chambers

To evaluate the maintenance of epithelial ion transport secretory function of the tissue a quality assurance test consisted of addition of carbachol (CCh) (0.1-10 μM) to the basolateral compartment at 2 h. CCh is a cholinomimetic drug which activates acetylcholine muscarinic receptors on the basolateral side of GI epithelia. This leads to an increase of electrogenic chloride ion secretion by the cells as reflected in a transient ΔI_{sc} [49]. In the absence of such an I_{sc} increase, the epithelial secretory function at the experimental endpoint can be considered compromised. Electrogenic ion transport capacity was therefore used as a surrogate for tissue viability.

2.3 Transport studies using non-everted rat intestinal sacs

2.3.1 Sac preparation

Maintenance and welfare of animals along with approved methods of humane killing were in accordance with those approved by the UCD Animal Research Ethics Committee (AREC). Male Wistar rats (280-320 g) were obtained from UCD Biomedical Facility and fasted overnight prior to sacrifice by cervical dislocation. The intestine (jejunum and colon) was rapidly removed after a midline incision and flushed with 37°C pre-oxygenated Medium 199. Sacs (without Peyer's patches) were prepared according to the method of Barthe *et al.* [50]. With the jejunum, 6 sacs, each 5 cm long were immediately placed in oxygenated Medium 199 at 37 °C, whereas 2 sacs, each 5 cm long, could be harvested from the colon. Intestinal sacs were pre-treated with the mucolytic, NAC (10 mM for 15 min), which was then flushed out with 20 ml Medium 199 [51].

Jejunal and colonic sacs (non-everted) were prepared by tying both ends of a 4 cm segment of intestine with braided silk (Mersilk, Ethicon Ltd., UK) (Figure 2A). 400 μl of FD4 solution (2 mg/ml) with or without SNAC or C_{10} was injected with a 1 ml syringe with a sterile 30G needle

in the sacs (Figure 2B). Each sac was placed in a separate organ bath (37 °C) containing 10 ml oxygenated Medium 199 (Figure 2C). 100 mM C_{10} was used as positive control in both colonic and jejunal sacs using Ca^{2+} free KH instead of Medium 199.

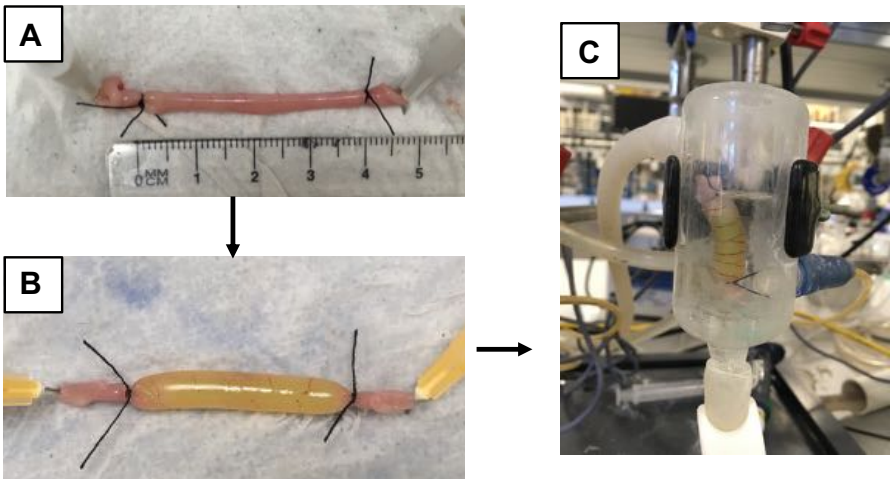

Figure 2: Non-everted gut sacs methodology showing **(A)** Empty non-everted jejunal intestinal sacs**, (B)** Non-everted jejunal intestinal sacs containing FD4 solution (yellow), **(C)** Intestinal sac submerged in 10 ml Medium 199 in a heated organ bath.

Concentrations of PEs were selected based on those that achieved permeation enhancement in Ussing chamber studies and on concentrations that are used *in vivo*. Samples of bath medium (200 µl) were taken every 5 min for the first 20 min and every 10 min thereafter up to a total of 90 min. They were pipetted directly onto a Nunclon 96 well white Maxisorp plate (Thermo Scientific, USA). The FITC signal intensity was measured as mentioned in Section 2.2.4.

2.4 Investigation of SNAC and C_{10} effect on mucus properties

2.4.1 Mucin removal experiments

Mucus secreted from jejunal and colonic mucosae challenged with SNAC or C_{10} in Ussing chambers on the mucosal side were quantified as previously described [39]. At 5, 10, 20, 30, 40, 50, and 60 min, 300 µl of liquid from the mucosal reservoir was removed and replaced with fresh KH, SNAC (20, 40 mM) or C_{10} (10, 30 mM). Mucin concentration was quantified using the Alcian Blue assay. Specifically, 100 µl of sample was loaded into a 96 well plate and 33 µl of Alcian Blue was added. The plate was equilibrated on a shaker for 2 h at room temperature and then centrifuged for 30 min at 1870 g. The plate was washed twice with wash buffer (40% ethanol, 0.1 M sodium acetate, 25 mM magnesium chloride, at pH 5.8). The pellet was then resuspended in 100 µl of 10% SDS. Sample absorbance was measured at 620 nm.

2.4.2 Rheological properties of native pig mucus exposed to PEs

2.4.2.1 Collection of porcine jejunal mucus

Jejunum was dissected from fresh small intestinal entrails obtained from an abattoir and transported to the laboratory within 60 min. The jejunum was cut into segments, opened with an incision and the tissue was pinned with the mucosal side facing upwards. Debris were washed away with PBS at room temperature. Mucus was collected from dissected pig jejunum segment with a hand-held nozzle attached to a foot-operated suction pump, which delivered mucus into Falcon tubes [52]. Special attention was paid during the process to avoid damaging the tissue. Unlike colonic mucus, small intestinal mucus does not exhibit a typical bilayer arrangement and thus, could be harvested intact in a single collection from each mucosal sheet [53] [54]. Samples were snap-frozen in liquid nitrogen and stored at -80°C. Prior to use for experiments, mucus was incubated for 20 min at room temperature. The pH of native mucus samples was checked with pH paper and was approximately neutral (7.0 ± 0.5). As found previously, the freezing procedure did not significantly affect rheological properties [55].

2.4.2.2 Rheological characterization of mucus

950 µl mucus aliquots were mixed with 50 µl stock solutions of PEs (in calcium-free PBS for C_{10} and Medium 199 for SNAC) to obtain a final concentration of C_{10} or SNAC of 10-100 mM. Mucus mixed with either PBS or Medium 199 was used as negative controls to cater for the change in ionic strength from adding PE solutions and to account for any unwanted effects of dilution. Mucus (950 µl) mixed with 50 µl of NAC solution (100 mM) was used as a positive control. Rheological properties of *ex vivo* mucus samples were analyzed using a rotational rheometer (MCR 301, Anton Paar, Graz, Austria), which was controlled using Rheoplus software V3.21 [56]. Oscillatory rheology measurements were carried out after 2 h exposure to PEs at 37 °C in a parallel-plate configuration (diameter 25 mm, TruGap®) [52]. Mucus samples were placed onto the base plate and the gap was set to 1 mm [57]. Samples were allowed to rest for 5 min to achieve a constant test temperature (37°C) and for relaxation of residual stresses. The temperature was maintained at 37 °C throughout the experiment with a Peltier heating system.

(i) A strain sweep test was done using native mucus to determine the linear viscoelastic region at fixed frequency 1 Hz where the strain amplitude was increased stepwise from 0.01-10% over a period of 10 min. This allowed to determine the linear region of strain where the viscoelastic characteristics of mucus were preserved (no yielding occurs).

(ii) Frequency sweeps were performed with angular frequency (ω) increasing linearly from 0.0628–62.8 s^{-1} at a fixed strain 1% over 19.5 min. Viscoelastic parameters including complex modulus (G*), elastic (G') and viscous (G") modulus and damping factor (tanδ) were

used to evaluate the alteration of rheology by addition of SNAC or C_{10}. G* was computed based $G^* = \sqrt{((G')^2 + (G'')^2}$ and $\tan\delta = G''/G'$ [53].

(iii) Viscosity ramps test were performed for thixotropic measurements of mucus-treated samples with SNAC or C_{10} (10 and 100 mM), where the shear rate was increased gradually from 0.01-100 s^{-1}over 19.2 min.

2.5 *In situ* instillations of PEs for histology assessments

Procedures were performed under license AE18982/P036 from the Health Products Regulatory Authority (HPRA) with Ethics approval number, UCD AREC 13-40-Brayden. Male Wistar rats (UCD Biomedical Facility) weighing 300-450 g were selected for experiments. Animals were housed under controlled conditions of temperature and humidity with a 12:12 h light/dark cycle. Rats received filtered water and standard laboratory chow *ad lib* and were fasted 16-20 h prior to the procedure with free access to water. All procedures were carried out under anesthesia by Dr. Fiona McCartney. *In situ* instillations were performed as previously described with minor modifications [13]. Briefly, following a midline laparotomy, the jejunum was identified and tied off in 3 segments of 4 cm each with a size 4 braided silk suture to create loops. 400 µl SNAC solution (40 or 100 mM) in Medium 199 and C_{10} solution (30 or 100 mM) in PBS were injected into the lumen using a 1-ml syringe with 30G needle. PBS and Media 199 alone were used as negative controls. Experiments were carried out in rats over 90 min as for the gut sacs experiment. Animals were euthanized at the end of the experiment with intra-cardiac injection of 0.4 ml pentobarbital sodium (EUTHATAL™, Merial Animal Health Ltd., UK). Histology was carried out as per Section 2.6.

2.6 Histology

Mucosal sheets from Ussing chamber experiments were removed after 120 min exposure and immersed in 10% (v/v) buffered formalin for 48 h. Tissue from the non-everted intestinal sacs and *in vivo* instillations were tied at both ends and submerged in 10% formalin after 90 min exposure. Tissues were then dehydrated in 80%, 95%, and 100% ethanol before xylene fixation and paraffin embedding. 5 µm tissue sections were cut on a microtome (Leitz 1512; GI, USA), mounted on adhesive coated slides and stained with haematoxylin and eosin (H&E), Alcian Blue and Neutral Red or Periodic Acid Schiff (PAS). Slides were visualized under a light microscope (NanoZoomer 2.0-HT light microscopy, Hamamatsu) and images were taken with high-resolution camera (Micropublisher 3.3 RTV, Imaging) and processing software (Image-Pro® Plus version 6.3; Media Cybernetics Inc., USA).

2.7 Data analysis

Unless stated otherwise, experiment was carried out on three independent occasions. All values are expressed as the mean ± SEM. Statistical significance was measured by one-way ANOVA or two-way ANOVA with either Dunnett's or Bonferroni's *post-hoc* tests using GraphPad® Prism-5 software. The threshold for significance was set at $P<0.05$.

3. Results

3.1 Transport studies using isolated rat colonic mucosae in Ussing chambers

3.1.1 Effect of SNAC and C_{10} on basal TEER and the P_{app} of FD4 and [^{14}C]-mannitol

The TEER and P_{app} of FD4 and [^{14}C]-mannitol across isolated colonic mucosae after apical-side incubation with 5-40 mM SNAC or 10 mM C_{10} for 120 min were measured. Colonic tissue was initially used in preference to small intestine tissue mucosae due to the ease of reproducible epithelial dissection and more robust viability in chambers [28], [42]. The mean basal TEER in KH buffer for colonic tissue was 104.9 ± 8.5 $\Omega.cm^2$ (n=15), which was above the acceptable cut-off value of 70 $\Omega.cm^2$. These values were similar to those obtained in other studies [42] [13]. With 30 mM SNAC emerging as the threshold for increasing fluxes in Caco-2 monolayers, it was expected that similar concentrations would be needed to be efficacious in this bioassay. Addition of SNAC caused a concentration-dependent and rapid decrease in TEER in rat colonic mucosae (Figure 3). 5 mM SNAC did not cause a TEER decrease and it remained similar to untreated control colonic tissue over 120 min (Table 1). 10 mM SNAC induced a reduction in TEER at 60 min to 60% of control. From 60-120 min, 10 mM SNAC reduced TEER to 33% of initial control values. Concentrations in the range 20-40 mM SNAC induced a reduction in TEER to 50% of control values in less than 15 min. A similar TEER decrease as for 20 mM SNAC was seen within 15 min with 10 mM C_{10}, confirming previous data for that concentration [28]. The % TEER remaining after incubation for 120 min was for SNAC: 5 mM (93%), 10 mM (33%), 20 mM (9%), and 40 mM (10%), while it was 14% for 10 mM C_{10}.

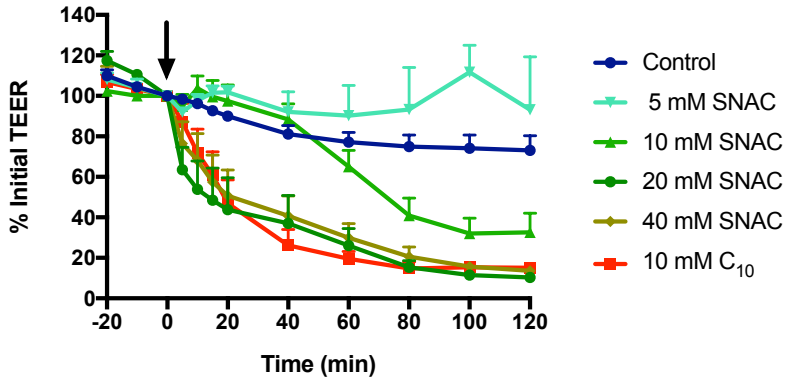

Figure 3: The effect of SNAC and C_{10} on % initial TEER in isolated colonic mucosae. Control group: n= 13; Treatments groups with SNAC: n= 3-10. (10 mM C_{10}, red squares) was included as a positive control in this and subsequent Figures (n=9). Statistics are provided in Table 1.

Table 1: Statistical analysis of % Initial TEER following apical addition of SNAC or C_{10} to rat colonic mucosae with respect to data in Figure 3. Values were treated using two-way ANOVA with Bonferroni's *post-test*. *p<0.05, **p<0.01, *** p<0.001 and **** p<0.0001 compared to control compared to KH; ns: not significant.

Time (min)	5 mM SNAC	10 mM SNAC	20 mM SNAC	40 mM SNAC	10 mM C_{10}
0	ns	ns	ns	ns	ns
5	ns	ns	***	**	ns
10	ns	ns	****	****	*
15	ns	ns	****	****	****
20	ns	ns	****	****	****
40	ns	ns	****	****	****
60	ns	ns	****	****	****
80	ns	***	****	****	****
100	ns	****	****	****	****
120	ns	****	****	****	****

The basal P_{app} values in the apical-to-basolateral direction for colonic mucosae were 0.4 ± 0.1 $x10^{-6}$ $cm.s^{-1}$ and $0.3 \pm 0.1x10^{-5}$ $cm.s^{-1}$ for FD4 and [^{14}C]-mannitol respectively (Table 2). These values were consistent with previously published data [21], [58]. SNAC caused a significant increase in the P_{app} of both markers at a threshold 20 mM (Figure 4). At 10 mM, SNAC caused only a 1.1-fold increase in the P_{app} of FD4 compared to an 8.1-fold increase for C_{10} at this concentration. Similarly, 10 mM SNAC caused only a 1.5-fold P_{app} enhancement for [^{14}C]-mannitol, compared to a 3.9 increase with C_{10}. However, when the SNAC concentration was increased to 20 mM, a similar P_{app} fold increase was obtained for [^{14}C]-mannitol (4.7-fold) and FD4 (9.8-fold), as 10 mM C_{10} (3.9- and 8.1-fold respectively). At 40 mM SNAC, the P_{app} was either similar to that seen with 20 mM SNAC for [^{14}C]-mannitol, or lower in respect of FD4.

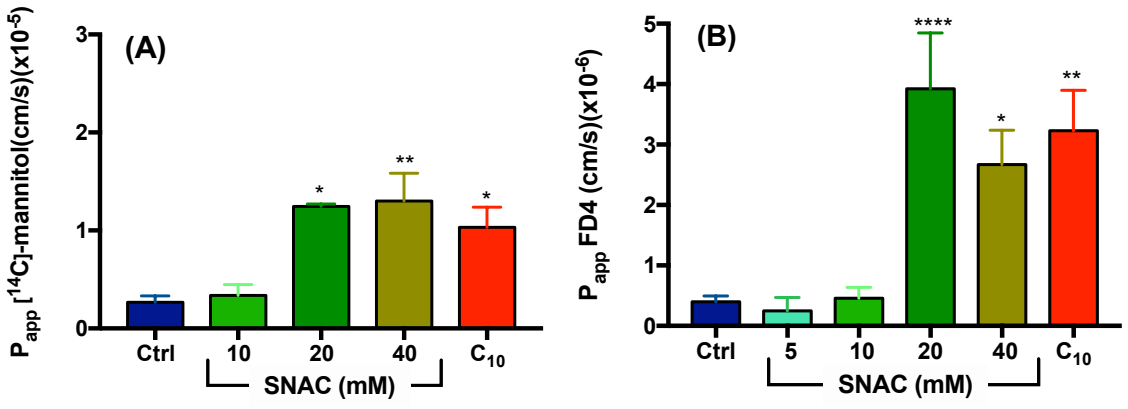

Figure 4: The effect of SNAC and C_{10} on parameters of isolated rat colonic mucosae. **(A)** P_{app} of [^{14}C]-mannitol and **(B)** P_{app} of FD4, both measured over 120 min compared to control. Concentrations of SNAC are given on the *x*-axis. C_{10} concentration was 10 mM. *p<0.05, **p<0.01, ****p<0.0001 compared to control. Each value represents the mean ± SEM of 3 to 8 independent replicates.

Table 2: P_{app} of [^{14}C]-mannitol and FD4 across isolated rat colonic mucosae when incubated with SNAC or C_{10} for 120 min. Fold increases relative to control.

Concentration (mM)	[^{14}C]-mannitol P_{app} (x10^{-5}cm s^{-1})	Fold increase	FD4 P_{app} (x10^{-6}cm s^{-1})	Fold increase
Untreated control	0.3 ± 0.1 (n=5)	-	0.4 ± 0.1 (n=9)	-
5 mM SNAC	-	-	0.2 ± 0.1 (n=5)	0.6
10 mM SNAC	0.4 ± 0.1 (n=5)	1.5	0.5 ± 0.1 (n=5)	1.1
20 mM SNAC	1.2 ± 0.1 (n=3)	4.7	4.0 ± 0.9 (n=7)	9.8
40 mM SNAC	1.3 ± 0.3 (n=3)	4.9	2.7 ± 0.6 (n=7)	6.7
10 mM C_{10}	1.0 ± 0.2 (n=5)	3.9	3.2 ± 0.7 (n=6)	8.1

3.1.2 Effects of PEs on electrogenic ion transport in isolated colonic mucosae

Tissue capacity to undergo active ion transport was evaluated during the experiment by two ways: (i) measuring the variation in epithelial electrogenic ion secretion ΔI_{sc} over time after PE apical addition compared to control mucosae (Figure 5A) and (ii) stimulating the I_{sc} with CCh (0.1-10 µM) across colonic mucosae at 120 min (Figure 5B) [28]. Control rat colonic mucosae had a basal I_{sc} of 32.1 ± 7.8 µA.cm^{-2} (n=9), a value within reported ranges indicating that tissue functionality was retained [60], [61]. An increase I_{sc} in response to carbachol confirmed that the mucosae retained ion transport functional capacity (Figure 5B). 5- and 10-mM SNAC caused a large sustained increase in ΔI_{sc} that reached a plateau around 50 µA.cm^{-2} compared to control (Figure 5A). Consequently, it led to a partial attenuation of the CCh-stimulated ΔI_{sc} (Figure 5B). At equimolar concentration, 10 mM C_{10} caused a slight decrease of ΔI_{sc}, -17 µA.cm^{-2} compared to control at 120 min. The complete loss of the CCh-stimulated ΔI_{sc} at 10 mM C_{10} has to be considered carefully as confounding interaction was previously shown between C_{10} and carbachol [59] (Figure 5B). Higher concentrations of 20 and 40 mM SNAC caused a biphasic change in basal I_{sc}: a transient increase within the first 20 min followed by

a long lasting fall reaching -39.8 ± 22.7 and -78.5 ± 20.1 $\mu A.cm^{-2}$ compared to the control respectively at 120 min (Figure 5A). This impaired I_{sc} was confirmed by a near complete inhibition of I_{sc} in response to carbachol (Figure 5B). A good correlation was obtained between data for I_{sc} variation over time or when challenged with carbachol for SNAC, however, due to the similarity in SNAC and C_{10} structure, artifact could also arise for data obtain with SNAC. Therefore, this functional electrophysiological assay is not helpful in detecting damage caused by pharmacological agents that directly interact with ion secretion.

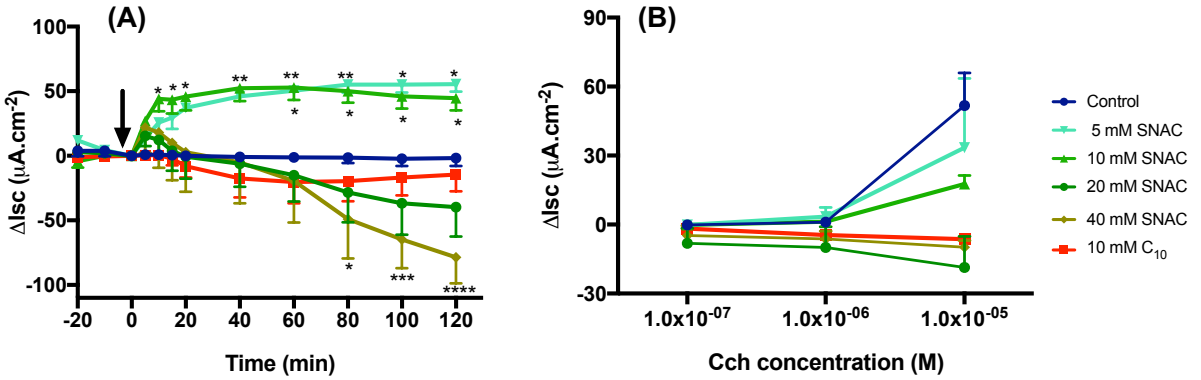

Figure 5: The effect of SNAC and C_{10} on **(A)** I_{sc} changes of colonic mucosae *ex vivo* over 120 min compared to control *p<0.05, **p<0.01, ***p<0.001, ****p<0.0001 compared to control. Control group: n= 9; Treatments groups with SNAC: n= 4-9. (10 mM) (n=7). Each value represents the mean ± SEM and **(B)** I_{sc} changes in response to carbachol (CCh) on colonic mucosae *ex vivo* after 120 min. Each value represents the mean ± SEM of 3 independent replicates.

3.1.3 Histology of isolated colonic mucosae after exposure to SNAC or C_{10}

Rat colonic mucosae were assessed for gross histology changes in the presence of 5-40 mM SNAC or 10 mM C_{10} following 2 h exposure (Figure 6). Control colonic tissues (KH buffer alone) showed an intact mucosal epithelium with a homogenous distribution of tightly packed cells and an unperturbed submucosa (Figure 6A). Tissue exposed to 5 mM SNAC was visually similar to control tissue (Figure 6B). With exposure to 10 mM SNAC, minor oedema was observed and, at the tips of the cells, some cell sloughing could be seen (Figure 6C). With 20 mM SNAC, the level of damage at the tops of the cells was increased and a layer of mucus was detected on the apical side of the tissue (Figure 6D). 40 mM SNAC led to a significant disruption of enterocytes on the tips, similar to that induced by C_{10} (10 mM) (Figure 6E, 6F). Even though cell sloughing was present with 40 mM SNAC, the crypts had comparable morphology to control images. Overall, the histology of the mucosae of SNAC- or C_{10}- treated colonic samples was mostly comparable to controls at 2 h and the physiological structure of the exposed tissue was retained at a gross level.

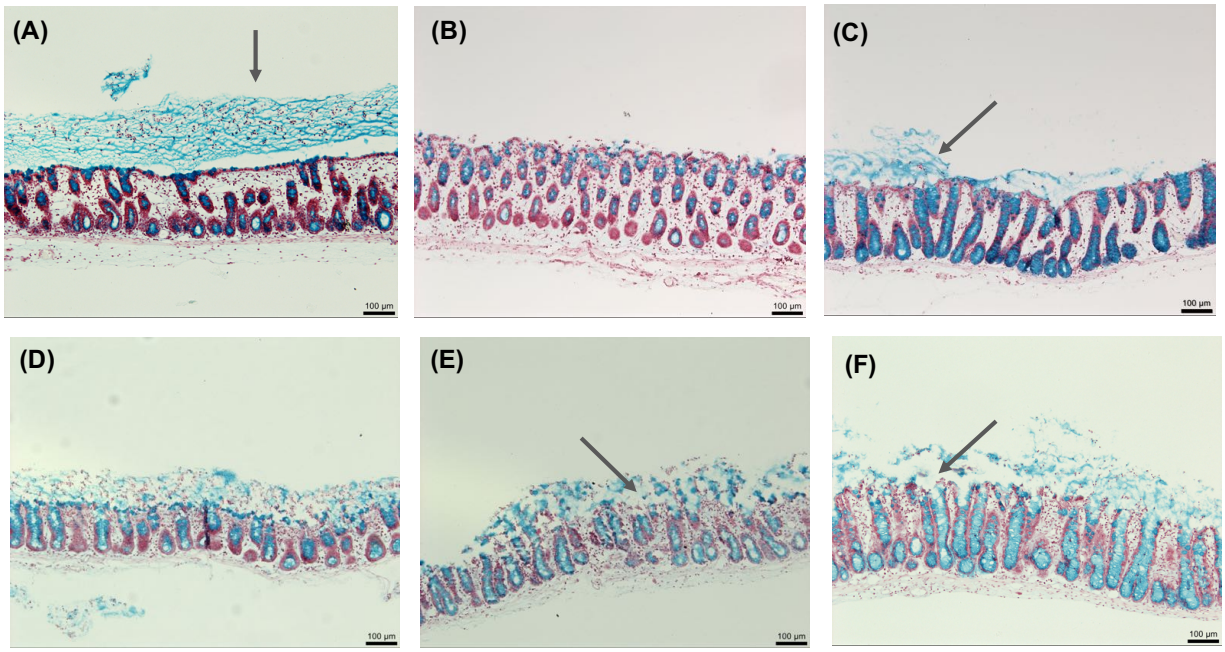

Figure 6: Representative histology of colonic tissue mucosae after 120 min exposure to SNAC or C_{10} with Neutral Red and Alcian blue staining**. (A)** KH control**, (B)** 5 mM SNAC, **(C)** 10 mM SNAC, **(D)** 20 mM SNAC, **(E)** 40 mM SNAC and **(F)** 10 mM C_{10}. Bar=100 µm. Arrows denote mucus. Representative of at least 3 sections in each case.

3.2 Transport studies using isolated rat jejunal mucosae in Ussing chambers

3.2.1 Effect of SNAC and C_{10} on basal TEER and the P_{app} of FD4 and [^{14}C]-mannitol

Jejunal basal TEER values were 34.5 ± 2.6 Ω.cm^2 (n=13), within the published range and above the cut-off value of 30 Ω.cm^2 [62]. Jejunal TEER gradually decreased to 70% of initial basal values even for untreated controls (Figure 7). A concentration of 30 mM C_{10} was selected as this was previously shown to be efficacious in isolated jejunal mucosae [63]. Apical addition of 30 mM C_{10} decreased TEER to 30% of basal value over 120 min, a decrease that was significant between 40-120 min (Table 3). The decrease in TEER after addition of C_{10} did not recover over 120 min. In contrast, apical addition of 20 mM SNAC did not alter TEER and it ended up even higher than the control. Similarly, 40- and 60-mM SNAC caused an increase in initial TEER up to 20% over basal value of exposed tissue and also compared to untreated control tissue.

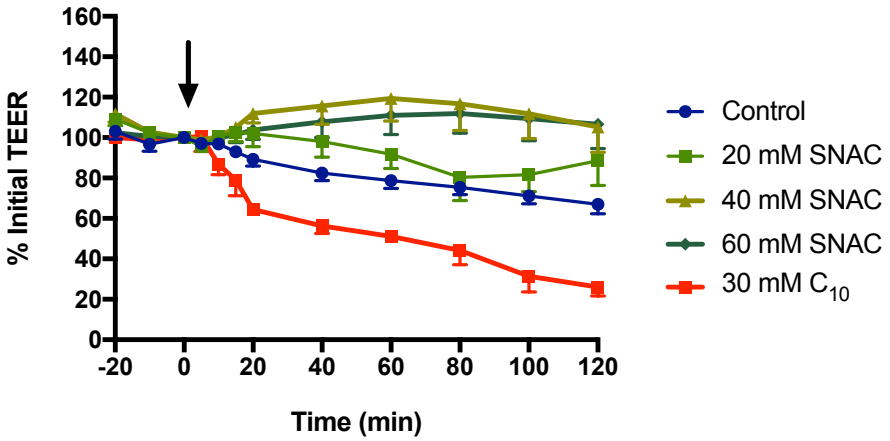

Figure 7: The effect of SNAC and C_{10} on % initial TEER in isolated jejunal mucosae. Control group: (n=12); Treatments groups with SNAC (n = 5-10) or 30 mM C_{10} (n = 11). Statistics are provided in Table 3.

Table 3: Statistical analysis of % Initial TEER following apical addition of SNAC to rat jejunal mucosae with respect to data in Figure 7. Values were treated using two-way ANOVA with Bonferroni's post-test. *p<0.05, **p<0.01, *** p<0.001 and **** p<0.0001 compared to control; ns: not significant.

Time (min)	20 mM SNAC	40 mM SNAC	60 mM SNAC	C_{10} (30 mM)
0	ns	ns	ns	ns
5	ns	ns	ns	ns
10	ns	ns	ns	ns
15	ns	*	ns	ns
20	ns	***	ns	ns
40	*	****	*	**
60	**	****	***	***
80	*	****	****	****
100	**	****	****	****
120	***	****	****	****

The P_{app} values of FD4 and [^{14}C]-mannitol were assessed across isolated rat jejunal tissue in the apical-to-basolateral direction (Figure 8). The basal P_{app} for control jejunal mucosae was $3.4 \pm 0.8 \times 10^{-6}$ cm.s^{-1} and $1.5 \pm 0.3 \times 10^{-6}$ cm.s^{-1} for [^{14}C]-mannitol and FD4 respectively (Table 4). In the presence of SNAC, even though TEER was similar to the untreated control over 120 min, the P_{app} value of markers trended higher compared to control. However, no statistical difference was found for any of SNAC concentrations, perhaps due to the already high basal P_{app} of the markers. At 20 mM, SNAC caused a 2.3-fold increase in the P_{app} of FD4 and a 1.9-fold increase for [^{14}C]-mannitol. At 40 mM SNAC, a slightly lower P_{app} enhancement of FD4 was obtained compared to 20 mM SNAC, 2.1-fold versus 2.3-fold respectively. The same trend was observed when using [^{14}C]-mannitol with a 1.5-fold increase only with 40 mM compared to 1.9-fold obtained with twice less the concentration (20 mM SNAC). The same trend of P_{app} enhancement with 20 mM and 40 mM SNAC for both markers was therefore apparent. To

further explore this loss of P_{app}, 60 mM SNAC was tested with FD4 marker and did not lead to any permeation enhancement of FD4. The P_{app} value with 60 mM SNAC was lower than the P_{app} value for control (0.8 ± 0.2 x 10^{-6} cm.s^{-1} versus 1.5 ± 0.3 x 10^{-6} cm.s^{-1} respectively), likely due to low solubility and physical interactions. Therefore, the changes in the P_{app} of the markers were not SNAC concentration-dependent and followed the order 20 mM > 40 mM > 60 mM SNAC. The rapid decrease in TEER across rat jejunal mucosae with 30 mM C_{10} was accompanied by a significant increase in the P_{app} of both paracellular markers. It caused a 2.4-fold and a 3.2-fold increase in the P_{app} of FD4 and [^{14}C]-mannitol respectively. P_{app} values obtained with 30 mM C_{10} were higher than all P_{app} values obtained for all SNAC concentration screened.

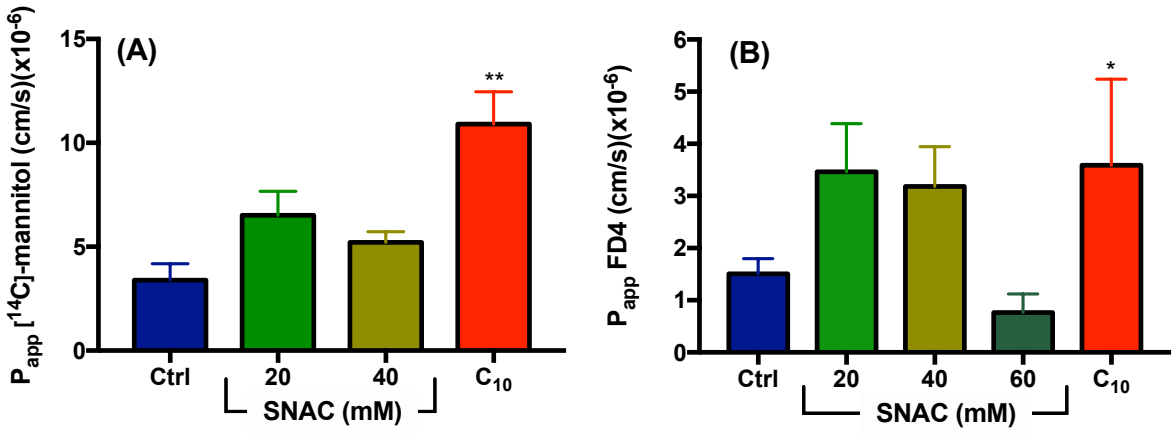

Figure 8: The effect of SNAC and C_{10} on parameters of jejunal mucosae *ex vivo* **(A)** P_{app} of [^{14}C]-mannitol **(B)** P_{app} of FD4 over 120 min compared to control. Concentrations of SNAC are given on the *x*-axis. *p<0.05, **p<0.01, ***p<0.001 compared to control. Mean ± SEM (n = 4-7 per group).

Table 4: P_{app} of [^{14}C]-mannitol and FD4 across rat jejunal mucosae incubated with SNAC or C_{10} for 120 min. Fold increases are relative to control (KH alone).

Concentration (mM)	[^{14}C]-mannitol P_{app} (x10^{-6}cm. s^{-1})	Fold increase	FD4 P_{app} (x10^{-6}cm. s^{-1})	Fold increase
Untreated control	3.4 ± 0.8 (n=7)	-	1.5 ± 0.3 (n=5)	-
20 mM SNAC	6.5 ± 1.1 (n=7)	1.9	3.5 ± 0.9 (n=5)	2.3
40 mM SNAC	5.2 ± 0.5 (n=5)	1.5	3.2 ± 0.8 (n=5)	2.1
60 mM SNAC	-	-	0.8 ± 0.2 (n=5)	0.5
30 mM C_{10}	11.0 ± 1.6 (n=7)	3.2	3.6 ± 0.7 (n=4)	2.4

3.2.2 Effects of PEs on active ion transport in isolated rat jejunal mucosae

In jejunal tissues, the mean basal I_{sc} for controls was 39.7 ± 5.8 μA.cm^{-2} (n=9) and tissue responded to carbachol with an increase in I_{sc} (Figure 9B). Apical treatment with all SNAC concentrations caused a slight decrease within 5 min of ΔI_{sc} followed by an increase in I_{sc} compared to control values in the order 20 mM (ΔI_{sc}: 11.1 ± 4.4 μA.cm^{-2}) > 40 mM (ΔI_{sc}: 2.5 ±

1.6 μA.cm^{-2}) > 60 mM (ΔI_{sc} : 0.4 ± 1.3 μA.cm^{-2}) at 120 min (Figure 9A). Unexpectedly, SNAC treatment led to a complete loss of the CCh-stimulated I_{sc} indicating that electrogenic chloride secretion of the jejunal tissue was impaired (Figure 9B). Apical addition of 30 mM C_{10} induced a progressive decrease in I_{sc} compared to control that became significant at 100 min (40.5 ± -18.5 μA.cm^{-2} less) (Figure 9A).

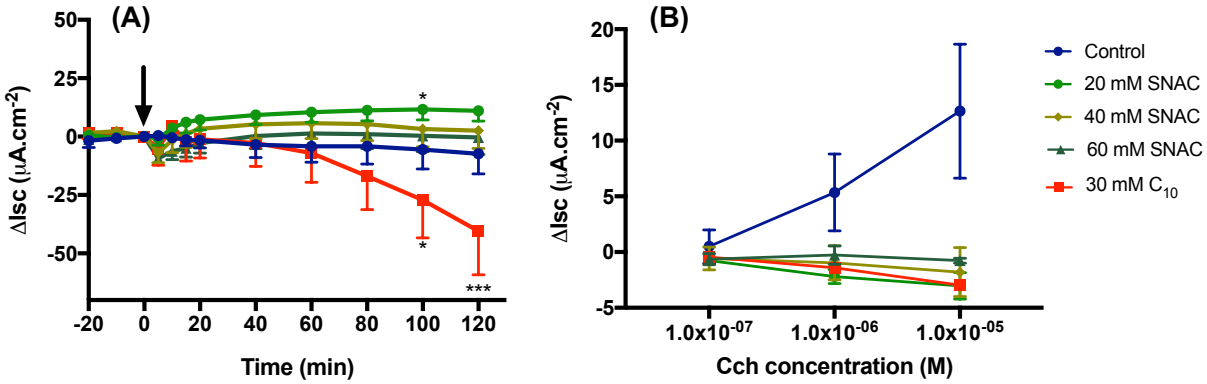

Figure 9: The effect of SNAC and C_{10} on **(A)** I_{sc} changes of jejunal mucosae *ex vivo* over 120 min compared to control *p<0.05, ***p<0.001 compared to control. Control group: n=9; Treatments groups with SNAC: n= 4-9. C_{10} (30 mM) (n=7). Each value represents the mean ± SEM and **(B)** I_{sc} changes in response to carbachol (CCh) on jejunal mucosae *ex vivo* after 120 min. Each value represents the mean ± SEM of 3 independent replicates.

3.2.3 Histology of isolated jejunal mucosae after exposure to SNAC or C_{10}

Histological analysis of jejunal tissue was carried out following 120 min exposure to SNAC (20-60 mM) and 30 mM C_{10} in Ussing chambers (Figure 10). In control jejunal tissue, normal morphological features can be observed with an intact epithelium with active goblet cells likely to be present due to the mucus produced. Some debris can be seen but the overall structure of the submucosa appeared intact (Figure 10A). Mild histological damage was observed following exposure to SNAC and C_{10}. 20 mM SNAC seems to cause more mucosal injury with truncated villi compared to 40 and 60 mM and with less apparent individual villi (Figure 10B, C and D respectively). The epithelium still remained continuous, without complete cell exfoliation or surface abrasion. C_{10} (30 mM) caused sloughing of the jejunal villi and an almost complete exfoliation of enterocytes from the mucosal surface (Figure 10E).

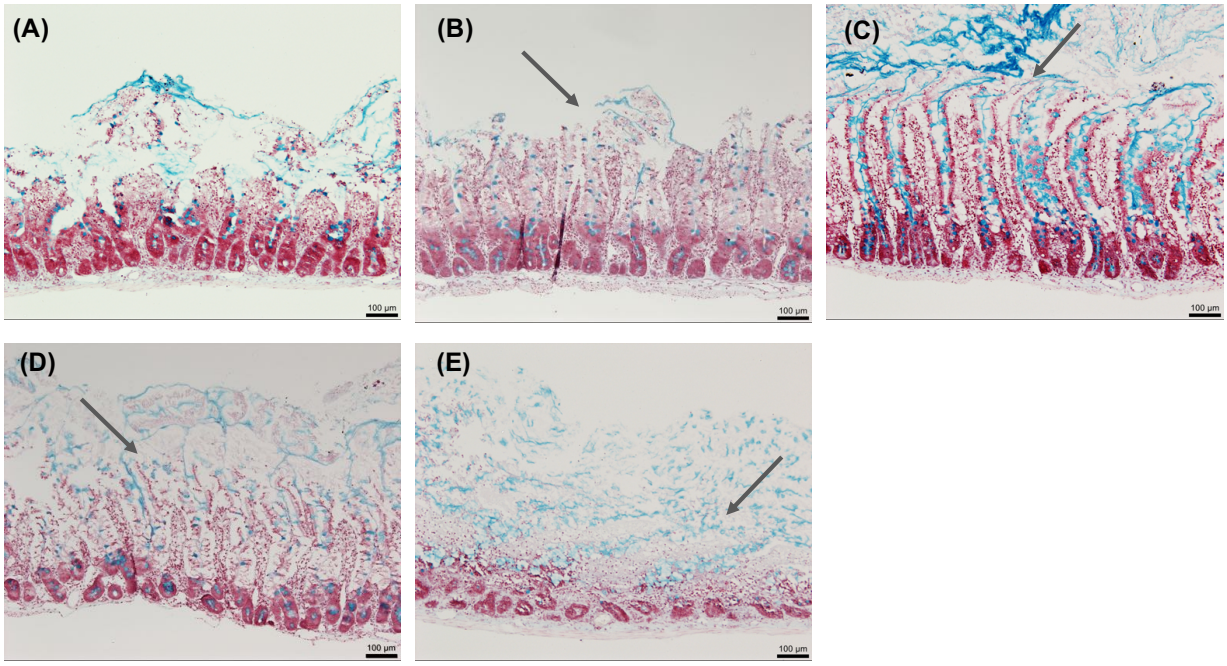

Figure 10: Representative histology of jejunal tissue mucosae after 120 min exposure to SNAC or C_{10} with Neutral Red and Alcian Blue staining. **(A)** KH control, **(B)** 20 mM SNAC, **(C)** 40 mM SNAC, **(D)** 60 mM SNAC and **(E)** 30 mM C_{10}. Bar=100 µm. Arrows denote mucus. Representative of at least 3 sections in each case.

3.3 Transport studies using isolated rat gastric mucosae in Ussing chambers

3.3.1 Effect of SNAC and C_{10} on TEER and P_{app} of FD4

According to a recent study using ligated dogs, the site of absorption for the recently approved tablet of semaglutide co-formulated with SNAC takes place in the stomach [16]. Here, studies were carried out in isolated rat stomach mucosae in the Ussing chambers to determine if SNAC or C_{10} could enhance the P_{app} of FD4. The two selected concentrations of C_{10} for the gastric mucosa study were derived from the experiments with C_{10} in rat jejunal (30 mM) and colonic mucosae (10 mM) in Ussing chambers. The three concentrations of SNAC used for stomach studies were based on previously published studies [16]. The mean basal TEER for stomach mucosae was 69.3 ± 6.3 $\Omega.cm^2$, above the cut off 35 $\Omega.cm^2$ [44]. Stomach TEER for untreated tissues remained stable over 120 min (Figure 11). Apical addition of either SNAC or C_{10} caused a concentration-dependent decrease in TEER. Addition of SNAC decreased TEER to 44%, 66% and 43% of the initial basal values at 20, 50- and 100-mM concentrations respectively after 120 min exposure (Table 5). Increasing the concentration of SNAC decreased the time required for a reduction in TEER from 40 min (20 mM), to 10 min (50 mM) and to 5 min (100 mM). 10 mM C_{10} reduced the TEER after 60 min and reached 50% of the initial TEER value after 120 min. Just 5 min exposure of mucosae to 30 mM C_{10} was enough to decrease TEER to 20% of the initial value after 120 min.

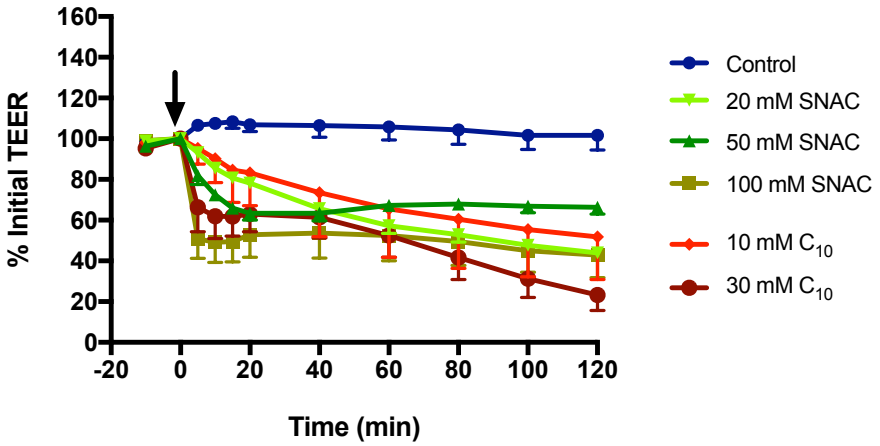

Figure 11: The effect of SNAC and C_{10} on % initial TEER in isolated gastric mucosae. Control group: n=6; Treatments groups with SNAC or C_{10}. n=3-5. Each value represents the mean ± SEM. Statistics for the group comparisons in the Figure 11 are shown in Table 5.

Table 5: Statistical analysis of % Initial TEER following apical addition of SNAC to rat gastric mucosae with respect to data in Figure 11. Values were using two-way ANOVA with Bonferroni's post-test. *p<0.05, **p<0.01, ***p<0.001, and ****p < 0.0001 compared to KH buffer; ns: not significant

Time (min)	20 mM SNAC	50 mM SNAC	100 mM SNAC	C_{10} (10 mM)	C_{10} (30 mM)
0	ns	ns	ns	ns	ns
5	ns	ns	****	ns	**
10	ns	***	****	ns	***
15	ns	****	****	ns	***
20	ns	****	****	ns	***
40	***	****	****	ns	***
60	****	****	****	*	****
80	****	***	****	**	****
100	****	***	****	**	****
120	****	***	****	***	***

The P_{app} of FD4 was assessed across gastric tissue mounted in Ussing chambers in the apical-to-basolateral direction when exposed to SNAC or C_{10} (Figure 12). A 6.3-fold increase in FD4 P_{app} was obtained following exposure to 20 mM SNAC (Table 6). Even though C_{10} displayed equal capacity as SNAC for TEER reduction, permeation enhancement of FD4 across the gastric mucosa was modest for it, with just 1.2- and 1.9-fold increases at 10 and 30 mM C_{10} respectively compared to control tissue. SNAC produced increases in the P_{app} of FD4 at much lower concentrations than C_{10}.

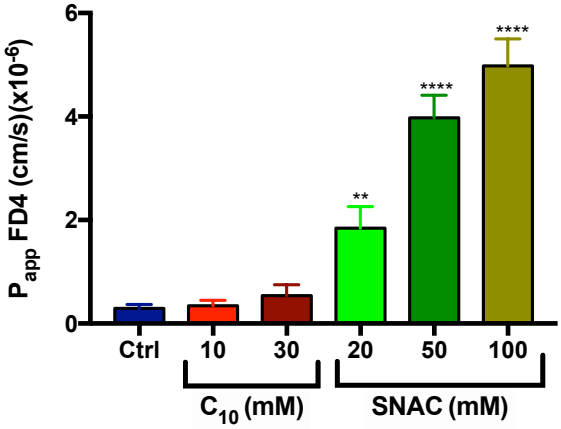

Figure 12: The effect of SNAC and C_{10} on the P_{app} of FD4 across isolated rat gastric mucosae over 120 min compared to control. **p < 0.01, ***p < 0.001 and ****p<0.0001 compared to control. Each value represents the mean ± SEM of 3 to 6 independent replicates.

Table 6: P_{app} of FD4 across isolated rat gastric mucosae incubated with SNAC or C_{10} for 120 min. Fold increases are relative to control (KH alone).

Concentration (mM)	FD4 P_{app} (x10^{-6}cm. s^{-1})	Fold increase
Untreated control	0.3 ± 0.1 (n=6)	-
10 mM C_{10}	0.3 ± 0.1 (n=3)	1.2
30 mM C_{10}	0.5 ± 0.2 (n=3)	1.9
20 mM SNAC	1.8 ± 0.2 (n=4)	6.3
50 mM SNAC	5.0 ± 0.5 (n=5)	13.6
100 mM SNAC	4.0 ± 0.4 (n=4)	17.1

3.3.2 Effects of PEs on active ion transport in isolated rat gastric mucosae

Apical addition of C_{10} caused a slight increase in $I_{sc.}$ at 5 min compared to control (ΔI_{sc}: 27.1 ± 7.5 μA.cm^{-2} for 10 mM C_{10} and 63.9 ± 32.6 μA.cm^{-2} for 30 mM C_{10}) (Figure 13). Similarly, low SNAC concentration 20 mM caused an increase I_{sc} compared to control that remained stable over time (27.5 ± 8.8 μA.cm^{-2} at 120 min). Higher SNAC concentrations 50 and 100 mM impacted transepithelial ion transport and led to a decrease in I_{sc} below control values (-14.8 ± 8.6 μA.cm^{-2} and -26.5 ± 11.1 μA.cm^{-2}).

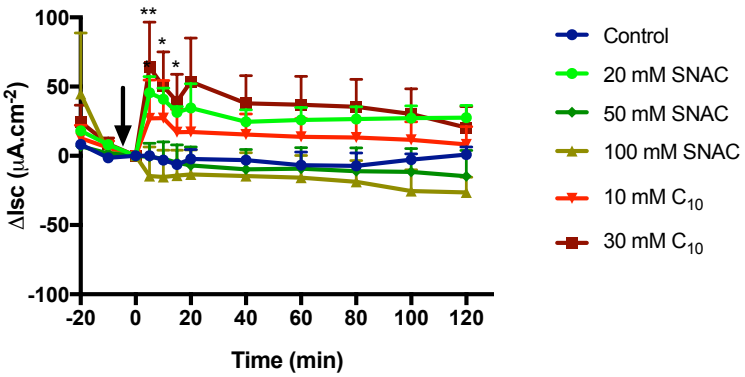

Figure 13: The effect of SNAC and C_{10} on I_{sc} changes of gastric mucosae over 120 min compared to control. *p<0.05, **p<0.01 compared to control. Control group: n= 4; Treatments groups with SNAC and C_{10}: n= 3-4. Each value represents the mean ± SEM.

3.3.3 Histology of isolated rat gastric mucosae after exposure to SNAC or C_{10}

The effect of SNAC and C_{10} on gastric mucosae was examined by histological analysis following exposure for 120 min in the Ussing chamber (Figure 14). Control mucosae showed normal morphological features with no evidence of sloughing or loss of barrier continuity (Figure 14A). Following exposure to 20 mM SNAC, gastric pits and undamaged lamina propria were seen along with normal levels of mucus (Figure 14B). The epithelium remained continuous and comparable to untreated control. No histological damage was observed in response to SNAC even when the P_{app} of FD4 was increased. 50 mM SNAC, as well as 10 and 30 mM C_{10} slightly perturbed the top layer of the tissue, but the lower layers remained undamaged (Figure 14 C, E and F respectively). However, 100 mM SNAC caused sloughing and mild focal perturbation of the epithelium (Figure 14D). Overall no increase in mucus levels occurred and the physiological structure of the tissue with the PEs added was retained.

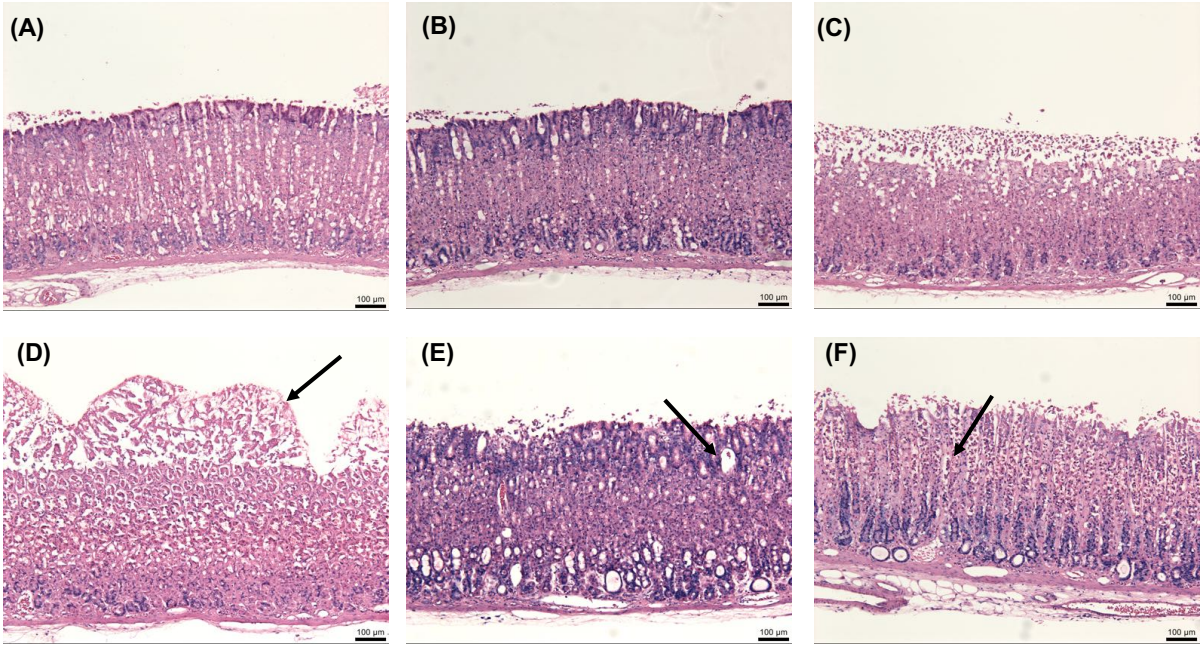

Figure 14: Representative histology of gastric tissue mucosae after 120 min exposure to SNAC or C_{10} with H & E staining. **(A)** KH control, **(B)** 20 mM SNAC, **(C)** 50 mM SNAC, **(D)** 100 mM SNAC, **(E)** 10 mM C_{10}, **(F)** 30 mM C_{10}. Black arrows indicate changes. Bar=100 µm.

3.4 Attempts to assay the P_{app} of [^{3}H]-exenatide across isolated rat jejunal mucosae

[^{3}H]-exenatide was selected as a labelled therapeutic peptide with which to further study the permeation enhancement capacity of SNAC or C_{10} across isolated rat jejunal mucosae. Initial experiments with [^{3}H]-exenatide, however, showed an unexpectedly high basal P_{app} for the molecule (Figure 15A). Optimization was attempted, including changing the gas for bubbling, using a different ratio of hot to cold exenatide, and varying the methods of mixing in buffers. However, the high concentration of the labeled peptide reaching the basolateral compartment

remained high and was suspected to be an artifact. The P_{app} of [^{3}H]-exenatide should have been in the same range as FD4 due to their similar MW, but instead it was 26 times higher (Figure 15B). As the Ussing chamber is a complex technique and includes variability associated with animal tissue, we carried out permeability studies on Caco-2 monolayers where five times less peptide was required, and the flux variability should be less. However, a very high basal P_{app} for [^{3}H]-exenatide was still obtained across monolayers. Traces of unattached tritium were then detected in [^{3}H]-exenatide samples, thereby preventing calculation of a valid P_{app}. Even after another filtration step was added in order to remove unattached tritium from [^{3}H]-exenatide, traces of free tritium were still present in samples (Figure 16). When the P_{app} of [^{3}H]-H_20 was measured, it was increased over that of [^{3}H]-exenatide, but the P_{app} value was closer to that of [^{3}H]-exenatide than to those of FD4 and [^{14}C]-mannitol, strong evidence that the [^{3}H]-exenatide was contaminated with unattached tritium (Figure 15 A and 15B).

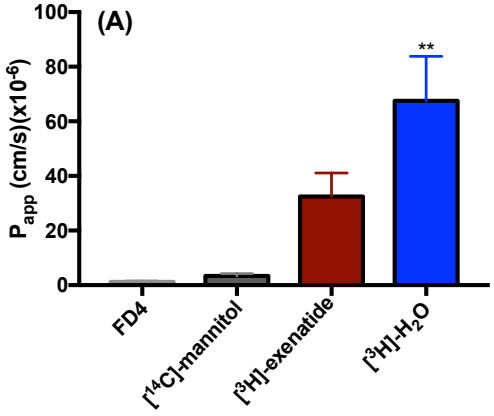

(B)

Markers	P_{app} (x10^{-6}cm s^{-1})	Fold increase
FD4	1.5 ± 0.3 (n = 5)	-
[^{14}C]-mannitol	3.4 ± 0.8 (n = 7)	2.7
[^{3}H]-exenatide	32.5 ± 4.3 (n = 4)	26.1
[^{3}H]-H_2O	67.5 ± 16.3 (n = 8)	54.2

Figure 15: Permeability measurements for different molecules across isolated rat jejunal mucosae over 120 min. **(A)** P_{app} screening with FD4, [^{14}C]-mannitol, [^{3}H]-exenatide and [^{3}H]-H_2O. **p<0.003, compared to FD4. Each value represents the mean ± SEM of 3 to 9 independent replicates. **(B)** P_{app} value of molecules and fold increases relative to FD4.

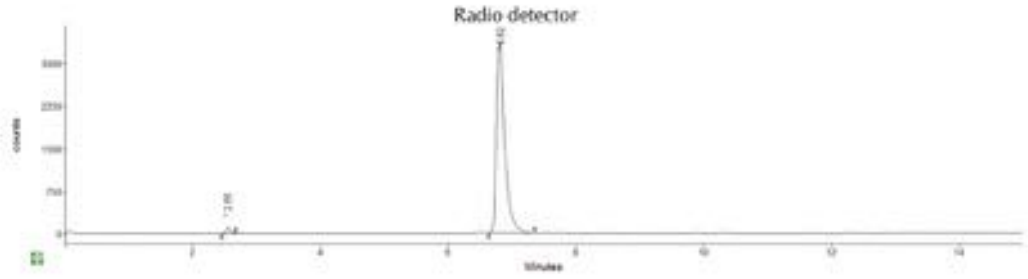

Results radio detector:

#	Peak name	R$_t$	Area	% Area
1		2.55	428.00	1.39
2	Exenatide	**6.82**	**30291.00**	**98.61**
Sum			30719.00	100.00

Figure 16: Certificate of analysis of [^{3}H]-exenatide with presence of free tritium traces on the radio-chromatograph.

3.5 Transport studies using isolated non-everted rat gut sacs

Non-everted gut sacs have been used in drug permeability studies and give comparable results to everted sacs for passively transported molecules [64]. They are easier and quicker to prepare, as tissue does not need to be everted. They spend less time outside physiological conditions and offer a more economical usage of test compounds as the apical compartment volume is much smaller [65]. Furthermore, because the lumen is merely flushed and the handling involved in the technique is far less than in everted intestinal sac preparation, there is less disruption to the mucus gel layer [20]. For these reasons, non-everted rat intestinal sacs were preferred to everted sacs as an *ex-vivo* model for examining FD4 permeability enhancement with SNAC and C_{10}. However, the secretory state of epithelium can lead to mucus over-production, as the tissue is still stressed during handling [65].

3.5.1 Effect of SNAC and C_{10} on FD4 permeation across rat non-everted jejunal and colonic sacs

The effect of SNAC and C_{10} on FD4 permeation across non-everted jejunal and colonic sacs over a 90 min period using 10, 20, 40, and 100 mM SNAC concentrations compared to 100 mM C_{10} is shown in Figures 17 and 18. 100 mM C_{10} is a reference concentration that is commonly used *in vivo* and was used in both regions [13]. The FD4 permeability increase across jejunal sacs was progressive and linear over time with 10, 20, and 40 mM SNAC. A steep increase was observed with 100 mM SNAC and 100 mM C_{10} at 5 min that reached a plateau after 20 min (Figure 17A). The FD4 AUC across jejunal sacs was increased compared to control in the order 10 mM SNAC < 20 mM SNAC < 40 mM SNAC < 100 mM SNAC < 100 mM C_{10} (Figure 17B). Overall, after 90 min, the maximal flux of FD4 across jejunal sacs was 13.0 ± 0.9 µg/ml for control, 20.9 ± 1.6 µg/ml (10 mM SNAC), 20.4 ± 2.5 µg/ml (20 mM SNAC), 19.4 ± 1.9 µg/ml (40 mM SNAC), 21.1 ± 1.0 µg/ml (100 mM SNAC) and 22.8 ± 0.7 µg/ml (100 mM C_{10}). A slightly higher FD4 flux was achieved using C_{10} instead of SNAC at the 100 mM concentration.

An increase in FD4 cumulative flux was also achieved from colonic gut sacs loaded with SNAC and C_{10} compared to FD4 control (Figure 18A). Similar to the Ussing chamber results, the basal FD4 flux across colonic sacs was lower than that of jejunal sacs (3.6 ± 1.1 µg/ml versus 13.0 ± 0.9 µg/ml after 90 min). The same trend as for jejunal sacs was found for colonic sacs for the FD4 flux profile but the order for efficacy was: 100 mM SNAC > 100 mM C_{10} > 20 mM SNAC > 40 mM SNAC = 10 mM SNAC (Figure 18B). SNAC seems more efficacious than C_{10} in promoting FD4 permeation across colonic sacs at 100 mM. However, in general, the overall FD4 fluxes in the presence of the PEs was lower across colonic sacs than jejunal sacs.

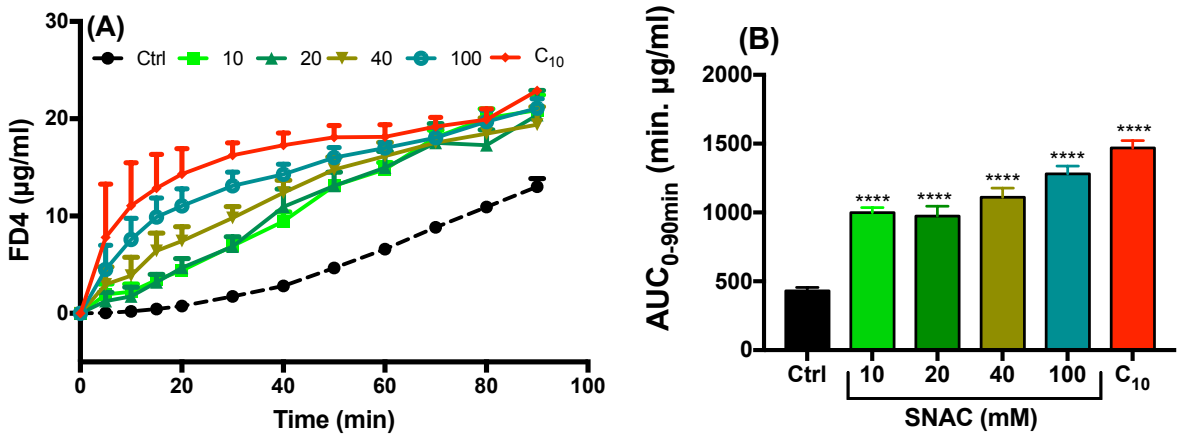

Figure 17: Effects of SNAC and C_{10} on FD4 permeation (2mg/ml in sac) across isolated jejunal non-everted sacs. **(A)** Rate of FD4 accumulation in basal medium **(B)** FD4 AUC. Values are given mean ± SEM. ****p < 0.0001 compared to control. Control (n = 8), 10 mM SNAC (n = 5), 20 mM SNAC (n = 5), 40 mM SNAC (n = 5), 100 mM SNAC (n = 3) and 100 mM C_{10} (n = 3).

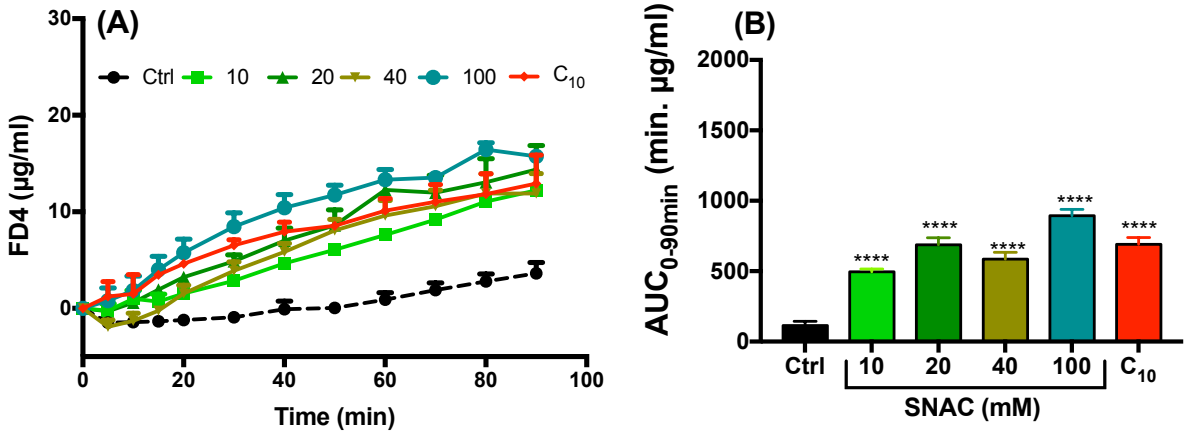

Figure 18: Effects of SNAC and C_{10} on FD4 permeation (2mg/ml in sac) across isolated colonic non-everted sacs. **(A)** Rate of FD4 accumulation in basal medium **(B)** FD4 AUC. Values are given mean ± SEM. ****p<0.0001 compared to control. Control (n = 5), 10 mM SNAC (n = 3), 20 mM SNAC (n = 3), 40 mM SNAC (n = 4), 100 mM SNAC (n = 4) and 100 mM C_{10} (n = 3).

3.5.2 Morphological assessments of non-everted sacs exposed to SNAC and C_{10}

To further understand SNAC and C_{10} effects on the epithelium of non-everted jejunal and colonic sacs, tissue samples were taken from light microscopy histology with PAS staining (Figure 19 and 20). There was minor oedema and cell sloughing in control jejunal samples after 90 min incubation in Medium 199 (Figure 19A). The increased FD4 flux induced by SNAC was associated with mucosal perturbation and with less mucus covering the villi, especially at 40- and 100-mM SNAC (Figure 19D and 19E). Sloughing and erosion of the epithelium was more prevalent at high SNAC or C_{10} concentrations (Figure 19E, 19F respectively). Compared to jejunal tissue samples, colonic sacs were more resistant to damage induced by SNAC and C_{10} (Figure 20). In control colon, the epithelial surface was organized and oedema-free (Figure 20A). An intact colonic epithelium was also observed in the presence of 10 mM and 20 mM SNAC (Fig 20B and 20C). Slight mucosal sloughing was observed at 40 mM SNAC in colonic

sacs, which became severe at 100 mM (Figure 20D and 20E). Changes induced by C_{10} (100 mM) on colonic sac epithelium were similar to SNAC (100 mM) (Figure 20F).

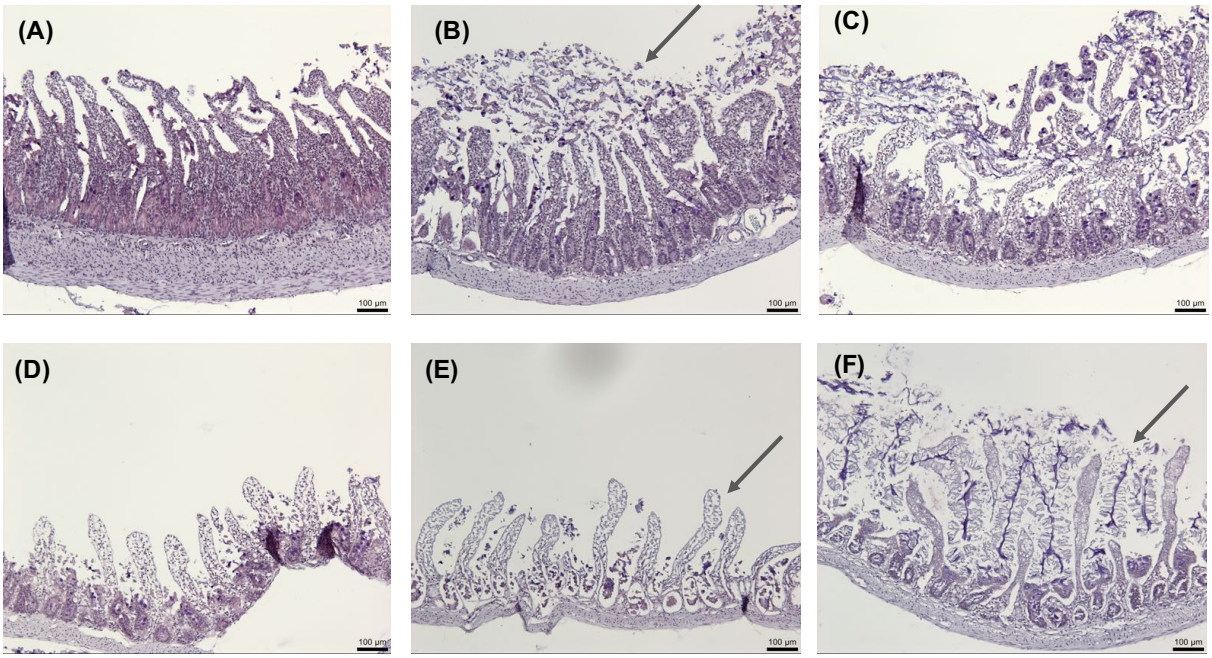

Figure 19: Representative histology of rat non-everted jejunal sacs after 90 min exposure to SNAC or C_{10} with PAS staining. **(A)** Control, **(B)** 10 mM SNAC, **(C)** 20 mM SNAC, **(D)** 40 mM SNAC, **(E)** 100 mM SNAC, **(F)** 100 mM C_{10}. Black arrows indicate mucosal perturbations. Bar=100 µm. Representative images from 4 sections.

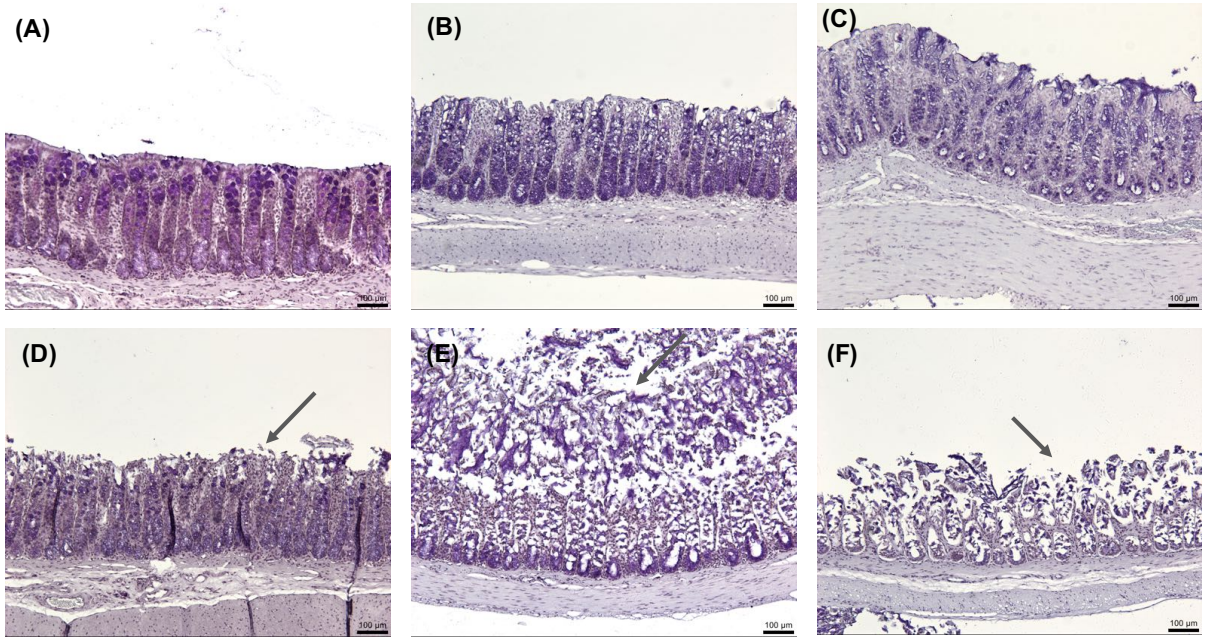

Figure 20: Representative histology of rat non-everted colonic sacs after 90 min exposure to SNAC or C_{10} with PAS staining. **(A)** Control, **(B)** 10 mM SNAC, **(C)** 20 mM SNAC**, (D)** 40 mM SNAC, **(E)** 100 mM SNAC, **(F)** 100 mM C_{10}. Black arrows indicate mucosal perturbation. Bar=100 µm. Representative images from 4 sections.

3.6 Morphological assessment of rat jejunal mucosae after SNAC- and C_{10}-*in situ* instillations

To compare SNAC and C_{10} effects on intestinal mucosa, we further examined the morphology of instilled intact rat jejunal loops exposed at the two concentrations of each PE that promoted FD4 permeability in Ussing chambers (40 mM SNAC and 30 mM C_{10}), and also at the 100 mM concentration previously used for instillation studies [29]. Examination of PAS-stained control jejunal sections treated with either instilled PBS (for C_{10}) or Medium 199 (for SNAC) showed that control tissue in both buffers remained unaffected (Figure 21). An intact mucosal epithelium with a homogeneous distribution of tightly packed villi and an unperturbed submucosa was observed. There was no sloughing of cells or damage to enterocytes at the tips of the villi. Bundles of mucin secretory vesicles were distributed along the microvilli showing that mucus-secreting goblet cells were intact (dark purple color).

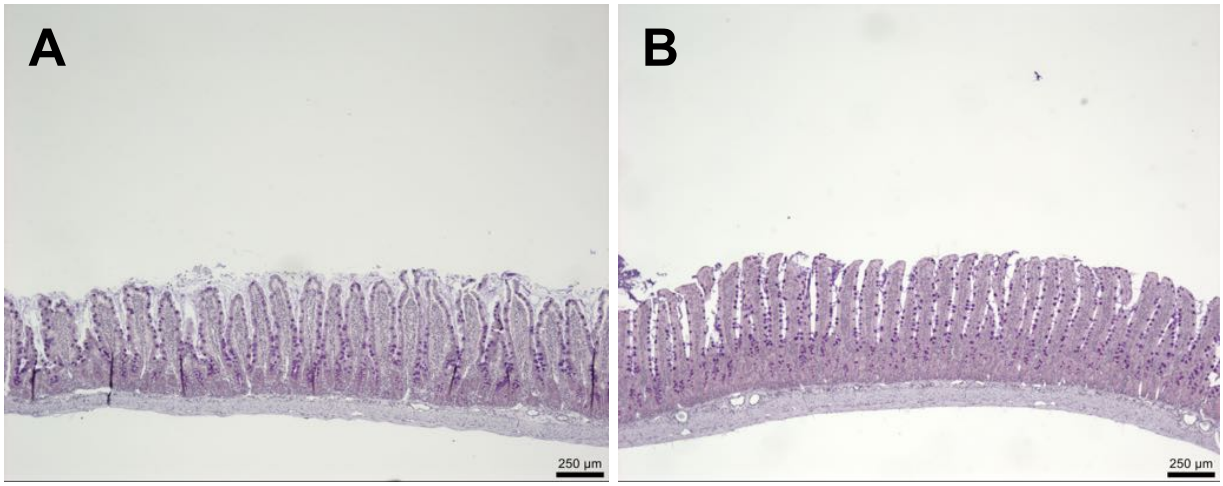

Figure 21: Representative histology after intra-jejunal instillation for 90 min with exposure to **(A)** PBS or **(B)** Medium 199 as controls with PAS staining. Bars=250 µm.

The histological effects of SNAC and C_{10} in jejunal tissue over 90 min of instillation is shown in Figure 22. There was evidence of only minor mucosal sloughing in the jejunal lumen following 40 mM and 100 mM SNAC instillation (Figure 22B and C). Separation of the epithelium from the lamina propria when exposed to 40 mM SNAC was likely to be an artifact during pre-fixation and not a direct effect of SNAC (Figure 22B) [66]. In intact jejunal segments instilled with 100 mM SNAC, mucosae had a tightly- bound epithelial surface that was homogeneous from the base of the crypts to the tips of the villi (Figure 22C). Only minor oedema of lamina propria were observed. There was no increase in the amount of mucus, but goblet cells were less apparent compared to the control tissue. Histology also revealed that did not dramatically affect the jejunal tissue, with only minor changes observed at 90 min (Figure 22E, F). At 30 mM C_{10}, the tops of the villi are prone to cell sloughing (Figure 22E). The effects of 100 mM C_{10} were heterogenous, with some parts of the tissue comparable to control and some levels of villi

flattening and sparseness (Figure 22F). Overall, for SNAC- and C_{10}- exposed jejunal epithelia displayed a normal appearance with undisturbed mucosa following *in vivo* instillations, even at concentrations higher than those used for Ussing chambers and sac studies. The crypts and submucosae did not show signs of disrupted morphology either.

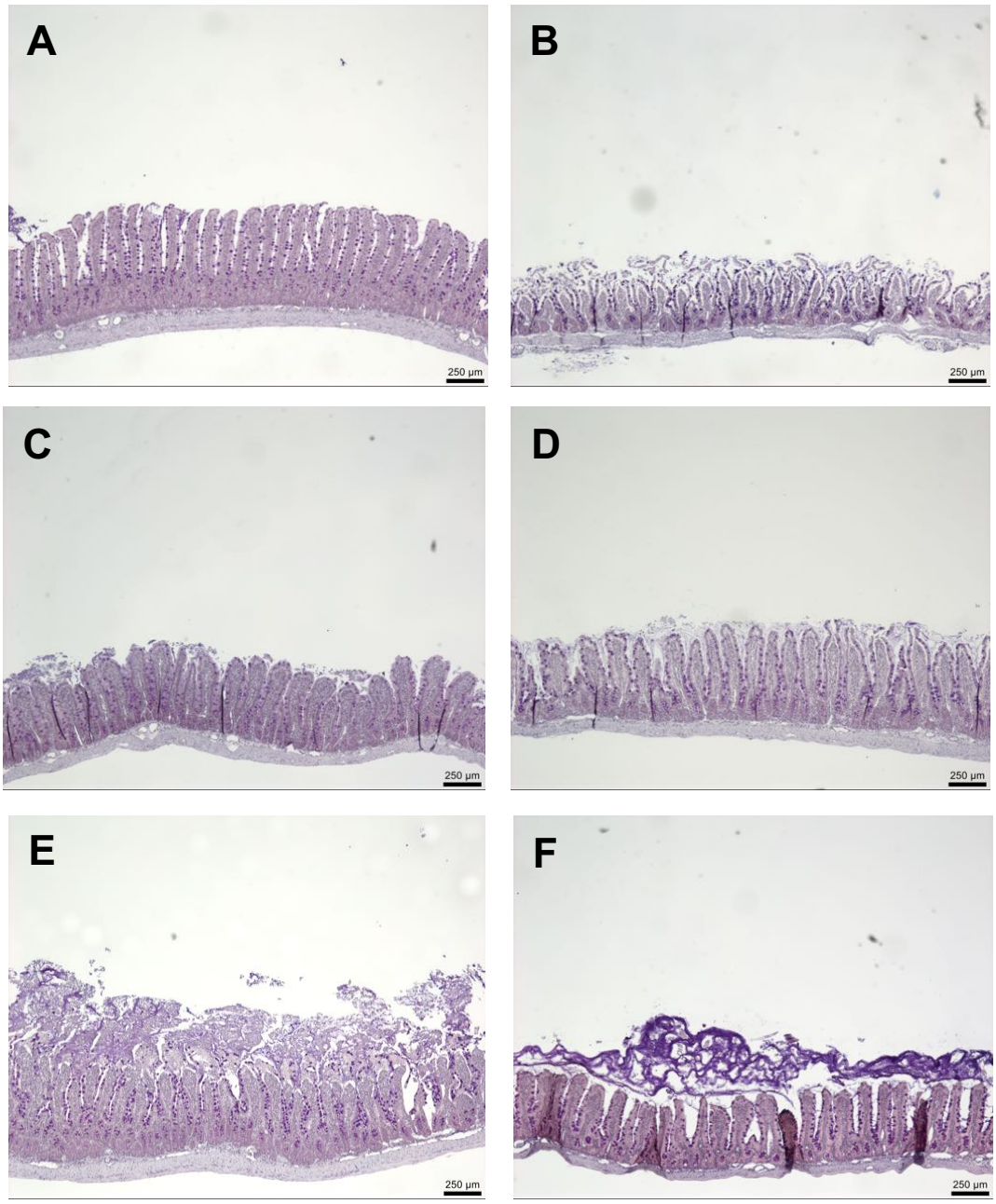

Figure 22: Representative histology obtained after intra-jejunal instillations of SNAC or C_{10} for 90 min using PAS staining. **(A)** Medium 199 control; **(B)** 40 mM SNAC; **(C)** 100 mM SNAC; **(D)** PBS **(E)** 30 mM C_{10} and **(F)** 100 mM C_{10}. Bar=250 µm.

3.7 Influence of PEs on mucus properties

3.7.1 Mucin removal from isolated rat intestinal tissue upon exposure to PEs

To test if removal of mucus is a mechanism SNAC or C_{10} may induce at mucosal surfaces, mucus secretion from tissue exposed to PEs mounted in Ussing chambers was quantified

using Alcian Blue assay. Apical exposure of the mucosae to SNAC and C_{10} increased mucus secretion relative to KH buffer control in both jejunal and colonic mucosae, as indicated indirectly by UV spectrophotometry measurements (Figure 23). 40 mM SNAC resulted in more mucus secretion than 20 mM. In both colon and jejunum, higher detection of mucus in the apical buffer was obtained in the presence of SNAC compared to C_{10}.

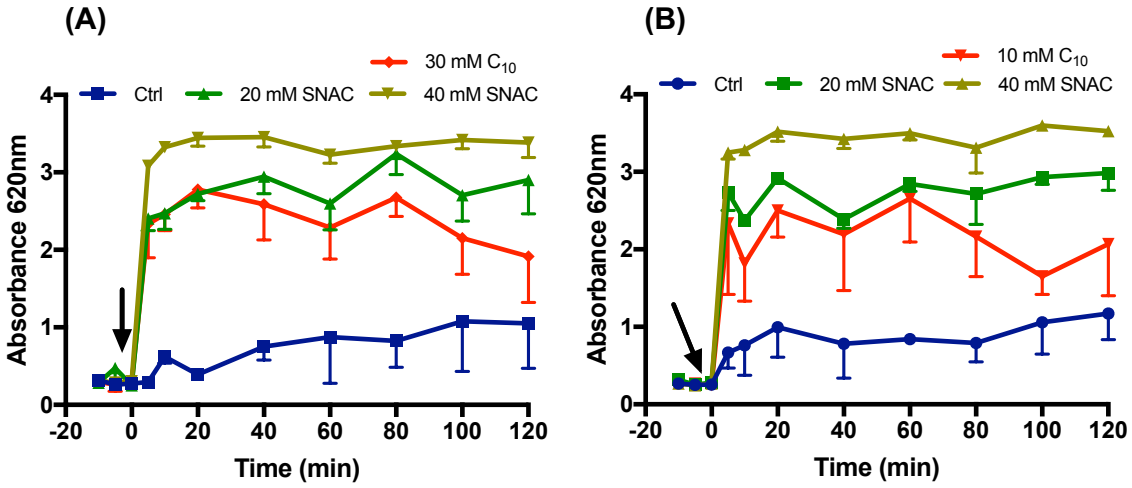

Figure 23: Mucin detected in the apical buffer from mucosae exposed to SNAC and C_{10} during Ussing experiment measured by Alcian Blue staining in **(A)** Jejunum and **(B)** Colon. n=3.

3.7.2 Rheological properties of native porcine small intestinal mucus treated with PEs

Based on previous experiments, we hypothesized that SNAC could interact with intestinal mucus as it: (i) liquifies mucus contained in the gut sacs (visual observations), (ii) washes away the mucus from the surface of tissue (histology in gut sacs), (iii) removes mucus from isolated rat tissue mounted in Ussing chamber studies (Alcian Blue assay). Also due to their surfactant-like properties, SNAC and C_{10} are likely to penetrate mucus and have direct permeation enhancement properties at the intestinal epithelium. However, changes in mucus production and structure could compromise mucosal protection. Consequently, we performed rheological studies with porcine small intestinal mucus treated with either SNAC or C_{10} to study any gross changes in mucus structure.

First, the linear viscoelastic region (LVR) of the native intestinal pig mucus was determined (Figure 24). Across the strain range (0.01-10%) the predominance of elastic behavior (G') over viscous behavior (G'') indicates gel-like character of the mucus. As a consequence, a constant strain of 1% corresponding to a small deformation that is within the LVR was selected for the frequency sweep and viscosity ramp test. The concentrations of SNAC (10, 20, 40, 100 mM) and C_{10} (10, 30, 100 mM) screened corresponded to concentrations used *ex vivo* and *in vivo*. 100 mM NAC was used as a positive control.

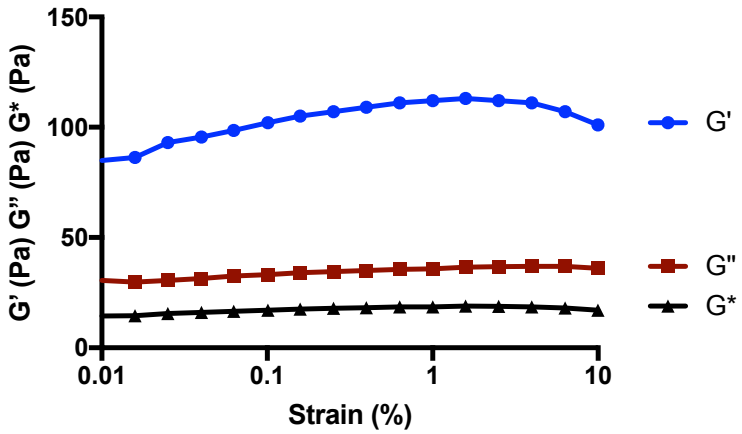

Figure 24: Evolution of G', G'' and G* versus strain at a constant frequency of 1% at 37°C for native pig mucus to determine the LVR.

The change of mucus viscoelastic properties in terms of G', G", the complex modulus (G*), and the damping factor were evaluated when exposed to both PEs (Figure 25 and 26). For control mucus, G' was consistently higher than G" by a factor of 4 across the frequency range, with no tendency to flow at low frequencies. These results fit with previously reported data for pig small intestinal mucus [67] [68]. The incubation of SNAC or C_{10} with mucus gradually increased all moduli values in a concentration-dependent manner compared to control (Figure 25 and 26). As indicated in Table 7, at 1 s^{-1}, the impact of SNAC on modulus is high, as G' and G" were 40 and 27-fold higher in the presence of 100 mM SNAC compared to control. With 100 mM C_{10}, the impact on modulus was lower, as G' and G" were increased by only 9.2 and 7.5-fold compared to control (Table 8). 100 mM NAC was suitable as positive control as it had a greater effect than SNAC or C_{10} on the modulus. The predominance of elastic behavior (G'>G'') over viscous indicates that mucus treated with either SNAC or C_{10} maintains its gel-like character even when PE concentrations were very high. Furthermore, in both cases, the damping factor of mucus was less than 1 (tan δ < 1) over the whole sweep frequency range (Figure 25D and 26D). This confirms that the mucus tended to exhibit high elasticity, while its viscous property remained intact in the presence of both PEs. Overall, neither SNAC nor C_{10} altered the pattern of moduli, as G' was greater than G", indicating stable mucus with little change to flow characteristics.

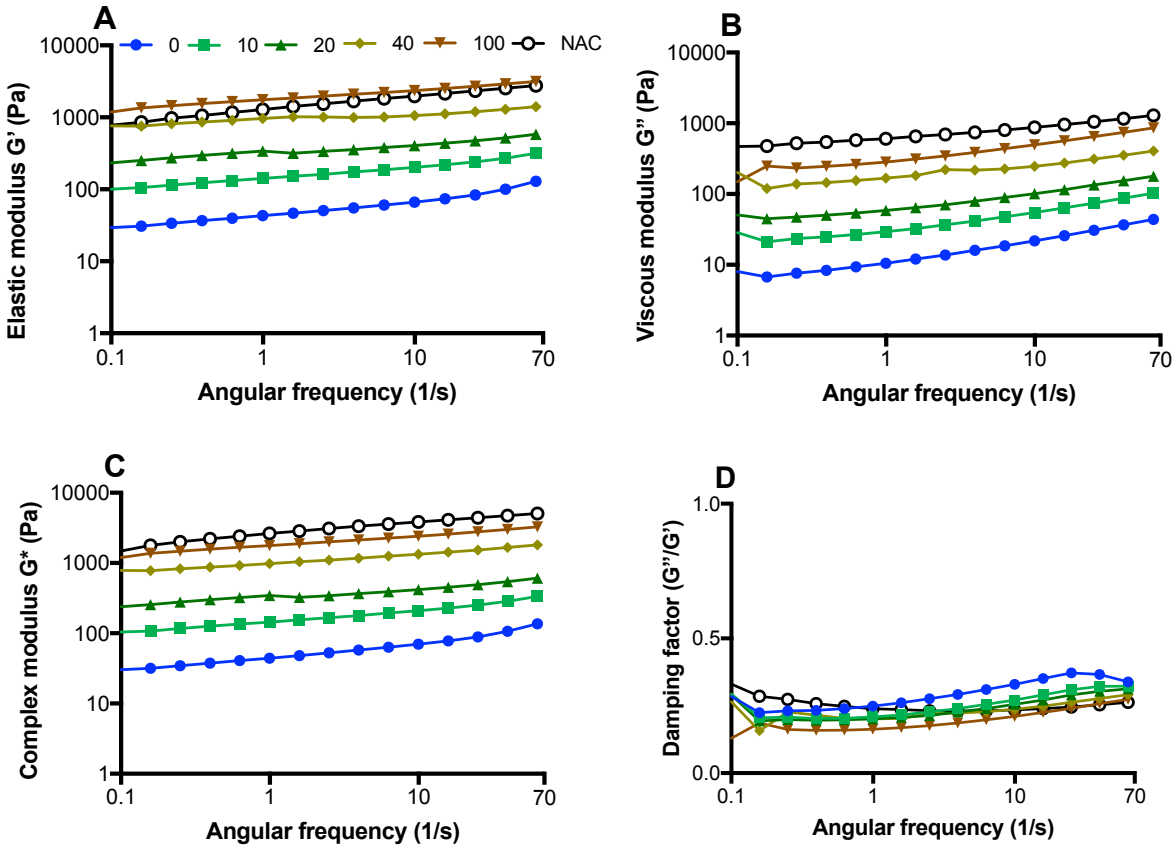

Figure 25: Viscoelastic modulus values for native mucus treated with SNAC at concentrations of 10, 20, 40 or 100 mM. Mucus-treated NAC (100 mM) was used as positive control (n = 2). **(A)** Elastic modulus (G'), **(B)** Viscous modulus (G''), **(C)** Complex modulus (G*) and **(D)** Damping factor (G''/G'). Symbols in (A) were used for the other panels (n=2).

Table 7: Average values and fold-increase of modulus and damping factor recorded at frequency $1s^{-1}$ for mucus treated with SNAC compared to the control mucus.

Challenge	G' (Pa)	Fold-increase	G'' (Pa)	Fold-increase	G* (Pa)	Fold-increase	Damping factor
Control	43.0 ± 8.3	-	10.5 ± 1.3	-	44.3 ± 8.4	-	0.3 ± 0.1
10 mM SNAC	141.5 ± 17.5	3.3	29.4 ± 2.1	2.8	144.5 ± 17.5	3.3	0.2 ± 0.1
20 mM SNAC	341.0 ± 45.0	7.9	58.6 ± 0.1	5.6	346.0 ± 45.0	7.8	0.2 ± 0.1
40 mM SNAC	966.0 ± 2.2	22.5	168.0 ± 0.5	16.0	980.0 ± 2.2	22.1	0.2 ± 0.1
100 mM SNAC	1755.0 ± 285.0	40.8	284.0 ± 38.0	27.0	1775.0 ± 285.0	40.1	0.2 ± 0.1
100 mM NAC	1288.0 ± 522.0	30.0	606.0 ± 160	57.7	2640.0 ± 780.0	59.6	0.2 ± 0.1

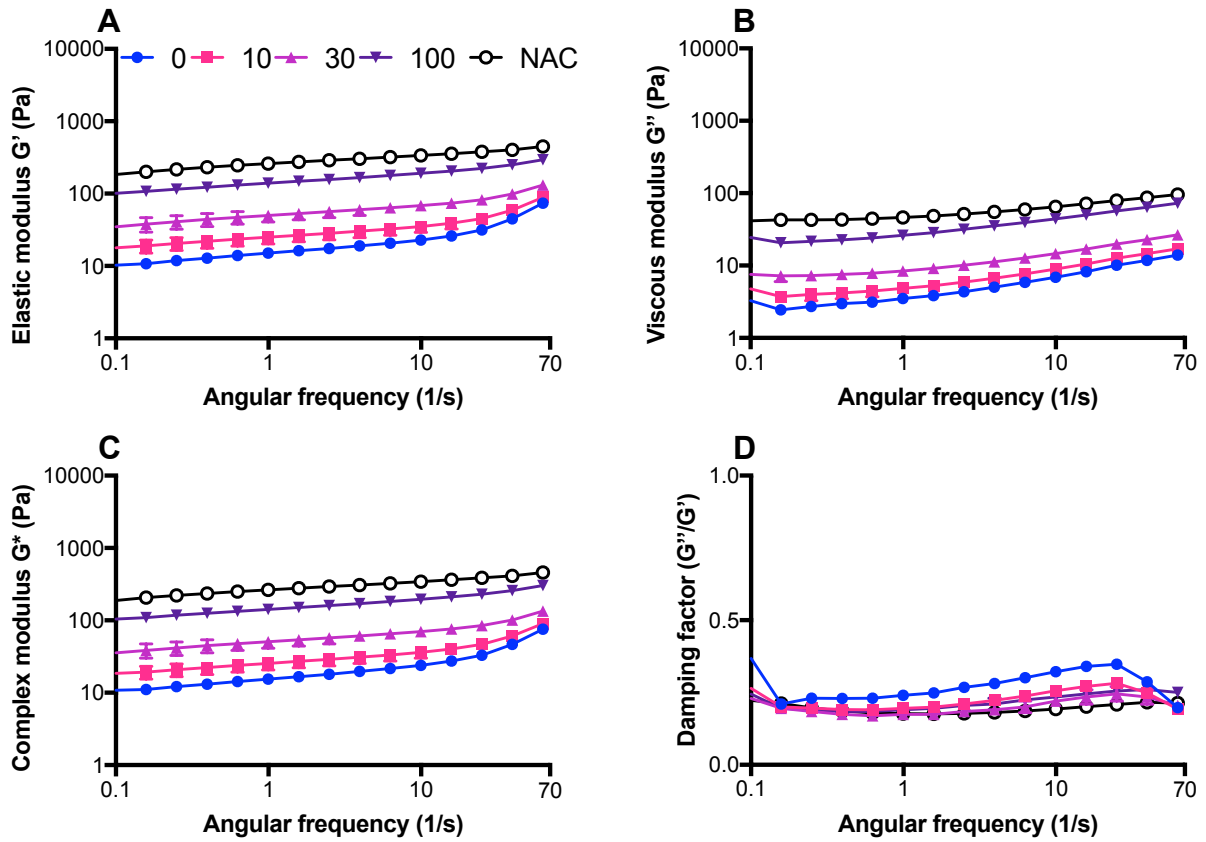

Figure 26: Viscoelastic modulus values for native mucus treated with C_{10} at a concentration of 10, 30 or 100 mM. Mucus treated with NAC (100 mM) was used as positive control (n = 2). **(A)** Elastic modulus (G'), **(B)** Viscous modulus (G''), **(C)** Complex modulus (G*) and **(D)** Damping factor (G''/G'). Symbols in (A) were used for other panels (n = 2).

Table 8: Average values and fold-increase of moduli and damping factor recorded at frequency of 1 s^{-1} for mucus treated with C_{10} compared to the control mucus.

Challenge	G' (Pa)	Fold-increase	G'' (Pa)	Fold-increase	G* (Pa)	Fold-increase	Damping factor
Control	15.1 ± 1.1	-	3.5 ± 0.1	-	15.5 ± 1.1	-	0.2 ± 0.1
10 mM C_{10}	24.9 ± 4.8	1.6	4.8 ± 0.8	1.4	25.5 ± 4.9	1.6	0.2 ± 0.1
30 mM C_{10}	50.1 ± 9.5	3.3	8.4 ± 0.9	2.4	50.8 ± 9.5	3.3	0.2 ± 0.1
100 mM C_{10}	139.5 ± 10.5	9.2	26.2 ± 0.5	7.5	142.0 ± 10.0	9.2	0.2 ± 0.1
100 mM NAC	261.0 ± 1.0	17.3	46.2 ± 0.7	13.2	265.0 ± 0.5	17.1	0.2 ± 0.1

The capacity of recovery of the mucus when challenged with increasing and decreasing shear rate (also called thixotropy) was evaluated when exposed to C_{10} or SNAC using the same mucus batch (Figure 27). As indicated in Figure 27A and 27B, addition of SNAC or C_{10} gradually increased the initial viscosity of mucus samples at low shear rate (0.01 s^{-1}) compared to control mucus. After 2 h incubation at 37°C, the initial viscosity was similar for both mucus

control sample either with Medium 199 (buffer used for SNAC) or with PBS (buffer used for C_{10}) with 490 and 437 Pa.s respectively. At 10 mM, the initial viscosity was increased similarly for both PEs, reaching 625 and 609 Pa.s for SNAC and C_{10} respectively. However, at 100 mM, a 2.2-fold higher viscosity was obtained with SNAC compared to C_{10} (7290 and 3270 Pa.s respectively). Overall, thixotropic measurements showed that mucus samples exposed to either SNAC or C_{10} retained viscosity. All mucus samples displayed shear-thinning behavior (decreased viscosity with increasing shear rate) typically found in non-Newtonian fluids. The mucus therefore had the capacity to recover its viscous properties after coming into contact with SNAC or C_{10}. In spite of significant changes in the G' and G'' (micro-rheology effect) of mucus due to the exposure to SNAC or C_{10}, the thixotropic properties (macro-rheology effect) were retained.

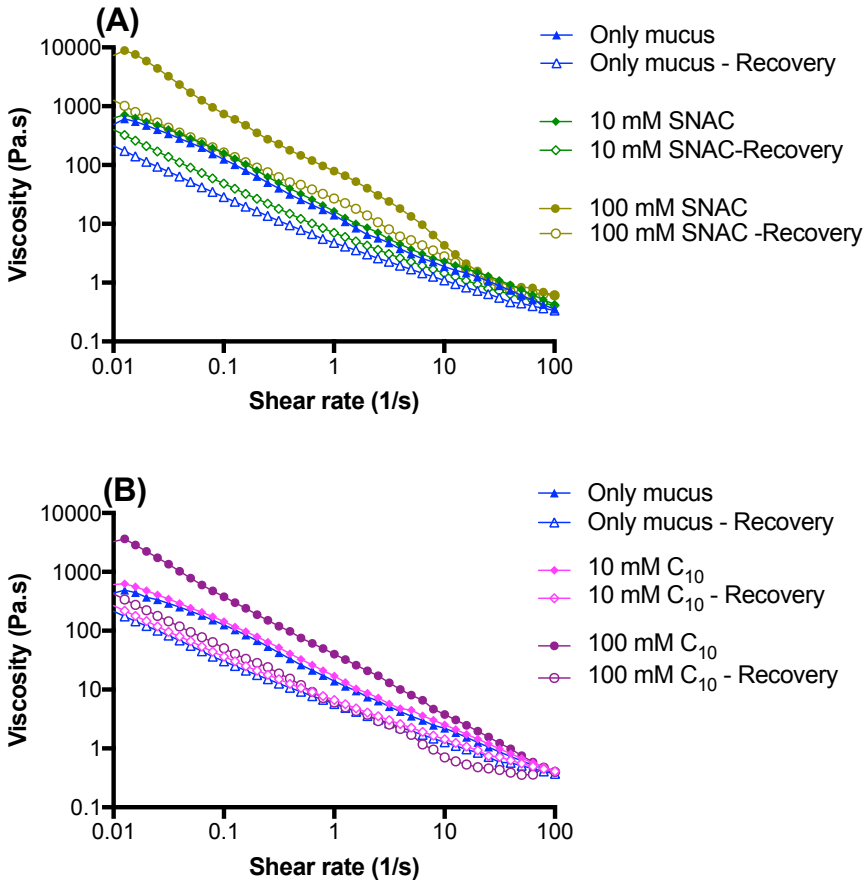

Figure 27: Thixotropic measurements on mucus after exposure to **(A)** SNAC and **(B)** C_{10} at concentrations of 10 mM and 100 mM. Full symbols indicate an increase in the shear rate and empty symbols indicate a decrease in shear rate (Recovery).

.

4. Discussion

Although it has been known from clinical trials that SNAC displays permeation enhancement capacity for a range of macromolecules including heparin, sCT, and semaglutide, it has not been examined in detail in relation to its mechanism of action on isolated intestinal mucosae, except in the stomach [16]. We examined SNAC's capacity to contribute to permeability enhancement through three distinct regions of the intestine in comparison with using isolated muscle-stripped rat tissue mucosae mounted in Ussing chambers. As a second and more robust *ex vivo* model, non-everted gut sacs from jejunum and colon were used to further explore SNAC permeability enhancement effects compared to C_{10} [69]. A third bioassay, rat jejunal instillation, was used to examine effects of the PEs solely on epithelial histology *in vivo*. In each model, histological evaluation was carried out in order to discriminate eventual mucosal damage. Finally, we examined if both SNAC and C_{10} could destabilize porcine intestinal mucus structure.

Initial studies were carried using isolated rat intestinal mucosae mounted in the Ussing chamber. The GI tract is divided into three distinct sections, namely the stomach, small intestine (comprising duodenum, jejunum and ileum), and the colon. The functional differentiation of the GI mucosa differs between those three organs leading to region-dependent properties affecting drug absorption [70]. Consequently, the permeation-enhancement capacity of SNAC can vary to a great extent in these intestinal regions. In this study, the mean basal TEER followed the order, jejunum < stomach < colon with values of 34.3 $\Omega.cm^2$ < 69.3 $\Omega.cm^2$ < 107.9 $\Omega.cm^2$, respectively. In addition, P_{app} value for control tissue for FD4 followed the order jejunum > colon = stomach, with values of $1.5 \pm 0.3 \times 10^{-6}$ $cm.s^{-1}$ > $0.4 \pm 0.1 \times 10^{-6}$ $cm.s^{-1}$ = $0.3 \pm 0.1 \times 10^{-6}$ $cm\ s^{-1}$, respectively. The TEER values reflects mostly paracellular ion flux in electrically-leaky epithelia and therefore the tightness of the intercellular junctional complex [71]. The lowest TEER together with the highest P_{app} recorded in the jejunum confirmed that the small intestine is a relatively leaky epithelium, whereas the colon and stomach are of intermediate tightness due to the variation of tight junction expression [72].

C_{10} was used as a benchmark positive control as it is a known efficacious intestinal PE [15]. In the intestinal mucosae permeability studies, we confirmed that C_{10} had the capacity to induce flux of the paracellular markers, FD4 and [^{14}C]-mannitol, across isolated rat jejunal and colonic tissue mucosae, while decreasing TEER. This behavior was well established from previous studies using a wide range of co-administered poorly permeable drugs on isolated animal and human intestinal mucosae [73]. We also confirmed that the permeation-enhancing effect of C_{10} was greater across the colon than in jejunum, reaching an 8.1-fold increase compared to 2.4-

fold increase in FD4 permeability compared to control respectively. Previous studies also emphasized such regional differences in the absorption promoting effect of C_{10} with a range of molecules [42] [74] [75]. In isolated human colonic mucosae, C_{10} increased the permeability of [^{51}Cr]-EDTA and horseradish peroxidase [76]. Mechanistic studies on isolated tissue revealed that C_{10} worked by primarily opening TJs thorough contraction of the peri-junctional action and myosin ring [77]. This effect on actin was confirmed in studies in rat ileal mucosae carried out in the Ussing chambers [78].

The actions of SNAC in tissue mucosae have not been well studied and this is a novel aspect of this Chapter. In the intestinal mucosae, SNAC increased the P_{app} of both FD4 and [^{14}C]-mannitol at a concentration threshold of 20 mM, which was below its CMC in Krebs buffer (34.2 mM) (Chapter 2, Table 3). This effect was somewhat surprising, as no FD4 flux enhancement was seen in Caco-2 monolayers, even at SNAC concentrations of > 30 mM. Similarly, to C_{10}, the effect of SNAC on marker flux increases was greater in the colon, with an enhancement ratio of 9.8 versus 2.3 in the jejunum. No TEER change was evident for SNAC in isolated jejunal rat mucosae, but it still increased the P_{app} of FD4. It is worth noting that TEER reduction and permeability increases to paracellular marker molecules do not always correlate, depending on how much of the TEER actually relates to the tight junction resistors and to transcellular parallel resistors in leaky epithelia [45]. Although colonic mucosae present a much lower surface area than small intestine mainly due to a lack in villi structures, the membrane fluidity is higher [74]. The colonic apical membrane may have increased susceptibility to PEs. Also, the small intestine presents a more rigid plasma membrane and is routinely exposed to bile salts at concentration up to 8 mM in the fasted state and 18 mM in the fed state [79]. Consequently, the jejunum is able to cope better with mild surfactants. In Chapter 3, we showed that SNAC acts in part by disrupting claudin-5 at tight junctions. On the one hand, the colon may be a better target for enhancement, as the highest expression of claudin-5 was seen in the colon of rat tissue, with lower expression seen in jejunal tissue [80]. The colon also has a longer transit time and a lower level of peptidases which might degrade peptides [74]. On the other hand, for systemic peptide delivery purpose, the colon might not be the route of choice for absorption due to the long and variable transit time, the complexity around tablet dissolution, and the interactions with the colonic microbiome.

Higher SNAC concentrations were necessary to obtain similar permeation enhancement as C_{10} in colonic mucosae. At concentrations above its CMC, 60 mM SNAC induced P_{app} values that were lower than controls P_{app} ($0.8 \pm 0.2 \times 10^{-6}$ cm.s^{-1} versus $1.5 \pm 0.3 \times 10^{-6}$ cm.s^{-1}). This suggests that above a certain concentration, SNAC is not efficacious, and that its effects are not concentration dependent, unlike for C_{10} [81]. One explanation could be the transition from

micelle formation to aggregates above the CMC, thus reducing SNAC's capacity to interact directly with mucosae. In previous studies on isolated rat jejunal mucosae mounted in Ussing chambers, concentrations of SNAC of up to 66 mM did not alter TEER [17]. This is in agreement with our own observation. In that study, SNAC (66 mM) resulted in a 7.2-fold increase in the transcellular flux component of a polar negatively charged marker molecule, 6-carboxy-fluorescein (6-CF), but the paracellular component was largely unaffected. Furthermore, neither did SNAC (66 mM) boost the flux of [^{3}H]-mannitol, across the epithelium in contrast to the effects of EDTA.

When SNAC was added to jejunal mucosae at a concentration of 165 mM, TEER dropped and the P_{app} of [^{3}H]-mannitol was increased [17], suggesting a compromising event at such a high concentration and a likely artifact. The authors concluded that the permeating-enhancing effect of SNAC may not involve tight junction complex opening but favored transcellular pathways. From our point of view, this study used such high concentrations of SNAC that loss of TEER was inevitable and is likely associated with epithelial damage, so no conclusions on mechanism can be made. In our study, the increase in the P_{app} of both paracellular markers in response to SNAC was achieved at much lower concentrations in jejunal and colonic mucosa and might be consistent with epithelial tight junction opening. However, it is not a direct proof of a paracellular mode of action, as transcellular perturbation might also reduce TEER and increase such fluxes. To obtain more insights about a specific mechanism of action of SNAC, it could be beneficial to further study the enhancement permeability of (i) transcellular markers such as [^{3}H]-propranolol [42], (ii) other FITC-dextran analogues with varying MW to probe tight junction permeability and (iii) a model peptide such as exenatide or insulin that would confirm if SNAC is able to enhance macromolecule and not just polar low MW small molecule markers.

Different patterns of enhancing effects were observed in the gastric mucosa: increasing SNAC concentrations lead to an increase in the FD4 P_{app} that was higher than C_{10} in any other region, while increasing C_{10} concentrations (effective in the jejunum and colon) surprisingly did not increase FD4 fluxes. Indeed, with C_{10}, even if the TEER was decreased, the resulting FD4 flux across stomach was similar to control giving an enhancement ratio of 1.2 (at 10 mM C_{10}) and 1.9 (at 30 mM C_{10}). To our knowledge no studies were assessed previously on isolated gastric mucosae using C_{10} as a PE. One explanation for *in vivo* behavior could be that near the gastric mucosa the pH is decreased below the pKa of C_{10}, which leads to formation of insoluble capric acid, which does not form micelles and is less efficient PE surfactant that interacts poorly with the gastric epithelium. However, in our studies, pH 7.4 was used on the apical side of the chamber so capric acid should not form. On the opposite side, SNAC enhanced FD4 transport across gastric mucosae with surprisingly higher efficacy than jejunum or colon.

Buckley *et al.* [16] investigated the mechanism of absorption mediated by SNAC through a variety of *in vitro* and *ex vivo* assays and clinical trials. As part of their study, sheets of isolated rat gastric mucosae were mounted in Ussing chambers and exposed to SNAC (30 mM) for 10 min only. First, a time-course profile was carried out by monitoring TEER changes pre- and post-SNAC exposure and second, the P_{app} of semaglutide was monitored at different times post-SNAC exposure. A 25% TEER decline was recorded after 10 min exposure to SNAC, which fully recovered after 60 min. Epithelial integrity was also confirmed by intact histological sections of the gastric mucosa 30 min after SNAC exposure. Flux of semaglutide was increased immediately after SNAC exposure, but gradually declined at 30 min and 60 min. Those elements emphasized SNAC's transient and short duration of action with Ussing studies where exposure was limited to a short time; this is likely to be similar *in vivo*. Buckley *et al.* [16] concluded that SNAC promoted absorption of semaglutide across gastric mucosa in a concentration-dependent manner via effects on transcellular pathways as demonstrated with fluorescent peptide, which were transient and reversible. In our study we confirmed SNAC enhancement capacity in gastric mucosa with a similar size molecule marker FD4 compared to semaglutide (4 kDa versus 4.1 kDa). However, an increase of paracellular marker permeability such as FD4 suggest the opening of the sealing TJ proteins and thus an enabling effect on the paracellular pathway. In that event, the SNAC mechanism of action cannot be accounted only by transcellular transport. It is worthwhile noting that a major difference in our study was the continuous exposure of the gastric mucosa with SNAC over 2 h compared to just 10 min in Buckley *et al.* [16].

Permeability experiments were also conducted in a non-everted gut sac model. Compared to the Ussing chamber, the lumen is merely flushed allowing to keep the mucus gel layer intact and the seromuscular layer is not stripped. This study also showed that treatment with SNAC or C_{10} led to permeation enhancement of FD4: the presence of mucus in the sac did not prevent either agent from acting as PEs [26].

Understanding local mucosal toxicity induction is critical for the eventual safe use of permeation enhancer in oral formulation [82], [10]. We examined potential mucosal damage that could arise from SNAC or C_{10} absorption-enhancing activity [83]. Qualitative morphological examinations of the gross histology in our study found only minor damage after administration at relatively high concentrations of SNAC or C_{10} both *ex vivo* and in *in situ* jejunal instillations. This occurred even though the concentrations tested *in vivo* were up to 10 times higher compared to those tested *ex vivo*. This is in agreement with previous studies reporting intact human and rat intestinal epithelia after C_{10} exposure (10-13 mM) assessed by histology [84] and by TEM [76]. Also, SNAC increased the rat ileal permeation of heparin *in situ* without

altering mucosal histologic findings [32]. In general, at permeation-enhancing concentrations, C_{10} induced more pronounced damage than SNAC on isolated intestinal mucosae in the Ussing chambers, perhaps due to its higher detergent capacity. This has been observed previously for comparison to other PEs [85]. However, repair of the intestinal barrier was confirmed within 30-60 min after exposure to 100 mM C_{10} using *in situ* instillations of rat [29]. The majority of *in vivo* studies in rat [86], dogs [87], pigs [88] and man [89] has shown that C_{10} (10-100 mM) does not damage the mucosa. Importantly, no safety issues were identified from several human trials of solid-dose oral formulations containing for some either 300 mg SNAC per tablet with semaglutide (up to 600 mg SNAC for ibandronate) [90] or 550 mg C_{10} with insulin [91]. Reduced toxicity *in vivo* may be explained by fluctuating concentrations of PE at the mucosal surface due to restricted access to the mucosal surface, dilution, variation of transit time and intestinal fluid volumes, the presence of mucus, large capacity for epithelial restitution, and fast absorption of the PE itself [92],[88].

In vivo, the mucus gel layer itself offers a protective function to underlying epithelial cells, acting as a molecular weight sieve that impedes the passage of macromolecules such as therapeutic peptides or proteins. At PE concentrations of 100 mM, above the CMC for both SNAC and C_{10}, a non-specific “detergent” effect could be able to disperse the mucus gel covering in the intestine. This mucolytic effect of SNAC or C_{10} was explored by measuring their impact of the rheology of porcine intestinal mucus. Although the mucus viscoelastic modulus was increased by the presence of SNAC or C_{10}, there was still sufficient network remaining to resist the shear strain similar to untreated mucus. Thus, mucus retains its protective function in the presence of either agent. SNAC changed the viscoelastic parameters of the mucus to a higher extent than C_{10}. A study on the components of porcine intestinal crude mucus suggested that it was lipids (37% w/w dry weight) rather than mucin glycoproteins (5%) that are the major components [93]. Hence, SNAC and C_{10} could interact with those particular lipids altering the moduli, but not strongly enough to break the network of mucus.

5. Conclusion

SNAC and C_{10} increased the flux of the paracellular markers, FD4 and [^{14}C]-mannitol, across isolated colonic and jejunal rat mucosae. Both agents also increased FD4 flux from non-everted gut sacs. There was a larger effect on colonic permeability than jejunal permeability, providing evidence of the increased sensitivity of the colonic mucosae to the actions of SNAC and C_{10}. Only SNAC enhanced FD4 transport across gastric mucosae, suggesting a greater efficacy in this region than C_{10}. However, the threshold concentration for enhancement in gastric mucosae was high with SNAC, indicative of its low potency. Tissue histology following *ex vivo* and intra jejunal instillation exposure to the PEs only showed slight perturbation at

permeation-enhancing concentrations. Also, both PEs modulated the viscoelastic properties of porcine jejunal mucus without altering rheological properties. Consequently, the gel-like structure of mucus was preserved and the capacity to recover when challenged with high strain was retained. Those elements indicate many common mechanistic features of surfactants between SNAC and C_{10}. They are also consistent with their established safety profiles in clinical trials of oral peptides. Finally, although SNAC has been touted as a PE with a unique pH mechanism for enhancing semaglutide delivery across the stomach [16], its effects on the gastric epithelium appear similar to its effects on epithelia in other intestinal regions.

Acknowledgments

I wish to thank Dr. Fiona McCartney for her guidance with the Ussing chambers and for performing *in situ* instillations. Also, thanks to Marc Farrelly and Dr. Bridget Hogg for their help in harvesting the pig mucus. I thank Kevin Thornton, Margot Coady and Catherine Lawson for their assistance with histology. Dr. Sourav Bhattacharjee is thanked for helpful discussions about rheology of porcine mucus, and Dr. Sabine Harrison is also acknowledged for her help in the rheological experiments.

References

1. Blutt, S.E., et al., *Engineered Human Gastrointestinal Cultures to Study the Microbiome and Infectious Diseases.* Cellular and Molecular Gastroenterology and Hepatology, 2018. **5**(3): p. 241-251.
2. Beloqui, A., et al., *A human intestinal M-cell-like model for investigating particle, antigen and microorganism translocation.* Nat Protoc, 2017. **12**(7): p. 1387-1399.
3. Beduneau, A., et al., *A tunable Caco-2/HT29-MTX co-culture model mimicking variable permeabilities of the human intestine obtained by an original seeding procedure.* Eur J Pharm Biopharm, 2014. **87**(2): p. 290-8.
4. Akazawa, T., et al., *Application of Intestinal Epithelial Cells Differentiated from Human Induced Pluripotent Stem Cells for Studies of Prodrug Hydrolysis and Drug Absorption in the Small Intestine.* Drug Metab Dispos, 2018. **46**(11): p. 1497-1506.
5. Bain, S.C., et al., *Cardiovascular safety of oral semaglutide in patients with type 2 diabetes: Rationale, design and patient baseline characteristics for the PIONEER 6 trial.* Diabetes Obes Metab, 2019. **21**(3): p. 499-508.
6. Costa, J. and A. Ahluwalia, *Advances and Current Challenges in Intestinal in vitro Model Engineering: A Digest.* Front Bioeng Biotechnol, 2019. **7**: p. 144.
7. Kim, H.J. and D.E. Ingber, *Gut-on-a-Chip microenvironment induces human intestinal cells to undergo villus differentiation.* Integr Biol (Camb), 2013. **5**(9): p. 1130-40.
8. Le Ferrec, E., et al., *In vitro models of the intestinal barrier. The report and recommendations of ECVAM Workshop 46. European Centre for the Validation of Alternative methods.* Altern Lab Anim, 2001. **29**(6): p. 649-68.
9. Quan, Y.S., et al., *Effectiveness and toxicity screening of various absorption enhancers using Caco-2 cell monolayers.* Biol Pharm Bull, 1998. **21**(6): p. 615-20.
10. Whitehead, K. and S. Mitragotri, *Mechanistic analysis of chemical permeation enhancers for oral drug delivery.* Pharm Res, 2008. **25**(6): p. 1412-9.
11. Luo, Z., et al., *Ex vivo and in situ approaches used to study intestinal absorption.* J Pharmacol Toxicol Methods, 2013. **68**(2): p. 208-216.
12. Maher, S., et al., *Effects of surfactant-based permeation enhancers on mannitol permeability, histology, and electrogenic ion transport responses in excised rat colonic mucosae.* Int J Pharm, 2018. **539**(1-2): p. 11-22.
13. McCartney, F., M. Rosa, and D.J. Brayden, *Evaluation of Sucrose Laurate as an Intestinal Permeation Enhancer for Macromolecules: Ex Vivo and In Vivo Studies.* Pharmaceutics, 2019. **11**(11).
14. Petersen, S.B., et al., *Colonic absorption of salmon calcitonin using tetradecyl maltoside (TDM) as a permeation enhancer.* Eur J Pharm Sci, 2013. **48**(4-5): p. 726-34.
15. Maher, S., et al., *Safety and efficacy of sodium caprate in promoting oral drug absorption: from in vitro to the clinic.* Adv Drug Deliv Rev, 2009. **61**(15): p. 1427-49.
16. Buckley, S.T., et al., *Transcellular stomach absorption of a derivatized glucagon-like peptide-1 receptor agonist.* Sci Transl Med, 2018. **10**(467).
17. Hess, S., V. Rotshild, and A. Hoffman, *Investigation of the enhancing mechanism of sodium N-[8-(2-hydroxybenzoyl)amino]caprylate effect on the intestinal permeability of polar molecules utilizing a voltage clamp method.* Eur J Pharm Sci, 2005. **25**(2-3): p. 307-12.
18. Alam, M.A., F.I. Al-Jenoobi, and A.M. Al-Mohizea, *Everted gut sac model as a tool in pharmaceutical research: limitations and applications.* J Pharm Pharmacol, 2012. **64**(3): p. 326-36.
19. Barthe, L., et al., *An improved everted gut sac as a simple and accurate technique to measure paracellular transport across the small intestine.* Eur J Drug Metab Pharmacokinet, 1998. **23**(2): p. 313-23.

20. Mateer, S.W., et al., *Ex Vivo Intestinal Sacs to Assess Mucosal Permeability in Models of Gastrointestinal Disease.* Journal of visualized experiments : JoVE, 2016(108): p. e53250-e53250.
21. McCartney, F., et al., *Labrasol(R) is an efficacious intestinal permeation enhancer across rat intestine: Ex vivo and in vivo rat studies.* J Control Release, 2019. **310**: p. 115-126.
22. Aguirre, T.A.S., et al., *Coated minispheres of salmon calcitonin target rat intestinal regions to achieve systemic bioavailability: Comparison between intestinal instillation and oral gavage.* J Control Release, 2016. **238**: p. 242-252.
23. Taverner, A., et al., *Enhanced paracellular transport of insulin can be achieved via transient induction of myosin light chain phosphorylation.* Journal of Controlled Release, 2015. **210**: p. 189-197.
24. Khafagy el, S., et al., *Region-Dependent Role of Cell-Penetrating Peptides in Insulin Absorption Across the Rat Small Intestinal Membrane.* Aaps j, 2015. **17**(6): p. 1427-37.
25. Ward, P.D., T.K. Tippin, and D.R. Thakker, *Enhancing paracellular permeability by modulating epithelial tight junctions.* Pharmaceutical Science & Technology Today, 2000. **3**(10): p. 346-358.
26. Sharma, P., et al., *Absorption enhancement, mechanistic and toxicity studies of medium chain fatty acids, cyclodextrins and bile salts as peroral absorption enhancers.* Farmaco, 2005. **60**(11-12): p. 884-93.
27. Narkar, Y., et al., *Evaluation of mucosal damage and recovery in the gastrointestinal tract of rats by a penetration enhancer.* Pharm Res, 2008. **25**(1): p. 25-38.
28. Maher, S., et al., *Evaluation of intestinal absorption enhancement and local mucosal toxicity of two promoters. I. Studies in isolated rat and human colonic mucosae.* Eur J Pharm Sci, 2009. **38**(4): p. 291-300.
29. Wang, X., S. Maher, and D.J. Brayden, *Restoration of rat colonic epithelium after in situ intestinal instillation of the absorption promoter, sodium caprate.* Ther Deliv, 2010. **1**(1): p. 75-82.
30. Swenson, E.S., W.B. Milisen, and W. Curatolo, *Intestinal permeability enhancement: efficacy, acute local toxicity, and reversibility.* Pharm Res, 1994. **11**(8): p. 1132-42.
31. Scott Swenson, E. and W.J. Curatolo, *(C) Means to enhance penetration: (2) Intestinal permeability enhancement for proteins, peptides and other polar drugs: mechanisms and potential toxicity.* Advanced Drug Delivery Reviews, 1992. **8**(1): p. 39-92.
32. Brayden, D., et al., *Heparin absorption across the intestine: effects of sodium N-[8-(2-hydroxybenzoyl)amino]caprylate in rat in situ intestinal instillations and in Caco-2 monolayers.* Pharm Res, 1997. **14**(12): p. 1772-9.
33. Cone, R.A., *Barrier properties of mucus.* Adv Drug Deliv Rev, 2009. **61**(2): p. 75-85.
34. Leal, J., H.D.C. Smyth, and D. Ghosh, *Physicochemical properties of mucus and their impact on transmucosal drug delivery.* International journal of pharmaceutics, 2017. **532**(1): p. 555-572.
35. Lundquist, P. and P. Artursson, *Oral absorption of peptides and nanoparticles across the human intestine: Opportunities, limitations and studies in human tissues.* Adv Drug Deliv Rev, 2016. **106**(Pt B): p. 256-276.
36. Chater, P.I., M.D. Wilcox, and J.P. Pearson, *Efficacy and safety concerns over the use of mucus modulating agents for drug delivery using nanoscale systems.* Advanced Drug Delivery Reviews, 2018. **124**: p. 184-192.
37. Iiboshi, Y., et al., *Adhesive mucous gel layer and mucus release as intestinal barrier in rats.* JPEN J Parenter Enteral Nutr, 1996. **20**(2): p. 98-104.
38. Chassaing, B., et al., *Dietary emulsifiers impact the mouse gut microbiota promoting colitis and metabolic syndrome.* Nature, 2015. **519**(7541): p. 92-6.
39. Lock, J.Y., et al., *Acute Exposure to Commonly Ingested Emulsifiers Alters Intestinal Mucus Structure and Transport Properties.* Scientific Reports, 2018. **8**(1): p. 10008.
40. Banerjee, A., et al., *Ionic liquids for oral insulin delivery.* Proc Natl Acad Sci U S A, 2018. **115**(28): p. 7296-7301.

41. Zhang, X., et al., *Modulating intestinal mucus barrier for nanoparticles penetration by surfactants.* Asian Journal of Pharmaceutical Sciences, 2019. **14**(5): p. 543-551.
42. Petersen, S.B., et al., *Evaluation of alkylmaltosides as intestinal permeation enhancers: comparison between rat intestinal mucosal sheets and Caco-2 monolayers.* Eur J Pharm Sci, 2012. **47**(4): p. 701-12.
43. Brayden, D.J. and E. Walsh, *Efficacious intestinal permeation enhancement induced by the sodium salt of 10-undecylenic acid, a medium chain fatty acid derivative.* Aaps j, 2014. **16**(5): p. 1064-76.
44. Hopkins, A.M., et al., *Omeprazole increases permeability across isolated rat gastric mucosa pre-treated with an acid secretagogue.* J Pharm Pharmacol, 2002. **54**(3): p. 341-7.
45. Clarke, L.L., *A guide to Ussing chamber studies of mouse intestine.* Am J Physiol Gastrointest Liver Physiol, 2009. **296**(6): p. G1151-66.
46. Brayden, D.J. and A.W. Baird, *A distinctive electrophysiological signature from the Peyer's patches of rabbit intestine.* Br J Pharmacol, 1994. **113**(2): p. 593-9.
47. Li, H., D.N. Sheppard, and M.J. Hug, *Transepithelial electrical measurements with the Ussing chamber.* Journal of Cystic Fibrosis, 2004. **3**: p. 123-126.
48. Gleeson, J.P., et al., *Stability, toxicity and intestinal permeation enhancement of two food-derived antihypertensive tripeptides, Ile-Pro-Pro and Leu-Lys-Pro.* Peptides, 2015. **71**: p. 1-7.
49. Baldassano, S., et al., *Glucagon-like peptide-2 modulates neurally evoked mucosal chloride secretion in guinea pig small intestine in vitro.* Am J Physiol Gastrointest Liver Physiol, 2009. **297**(4): p. G800-5.
50. Barthe, L., et al., *An improved everted gut sac as a simple and accurate technique to measure paracellular transport across the small intestine.* European Journal of Drug Metabolism and Pharmacokinetics, 1998. **23**(2): p. 313-323.
51. Tomkiewicz, R.P., et al., *A comparison of a new mucolytic N-acetylcysteine L-lysinate with N-acetylcysteine: airway epithelial function and mucus changes in dog.* Pulm Pharmacol, 1995. **8**(6): p. 259-65.
52. Bhattacharjee, S., et al., *Nanoparticle passage through porcine jejunal mucus: Microfluidics and rheology.* Nanomedicine, 2017. **13**(3): p. 863-873.
53. Lai, S.K., et al., *Micro- and macrorheology of mucus.* Adv Drug Deliv Rev, 2009. **61**(2): p. 86-100.
54. Pearson, J.P., P.I. Chater, and M.D. Wilcox, *The properties of the mucus barrier, a unique gel--how can nanoparticles cross it?* Ther Deliv, 2016. **7**(4): p. 229-44.
55. Macierzanka, A., et al., *Transport of particles in intestinal mucus under simulated infant and adult physiological conditions: impact of mucus structure and extracellular DNA.* PLoS One, 2014. **9**(4): p. e95274.
56. Siddhanta, S., et al., *Shedding Light on the Trehalose-Enabled Mucopermeation of Nanoparticles with Label-Free Raman Spectroscopy.* Small, 2019. **15**(33): p. 1901679.
57. Bhattacharjee, S., et al., *Track analysis of the passage of rhodamine-labeled liposomes across porcine jejunal mucus in a microchannel device.* Ther Deliv, 2018. **9**(6): p. 419-433.
58. Sjoberg, A., et al., *Comprehensive study on regional human intestinal permeability and prediction of fraction absorbed of drugs using the Ussing chamber technique.* Eur J Pharm Sci, 2013. **48**(1-2): p. 166-80.
59. Schultheiss, G., Ribeiro, R. & Diener, M. Pflügers, *Fatty acids inhibit anion secretion in rat colon: apical and basolateral action sites.* Arch - Eur J Physiol, 2001. **442**(4): p. 603-613.
60. Saunders, P.R., et al., *Physical and psychological stress in rats enhances colonic epithelial permeability via peripheral CRH.* Dig Dis Sci, 2002. **47**(1): p. 208-15.
61. Bzik, V.A., et al., *Mechanisms of action of zinc on rat intestinal epithelial electrogenic ion secretion: insights into its antidiarrhoeal actions.* J Pharm Pharmacol, 2012. **64**(5): p. 644-53.

62. Sjogren, E., et al., *Excised segments of rat small intestine in Ussing chamber studies: A comparison of native and stripped tissue viability and permeability to drugs.* Int J Pharm, 2016. **505**(1-2): p. 361-8.
63. Gleeson, J.P., et al., *Sodium caprate enables the blood pressure-lowering effect of Ile-Pro-Pro and Leu-Lys-Pro in spontaneously hypertensive rats by indirectly overcoming PepT1 inhibition.* Eur J Pharm Biopharm, 2018. **128**: p. 179-187.
64. Genty, M., et al., *Determination of the passive absorption through the rat intestine using chromatographic indices and molar volume.* Eur J Pharm Sci, 2001. **12**(3): p. 223-9.
65. Keely, S., et al., *In vitro and ex vivo intestinal tissue models to measure mucoadhesion of poly (methacrylate) and N-trimethylated chitosan polymers.* Pharmaceutical research, 2005. **22**(1): p. 38-49.
66. Taqi, S.A., et al., *A review of artifacts in histopathology.* J Oral Maxillofac Pathol, 2018. **22**(2): p. 279.
67. Nordgård, C.T. and K.I. Draget, *Dynamic responses in small intestinal mucus: Relevance for the maintenance of an intact barrier.* European Journal of Pharmaceutics and Biopharmaceutics, 2015. **95**: p. 144-150.
68. Boegh, M., et al., *Property profiling of biosimilar mucus in a novel mucus-containing in vitro model for assessment of intestinal drug absorption.* European Journal of Pharmaceutics and Biopharmaceutics, 2014. **87**(2): p. 227-235.
69. Antunes, F., et al., *Models to predict intestinal absorption of therapeutic peptides and proteins.* Curr Drug Metab, 2013. **14**(1): p. 4-20.
70. Vertzoni, M., et al., *Impact of regional differences along the gastrointestinal tract of healthy adults on oral drug absorption: An UNGAP review.* Eur J Pharm Sci, 2019. **134**: p. 153-175.
71. Dahlgren, D., et al., *Regional Intestinal Permeability of Three Model Drugs in Human.* Mol Pharm, 2016. **13**(9): p. 3013-21.
72. Lu, Z., et al., *Claudins in intestines: Distribution and functional significance in health and diseases.* Tissue Barriers, 2013. **1**(3): p. e24978.
73. Maher, S., et al., *Evaluation of intestinal absorption and mucosal toxicity using two promoters. II. Rat instillation and perfusion studies.* Eur J Pharm Sci, 2009. **38**(4): p. 301-11.
74. Maroni, A., et al., *Oral colon delivery of insulin with the aid of functional adjuvants.* Adv Drug Deliv Rev, 2012. **64**(6): p. 540-56.
75. Yamamoto, A., et al., *Effects of Different Absorption Enhancers on the Permeation of Ebiratide, an ACTH Analogue, across Intestinal Membranes.* Journal of Pharmacy and Pharmacology, 1997. **49**(11): p. 1057-1061.
76. Wallon, C., et al., *Endoscopic biopsies in Ussing chambers evaluated for studies of macromolecular permeability in the human colon.* Scand J Gastroenterol, 2005. **40**(5): p. 586-95.
77. Shimazaki, T., et al., *Absorption-enhancing effects of sodium caprate and palmitoyl carnitine in rat and human colons.* Dig Dis Sci, 1998. **43**(3): p. 641-5.
78. Soderholm, J.D., et al., *Reversible increase in tight junction permeability to macromolecules in rat ileal mucosa in vitro by sodium caprate, a constituent of milk fat.* Dig Dis Sci, 1998. **43**(7): p. 1547-52.
79. Porter, C.J.H., N.L. Trevaskis, and W.N. Charman, *Lipids and lipid-based formulations: optimizing the oral delivery of lipophilic drugs.* Nature Reviews Drug Discovery, 2007. **6**(3): p. 231-248.
80. Markov, A.G., et al., *Segmental expression of claudin proteins correlates with tight junction barrier properties in rat intestine.* J Comp Physiol B, 2010. **180**(4): p. 591-8.
81. Brayden, D.J., et al., *Sodium caprate-induced increases in intestinal permeability and epithelial damage are prevented by misoprostol.* Eur J Pharm Biopharm, 2015. **94**: p. 194-206.
82. McCartney, F., J.P. Gleeson, and D.J. Brayden, *Safety concerns over the use of intestinal permeation enhancers: A mini-review.* Tissue Barriers, 2016. **4**(2): p. e1176822.

83. Swenson, E.S., W.B. Milisen, and W. Curatolo, *Intestinal permeability enhancement: structure-activity and structure-toxicity relationships for nonylphenoxypolyoxyethylene surfactant permeability enhancers.* Pharm Res, 1994. **11**(10): p. 1501-4.
84. Soderholm, J.D., et al., *Augmented increase in tight junction permeability by luminal stimuli in the non-inflamed ileum of Crohn's disease.* Gut, 2002. **50**(3): p. 307-13.
85. Maher, S., et al., *Evaluation of intestinal absorption enhancement and local mucosal toxicity of two promoters.I. Studies in isolated rat and human colonic mucosae.* Eur J Pharm Sci (submitted), 2009.
86. Chao, A.C., et al., *In vitro and in vivo evaluation of effects of sodium caprate on enteral peptide absorption and on mucosal morphology.* Int J Pharm, 1999. **191**(1): p. 15-24.
87. Raoof, A.A., et al., *Oral bioavailability and multiple dose tolerability of an antisense oligonucleotide tablet formulated with sodium caprate.* J Pharm Sci, 2004. **93**(6): p. 1431-9.
88. Raoof, A.A., et al., *Effect of sodium caprate on the intestinal absorption of two modified antisense oligonucleotides in pigs.* Eur J Pharm Sci, 2002. **17**(3): p. 131-8.
89. Leonard, T.W., et al., *Promoting absorption of drugs in humans using medium-chain fatty acid-based solid dosage forms: GIPET.* Expert Opin Drug Deliv, 2006. **3**(5): p. 685-92.
90. Bittner, B., et al., *Phase I clinical study to select a novel oral formulation for ibandronate containing the excipient sodium N-[8-(2-hydroxybenzoyl) amino] caprylate (SNAC).* Pharmazie, 2012. **67**(3): p. 233-41.
91. Halberg, I.B., et al., *The Effect of Food Intake on the Pharmacokinetics of Oral Basal Insulin: A Randomised Crossover Trial in Healthy Male Subjects.* Clin Pharmacokinet, 2019.
92. Schiller, C., et al., *Intestinal fluid volumes and transit of dosage forms as assessed by magnetic resonance imaging.* Aliment Pharmacol Ther, 2005. **22**(10): p. 971-9.
93. Larhed, A.W., P. Artursson, and E. Bjork, *The influence of intestinal mucus components on the diffusion of drugs.* Pharm Res, 1998. **15**(1): p. 66-71.

Chapter 5

General discussion

1. Thesis overview

Since the first isolation and commercialization of insulin in the early 1920s, peptide drugs have greatly reshaped our modern pharmaceutical industry [1]. A global industry analysis of peptide therapeutics predicted sales of peptide drugs to exceed 70 billion USD in 2019 [2]. The protein-based therapeutics market and pipeline has expanded substantially in the last 30 years, and new peptide drugs are constantly emerging [3]. One of the reasons is due to their high therapeutic potential and their specificity has been seen to translate into excellent safety, tolerability and efficacy profiles in humans [4].

Oral delivery for these macromolecular drugs, however, is challenging due to their metabolic instability and poor absorption [5]. Indeed, the oral route exposes therapeutic macromolecules to chemical barriers (enzymes and pH) and physical barriers (mucus and intestinal epithelia) resulting in limited access to the systemic circulation and poor bioavailability [6]. Investigations to enable oral delivery of peptides have been extensively carried out by pharmaceutical companies and academic researchers developing technologies such as enzyme inhibitors [7], enteric coating [8], nanoparticle encapsulation [9], use of intestinal PE [10], devices (patches, microneedles, SOMA) [11,12] or combinations of such technologies [13]. Generally, the peptides clinically tested for oral delivery aim at treating endocrine disorders and are large polypeptides such as insulin, sCT, glucagon-like peptide-1 (GLP-1), and octreotide [6]. Even if they can reach the intestinal epithelium, their absorption is still impaired due to their high molecular mass, low lipophilicity, labile nature, and charged functional substructures [14]. Improved epithelial membrane permeability have been obtained by utilizing intestinal PE technologies. Those compounds increase transport via either the paracellular route, by modifying the integrity of the TJs between cells in the epithelial layer or the transcellular route by disrupting the epithelial cell membrane [15,16]. PEs have become an essential component of the most advanced oral peptide formulations [17,18].

The formulations in clinical trials for oral peptide delivery usually comprise high doses of PEs and peptidase inhibitors in the same formulation, typically accompanied by enteric coating [19]. Even if oral peptide bioavailability remains low (1-2%) with PEs relative to s.c. administration, PEs are among the most popular oral delivery strategies due to their easy inclusion in a common solid dosage form. The dominant enhancers in clinical trials are based on pharmacopeia-approved or GRAS-listed excipients, many of which are amphiphilic surfactants including medium chain fatty acids (MCFA), sodium caprate (C_{10}) and the C_8 derivative, salcaprozate sodium (SNAC), the focus of this PhD thesis. To date, following hundreds of human dosings, SNAC and C_{10} have demonstrated effective and safe delivery of a range of

macromolecules. In September 2019, FDA approval was granted for the first daily oral delivery of semaglutide (Rybelsus®) for the treatment of T2D containing SNAC as its other main tablet component. Undoubtedly, this approval is a significant advance for oral peptide and protein delivery. C_{10} could be in line for future approval in an oral product if it can be matched with a suitable stable long t½ payload, given that its effects on PK in clinical trials across many macromolecules are of the same order as those induced by SNAC [20,21].

The main objective of the thesis was to perform a head to head comparison of the mechanism of action of SNAC and C_{10}, and to decipher whether they have common features or major differences. The comparison was based on three main criteria, interaction with payloads, i.e. exenatide (Chapter 2), cytotoxicity (Chapter 3) and their permeation enhancing properties in *in vitro* and *ex vivo* models (Chapter 4) (Figure 1).

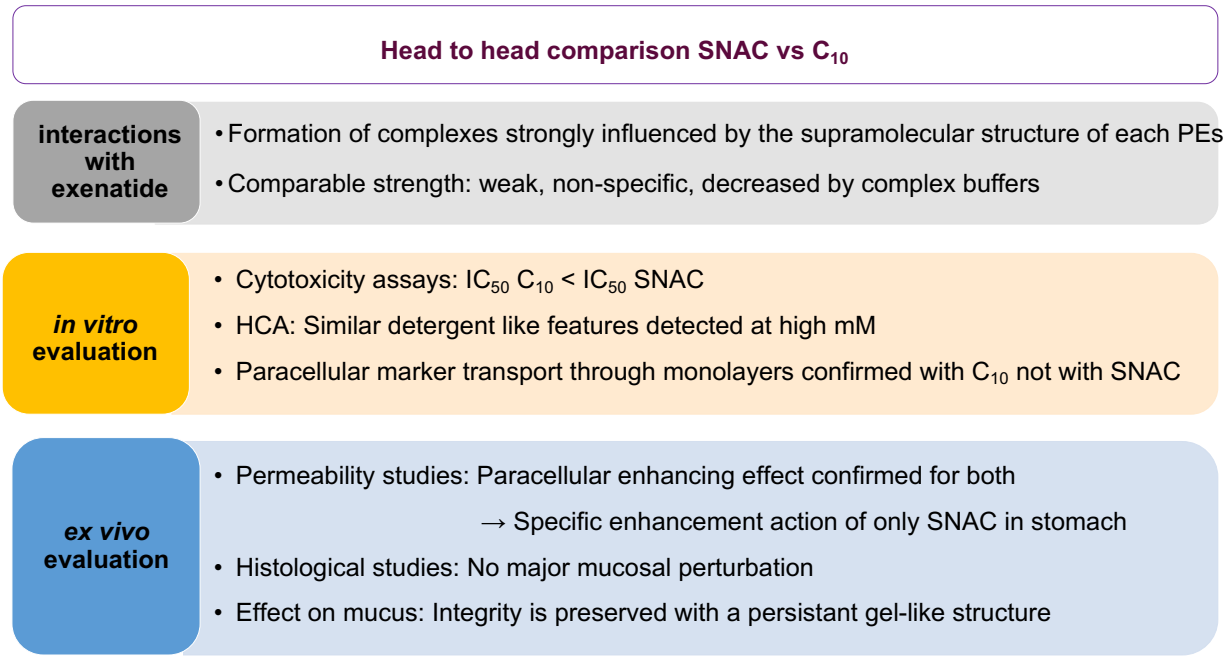

Figure 1: Overview of the main findings of the PhD thesis.

The first half of the thesis focused on characterizing their supramolecular behavior when admixed with exenatide. We evaluated PE capacity for interaction with the peptide using advanced biophysical techniques, namely, DLS, ITC, SPR and ACE. We obtained a better understanding of the PE/exenatide interaction: it was complex due to the PE's supramolecular organization and non-specific weak binding to exenatide. This interaction was highly variable in complex buffers. The second half of the thesis consisted of comparing the mechanism of action of SNAC and C_{10} in *in vitro/ex vivo* bioassays. Their cytotoxicity profile was assessed by conventional endpoint assays together with High Content Analysis (HCA) in Chapter 3. SNAC and C_{10} exhibited similar cellular changes in Caco-2 cells, but with different patterns in

generating intracellular calcium and mitochondrial membrane potential (MMP). Permeation enhancing effects on Caco-2 monolayers were concentration-dependent for C_{10} on paracellular pathways, but not so with SNAC. In Chapter 4, permeability enhancement effects were further assessed using two different *ex vivo* models (isolated rat tissue mucosae and non-everted gut sacs) with subsequent histological assessment and mucus interaction studies. Overall, SNAC and C_{10} were both efficient PE with slightly higher efficacy for $C_{10.}$ Both were associated with mild mucosal damage and a degree of mucus structure perturbation.

2. SNAC and C_{10} interact weakly and non-specifically with exenatide

SNAC and C_{10} are both fatty acid-based surfactants but were long believed to act very differently as PEs [22]. Both have PE potential, but with a specific feature for SNAC claimed by Emisphere researchers: the forming of a non-covalent structure with several different payloads [23]. To further explore this hypothesis, our two step approach was to understand (i) the aggregation behavior of C_{10} and SNAC alone and then (ii) study their interactions with exenatide. First, in chapter 2, DLS was employed to identify the supramolecular behavior of PEs in solution by determining the size distribution of the structures alone. This information was crucial, as free monomers present near the small intestinal epithelium can directly impact the extent of transient permeability. DLS results revealed, for the first time, that SNAC had the capacity to form polydisperse structures in various buffers. Compared to each other, both PEs showed similar self-assembly behavior [24]. They presented a common size distribution profile, with heterogenic-sized particles structures found in the 200 nm and 5 nm size range. The size of those structures should be further investigated by TEM and SEM studies.

A large number of studies have investigated aggregation behavior and determined the CMC values of MCFAs using different experimental techniques such as surface tension measurement [25], the dye micellization method [26], capillary electrophoresis [27], and conductimetry techniques [28]. Those methods provided large variation in results mainly due to the variation of the measurement methods and the use of different buffer solutions [24]. Hence, we applied alternative techniques to confirm the CMC values for C_{10} and determined for the first time here the CMC for SNAC in various buffers. DLS and tensiometry studies allowed the determination of the CMC for SNAC and C_{10} using common experimental conditions. The CMC is considered a good parameter for identifying threshold concentration of a PE to enhance intestinal absorption: typically, the lower the CMC, the lower the concentration needed to induce permeability enhancement [25,29]. SNAC and C_{10} exhibited CMC values in a similar concentration range (~ 30 mM) depending on the buffer and were a

threshold for colloidal organization. The most recent CMC determination of C_{10} was done using coarse-grained molecular dynamics (CG-MD) simulation in water and revealed that the calculated CMC values correlated with the experimental values, as determined by the Wilhelmy method [30]. These authors reasonably concluded that the CMC value was highly dependent on the buffer solution of the system under the key criteria of pH and ionic strength [30]. Another point to be further investigated should include CMC measurement in biorelevant buffers. Ultrasonic resonance technology has been used previously to determine CMC of surfactants in simulated bio-relevant small intestinal fluid buffers: their interaction with bile salts would also aid understanding of their behavior *in vivo* [31].

In addition, in Chapter 2, the interaction mechanism in the mixed system of C_{10} or SNAC with exenatide was studied under different environmental conditions using multiple techniques. With DLS, at a precise ratio between C_{10} and exenatide, a broad peak with a mean hydrodynamic diameter of approximately 120 nm appeared, which indicated the formation of a self-assembled structure in aqueous solution. The presence of those structures results from a finely balanced interplay between the various hydrophobic, electrostatic and dipole-dipole interactions. A major difference between C_{10} and SNAC was emphasized in these studies, as SNAC mixed with exenatide led to colloidal suspension no matter the ratio used in contrast to C_{10}. The morphology of the exenatide/PEs complexes may be further observed by use of atomic force microscopy (AFM) and TEM. Aguirre *et al.* used AFM to image distinct structures that were formed for sCT combined with PEs (sodium taurodeoxycholate, C_{10} and sodium glycocholate) [32]. Also, nanoparticle tracking analysis could be exploited to investigate different micelle or mixed micelles populations. The use of orthogonal techniques including ITC, SPR and ACE supported a common conclusion about the interaction of both SNAC and C_{10} with exenatide: non-covalent binding of low affinity. Complementary techniques are necessary to obtain robust conclusions on such complex interactions, as both PEs and exenatide form supramolecular structures by themselves. Taboada *et al.* studied the interactions between a non-ionic di-block copolymer with anionic SDS in aqueous solutions by combining static and dynamic light scattering, ITC and ^{13}C and self-diffusion nuclear magnetic resonance techniques [33]. It was found that the increasing SDS concentration created a transition of the interaction switching from the copolymer-rich-SDS mixed micelles complexes to give the surfactant-rich-copolymer mixed micelles.

It is worthwhile noting also that the intrinsic properties of the exenatide structure including hydrophobicity, charge, secondary structure propensity and sequence patterning are mainly responsible for the interactions with SNAC and C_{10}. Thus, investigating the interactions between oppositely-charged systems of SNAC and C_{10} and selected peptides could lead to

better interactions. Hydrophobic ion pairing (HIP) involves electrostatic-based complexation of an ionizable lead (usually a peptide) with an oppositely charged counterion [34]. In oral delivery of peptide, PEs with a hydrophobic moiety can perform as a counterion, neutralizing the charge of the macromolecule to allow passive diffusion of the ion-pair complex through intestinal membranes [35]. HIP complexes are usually characterized using complementary techniques such as differential scanning calorimetry (DSC), X-ray diffraction (XRD), NMR and FTIR, etc. Usually, HIP complexes present higher lipophilic properties thus lower aqueous solubility and consequently are encapsulated in nanoparticles [36], incorporated in lipid-based formulations [37,38] or in non-aqueous solvents [39]. One of the major considerations with this approach that would require more investigation is the thermodynamic assessment of the dissociation of the hydrophobized peptide complex during permeation. HIP cannot account for the exenatide interactions with SNAC and C_{10} however, as the electrostatic component, if present, seems to only contribute to a minor extent compared to other non-covalent forces, including dipole-dipole interaction and van der Waals forces. If HIP was dominant, why would SNAC and C_{10} act as PEs with payloads that were not oppositely charged? Nonetheless, at least in the case of SNAC, increased hydrophobic insoluble structures result and this is a similar outcome to HIP.

Molecular dynamic simulation has been carried out previously to visualize potential interactions between cromolyn and SNAC [40]. The authors concluded that the predominant type of interaction was ring stacking. Molecular dynamic simulation has also been used to calculate the stability constants between bile salts with alpha cyclodextrins and to facilitate the interpretation of the weak interaction [41]. Holm *et al.* [41] emphasized that the mode of binding was the insertion of the conjugated chain of the bile salt into the cyclodextrins secondary site cavity. Hence, more information concerning our system could be obtained with molecular modelling.

Other work has focused not only on the interaction between PEs and the therapeutic peptide, but between PEs and the lipid and surfactant components present in the complex milieu of the small intestine, as modelled in simulated biorelevant buffers [42]. Since SNAC and C_{10} are amphiphilic in nature, interactions with bile salt-phospholipid mixed micelles *in vivo* are very likely. Gradauer *et al.* demonstrated interaction of maltosides with NaTC/lecithin when dramatic reduction in the permeation enhancing potential of maltosides was evident in FaSSIF and FeSSIF buffers [42]. Thus, additional characterization is necessary to confirm the hypothesis that PEs such as SNAC and C_{10} might also be incorporated into NaTC/lecithin mixed micelles. In terms of permeation enhancement potential, PEs associated with mixed micelles have not yet been assessed as to their actions on the plasma membrane.

Similarly, conformational properties of exenatide when mixed with such high concentrations of anionic PEs should be investigated, as conformational changes can reduce biological activity [43]. A combination of techniques such as CD, X-ray crystallography and NMR would be giving information about the overall structure and conformation of peptides at an atomic level. Non-destructive techniques that perform structural analysis under conditions that mimic biological conditions should be prioritised.

3. Investigation of SNAC and C_{10}: *in vitro* and *ex vivo* bioassays

One of the goals in oral delivery formulation is to release high concentrations of intact peptide with PEs close to the intestinal wall to facilitate permeation and uptake across the epithelium. Therefore, it is necessary to better understand potential intestinal epithelial toxicity that might be caused by high concentrations of SNAC and C_{10} on Caco-2 cells. To explore the cytotoxicity profile for SNAC compared to C_{10}, we compared cellular parameters using a series of five end-point conventional assays and quantitative HCA of multiple sub-lethal parameters in Caco-2 cells. The comparison of IC_{50} values of SNAC and C_{10} across the conventional assays indicated that there was initial mitochondrial membrane potential perturbation at relatively low concentrations, followed by an increased nuclear, lysosomal, and plasma membrane permeability at excessively high concentrations. Importantly, SNAC did not affect cell viability, plasma membrane integrity, or nuclear permeability at concentration higher than 40 mM.

Testing of C_{10} and SNAC using HCA allowed a head to head comparison of multiple parameters, simultaneously on live cells, such as plasma membrane potential and intracellular calcium [44]. HCA has been previously used to compare effects of a group of MCFAs in Caco-2 cells, but SNAC has not yet been assessed by HCA in any cell type [45]. High-contents readouts were more sensitive for detection of sub-lethal changes compared to conventional cytotoxicity assays. Indeed, with both approaches the mitochondrial physiology was the first metric affected by PEs, but the detection of hormesis in mitochondrial membrane potential caused by C_{10} was measured only by HCA. HCA confirmed that SNAC and C_{10} showed sub-lethal cytotoxic events in Caco-2 due to multiple processes that occurred simultaneously. HCA also identified different patterns concerning the mitochondrial membrane potential and intracellular calcium profile. More importantly, HCA revealed that high SNAC concentrations induced plasma membrane permeabilization, a membrane perturbation that was not detected with traditional cell-based screens (LDH and CellToxGreen assay). Thus, HCA proved that both surfactants display detergent-like features that reflect initial membrane fluidization flowed by changes in intracellular parameters. Overall, surfactant-induced membrane perturbation associated with membrane permeabilization was more pronounced at low C_{10} concentrations,

whereas higher SNAC concentrations were required to induce similar effects. Effects were seen in the mM concentrations range indicating that drug delivery systems may release high concentrations of C_{10} or SNAC at the intestinal wall.

Transport studies across Caco-2 monolayers in Transwells showed that with C_{10}, FD4 flux increases were concentration-dependent with an associated reduction in TEER that was reversible at low C_{10} concentrations and became partially recoverable (8.5 mM C_{10}) or non-recoverable (10 mM C_{10}) depending on the concentration. The mechanism of paracellular enhancement first outlined for C_{10} in Caco-2 monolayers over 20 years ago [46,29] was further verified in this study and allowed for a direct comparison with SNAC action. Immunostaining of TJs proteins further confirmed the paracellular mechanism of action of C_{10} in monolayers grown on coverslips that triggered ZO-1 internalization, and redistribution of claudin-5 and occludin. A notable and new finding from the transport studies was that SNAC differed from C_{10} in that the former did not enhance FD4 flux nor reduce TEER at concentrations < 40 mM. That could supposedly denote for a different mechanism of action than C_{10}. However, paracellular enhancement by SNAC cannot be entirely ruled out, since a progressive removal of claudin-5 from the TJs at high concentrations of SNAC was observed, although expression of ZO-1 and occludin was maintained. Higher SNAC concentrations were screened but gave unreliable flux data as cells were detached suggesting a compromised monolayer. This is a major limitation of Caco-2 model where the SNAC concentrations associated with membrane perturbation enhancement were not distinguishable from concentrations causing membrane damage [47].

Our results confirmed that very high SNAC concentrations were required to permit even a weak detergent action based on a non-specific mechanism of action. Previously, sodium salicylate, which has a structural similarity with SNAC, only significantly enhanced the transport of fluorescein (MW 376 Da) through Caco-2 monolayers at very high concentration 173 mM and did not with FD4 [48]. In this thesis, this transport study was not designed to address the potential permeation enhancement of SNAC via the transcellular pathways as it has not been established if a transcellular marker probe could permeate in the presence of SNAC. Further investigations are necessary to definitively prove whether SNAC acts transcellularly or paracellularly *in vitro* with multi-modal mechanisms of action. For example, other proteins involved in TJs regulation and that can be affected by PEs should be tested by immunofluorescence including tricellulin [59], claudin-2 [60,61], E-cadherin [62] JAM-1 [63].

Testing of SNAC and C_{10} permeability enhancing effects was done using conventional fully differentiated and confluent Caco-2 monolayers that required 21 days to culture [49]. It is worth

noting that Caco-2 monolayers are reported to develop tight junctions of different tightness (TEER ~300 $\Omega.cm^2$), compared to human small or large intestine *in vitro* (TEER ~50-100 $\Omega.cm^2$) [50]. Hence, screening of SNAC and C_{10} effect could be done on alternative *in vitro* models. For example, a more recent 3-day Caco-2 system using modified culture conditions provides a more physiologically relevant TEER values and an increased throughput [51]. Permeability values for macromolecules exenatide, insulin and calcitonin obtained with this system correlated well with predicted *in vivo* intestinal permeability values, but this has never been tested with PEs [52]. Authors testing the 3-day Caco-2 epithelia, a.k.a. Thrifty Rapid Intestinal Monolayers (TRIM) recently demonstrated comparable results to 21-day monolayers when examining intestinal permeability with several PEs [53]. Also, it would be advantageous to test the effect of PEs on emerging models such as co-cultures expressing different types of intestinal epithelial cells [54,55], organoids [56], and microfluidic organ chip systems [57] that better reflect *in vivo* small intestine physiology and might better predict PEs enhancing effect in humans [58].

To complement imaging, the expression levels of TJs can be evaluated using Western blotting to give another valuable indication of their alteration in presence of PEs [60]. Other imaging techniques such as TEM could help to elucidate the ultrastructural details of TJ opening in Caco-2 cell monolayers [63]. Recently, Zheng *et al.* visualized the mechanical reorganization of epithelial cells in response to two piperazine derivatives with the use of chromatin dynamics (a technique termed SINK (sensors from intranuclear kinetics [64]). Authors gained valuable insight of the mechanism of action of piperazines that increased cellular force generation by myosin that leads to a breakdown of cadherins and then tight junctions ultimately [65]. It is not known if SNAC or C_{10} can dissociate TJs by way of transient actin-myosin forces via cadherins. Of all the absorption-enhancing mechanisms, an increase in the membrane fluidity is one of the most important and largely ignored mechanisms of action of many C_{10} and SNAC. DSC revealed physical interactions between SNAC and the cellular lipid membrane [21]. Labeling the cell membrane with fluorescent compounds allow the tracking of membrane fluidity changes by fluorescence polarization techniques, this could also be applied to SNAC [59].

For the first time, the SNAC mechanism of action was examined on isolated intestinal mucosae along with additional studies in the stomach mucosae and they were compared with that of C_{10}. Common points were detected: paracellular marker flux enhancement was increased with both PEs and the degree was higher across colonic mucosae than jejunal. C_{10} showed higher efficacy than SNAC and with lower concentrations necessary to obtain similar P_{app}. A major difference was that the SNAC effect on permeability was not concentration-dependent as it was with C_{10}, with the loss of permeation effect above the threshold concentration of 20 mM.

Surprisingly *in vivo*, there seems to be also a critical range of concentrations for co-formulated SNAC to optimize semaglutide absorption in dogs and humans, as 600 mg of SNAC resulted in lower levels of systemic semaglutide than the 300-mg dose [21,66]. In our study, concentrations lower and higher than 20 mM SNAC did not exert an enhancing effect on Caco-2 monolayers. This result demonstrates that combination of *in vitro* and *ex vivo* must be tested for an initial screen of PEs to conclude for permeation enhancement capacity.

We demonstrated that there are regional differences in the permeation-enhancing effects of SNAC and C_{10} for improving the flux of FD4 through mucosae. Different patterns of enhancing effects were observed in the gastric mucosa: increasing SNAC concentrations led to an increase in the FD4 P_{app} that was higher than in any other region, while increasing C_{10} concentrations (one that were effective in the jejunum and colon) surprisingly did not increase FD4 fluxes. This study was the first to discover the lack of permeation from C_{10} across gastric mucosae when other studies also emphasized the loss of C_{10} enhancement capacity through guinea pig gallbladder mounted in Ussing chambers [67]. Previous studies emphasized SNAC enhancement capacity in the gastric mucosa but with effects on transcellular pathways [21]. Our study confirmed TEER perturbation and paracellular markers flux that suggest an enabling effect of SNAC on the paracellular pathway. This paracellular effect of SNAC was confirmed even in the presence of a mucus gel layer present in non-everted gut sac and was similar to C_{10}. Also the new mechanism suggested for SNAC arising from ligated dog studies argues for a local increase in stomach pH around semaglutide, a mechanism that appears to be specific for this molecule [21].

Ideally, biorelevant matrices such as fasted-state simulated intestinal fluid (FaSSIF) or fed-state simulated intestinal fluid (FeSSIF) could be combined with *ex vivo* permeability assays to get a better insight in the influence and interactions of luminal factors on *in vivo* permeability. In the case of permeation enhancement, the physical properties and consequently enhancement action of PEs will likely be modulated by the presence of endogenous bile salts/lecithin/cholesterol micelles [68]. Phospholipid and bile salts constituents of simulated intestinal media can attenuate the effects of alkyl maltopyranosides through the formation of mixed micelles [42]. Screening the effect of PEs using biorelevant media would aid at understanding the complexity of absorption enhancement *in vivo*. Westerhout *et al.* reported the successful use of porcine intestinal tissue as an alternative for human intestinal tissue for permeability studies using biorelevant buffers [69]. Recent studies have looked at the effect of simulated intestinal buffers in the Caco-2 model and isolated rat ileum in Ussing chambers on the transport of a range of paracellular and transcellular compounds and also in rat *in situ* intestinal instillations using alkylmaltoside PEs [42,70,71]. The importance of fasting for

semaglutide absorption is highlighted by findings of no meaningful detectable systemic semaglutide exposure when the tablet was dosed in the fed state [21]. Patients are required to wait 30 min before eating and drinking after taking tablets of semaglutide/SNAC each morning to avoid food effects.

In this thesis, a specific attention was given to potential epithelial damage resulting from SNAC and C_{10} via a qualitative histological assessment of isolated mucosae, non-everted sacs and jejunal mucosa after intra jejunal instillations. Histology revealed that both PEs induced minor epithelial damage to the mucosa at the concentrations required to increase marker fluxes. Jejunal tissue could better withstand epithelial damage in the following order: intra jejunal *in situ* instillations > jejunal sacs > isolated jejunal mucosae. The implementation of standardized scoring of histology as proposed by Maher *et al*. could be a helpful way to compare PEs and aid the investigation of safety margins for PEs [17]. Also, comparisons of PEs to established excipients would help to show that mild mucosal perturbation may be common. Previously removal and wash out of C_{10} lead to recovery of permeability and TEER across rat colonic mucosae in Ussing chambers [72], or intact epithelium within the hour after rat *in situ* colonic instillation [73]. In addition*, in vivo* the epithelium has the ability to repair itself after permeation enhancer damage unlike excised tissue section [74]. Reversibility studies performed with C_{10} (0.5 g) in humans using the lactulose:mannitol urinary excretion ratio (LMER) assay showed that, following intra-jejunal administration to human subjects, the enhancer only increased permeability in a 20-min window [75]. No increase in LMER was detected in the urine at 40 and 60 min gaps suggesting the epithelium repaired from the mild challenge before the sugars were ingested. It seems that dilution, spreading, and rapid intestinal absorption of both C_{10} and SNAC prevents prolonged exposure in vivo.

Surfactants may impair the protective mucus layer, facilitating the diffusion of luminal bacteria to the intestinal epithelium and ultimately disturbing the host microbiota [76]. Hence, an ideal enhancer should be able to promote peptide absorption through the intestinal mucosa without compromising the mucus layer. In this thesis, we explored for the first time the eventual mucolytic effect of SNAC and C_{10} by measuring their impact of the rheology of porcine intestinal mucus. SNAC changed the viscoelastic parameters of the mucus to a higher extent than C_{10}. However, mucus retains its protective function as remaining network resisted to shear strain similar to untreated mucus.

To date, no significant toxicity has been attributed solely to the use of SNAC or C_{10} in clinical trials even with repeated high dosing. There is no direct evidence of abrasive mucosal damage due to PEs action, no toxicity reports claiming stomach or duodenal ulcers even from studies

with a duration as long as six months. One plausible explanation is that impact of the PE is compensated by the high turnover rate of enterocytes combined with dilution, spreading and absorption of the enhancer itself could defer such effects. Also, the clinical trial experience with both SNAC and C_{10} in hundreds of subjects over more than 20 years suggest that only very low numbers of subjects experienced side-effects that caused drop out from trials, and the majority of reports were related to mild GI effects including nausea and diarrhea for GIPET™ [75, 77] and SNAC [78]. With recent FDA approval for daily administration of oral semaglutide containing SNAC, post-marketing surveillance will provide more safety data over several years.

To summarize the key findings of this thesis, the comparison of both enhancers to increase paracellular permeability across Caco-2 and intestinal mucosa showed that C_{10} had the greatest efficacy. The increase in enhancement with C_{10} tends to be accomplished by an increase in cytotoxicity in reductionist models and more damage on intestinal mucosae compared to SNAC. However, in comparing the safety and efficacy of C_{10} and SNAC as PEs in clinical studies, they both permit oral bioavailability of a range of macromolecule payloads of around 1%. Aspects that tip the balance to SNAC compared to C_{10} include the following: broader clinical experience and an approved vitamin B_{12} product, more extensive toxicology studies and GRAS status, and the lack of requirement for protection against stomach acid.

References

1. Bliss, M., *Banting's, Best's, and Collip's accounts of the discovery of insulin.* Bull Hist Med, 1982. **56**(4): p. 554-68.
2. T.M, R., *Global Industry Analysis, Size, Share, Growth, Trends and Forecast.* Pept. Mark. 2016:2016–2024.
3. Kaspar, A.A. and J.M. Reichert, *Future directions for peptide therapeutics development.* Drug Discov Today, 2013. **18**(17-18): p. 807-17.
4. Lee, A.C., et al., *A Comprehensive Review on Current Advances in Peptide Drug Development and Design.* Int J Mol Sci, 2019. **20**(10).
5. Drucker, D.J., *Advances in oral peptide therapeutics.* Nature Reviews Drug Discovery, 2019.
6. Moroz, E., S. Matoori, and J.C. Leroux, *Oral delivery of macromolecular drugs: Where we are after almost 100years of attempts.* Adv Drug Deliv Rev, 2016. **101**: p. 108-121.
7. Maroni, A., et al., *Oral colon delivery of insulin with the aid of functional adjuvants.* Adv Drug Deliv Rev, 2012. **64**(6): p. 540-56.
8. Cole, E.T., et al., *Enteric coated HPMC capsules designed to achieve intestinal targeting.* Int J Pharm, 2002. **231**(1): p. 83-95.
9. Hristov, D.R., et al., *Silica-coated nanoparticles with a core of zinc, L-arginine and a peptide designed for oral delivery.* ACS Applied Materials & Interfaces, 2019.
10. McCartney, F., M. Rosa, and D.J. Brayden, *Evaluation of Sucrose Laurate as an Intestinal Permeation Enhancer for Macromolecules: Ex Vivo and In Vivo Studies.* Pharmaceutics, 2019. **11**(11).
11. Abramson, A., et al., *An ingestible self-orienting system for oral delivery of macromolecules.* Science, 2019. **363**(6427): p. 611-615.
12. Banerjee, A. and S. Mitragotri, *Intestinal patch systems for oral drug delivery.* Curr Opin Pharmacol, 2017. **36**: p. 58-65.
13. Parmentier, J., F.J. Hartmann, and G. Fricker, *In vitro evaluation of liposomes containing bio-enhancers for the oral delivery of macromolecules.* Eur J Pharm Biopharm, 2010. **76**(3): p. 394-403.
14. Goldberg, M. and I. Gomez-Orellana, *Challenges for the oral delivery of macromolecules.* Nat Rev Drug Discov, 2003. **2**(4): p. 289-95.
15. Whitehead, K. and S. Mitragotri, *Mechanistic analysis of chemical permeation enhancers for oral drug delivery.* Pharm Res, 2008. **25**(6): p. 1412-9.
16. Maher, S., et al., *Application of Permeation Enhancers in Oral Delivery of Macromolecules: An Update.* Pharmaceutics, 2019. **11**(1).
17. Maher, S., R.J. Mrsny, and D.J. Brayden, *Intestinal permeation enhancers for oral peptide delivery.* Adv Drug Deliv Rev, 2016. **106**(Pt B): p. 277-319.
18. Jørgensen, J.R., et al., *Microcontainers for oral insulin delivery – In vitro studies of permeation enhancement.* European Journal of Pharmaceutics and Biopharmaceutics, 2019. **143**: p. 98-105.
19. Anselmo, A.C., Y. Gokarn, and S. Mitragotri, *Non-invasive delivery strategies for biologics.* Nat Rev Drug Discov, 2019. **18**(1): p. 19-40.
20. Halberg, I.B., et al., *Efficacy and safety of oral basal insulin versus subcutaneous insulin glargine in type 2 diabetes: a randomised, double-blind, phase 2 trial.* The Lancet Diabetes & Endocrinology, 2019. **7**(3): p. 179-188.
21. Buckley, S.T., et al., *Transcellular stomach absorption of a derivatized glucagon-like peptide-1 receptor agonist.* Sci Transl Med, 2018. **10**(467).
22. Twarog, C., et al., *Intestinal Permeation Enhancers for Oral Delivery of Macromolecules: A Comparison between Salcaprozate Sodium (SNAC) and Sodium Caprate (C10).* Pharmaceutics, 2019. **11**(2).

23. Leone-Bay, A., et al., *Acylated non-alpha-amino acids as novel agents for the oral delivery of heparin sodium, USP.* J Control Release, 1998. **50**(1-3): p. 41-9.
24. Maher, S., et al., *Safety and efficacy of sodium caprate in promoting oral drug absorption: from in vitro to the clinic.* Adv Drug Deliv Rev, 2009. **61**(15): p. 1427-49.
25. Kimura, Y., et al., *Physico-chemical Properties of Fatty Acids for Assessing the Threshold Concentration to Enhance the Absorption of a Hydrophilic Substance.* Biosci Biotechnol Biochem, 1998. **62**(3): p. 443-7.
26. Patist, A., et al., *On the measurement of critical micelle concentrations of pure and technical-grade nonionic surfactants.* Journal of Surfactants and Detergents, 2000. **3**(1): p. 53-58.
27. Stanley, F.E., et al., *Rapid determination of surfactant critical micelle concentrations using pressure-driven flow with capillary electrophoresis instrumentation.* J Chromatogr A, 2009. **1216**(47): p. 8431-4.
28. Wen, X. and E.I. Franses, *Effect of Protonation on the Solution and Phase Behavior of Aqueous Sodium Myristate.* J Colloid Interface Sci, 2000. **231**(1): p. 42-51.
29. Lindmark, T., T. Nikkila, and P. Artursson, *Mechanisms of absorption enhancement by medium chain fatty acids in intestinal epithelial Caco-2 cell monolayers.* J Pharmacol Exp Ther, 1995. **275**(2): p. 958-64.
30. Hossain, M.S., et al., *Aggregation Behavior of Medium Chain Fatty Acids Studied by Coarse-Grained Molecular Dynamics Simulation.* AAPS PharmSciTech, 2019. **20**(2): p. 61.
31. Horiuchi, S. and G. Winter, *CMC determination of nonionic surfactants in protein formulations using ultrasonic resonance technology.* European Journal of Pharmaceutics and Biopharmaceutics, 2015. **92**: p. 8-14.
32. Aguirre, T., *Oral liquid emulsion drug delivery systems for enabling oral delivery of salmon calcitonin*, in *UCD*. 2012, UCD.
33. Taboada, P., E. Castro, and V. Mosquera, *Surfactant/nonionic copolymer interaction: a SLS, DLS, ITC, and NMR investigation.* J Phys Chem B, 2005. **109**(49): p. 23760-70.
34. Ristroph, K.D. and R.K. Prud'homme, *Hydrophobic ion pairing: encapsulating small molecules, peptides, and proteins into nanocarriers.* Nanoscale Advances, 2019. **1**(11): p. 4207-4237.
35. Hintzen, F., et al., *In vitro and ex vivo evaluation of an intestinal permeation enhancing self-microemulsifying drug delivery system (SMEDDS).* Journal of Drug Delivery Science and Technology, 2013. **23**(3): p. 261-267.
36. Sun, S., et al., *Hydrophobic ion pairing of an insulin-sodium deoxycholate complex for oral delivery of insulin.* Int J Nanomedicine, 2011. **6**: p. 3049-56.
37. Griesser, J., et al., *Hydrophobic ion pairing: Key to highly payloaded self-emulsifying peptide drug delivery systems.* Int J Pharm, 2017. **520**(1-2): p. 267-274.
38. Phan, T.N.Q., et al., *Oral self-emulsifying delivery systems for systemic administration of therapeutic proteins: science fiction?* Journal of Drug Targeting, 2019. **27**(9): p. 1017-1024.
39. Li, P., et al., *Preparation and characterization of insulin-surfactant complexes for loading into lipid-based drug delivery systems.* J Pharm Sci, 2013. **102**(8): p. 2689-98.
40. Ding, X., et al., *Oral absorption enhancement of cromolyn sodium through noncovalent complexation.* Pharm Res, 2004. **21**(12): p. 2196-206.
41. Holm, R., et al., *Complexation of tauro- and glyco-conjugated bile salts with alpha-cyclodextrin and hydroxypropyl-alpha-cyclodextrin studied by affinity capillary electrophoresis and molecular modelling.* J Sep Sci, 2011. **34**(22): p. 3221-30.
42. Gradauer, K., et al., *Interaction with Mixed Micelles in the Intestine Attenuates the Permeation Enhancing Potential of Alkyl-Maltosides.* Molecular Pharmaceutics, 2015. **12**(7): p. 2245-2253.
43. Mach, H. and T. Arvinte, *Addressing new analytical challenges in protein formulation development.* Eur J Pharm Biopharm, 2011. **78**(2): p. 196-207.

44. Walsh, E.G., et al., *High content analysis to determine cytotoxicity of the antimicrobial peptide, melittin and selected structural analogs.* Peptides, 2011. **32**(8): p. 1764-73.
45. Brayden, D.J., J. Gleeson, and E.G. Walsh, *A head-to-head multi-parametric high content analysis of a series of medium chain fatty acid intestinal permeation enhancers in Caco-2 cells.* Eur J Pharm Biopharm, 2014. **88**(3): p. 830-39.
46. Tomita, M., M. Hayashi, and S. Awazu, *Absorption-enhancing mechanism of EDTA, caprate, and decanoylcarnitine in Caco-2 cells.* J Pharm Sci, 1996. **85**(6): p. 608-11.
47. Aungst, B.J., *Intestinal permeation enhancers.* J Pharm Sci, 2000. **89**(4): p. 429-42.
48. Hurni, M.A., et al., *Permeability enhancement in Caco-2 cell monolayers by sodium salicylate and sodium taurodihydrofusidate: assessment of effect-reversibility and imaging of transepithelial transport routes by confocal laser scanning microscopy.* J Pharmacol Exp Ther, 1993. **267**(2): p. 942-50.
49. Sambuy, Y., et al., *The Caco-2 cell line as a model of the intestinal barrier: influence of cell and culture-related factors on Caco-2 cell functional characteristics.* Cell Biol Toxicol, 2005. **21**(1): p. 1-26.
50. Collett, A., et al., *Comparison of HT29-18-C1 and Caco-2 cell lines as models for studying intestinal paracellular drug absorption.* Pharm Res, 1996. **13**(2): p. 216-21.
51. Chong, S., S.A. Dando, and R.A. Morrison, *Evaluation of Biocoat intestinal epithelium differentiation environment (3-day cultured Caco-2 cells) as an absorption screening model with improved productivity.* Pharm Res, 1997. **14**(12): p. 1835-7.
52. Gupta, V., N. Doshi, and S. Mitragotri, *Permeation of insulin, calcitonin and exenatide across Caco-2 monolayers: measurement using a rapid, 3-day system.* PLoS One, 2013. **8**(2): p. e57136.
53. Lamson, N.G., et al., *Thrifty, Rapid Intestinal Monolayers (TRIM) Using Caco-2 Epithelial Cells for Oral Drug Delivery Experiments.* Pharm Res, 2019. **36**(12): p. 172.
54. Beloqui, A., et al., *A human intestinal M-cell-like model for investigating particle, antigen and microorganism translocation.* Nat Protoc, 2017. **12**(7): p. 1387-1399.
55. Beduneau, A., et al., *A tunable Caco-2/HT29-MTX co-culture model mimicking variable permeabilities of the human intestine obtained by an original seeding procedure.* Eur J Pharm Biopharm, 2014. **87**(2): p. 290-8.
56. Akazawa, T., et al., *Application of Intestinal Epithelial Cells Differentiated from Human Induced Pluripotent Stem Cells for Studies of Prodrug Hydrolysis and Drug Absorption in the Small Intestine.* Drug Metab Dispos, 2018. **46**(11): p. 1497-1506.
57. Bain, S.C., et al., *Cardiovascular safety of oral semaglutide in patients with type 2 diabetes: Rationale, design and patient baseline characteristics for the PIONEER 6 trial.* Diabetes Obes Metab, 2019. **21**(3): p. 499-508.
58. Costa, J. and A. Ahluwalia, *Advances and Current Challenges in Intestinal in vitro Model Engineering: A Digest.* Front Bioeng Biotechnol, 2019. **7**: p. 144.
59. Krug, S.M., M. Fromm, and D. Gunzel, *Two-path impedance spectroscopy for measuring paracellular and transcellular epithelial resistance.* Biophys J, 2009. **97**(8): p. 2202-11.
60. Almansour, K., et al., *An intestinal paracellular pathway biased toward positively-charged macromolecules.* J Control Release, 2018. **288**: p. 111-125.
61. Turner, J.R., et al., *The role of molecular remodeling in differential regulation of tight junction permeability.* Semin Cell Dev Biol, 2014. **36**: p. 204-12.
62. Maher, S., et al., *Melittin as an epithelial permeability enhancer I: investigation of its mechanism of action in Caco-2 monolayers.* Pharm Res, 2007. **24**(7): p. 1336-45.
63. Sonaje, K., et al., *Opening of Epithelial Tight Junctions and Enhancement of Paracellular Permeation by Chitosan: Microscopic, Ultrastructural, and Computed-Tomographic Observations.* Molecular Pharmaceutics, 2012. **9**(5): p. 1271-1279.
64. Armiger, T.J., et al., *Determining mechanical features of modulated epithelial monolayers using subnuclear particle tracking.* J Cell Sci, 2018. **131**(12).

65. Zheng, S., et al., *Piperazine Derivatives Enhance Epithelial Cell Monolayer Permeability by Increased Cell Force Generation and Loss of Cadherin Structures.* ACS Biomaterials Science & Engineering, 2019.

66. Granhall, C., et al., *Pharmacokinetics, Safety and Tolerability of Oral Semaglutide in Subjects with Renal Impairment.* Clin Pharmacokinet, 2018. **57**(12): p. 1571-1580.

67. Bzik, V.A., et al., *Mechanisms of action of zinc on rat intestinal epithelial electrogenic ion secretion: insights into its antidiarrhoeal actions.* J Pharm Pharmacol, 2012. **64**(5): p. 644-53.

68. Swenson, E.S., W.B. Milisen, and W. Curatolo, *Intestinal permeability enhancement: efficacy, acute local toxicity, and reversibility.* Pharm Res, 1994. **11**(8): p. 1132-42.

69. Westerhout, J., et al., *A new approach to predict human intestinal absorption using porcine intestinal tissue and biorelevant matrices.* Eur J Pharm Sci, 2014. **63**: p. 167-77.

70. Wuyts, B., et al., *Evaluation of fasted and fed state simulated and human intestinal fluids as solvent system in the Ussing chambers model to explore food effects on intestinal permeability.* Int J Pharm, 2015. **478**(2): p. 736-44.

71. Wuyts, B., et al., *Evaluation of fasted state human intestinal fluid as apical solvent system in the Caco-2 absorption model and comparison with FaSSIF.* Eur J Pharm Sci, 2015. **67**: p. 126-135.

72. Feighery, L., *Modulation of epithelial tight junctions in rodent intestinal mucosae*. 2006, University College Dublin: Dublin.

73. Wang, X., S. Maher, and D.J. Brayden, *Restoration of rat colonic epithelium after in situ intestinal instillation of the absorption promoter, sodium caprate.* Ther Deliv, 2010. **1**(1): p. 75-82.

74. Barker, N., *Adult intestinal stem cells: critical drivers of epithelial homeostasis and regeneration.* Nat Rev Mol Cell Biol, 2014. **15**(1): p. 19-33.

75. Leonard, T.W., et al., *Promoting absorption of drugs in humans using medium-chain fatty acid-based solid dosage forms: GIPET.* Expert Opin Drug Deliv, 2006. **3**(5): p. 685-92.

76. Cani, P.D., *Human gut microbiome: hopes, threats and promises.* Gut, 2018. **67**(9): p. 1716-1725.

77. Walsh, E.G., et al., *Oral delivery of macromolecules: rationale underpinning Gastrointestinal Permeation Enhancement Technology (GIPET).* Ther Deliv, 2011. **2**(12): p. 1595-610.

78. Davies, M., et al., *Effect of Oral Semaglutide Compared With Placebo and Subcutaneous Semaglutide on Glycemic Control in Patients With Type 2 Diabetes: A Randomized Clinical Trial.* Jama, 2017. **318**(15): p. 1460-1470.

Conclusions & Perspectives

Conclusions

In summary during the course of the PhD studies for this thesis, we investigated a mechanistic head to head comparison of C_{10} and SNAC, two leading permeation enhancers used in advanced oral peptide formulation and recently accepted on the market in the case of SNAC (Rybelsus®). The use of complementary advanced biophysical methods could enlighten the understanding of the PEs/exenatide interaction as well as provide methodological insights. It was determined that SNAC and C_{10} do have the capacity to form supramolecular structures in solution. Their interaction process with exenatide was dominated by non-covalent weak interactions, which were even weaker in complex buffers. For the first time, the theory that SNAC is a chaperone system of the payload through non-covalent linkages was refuted by experimental data. However, more investigations with others peptide would be necessary to determine if this theory stands or not for specific peptides.

HCA and conventional cytotoxicity assays revealed that PEs shared common detergent-like features with minor differences. Cellular changes were detected at very high concentrations unlikely to be present at the epithelium *in vivo*. Indeed, the quantity of PEs from the tablet reaching the epithelium wall will be greatly reduced due to dilution, spreading and absorption of the PE itself as it is the case with SNAC and C_{10}. It has been shown that both C_{10} and SNAC improved intestinal permeation of paracellular markers through isolated rat tissue mucosae and non-everted gut sacs and favoring the colon over jejunum. Several parameters indicated that SNAC seems to work via a paracellular, and not solely via a transcellular mechanism. The unusual permeation mechanism of SNAC with semaglutide that occurs in the stomach seems to be highly specific for this peptide. However, in our study, we also emphasized a specific enhancement action of SNAC toward the isolated rat gastric mucosa with a paracellular marker. The *in vitro* evaluation together with the *ex vivo* histological assessment confirmed the safety of PEs on the enteric membrane, as only high mM concentrations caused perturbation.

An ideal enhancer must achieve sufficient transient disruption of the intestinal epithelium to enable meaningful peptide absorption, while maintaining an acceptable safety profile and minimal local or systemic toxicity. Only a few enhancers have shown sufficient safety and efficacy to progress into clinical trials, SNAC and C_{10} being amongst them. After completion of the largest phase III trial program conducted to date for an oral peptide, the first oral semaglutide containing SNAC received FDA approval in 2019. This is a landmark in the oral peptide delivery field that could energize the development of other oral peptide therapeutics. However, a tailored approach is needed to identify suitable combinations of peptides and

permeation enhancers for oral delivery. This thesis revealed numerous similarities between SNAC and C_{10} that may be beneficial for accelerating a future approval for C_{10}. Furthermore, the success and relative safety of C_{10} and SNAC in the clinic has fostered great interest in exploring opportunities for further enhancing the efficiency of transmucosal passage of protein therapeutics.

Additional work identified

Following the observations made during this thesis a number of areas warranting additional research including:

1. To characterize the interaction of SNAC with other peptides presenting different charge and molecular weight to allow a broader conclusion of the chaperone theory.
2. To develop a better understanding of the micellar behavior of PEs in the *in vivo* situation, especially in regard to their interaction with bile salts through the use of simulated intestinal fluid.
3. To establish conclusively whether SNAC permeation enhancement is via the transcellular and/or the paracellular routes *in vivo.*

Titre : Comparaison des promoteurs d'absorption intestinaux SNAC et C_{10} pour la délivrance orale de peptides : études biophysiques, *in vitro* et *ex vivo*

Mots clés : Délivrance orale de peptide, promoteurs d'absorption, cytotoxicité, interactions

Le caprate de sodium (C_{10}) et le salcaprozate de sodium (SNAC) sont des promoteurs d'absorption (PE) inclus comme composants clés dans les formulations développées pour la délivrance orale de peptides. Plus de 20 essais cliniques réalisés chez l'Homme ont évalués ces formes pharmaceutiques comprenant en quantité majoritaire SNAC ou C_{10}. Cependant, plusieurs propriétés de ces promoteurs font encore débats et sont explorées et comparées dans cette thèse, notamment : (i) leurs interactions avec la molécule active, (ii) leur cytotoxicité, (iii) leur capacité d'amélioration de la perméabilité intestinale et (iv) l'impact sur le mucus intestinal. Les interactions biophysiques entre SNAC ou C_{10} et l'exénatide se révèlent être de nature similaires, faibles et impactées par l'organisation supramoléculaire individuelle des PEs. Les tests de cytotoxicités combinés au *l'High Content Analysis* révèlent que SNAC et C_{10} fluidifient initialement la membrane plasmique des cellules Caco-2. Ils perturbent ensuite l'homéostasie cellulaire générale mais de façon différente. Dans les études de perméabilité, le SNAC diffère du C_{10} car il n'améliore pas le passage du marqueur FD4 au travers des monocouches de Caco-2. Pour les deux PE, l'augmentation de la perméabilité de marqueurs paracellulaires est confirmée au travers de tissus intestinaux isolés de rat (colon, jéjunum) et de sacs intestinaux non inversés. Seul le SNAC augmente cette perméabilité au travers du tissu gastrique de rat. Des mesures de rhéologie indiquent que la structure gélifiée du mucus intestinal de porc est préservée au contact des PEs. En conclusion, cette thèse révèle de nombreuses similarités entre SNAC et C_{10} avec de subtiles différences. C_{10} démontre une puissance légèrement supérieure au SNAC mais ils obtiennent une efficacité et un profil cytotoxique similaire.

Title: Comparison of the intestinal permeation enhancers, SNAC and $C_{10,}$ for oral peptides: biophysical, *in vitro* and *ex vivo* studies

Keywords: Oral peptide delivery, intestinal permeation enhancer, cytotoxicity, interactions

Sodium caprate (C_{10}) and salcaprozate sodium (SNAC) are permeation enhancers (PEs) included as key components in advanced oral peptide formulations. More than 20 clinical trials have evaluated oral peptide formulations comprising high quantities of SNAC or C_{10}. However, there is still debate concerning the comparative mechanistic properties of SNAC and C_{10}, which are studied in this thesis notably: (i) interactions with payloads, (ii) potential cytotoxicity, (iii) intestinal permeability enhancement capacity and (iv) effects on intestinal mucus. A head to head comparison between SNAC and C_{10} would assist a decision to opt for one over the other in an oral peptide formulation.
Biophysical interactions between SNAC or C_{10} and a model peptide, exenatide, were similar, dominated by non-covalent weak interactions resulting from supramolecular organization. Cytotoxicity assays combined with High Content Analysis revealed that SNAC and C_{10} initially fluidized Caco-2 cell apical plasma membranes. Intracellular parameters consequently varied, but with different patterns for each PEs. In transport studies, SNAC differed from $C_{10,}$ as only the latter enhanced FD4 fluxes across Caco-2 monolayers. However, permeation enhancing effects of both PEs were confirmed using rat intestinal tissue mucosae and non-everted gut sacs from jejunum and colon. A specific enhancing effect was measured for SNAC and not C_{10} across isolated rat gastric mucosae. Rheological studies indicate that the gel-like structure of intestinal porcine mucus was preserved when in contact with these PEs. In conclusion, this thesis has revealed the common mechanistic features of surfactants between C_{10} and SNAC along with subtle differences. C_{10} had a somewhat higher potency as a PE than SNAC, but efficacy and cytotoxicity profiles were similar.

Université Paris-Saclay
Espace Technologique / Immeuble Discovery
Route de l'Orme aux Merisiers RD 128 / 91190 Saint-Aubin, France